

ASSESSMENT OF NON-EXPONENTIAL SOUND ENERGY DECAYS WITHIN
MULTI-DOMED MONUMENTS BY NUMERICAL AND EXPERIMENTAL
METHODS

A THESIS SUBMITTED TO
THE GRADUATE SCHOOL OF NATURAL AND APPLIED SCIENCES
OF
MIDDLE EAST TECHNICAL UNIVERSITY

BY

ZÜHRE SÜ GÜL

IN PARTIAL FULFILLMENT OF THE REQUIREMENTS
FOR
THE DOCTOR OF PHILOSOPHY
IN
BUILDING SCIENCE IN ARCHITECTURE

JANUARY 2015

Approval of the thesis:

**ASSESSMENT OF NON-EXPONENTIAL SOUND ENERGY DECAYS
WITHIN MULTI-DOMED MONUMENTS BY NUMERICAL AND
EXPERIMENTAL METHODS**

submitted by **ZÜHRE SÜ GÜL** in partial fulfillment of the requirements for the degree of **Doctor of Philosophy in Building Science in Architecture Department, Middle East Technical University** by,

Prof. Dr. Gülbin Dural Ünver
Dean, Graduate School of **Natural and Applied Sciences** _____

Prof. Dr. Güven Arif Sargın
Head of Department, **Architecture** _____

Assoc. Prof. Dr. Ayşe Tavukçuoğlu
Supervisor, **Dept. of Architecture, METU** _____

Prof. Dr. Mehmet Çalışkan
Co-Supervisor, **Mechanical Engineering Dept., METU** _____

Examining Committee Members:

Prof. Dr. Ömür Bakırer
Dept. of Architecture, METU _____

Assoc. Prof. Dr. Ayşe Tavukçuoğlu
Supervisor, Dept. of Architecture, METU _____

Prof. Dr. Emine Caner Saltık
Dept. of Architecture, METU _____

Assoc. Prof. Ali Murat Tanyer
Dept. of Architecture, METU _____

Assoc. Prof. Dr. Semiha Yılmaz
Dept. of Interior Arch. and Env. Design, Bilkent University _____

Date: 22.01.2015

I hereby declare that all information in this document has been obtained and presented in accordance with academic rules and ethical conduct. I also declare that, as required by these rules and conduct, I have fully cited and referenced all material and results that are not original to this work.

Name, Last Name: Zühre SÜ GÜL

Signature :

ABSTRACT

ASSESSMENT OF NON-EXPONENTIAL SOUND ENERGY DECAYS WITHIN MULTI-DOMED MONUMENTS BY NUMERICAL AND EXPERIMENTAL METHODS

Sü Gül, Zühre

Ph.D., in Building Science, Department of Architecture

Supervisor: Assoc. Prof. Dr. Ayşe Tavukçuoğlu

Co-supervisor: Prof. Dr. Mehmet Çalışkan

January 2015, 308 pages

The key concern of this study is to investigate sound fields of single space superstructures sheltered with multiple-domes, in terms of their potential for featuring non-exponential sound energy decay characteristics. In this framework, Süleymaniye Mosque and Hagia Sophia Museum are selected as cases for investigating the effects of different material use and volumetric contribution on multi-slope decay formation. Methodology involves joint use of in-situ acoustical measurements and acoustical simulations. Relevant acoustical parameters including decay rates and decay times are computed by applying Bayesian decay parameter estimation. Analysis results of experimentally acquired and simulated data disclose double or triple decay formation in superstructures of Süleymaniye Mosque and Hagia Sophia Museum. To justify the phenomena and to understand the mechanism of energy exchanges, spatial sound energy distributions and energy flow vectors are studied by Diffusion Equation Model (DEM) simulations and intensity probe measurements over the case of Süleymaniye Mosque. Both computed and in-situ

flow vectors highlight the contribution of sound reflective central dome versus absorptive carpeted floor on providing later energy feedback, creating a nondiffuse sound field. On the other hand, for Süleymaniye Mosque trial by DEM simulations the case of floor with marble instead of carpet has resulted in a much diffuse sound field, implying that the use of sound reflective floor material has prevented the multi-slope decay formation. Results over various acoustical data collection and data analysis techniques proved that energy fragmentation in support of non-exponential energy decay formation is due to both materials' sound absorption characteristics and their distributions, as well as volumetric inter-space relations.

Keywords: Non-exponential Sound Energy Decay, Diffusion Equation Model, Intensity Probe Measurements, Acoustics of Süleymaniye Mosque, Acoustics of Hagia Sophia Museum

ÖZ

ÇOK KUBBELİ ANITSAL YAPILARDA BAĞLAŞIK AKUSTİK ALANLARIN SAYISAL VE DENEYSEL YÖNTEMLERLE ARAŞTIRILMASI

Sü Gül, Zühre

Doktora, Yapı Bilimleri, Mimarlık Bölümü

Tez Yöneticisi: Assoc. Prof. Dr. Ayşe Tavukçuoğlu

Ortak Tez Yöneticisi: Prof. Dr. Mehmet Çalışkan

Ocak 2015, 308 sayfa

Bu araştırmanın temel hedefi, çok kubbeli bir üst yapıya sahip tek hacimli anıtsal yapılarda bağlaşıklık ses alanlarının analizi ile çoklu ses enerjisi sönümlenme eğrilerinin oluşumu ve bu oluşumun sebeplerinin ortaya konmasıdır. Mimari ve malzeme değişkenlerinin enerji sönümlenme eğrisine etkisini belirlemek amacıyla, farklı hacim, plan şeması ve yer bitirme malzemelerine sahip olan Süleymaniye Camii ve Aya Sofya Müzesi üzerinde çalışmalar yürütülmüştür. Bu çalışmalar, sahada yapılan akustik ölçümler ve bilgisayar benzetimi sonuçlarının berimsel/hesaplamalı analizine dayanmaktadır. Çoklu sönümlenme eğrisi analizleri istatistiksel Bayesian kestirim yöntemi ile gerçekleştirilmiştir. Elde edilen akustik darbe yanıtı verilerinden, sönümlenme hızları/oranları ve sönümlenme süreleri hesaplanmıştır. Bu sonuçlara göre her iki yapıda iki hatta üç enerji sönümlenme eğrileri gözlenmiştir. Tek bir hacim içerisinde gözlenen bu olayı irdelemek üzere, sonlu elemanlarda difüzyon denklemi modelinin uygulaması ile Süleymaniye Camii'nin ses akış alanları çözümlenmiştir. Destekleyici olarak aynı mekanda parçacık hızı sensörü ile sahada toplanan gerçek

veriler üzerinden akış vektörleri hesaplanmıştır. Her iki teknik ile elde edilen enerji akış vektörleri, ses yutucu halı kaplı yer yüzeyine kıyasla yansıtıcı merkezi kubbenin geç enerji akışı ve dağınık olmayan ses alanı yaratmasına, dolayısıyla çoklu enerji sönümlenme eğrileri oluşumuna katkısını işaret etmektedir. Süleymaniye Camii'nde, yerlerin halı yerine mermer ile değiştirildiği diğer bir DEM çözümlemesi, enerji odak alanının daha merkezi bir noktaya taşınmasına sebep olmuş; ses yansıtıcı mermer kaplı döşeme yüzeylerinin varlığı sonucunda gelişen düzgün dağınık ses alanı geç enerji dönüşlerinin oluşumuna engel olmuştur. Tüm sonuçlar geometri, boyut ve malzeme özelliklerinin mekanların ses alanı dağılım karakteristiklerine etkilerini göstermiş ve tüm bu mimari parametrelerin çoklu sönümlenme veya akustik bağlaşıklıkla temel sebepleri olduğunu ortaya koymuştur.

Anahtar Kelimeler: Bağlaşıklık Akustik Alanlar, Difüzyon Denklemi Modeli, Akustik Parçacık Hızı Ölçümleri, Süleymaniye Camii Akustiği, Aya Sofya Müzesi Akustiği

*To all Working Mothers
and their Precious Ones..*

ACKNOWLEDGEMENTS

My utmost appreciation is to my mentor professor Mehmet Çalışkan. The reasons cannot be restricted by this research, but some to be expressed within this limited words; as for him lighting up the road within every aspect of my life, for not being a profound teacher and a life-time standing library, but as well for being a father of mine at all times. And, for him to be proud and in support of all of us, *all of his students*.

I would like to express sincere appreciation to my advisor Dr. Ayşe Tavukçuoğlu, for her special contributions in this research, for her excitement and motivation on me, and for her robust influence on all technical commentary. Special thanks are to my permanent advisor Dr. Ning Xiang, who grounded up all previous success of mine, and with his undocumented support for this research as well, to him for believing in me as in before and for guiding me in every step of my study.

I would like to extend my gratitude to the General Directorate of Pious Foundations (Vakıflar Genel Müdürlüğü) for providing measured drawings of Süleymaniye Mosque and for giving permissions on field measurements. Turkish Ministry of Culture and Tourism, and General Directorate of Turkish Cultural Heritage and Museums are gratefully acknowledged for their permissions on Hagia Sophia field measurements.

It is also my duty to express deepest appreciation to all talented and intelligent MEZZO Stüdyo team members for covering and filling all the gaps of my absence from the busiest working hours. Most of all, for their being as of a family member, for their sincerity, for their desire and enthusiasm to solve whatever research topic or

real-life problem we are searching for, which all makes us a special team that can hardly be sustained in any other business grounds.

Most private thanks are to my special men Murat and Manas, for their presence, for making my life much meaningful with their precious love and for their understanding of my stolen times. Solely, without their being nothing could be ended, or whatever ended wouldn't have any meaning. Lastly, but not least, my greatest indebtedness is for sure to my family, who are still with us or not, with their endless trust and for their pure happiness out of my every achievement.

TABLE OF CONTENTS

ABSTRACT	v
ÖZ.....	vii
ACKNOWLEDGEMENTS	x
TABLE OF CONTENTS	xii
LIST OF TABLES	xvi
LIST OF FIGURES.....	xvii
LIST OF SYMBOLS	xxiv
LIST OF ABBREVIATIONS	xxvi

CHAPTERS

1. INTRODUCTION.....	1
1.1. Argument	1
1.2. Objectives.....	6
1.3. Procedure	8
1.4. Disposition	10
2. STATE OF THE ART.....	11
2.1. Acoustical and Architectural Parameters	11
2.2. Acoustical Data Collection Methods.....	16
2.3. Review of Mosque Acoustics.....	18
2.3.1. Assessment and Comparison Studies of Mosques	19
2.3.2. Acoustical Renovations and Acoustical Design of Mosques.....	25

2.3.3. Acoustical Investigations on Virtual Mosques and Design Criteria Development.....	30
2.3.4. Concluding Remarks on Mosque Acoustics	34
2.4. Review of Coupled Spaces.....	38
2.4.1. Geometrical Room Acoustics	41
2.4.2. Geometrical Statistical Methods	48
2.4.2. Diffusion Equation Model (DEM).....	53
2.4.3. Wave Theory.....	56
2.4.4. Acoustical Coupling Quantifiers.....	59
2.4.5. Concluding Remarks on Coupled Spaces	65
3. RESEARCH MATERIALS	69
3.1. Case 1: Süleymaniye Mosque, İstanbul	71
3.1.1. Architectural Features	72
3.1.2. Restoration Works.....	79
3.2. Case 2: Hagia Sophia, İstanbul	81
3.2.1. Basic Repairs and Alterations	82
3.2.2. Architectural Features as of Today	86
4. METHODOLOGY.....	91
4.1. Room Acoustics Simulations	91
4.2. Room Acoustics Measurements	95
4.2.1. Süleymaniye Mosque Measurements.....	96
4.2.2. Hagia Sophia Measurements.....	99
4.3. Decay Parameter Estimations (DPE)	101
4.4. Diffusion Equation Model (DEM) Analysis	105
4.4.1. Interior Diffusion Equation	105

4.4.2. Boundary Conditions.....	108
4.5. Intensity Probe Impulse Response Measurements	111
5. RESULTS.....	115
5.1. Simulation and Field Measurement Data	115
5.1.1. Süleymaniye Mosque Field Data	115
5.1.2. Süleymaniye Mosque Simulation Data	118
5.1.3. Hagia Sophia Field Data	121
5.2. DPE Data.....	126
5.2.1. Süleymaniye Mosque Pre-Field Simulation DPE	126
5.2.2. Süleymaniye Mosque Field DPE	130
5.2.3. Süleymaniye Mosque Post-Field Simulation DPE.....	132
5.2.4. Hagia Sophia Field DPE	134
5.3. DEM Data (Süleymaniye Mosque)	138
5.4. Intensity Probe Data (Süleymaniye Mosque).....	151
6. DISCUSSIONS	167
6.1. Acoustical Field Comparison of Süleymaniye Mosque for Before and After 2007-2011 Restorations	167
6.2. Interpretation of Süleymaniye Mosque’s Acoustics for Its Original State	171
6.3. Coupling Trend Investigations of Süleymaniye Mosque by Comparison of Field and Simulation DPE.....	177
6.4. Coupling Trend Investigations of Süleymaniye Mosque by the Analysis of Simulated DEM and Intensity Probe Field Data.....	182
6.5. Multi-Slope Formation within Süleymaniye Mosque and Hagia Sophia in Relation to Basic Architectural Parameters	202
6.6. Evaluation of Data Collection and Data Analysis Methods.....	210

7. CONCLUSION	217
BIBLIOGRAPHY	231
APPENDICES	
A. SIMULATION RESULTS.....	241
B. DPE RESULTS	257
C. DEM RESULTS.....	273
D. INTENSITY PROBE RESULTS.....	287
CURRICULUM VITAE	303

LIST OF TABLES

TABLES

Table 5.1. Süleymaniye Mosque overall T30 (s) field test results in 1/3 octaves....	116
Table 5.2. Hagia Sophia INR and T30 (s) field test results in 1/1 octaves	123
Table 5.3. Süleymaniye Mosque multi-slope analysis, typical pre-field	128
Table 5.4. Decay parameters for impulse response collected at R ₃ S ₁	129
Table 5.5. Süleymaniye Mosque multi-slope analysis results, typical field	130
Table 5.6. Decay parameters for impulse response collected at S ₃ R ₇	131
Table 5.7. Süleymaniye Mosque multi-slope analysis results, typical post-field	132
Table 5.8. Decay parameters for impulse response collected at S ₂ R ₂	133
Table 5.9. Hagia Sophia multi-slope analysis results, typical field data.....	134
Table 5.10. Decay parameters for impulse response collected at S ₂ R ₆	137
Table 5.11. Süleymaniye Mosque intensity probe field measurement data.....	152
Table 6.1. Decay parameters for impulse response collected at S ₁ R ₁	196
Table B.1. Süleymaniye Mosque multi-slope analysis results, overall pre-field.....	257
Table B.2. Süleymaniye Mosque multi-slope analysis results, overall field	267
Table B.3. Süleymaniye Mosque multi-slope analysis results, overall post-field ...	269
Table B.4. Hagia Sophia multi-slope analysis results, overall field data.....	271

LIST OF FIGURES

FIGURES

Figure 1.1. Visual detection of non-exponential decay in Schroeder decay curve	4
Figure 1.2. A conceptual drawing of probable energy exchanges	5
Figure 2.1. Typical impulse response data graph.....	12
Figure 2.2. Reverberation time definition with sample decay	13
Figure 2.3. Recommended RT for different mosque volumes.....	33
Figure 2.4. A typical coupled volume system.....	39
Figure 2.5. A schematic drawing for stage house and distributed coupling	40
Figure 2.6. A typical appearance of energy time curve	60
Figure 2.7. Coupling quantifiers based on EDT and LDT.....	61
Figure 3.1. Süleymaniye complex - an old gravure	72
Figure 3.2. Süleymaniye Mosque plan view	73
Figure 3.3. Süleymaniye Mosque central section, looking towards mihrab	73
Figure 3.4. Süleymaniye Mosque, section view	74
Figure 3.5. Interior view of domes and <i>pendentives</i> in Süleymaniye Mosque	75
Figure 3.6. Süleymaniye Mosque fume room.....	77
Figure 3.7. Openings for resonators within the dome of Süleymaniye Mosque.....	78
Figure 3.8. <i>Muqarnas</i> detail - highlighted with pen paintings.....	78
Figure 3.9. Hagia Sophia exterior view - an old painting	81
Figure 3.10. Hagia Sophia interior view - an old painting.....	84
Figure 3.11. <i>Müezzin's mahfili</i> , Hagia Sophia	84
Figure 3.12. Imperial Pavilion and Loge	85
Figure 3.13. Plan view of Hagia Sophia	86
Figure 3.14. Section view from the central axis by Salzenberg, Hagia Sophia	87
Figure 3.15. Interior view from south gallery, Hagia Sophia	88
Figure 4.1. Süleymaniye Mosque, ODEON ray tracing view.....	93

Figure 4.2. 3D-OpenGL view of modelled Süleymaniye Mosque.....	94
Figure 4.3. Süleymaniye Mosque ODEON acoustical model.....	95
Figure 4.4. Measurement set-up of field tests	96
Figure 4.5. Süleymaniye Mosque field tests source(S) and receiver(R) locations	97
Figure 4.6. Süleymaniye Mosque field measurement photographs	98
Figure 4.7. Hagia Sophia field tests source(S) and receiver(R) locations.....	101
Figure 4.8. Hagia Sophia field measurement photographs	101
Figure 4.9. Süleymaniye Mosque solid mesh model	110
Figure 4.10. Measurement set-up for probe measurements	112
Figure 4.11. Plan layout of Süleymaniye Mosque probe measurements	113
Figure 4.12. Süleymaniye Mosque probe measurement photographs	113
Figure 5.1. Süleymaniye Mosque average EDT, T20, T30 field test results	116
Figure 5.2. Süleymaniye Mosque average C80 field test results	117
Figure 5.3. Süleymaniye Mosque background noise levels (Leq)	117
Figure 5.4. Comparison of T30 results for pre and post-field simulations	119
Figure 5.5. Comparison of T30 results for full and unoccupied Mosque	119
Figure 5.6. Unoccupied state of the Mosque, comparison of plasters	120
Figure 5.7. Occupied state of the Mosque, comparison of plasters	120
Figure 5.8. Hagia Sophia INR measurements in 1/1 octave bands	122
Figure 5.9. Hagia Sophia T30 measurements in 1/1 octave bands	125
Figure 5.10. Pre-field simulations source(S) and receiver(R) locations	127
Figure 5.11. Comparison of Schroeder curve and the model curve for R ₃ S ₁	129
Figure 5.12. Comparison between Schroeder curve and the model curve, S ₃ R ₇	131
Figure 5.13. Comparison between Schroeder curve and the model curve, S ₂ R ₂	133
Figure 5.14. Average # of slopes per 1/1 octave bands, Hagia Sophia.....	135
Figure 5.15. Average # of slopes per source locations, Hagia Sophia.....	135
Figure 5.16. Average # of slopes per receiver locations, Hagia Sophia	136
Figure 5.17. Total # of slopes per source-receiver configurations, Hagia Sophia ...	136
Figure 5.18. Comparison between Schroeder curve and the model curve, S ₂ R ₆	137
Figure 5.19. Field versus DEM results for S ₁ R ₄ , 1 kHz, 1 slope	139

Figure 5.20. Field versus DEM results for S ₁ R ₄ , 1 kHz, 2 slopes.....	139
Figure 5.21. Süleymaniye Mosque DEM results, spatial sound energy distributions and flow vectors for 250 Hz, time: 0.1s.....	140
Figure 5.22. Süleymaniye Mosque DEM results, spatial sound energy distributions and flow vectors for 250 Hz, time: 0.3s.....	141
Figure 5.23. Süleymaniye Mosque DEM results, spatial sound energy distributions and flow vectors for 250 Hz, time: 0.5s.....	141
Figure 5.24. Süleymaniye Mosque DEM results, spatial sound energy distributions and flow vectors for 250 Hz, time: 0.7s.....	142
Figure 5.25. Süleymaniye Mosque DEM results, spatial sound energy distributions and flow vectors for 250 Hz, time: 0.9s.....	142
Figure 5.26. Süleymaniye Mosque DEM results, spatial sound energy distributions and flow vectors for 250 Hz, time: 2s.....	143
Figure 5.27. Süleymaniye Mosque DEM results, , spatial sound energy distributions and flow vectors for 250 Hz, time: 13s.....	143
Figure 5.28. Süleymaniye Mosque DEM results, spatial sound energy distributions and flow vectors for 1 kHz, time: 0.1s.....	144
Figure 5.29. Süleymaniye Mosque DEM results, spatial sound energy distributions and flow vectors for 1 kHz, time: 0.3s.....	144
Figure 5.30. Süleymaniye Mosque DEM results, spatial sound energy distributions and flow vectors for 1 kHz, time: 0.5s.....	145
Figure 5.31. Süleymaniye Mosque DEM results, spatial sound energy distributions and flow vectors for 1 kHz, time: 0.7s.....	145
Figure 5.32. Süleymaniye Mosque DEM results, spatial sound energy distributions and flow vectors for 1 kHz, time: 0.9s.....	146
Figure 5.33. Süleymaniye Mosque DEM results, spatial sound energy distributions and flow vectors for 1 kHz, time: 2s.....	146
Figure 5.34. Süleymaniye Mosque DEM results, spatial sound energy distributions and flow vectors for 1 kHz, time: 6s.....	147

Figure 5.35. Süleymaniye Mosque DEM results, spatial sound energy distributions and flow vectors for 1 kHz, time: 0.1s; marble floor	148
Figure 5.36. Süleymaniye Mosque DEM results, spatial sound energy distributions and flow vectors for 1 kHz, time: 0.3s; marble floor	148
Figure 5.37. Süleymaniye Mosque DEM results, spatial sound energy distributions and flow vectors for 1 kHz, time: 0.5s; marble floor	149
Figure 5.38. Süleymaniye Mosque DEM results, spatial sound energy distributions and flow vectors for 1 kHz, time: 0.7s; marble floor	149
Figure 5.39. Süleymaniye Mosque DEM results, spatial sound energy distributions and flow vectors for 1 kHz, time: 0.9s; marble floor	150
Figure 5.40. Süleymaniye Mosque DEM results, spatial sound energy distributions and flow vectors for 1 kHz, time: 2s; marble floor	150
Figure 5.41. Süleymaniye Mosque DEM results, spatial sound energy distributions and flow vectors for 1 kHz, time: 8s; marble floor	151
Figure 5.42. Intensity vectors, 1kHz, t: 0 ms, full section view (XZ axis)	155
Figure 5.43. Intensity vectors, 1kHz, t: 50 and 100ms, section view	155
Figure 5.44. Intensity vectors, 1kHz, t: 150, 200, 250 and 300ms, section view	156
Figure 5.45. Intensity vectors, 1kHz, t: 350, 400, 450 and 500ms, section view	157
Figure 5.46. Intensity vectors, 1kHz, t: 550, 600, 650 and 700ms, section view	158
Figure 5.47. Intensity vectors, 1kHz, t: 750, 800, 850 and 900ms, section view	159
Figure 5.48. Intensity vectors, 1kHz, t: 950, 1000, 1150 and 1100ms, section	160
Figure 5.49. Intensity vectors, 1kHz, t: 0 ms, full axon view	161
Figure 5.50. Intensity vectors, 1kHz, t: 50 and 100ms, axon view	161
Figure 5.51. Intensity vectors, 1kHz, t: 150, 200, 250 and 300ms, axon view	162
Figure 5.52. Intensity vectors, 1kHz, t: 350, 400, 450 and 500ms, axon view	163
Figure 5.53. Intensity vectors, 1kHz, t: 550, 600, 650 and 700ms, axon view	164
Figure 5.54. Intensity vectors, 1kHz, t: 750, 800, 900 and 950ms, axon view	165
Figure 5.55. Intensity vectors, 1kHz, t: 950, 1000, 1050 and 1100ms, axon view ..	166
Figure 6.1. Comparison of T30 for field tests held in 1988, 1996, 2000, 2013	168
Figure 6.2. Average # of slopes per 1/1 octave bands, Süleymaniye Mosque	178

Figure 6.3. Average # of slopes per source locations, Süleymaniye Mosque.....	178
Figure 6.4. Average # of slopes per receiver locations, Süleymaniye Mosque	179
Figure 6.5. Total # of slopes per source-receiver configurations.....	179
Figure 6.6. Spatial sound energy level (dB) distribution, time: 0.1s, 1 kHz.....	183
Figure 6.7. Spatial sound energy level (dB) distribution, time: 2s, 1 kHz.....	185
Figure 6.8. Two-dimensional mapping of sound-energy flow vectors	187
Figure 6.9. Three-dimensional mapping of sound-energy flow vectors, 250 Hz	188
Figure 6.10. Flow vectors (DEM) versus intensity vectors (field), t: 0.1 to 0.3s.....	190
Figure 6.11. Flow vectors (DEM) versus intensity vectors (field), t: 0.4 to 0.6s.....	191
Figure 6.12. Flow vectors (DEM) versus intensity vectors (field), t: 0.7 to 0.9s.....	192
Figure 6.13. Intensity vectors, S ₁ R ₁ , 1 kHz, t: 655 to 1155ms, XZ axis.....	194
Figure 6.14. Comparison between Schroeder curve and the model curve, S ₁ R ₁	196
Figure 6.15. Intensity vectors, S ₁ R ₁ , 1 kHz, t: 1137 to 1170 ms, XZ axis.....	197
Figure 6.16. Spatial sound energy level (dB) distribution, marble floor	199
Figure 6.17. Two-dimensional mapping of flow vectors, marble floor	200
Figure 6.18. Süleymaniye Mosque, DEM multi-slope analysis results, S ₁ R ₄	201
Figure 6.19. Comparison of different T30 field test results of Hagia Sophia.....	203
Figure 6.20. Barrier wall separating left aisle from the main space	204
Figure 6.21. Photo of main dome and scaffoldings, Hagia Sophia in 2014.....	204
Figure 6.22. Comparison of T30 for Süleymaniye Mosque and Hagia Sophia.....	205
Figure 6.23. Partial plans of Süleymaniye (above) and Hagia Sophia (below)	206
Figure 6.24. Average # of decay slopes per 1/1 octave bands	207
Figure 6.25. Minimum and maximum # of decay slopes per 1/1 octave bands.....	207
Figure 6.26. Arches of Süleymaniye Mosque (above) and Hagia Sophia (below)..	209
Figure 7.1. Conceptual plan (a) and section (b) views for energy flows	223
Figure 7.2. Spatial sound energy distribution comparison of Süleymaniye Mosque floor finishes; carpet floor (a) versus marble floor (b).....	225
Figure 7.3. Flow vector distribution comparison of Süleymaniye Mosque floor finishes; carpet floor (a) versus marble floor (b).....	225
Figure 7.4. Conceptual sketch for early (clarity) and late (reverberance)	230

Figure A.1. T30 distribution map, 125 Hz, Süleymaniye Mosque	241
Figure A.2. T30 cumulative distribution graph, 125 Hz, Süleymaniye Mosque	242
Figure A.3. T30 distribution map, 250 Hz, Süleymaniye Mosque	242
Figure A.4. T30 cumulative distribution graph, 250 Hz, Süleymaniye Mosque	243
Figure A.5. T30 distribution map, 500 Hz, Süleymaniye Mosque	243
Figure A.6. T30 cumulative distribution graph, 500 Hz, Süleymaniye Mosque	244
Figure A.7. T30 distribution map, 1000 Hz, Süleymaniye Mosque	244
Figure A.8. T30 cumulative distribution graph, 1000 Hz, Süleymaniye Mosque ...	245
Figure A.9. T30 distribution map, 2000 Hz, Süleymaniye Mosque	245
Figure A.10. T30 cumulative distribution graph, 2000 Hz, Süleymaniye Mosque .	246
Figure A.11. T30 distribution map, 4000 Hz, Süleymaniye Mosque	246
Figure A.12. T30 cumulative distribution graph, 4000 Hz, Süleymaniye Mosque .	247
Figure A.13. C80 distribution map, 125 Hz, Süleymaniye Mosque	247
Figure A.14. C80 cumulative distribution graph, 125 Hz, Süleymaniye Mosque ...	248
Figure A.15. C80 distribution map, 250 Hz, Süleymaniye Mosque	248
Figure A.16. C80 cumulative distribution graph, 250 Hz, Süleymaniye Mosque ...	249
Figure A.17. C80 distribution map, 500 Hz, Süleymaniye Mosque	249
Figure A.18. C80 cumulative distribution graph, 500 Hz, Süleymaniye Mosque ...	250
Figure A.19. C80 distribution map, 1000 Hz, Süleymaniye Mosque	250
Figure A.20. C80 cumulative distribution graph, 1000 Hz, Süleymaniye Mosque .	251
Figure A.21. C80 distribution map, 2000 Hz, Süleymaniye Mosque	251
Figure A.22. C80 cumulative distribution graph, 2000 Hz, Süleymaniye Mosque .	252
Figure A.23. C80 distribution map, 4000 Hz, Süleymaniye Mosque	252
Figure A.24. C80 cumulative distribution graph, 4000 Hz, Süleymaniye Mosque .	253
Figure A.25. SPL(A) distribution map, Süleymaniye Mosque	253
Figure A.26. SPL(A) cumulative distribution graph, Süleymaniye Mosque	254
Figure A.27. STI distribution map, Süleymaniye Mosque	254
Figure A.28. STI cumulative distribution graph, Süleymaniye Mosque	255
Figure C.1. Süleymaniye Mosque DEM result for 250 Hz, t: 0.1s, carpeted floor..	273
Figure C.2. Süleymaniye Mosque DEM result for 250 Hz, t: 0.3s, carpeted floor..	274

Figure C.3. Süleymaniye Mosque DEM result for 250 Hz, t: 0.5s, carpeted floor..	275
Figure C.4. Süleymaniye Mosque DEM result for 250 Hz, t: 0.7s, carpeted floor..	276
Figure C.5. Süleymaniye Mosque DEM result for 250 Hz, t: 0.9s, carpeted floor..	277
Figure C.6. Süleymaniye Mosque DEM result for 250 Hz, t: 2s, carpeted floor.....	278
Figure C.7. Süleymaniye Mosque DEM result for 250 Hz, t: 13s, carpeted floor...	279
Figure C.8. Süleymaniye Mosque DEM results for 1 kHz, t: 0.1s, marbled floor ..	280
Figure C.9. Süleymaniye Mosque DEM results for 1 kHz, t: 0.3s, marbled floor ..	281
Figure C.10. Süleymaniye Mosque DEM results for 1 kHz, t: 0.5s, marbled floor	282
Figure C.11. Süleymaniye Mosque DEM results for 1 kHz, t: 0.7s, marbled floor	283
Figure C.12. Süleymaniye Mosque DEM results for 1 kHz, t: 0.9s, marbled floor	284
Figure C.13. Süleymaniye Mosque DEM results for 1 kHz, t: 2s, marbled floor ...	285
Figure C.14. Süleymaniye Mosque DEM results for 1 kHz, t: 8s, marbled floor ...	286
Figure D.1. Intensity vectors, R1S1, 1kHz, t: 0 to 185ms, XZ coordinates	288
Figure D.2. Intensity vectors, R1S1, 1kHz, t: 200 to 240ms, XZ coordinates.....	289
Figure D.3. Intensity vectors, R1S1, 1kHz, t: 245 to 325ms, XZ coordinates.....	290
Figure D.4. Intensity vectors, R1S1, 1kHz, t: 230 to 382ms, XZ coordinates.....	291
Figure D.5. Intensity vectors, R1S1, 1kHz, t: 283 to 425ms, XZ coordinates.....	292
Figure D.6. Intensity vectors, R1S1, 1kHz, t: 435 to 455ms, XZ coordinates.....	293
Figure D.7. Intensity vectors, R1S1, 1kHz, t: 475 to 555ms, XZ coordinates.....	294
Figure D.8. Intensity vectors, R1S1, 1kHz, t: 555 to 620ms, XZ coordinates.....	295
Figure D.9. Intensity vectors, R1S1, 1kHz, t: 625 to 725ms, XZ coordinates.....	296
Figure D.10. Intensity vectors, R1S1, 1kHz, t: 750 to 855ms, XZ coordinates.....	297
Figure D.11. Intensity vectors, R1S1, 1kHz, t: 895 to 975ms, XZ coordinates.....	298
Figure D.12. Intensity vectors, R1S1, 1kHz, t: 1000 to 1070ms, XZ coordinates...	299
Figure D.13. Intensity vectors, R1S1, 1kHz, t: 1075 to 1155ms, XZ coordinates...	300
Figure D.14. Intensity vectors, R1S1, 1kHz, t: 1160 to 1275ms, XZ coordinates...	301
Figure D.15. Intensity vectors, R1S1, 1kHz, t: 1375 to 1475ms, XZ coordinates...	302

LIST OF SYMBOLS

A_s	Amplitude level, dB
T_s	Decay time, s
c	Speed of sound, $\text{m}\cdot\text{s}^{-1}$
q	Particle density
P	Acoustic power, W
V	Volume, m^3
S	Surface area, m^2
$\bar{\alpha}$	Average surface absorption coefficient
Q	Particle scattering cross-section
λ	Mean free path, m
J	Particle-density flux
t	Time
r	Position in x,y,z direction
w	Acoustic energy density, $\text{J}\cdot\text{m}^{-3}$
∇^2	Laplace operator
D	Diffusion coefficient
m	Air absorption coefficient
δ	Dirac-delta function
E	Acoustic energy, J
n	Surface outgoing normal
A_x	Absorption factor
α	Sound absorption coefficient
A_S	Sabine absorption term

A_E	Eyring absorption term
A_M	Modified absorption term

LIST OF ABBREVIATIONS

BIC	Bayesian Information Criterion
BRIR	Binaural Room Impulse Responses
C80	Clarity
CAHRISMA	Conservation of the Acoustical Heritage by the Revival and Identification of the Sinan's Mosques Acoustics
D50	Definition
DEM	Diffusion Equation Model
DPE	Decay Parameter Estimations
DSE	Double Slope Effect
EDT	Early Decay Time
ETC	Energy Time Curve
EU	European Union
FEM	Finite Element Modeling
G	Strength
GA	Geometrical Room Acoustics
INR	Impulse to Noise Ratio
ITDG	Initial-Time-Delay Gap
LF60	Lateral Fraction
MFP	Mean Free Path
MFT	Mean Free Time
MLS	Maximum Length Sequence
MPH	Main Prayer Hall
NC	Noise Criteria
RIR	Room Impulse Response
RT	Reverberation Time
RTC	Randomized Tail-corrected Cone-tracing

SA	Statistical Acoustics
SEA	Statistical Energy Analysis
SPL	Sound Pressure Level
SPL-A	A-Weighted Sound (Pressure) Level
S/R	Signal to Noise Ratio
SRS	Sound Reinforcement System
STC	Sound Transmission Class
STI	Speech Transmission Index
T20	Reverberation that accounts for the first 20 dB decay
T30	Reverberation that accounts for the first 30dB decay
ULI	Upper Limit of Integration

CHAPTER 1

INTRODUCTION

In this research, from a broader perspective, the intersection level of two commonly distant research grounds that have affinity to a scientific field, so called ‘acoustics’ are investigated. Sound field analysis is an important method of scientific inquiries on acoustics, while acoustics is a diverse wheel of science covering multiple sub-branches as of architectural acoustics. The two up to day isolated inquiry areas are namely mosque structures and virtually/visually coupled spaces. The significance behind this exploration is initially to reveal the unexpected crossing outcomes of the two fields and to declare them as to be related and associate. Detailed arguments, objectives and motivation behind this study together with the procedure of the research and disposition of the thesis are presented in following sections.

1.1. ARGUMENT

Mosque as of a building typology is an enclosure for Islamic worship, which is essentially a good subject matter for room acoustics with its finely defined forms and involved activity patterns. In acoustical terms, the activity patterns are chiefly the intelligibility of conveys of *imam* in weekly Friday’s sermon and the speech-music interpolation of *imams* commands in a daily preaching activity called ‘*namaz*’. In architectural design of a mosque, the desired acoustical criteria must be incorporated within a visual aesthetic for the success of a mosque which satisfies the spiritual aspects of worship. Until today most of the mosque acoustics investigations have concentrated on the behavior of mosque typology in satisfaction of previously defined mosque activity patterns and corresponding acoustical criteria. Previously,

mosque as an architectural typology has not been the subject of investigations for a more scientific inquiry such as acoustical coupling.

Coupled volume systems, on the other hand, have far been investigated for theoretical understanding of particular sound energy decay characteristics, in other words non-exponential energy decay formation, within such enclosures. Non-exponential energy decay regarding to its inherent properties of early and late decay/s in very early studies have found to be detrimental due to creating an unfamiliar acoustical impression, then has become a design tool in providing a lingering reverberance while maintaining sense of intimacy and clarity. Main stimulus behind coupled space investigations is to better orient their use in real cases ranging from large concert halls to much smaller studios.

The curiosity behind acoustical coupling are not limited to existing real-case situations, but more to the understanding of the behavior of sound in the scale of wave acoustics, geometrical acoustics or statistical acoustics. The field is still scientifically developing and there are very few studies to provide real size data; collected in real architectural environments that have the possibility of possessing non-exponential energy decay phenomenon. Most work in the field is dependent on scale model tests or computer simulations. It is still a necessity to provide real data to the science of acoustics and accordingly to enlighten many inquiries over the formation of non-exponential energy decays.

Until very recently, the main focus of the studies has been the so-called double decay phenomenon. In one of very recent studies, double slope decay concept is furthered and methods are developed with an aim of identifying ‘multiple-slope’ decays and quantifying the degree of multiple coupling (Xiang, 2011). For that reason, in this research, the phenomenon is searched not only within the framework of double-slope context but in a more scientific approach under multiple non-exponential sound energy decay examinations.

As stated, none of the mosque acoustics researchers has had an inclination to find out dissimilar sound energy decay in compare to classical acoustical parameter and/or single decay analysis. On the other side, recent works on coupled spaces are mostly on theoretical formulation of energy exchange between coupled volumes, and none as a case investigates acoustic coupling in multi-domed single space sacred superstructures/monuments. To sum up, it can be stated that research topic is both original in mosque acoustics -specifically, domed single space monumental structures-, and in room acoustics coupling studies -specifically, non-exponential energy decay formation-.

This research is in quest of highlighting the single shell but acoustically divergent/nondiffuse environments that can form basis for further room acoustics coupling investigations. The major argument of this study is that *even single-volume systems with specific architectural compositions and material input can form non-exponential energy decays* with careful selection of source and receiver configurations. Thus, the prime research question is that whether acoustical coupling or non-exponential energy decay is an outcome of coupled-spaces solely, or if it could be observed in single-space enclosures with specific geometric and material attributes.

One major motivation behind this question is Kuttruff (2000)'s statement -depending upon his investigations- as '*coupling phenomena can even occur in single enclosures that are lack of sound field diffusion*'. Another motivation for probable occurrence of the coupling phenomena in mosque's acoustic field is Topaktaş's investigation on Süleymaniye Mosque in İstanbul (Topaktaş, 2003). In that research, the energy decay curves out of simulations depict a double slope curve in a visual inspection (Figure 1.1), which urges a deeper investigation/understanding and validation of the phenomenon with advanced tools of data collection and computational data analysis.

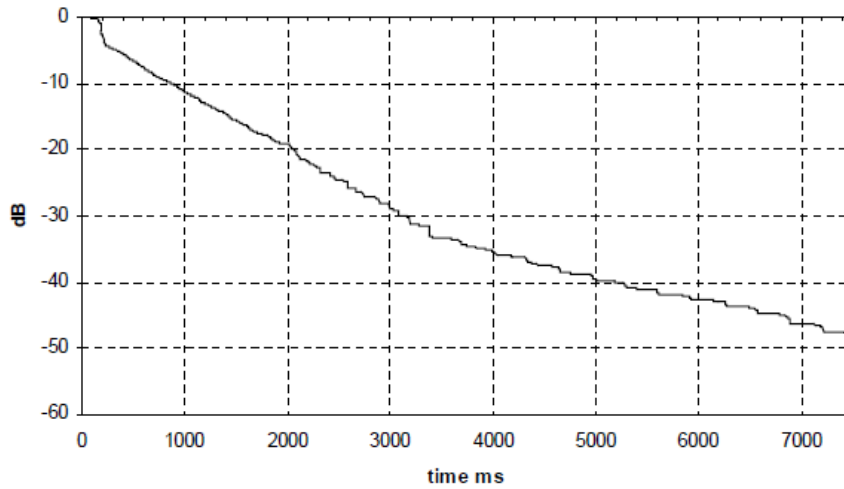


Figure 1.1. Visual detection of non-exponential decay in Schroeder decay curve of simulated room impulse response in 1 kHz, for Süleymaniye Mosque (Source: Topaktaş, 2003: 86)

Specific combinations of different architectural volumes are highly correlated with acoustical coupling. Thus, domed structures are thought to have a potential for featuring multi-slope sound energy decays (Figure 1.2). Instead of multiple volumes with defined enclosures, a single volume with specific geometric attributes is considered to be base for the multiple-slope formation (Sü Gül and Çalışkan, 2013c). None of other building/room typologies in a visually uncoupled enclosure format have been investigated yet for their potentials on different sound energy storages in the form of overlapping linear decays with dissimilar decay rates.

For all that reason, the uniqueness of this work is in bringing out the mosque typology or the multi-domed sacred superstructures with a single volume space, as disguised sources of acoustical coupling (or non-exponential energy decay formation). Findings can also motivate some future studies on the psycho-acoustic effects of non-exponential energy decay within a mosque's (or multi-domed sacred super-structures) sound field considering its function of use and spiritual aspects.

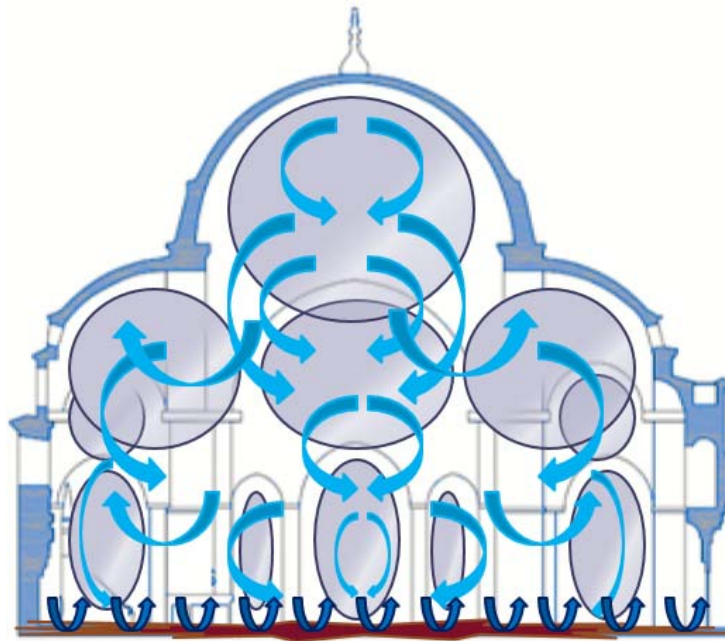


Figure 1.2. A conceptual drawing of probable energy exchanges within a multi-domed superstructure (Source: produced by the author)

From a theoretical point of view, single enclosures composed of large volumes within multiple dome scheme and that are deficient of sound field diffusion, such as mosques with highly reflective interior surfaces encountering with comparatively excessive floor absorption, are thought to have potential for creating non-exponential energy decays. Within that respect, multiple dome superstructures are identified to be the sample group for computational models and/or real size experiments on acoustical data collection and data analysis. Süleymaniye Mosque in İstanbul is chosen to be the major case, which has motivated this research out of previous simulation study results as previously discussed. Süleymaniye Mosque, with a multi-domed upper-structure and large main arches connected to main piers (elephant foot) provides a single space definition in architectural terms. In acoustical terms, the Mosque has the potential of generating noneven distribution of sound energy, due to the fragmentation of vertical interior acoustical field by a sound absorptive carpeted lower ground/floor zone versus sound reflective painted/plastered stone upper shelter.

Another monument that is investigated is Hagia Sophia Museum, which as well has a multi-domed upper shell morphology but a larger volume and a basilican plan layout. Another significant difference in terms of room acoustics conditions is that Hagia Sophia has a sound reflective floor -out of marble- in contrast to Süleymaniye Mosque with absorptive floor -out of carpet-. This material shift could augment or degrade the effects of acoustical coupling, which should also be considered and examined. For that reason Hagia Sophia is selected to be the supportive case to discuss some significant issues as of material changes, volumetric distribution and more specifically, its relatively much diffuse sound field in comparison to Süleymaniye Mosque's nondiffuse acoustical environment.

1.2. OBJECTIVES

Major intuitions to better understand and to broaden the definition of room acoustics coupling are highlighted in Section 1.1. Non-exponential decay formation in coupled spaces, known to be 'two or more volumes with well-defined enclosure limits coupled to each other with a coupling aperture', has found a revised definition in this study as of non-exponential decay formation within 'single-spaces with nondiffuse sound field separated/fragmented with virtual apertures'. In the light of basic arguments and/or research questions, specific objectives of the study can be listed as follows;

- to test the hypothesis/argument of 'the non-exponential decay formation is the resultant factor of both virtually coupled spaces in form of main dome spaces to sub dome spaces, and of well-defined/split zones of sound attenuation and amplification through absorptive floor and reflective upper enclosure finishes;
 - to examine the sound propagation under certain structural forms and architecturally finished spaces of mosques, or multiple-domed sacred superstructures, and acoustical coupling features of that specific medium.

- to test volumetric and material information in relation to non-exponential energy decay; to test the effects of different volumes, plan-layouts and different sound absorption areas/locations within multi-domed single space superstructure typology.
- to validate the effects of different material input and distribution (absorptive floor versus reflective upper structure to reflective floor and reflective upper-structure) in real-case scenarios.
- to provide more real-size input/data for better understanding of the non-exponential energy decay and to enlighten many inquiries within this specific research field;
 - to provide real data over both single space structures and structures that integrate both single space and coupled space systems; under single space structures as of Süleymaniye Mosque and partially single space structures as of Hagia Sophia's central space (virtually coupled by main geometric forms within their single shell) and under coupled volume structures as of Hagia Sophia's side aisles (geometrically coupled to its main space).
 - to search not only double-decay phenomenon but to pioneer in presenting real cases of 'multiple-decay' formation especially in single shell structures.
- to validate multiple-decay formation with further scientific tools as of diffusion equation modeling (never to be applied before in such a real case monumental scenario) and field probe measurements (very recent technology with very few applications in real-size environments), and to be pioneer in joint use of these tools/methodologies;
 - to provide/introduce new data collection and analysis tools to the field of architectural acoustics that can be applied in scientific/academic investigations as well as in practice.
- to motivate future investigations on the subjective effects of non-exponential energy decay within sacred monumental spaces.

- to motivate future investigations on historical materials (specifically lime-based plasters) by emphasizing their positive influence on reverberation control and thus acoustical comfort levels specific to function.

1.3. PROCEDURE

In this study, initially the literature on mosque acoustics and acoustically coupled spaces are investigated for better capturing of previous outcomes in relation to classical room acoustics parameters and most significantly in terms of acoustical coupling quantifiers. Besides, state of the art helps in detection of present and future tools of data collection and data analysis in room acoustics. In a scientific inquiry of non-exponential energy decays through data analysis, first of all the right tools/computational techniques have to be established for the estimation of coupling quantifiers. The data collection tools are also vital to gather reliable data, whether real or simulated. Field measurements and acoustical simulations/computations are the major tools for data collection.

Field measurements are grouped under pressure microphone and intensity transducer set-ups, the details of which are presented under Methodology section. Both in Süleymaniye Mosque and Hagia Sophia Museum, the data gathered through pressure microphone field measurements and simulations are further analyzed for multi-slope decay formation over pressure impulse responses. Studies over energy exchange between coupled volumes with focus on Bayesian formulation aim to estimate parameters associated with multiple slope decay and intend to characterize energy decays of multiple decay process. Decays out of pressure impulse provide some important decay parameters as of number of slopes, decay times and decay levels. Intensity impulses gathered by intensity probe over the case Süleymaniye Mosqu are utilized to validate and understand the mechanism of multi-slope decay formation.

Acoustical computation studies comprise both ray and image tracing based simulations and numerical methods as of diffusion equation modeling (DEM) within a finite element solution. DEM is also used to investigate the influence of material input in generation of nondiffuse sound field formation, specifically marble versus carpet floor. The estimated findings in a DEM solution have necessitated to be confirmed and/or to be supported by a real-case that has reflective surfaces both in floor and upper-structure/shelter that is Hagia Sophia museum. To obtain the real data and to highlight and observe above mentioned discussion points, field tests are held in Hagia Sophia Museum as well.

Data gathered through DEM model and intensity probe measurements of Süleymaniye Mosque are further analyzed in search of energy exchange mechanism that has provided the multi-slope decay formation. Spatial sound energy distributions and sound energy flow vectors are analyzed for highlighting the energy fragmentation patterns. Lastly, the comparison of energy flow vectors out of intensity probe measurements and pressure decay analysis are used for the validation of turning points, which are the crossing points of early versus later energy decays (linear decay terms) in a non-exponential energy decay.

Supplementary/side discussions are held over acoustical conditions of Süleymaniye Mosque for before and after some specific restorations, and for its original state. These studies basically involve the comparison of field test data for different times and include the experimentation of contemporary versus historical materials by the use of acoustical simulations. Results are evaluated both in terms of material changes (plaster and paint) in time and the contribution of basic architectural decisions (for the original state) on to the acoustical comfort parameters, as of the site location, main geometric sizes, geometric relations, interior forms/modulations and surface undulations/textures.

1.4. DISPOSITION

This study is presented under seven chapters, out of which this *'introduction'* is the first. In the second chapter *'state of the art'* is given, which comprises the acoustical and architectural parameters together with acoustical data collection tools in relation to the mosque acoustics and coupled spaces. The review sections indicate up to day information over technology and recent findings of both fields and instrumental in emphasizing the weak paths that necessitate further investigations.

In the third chapter is given the descriptions of *'research materials'*, which are Süleymaniye Mosque and Hagia Sophia. Both monuments are presented in terms of their architectural features as of today together with basic repairs and alterations within their timespan. The fourth chapter presents the information on *'methodology'* in terms of data collection and data analysis tools. Analysis/computation outcomes of real-size and computed data are presented under *'results'* in the fifth chapter.

The sixth chapter includes *'discussions'* over major and supplementary arguments in relation to results of acoustical field conditions of analyzed multi-domed single space monuments and non-exponential decay formation detection and validation within those case structures. All instructive and validating outcomes of arguments and motivational findings in regards to future studies are briefed under *'conclusion'* in the seventh chapter.

CHAPTER 2

STATE OF THE ART

As this research will be the first to deeply investigate the intersection points of two different interest areas namely mosque acoustics (or multi-domed monumental sacred spaces) and acoustical coupling, under this section the literature of two topics are discussed separately. In order to provide needed background, the basic acoustical indicators, architectural parameters and data collection tools are firstly presented as they relate both to mosque/sacred space acoustics and acoustical coupling in room acoustics.

2.1. ACOUSTICAL AND ARCHITECTURAL PARAMETERS

The quality of acoustics for a room is basically evaluated by some objective and subjective requirements. These subjective and objective measures should have good correlations in between to be considered as reliable. Subjective requirements comprise the criteria which are principally depending on the ears' interpretation of different measures. Some basic subjective acoustical parameters can be listed as intimacy, warmth, loudness, envelopment, reverberance, subjective clarity, diffusion, ensemble, balance, blend, brilliance and dynamic range.

Objective measures offer an intermediate description between design parameters and subjective effect (sound perception). According to the behavior of sound in rooms, the design creates a sound field at the listener's position, which can be described in objective acoustical measures. The major objective acoustical parameters are Reverberation Time (RT, T30, T20), Early Decay Time (EDT), Clarity (C80),

Definition (D50), Lateral Fraction (LF60), Speech Transmission Index (STI), Strength (G), Initial-Time-Delay Gap (ITDG) and A-Weighted Sound Pressure Level (SPL/-A).

Among listed objective acoustical metrics some specific ones are measured and/or assessed in mosque acoustics and acoustical coupling studies. According to the function of use or matter of scientific investigation of sound fields the parameters may vary. The very basic parameter which is discussed in both mosque acoustics and non-exponential decay formation in coupled spaces is the “decay rate”, which also relates to RT and EDT. Acoustical parameters are gathered through an impulse response (virtual or real) that is recorded for a room (Figure 2.1). Following to that, energy decay curves are obtained for observing the energy levels of the decay in time. Decay rate describes how fast or slow the sound decays in time in a particular section of the decay curve within a specific room.

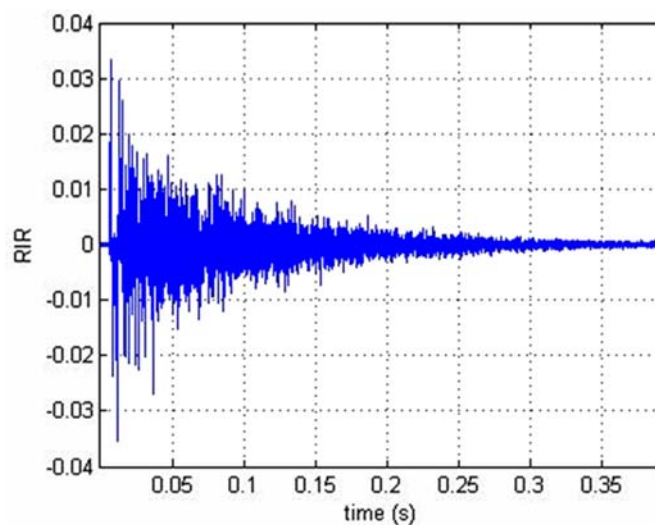


Figure 2.1. Typical impulse response data graph

In very rough terms ‘Reverberation Time (RT)’ is defined as the time required for a sound that is loud enough to decay to inaudibility (Everest, 1994). The general scientific description for the reverberation time is that the time required after stopping a sound source for the average sound energy density to decay by 60 dB

(one-millionth of its original value) from an equilibrium level (Figure 2.2). Since W.C. Sabine in 1900 studied the phenomenon reverberation time, it has been used as the most important indicator of the acoustic characteristics or the auditory environment of a room (Maekawa and Lord, 1994). Early Decay Time (EDT) is another parameter that is evaluated in both fields of interest. EDT is the sensation of RT or technically, it is the measure of the rate of a sound decay, expressed in the same way as RT, based on measuring the first 10 dB portion of the decay and multiplying it by 6 for corresponding with RT values (Barron, 1993).

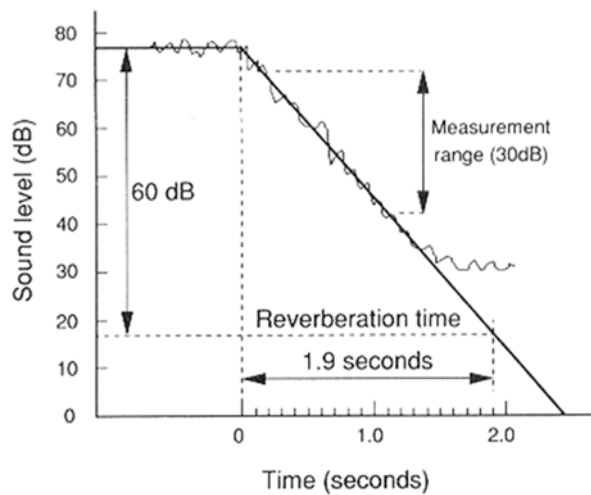


Figure 2.2. Reverberation time definition with sample decay. The slope of the decay is in practice measured between -5 dB and -35 dB of the initial level. (Source: Barron, 1993: 27)

Clarity (C80) or the early-to-late sound index is the quality characterizing the separation in time, of the sounds, of individual pieces of music. The technical description for the clarity is that the ratio of early sound energy arrives within 80 ms of direct sound to late or reverberant sound energy arriving later than 80 ms after the direct sound (Makrinenko, 1994). Distinctness of sound, obtained from the impulse response is named as definition (D50). This is the measure derived from the ear's response to consecutive impulses and characterizes the ratio of the effective energy to the total energy in an impulse response. The effective energy includes both the direct sound energy and the energy of reflections delayed with respect to the direct sound by up to 50 ms. As observed in this literature review, D50 has only been a

topic of acoustical indicator for mosque acoustics, while C80 is applied under both mosque acoustics and acoustical coupling investigations.

Intelligibility of speech is priority in a mosque, which is also one basic reason to uprise the acoustical considerations. Acoustic measures of speech intelligibility have concentrated on two concerns which are the signal-to-noise ratio and the level/strength of sound. The speech sound must be loud enough relative to the background noise. Speech Transmission Index (STI) has been strongly promoted for predicting speech intelligibility through impulse response. It accommodates both the signal-to-noise ratio and the strength of impulse -in level- which affect intelligibility. The idea behind this measure is that for good speech intelligibility the envelope of the signal should be preserved. It allows for different contributions of various frequency bands to speech quality, and estimates the mutual masking between adjacent frequency bands occurring in our hearing organ (Kuttruff, 1991).

The Sound Pressure Level (SPL) is last acoustical parameter to be mentioned as it correlates to both mosque acoustics and acoustical coupling investigations. The A-weighted level (SPL-A) is the most common single number measure of loudness and indicator of the acoustic wave strength. Strength (G), on the other hand, is the total sound level at a closed volume for a specific source and receiver configuration, that is assessed by the comparison of the sound level at volume/space under consideration for given source location, to the direct sound level at 10 m from the same source in an open/free field (Long, 2006).

There are two basic architectural parameters that to some extent the objective criteria depend on. These are room volume and total surface absorption (Barron, 1993). Volume is one major variable of room acoustics. Increase in volume enable changes in reverberation time, indicating a longer decay time. A monumentally large mosque would definitely have a different sound field and accordingly subjective acoustical field effect in comparison to a small mosque. On the other hand, experimental

variations of volumes of coupled rooms can affect the occurrence of multiple decay formations. Volume is proportional to decay rate and as it increases also the reverberance of a space.

Variation in acoustic absorption enables sound pressure and reverberation time changes. The balance in between acoustically absorptive and reflective surfaces - depending upon sound absorption coefficients over frequency spectrum of interior materials- depicts how live or dead a room is. Total sound absorption is inversely proportional to decay rate or reverberance of an enclosed space. Interior surface materials of a mosque such as plaster, stone, brick or wood are generally regarded as acoustically reflective materials as long as there are no special surface treatments to increase absorption and diffusion. Carpet floor finishes comprise the major sound absorptive surfaces within mosques except for the sound absorption due to the human body/the prayers and except for the absorption by air in specific frequency ranges.

Major room geometry and surface forms create different reflections and diffuseness within the space. Results may either be acoustically hazardous such as acoustical foci due to domed geometry of mosques or may be beneficial for creating an even sound field with efficient scattering of sound as by means of *muqarnases* or stalactites. Changes in diffuseness of a surface carry less impact than changes in absorption or orientation, but still is an important element for creating a diffuse sound field. Especially for coupling investigations diffusion within each coupled space over a wide range of frequency/octave bands is highly significant to experimentally search the nondiffuse sound field in the resultant coupled condition of rooms with different sound decays.

For non-exponential decay investigations in coupled spaces apart from the parameters such as absorption ratio of materials and volume ratio of sub-rooms, aperture size and partition properties are also significant architectural parameters.

Most of the acoustical coupling studies concentrate on the effects of aperture dimensions. Size and location of the aperture are highly correlated with the effective sound flow in between coupled sub-rooms. Aperture may be oversized and cause the sub-spaces to be perceived as a single large space, or may be too small to enable the adequate energy transfer for the interpolation of different decay terms. In a similar manner the Sound Transmission Class (STC/Rw) values of the common partitions should be high enough to provide the acoustical separation of two or more coupled enclosures.

2.2. ACOUSTICAL DATA COLLECTION METHODS

Real-size field tests are the major and most reliable method of acoustical data collection in existing mosques or coupled room configurations as long as the measurement set-up and equipment can be fulfilled. A general set-up for measurement of room acoustic parameters necessitates an omni-power sound source for acoustical signal generation, a power amplifier, a microphone for capturing direct and reflected sound energy -that can be incorporated into a hand held analyzer- and a software for both generating noise/source signal and post processing of the measured impulse response data. A wise selection of sound and receiver locations are upmost factor in acoustical coupling investigations as it is a location sensitive phenomenon. On the other hand, classical room acoustic parameter measurements for spaces such as mosques, are already defined in standards as ISO 3382-1 (2009).

There are some other techniques for acoustical data collection, specifically for spaces in project design phases or for virtual spaces. Early twentieth century acousticians built physical scale models to test acoustical design ideas (Long, 2006). This method was especially helpful when the hall is in design phase and for the time there is no other way of experimenting virtual spaces. The measurement system is similar to that of field tests yet the microphones and sound generators vary in scale in accordance with the scale of the model. For such models, ways of approximating air absorption

are searched, and nitrogen gas is found to be the most appropriate medium to be used in replacement of air. In coupled systems, scale modelling is still an important method of experimentation (Sü Gül, 2006) and considering reliability of the data stands in between real-size acoustical measurements and acoustical simulations.

Technological developments provide new opportunities for acoustical design. The modelling by ray tracing has undergone rapid development in the last thirty years through the work of computer graphics programmers (Long, 2006). The acoustical assessment of a space in the design phase through scale models that are time consuming and unpractical in the past, now is possible to be held by computer simulation within hours instead of weeks or months.

Academic researches on mosque acoustics are mostly on existing mosques or renovation of mosques, that use computer simulation in order to provide a comparison ground for the following field tests. Besides, computer simulations are practical ways to study design parameters of mosques in virtual cases. Computer simulation has mostly proven to be a viable tool in performance buildings such as concert halls, opera houses, and multi- purpose auditoria (Schmidt and Kirkegaard, 2004). Recently the geometrical room acoustics studies are also focused for providing mathematical sub-codes for hybrid-model based simulation software that work most appropriate with acoustically coupled systems.

A very recent method in room acoustics predictions is the application of Diffusion Equation Model (DEM). The local acoustic energy density in rooms with perfectly diffuse reflecting walls is named to be diffusion model, which is based on the mathematical theory of diffusion to the sound field within an enclosed space (Valeau et. al, 2006). Due to its computational efficiency and provided advantages as of spatial energy density and flow vector analysis, DEM is a viable tool in scientific investigations of sound fields of complex architectural spaces as of multiple-domed superstructures as well as acoustically coupled spaces. Within the context of this

research; field tests, ray and image tracing based simulations and DEM applications are utilized altogether for collection and analysis of data as detailed under Methodology section.

2.3. REVIEW OF MOSQUE ACOUSTICS

Evolved to meet Islamic needs, the mosque is an important building type of Muslim architecture. Within the context of architectural acoustics mosques are important subjects and have long been investigated considering speech and speech-music related activity patterns held in such religious spaces. Different worship activities necessitate different acoustical requirements. As in many other religions worshippers sometimes need solitude, while at other times they want to feel in absolute unity with the others presence. Acoustics is one of the basic means of creating different and desirable effects within such religious spaces.

In summary, there are three distinct acoustical requirements for mosques in relation to speech intelligibility as well as the spiritual effects of sound:

- audibility of the *namaz* -prayer orders of the Imam (prayer leader)-,
- recognizable sermon of the preacher,
- listening to or joining in the recital of the musical versions of the Holy Quran

Room acoustics investigations on mosque typology have been started as early as in 1991 (Abdelazeez et al.). Considering the room acoustics as a field of profession, as to be rooted back in 1940s by Beranek, the interest for the acoustical fields of mosques is not that late. It should be noted that apart from acoustics as a profession, there are the great architects in the history who synthesized acoustics within their designs for serving the functions of their edifices such as Sinan the Architect (1490-1588) of grand Ottoman Mosques or Jean Louis Garnier (1825-1898), the designer of the Paris Opera House. Only after the acoustics has been adopted as a field of

expertise in architecture, the literature on both academia and profession have been abruptly accumulated. The pre-acousticians and acoustics researchers' era can be best summarized by Garnier's words as follows:

“I gave myself pains to master this bizarre science of acoustics...nowhere did I find a positive rule to guide me; on the contrary, nothing but contradictory statements... I must explain that I have adopted no principle, that my plan has been based on no theory, and that I leave success or failure to chance alone... like an acrobat who closes his eyes and clings to the ropes of an ascending balloon (Long, 2006).”

The literature on mosque acoustics can be divided into three main categories. First group comprises the assessment or comparison studies, second group is on renovation or acoustic enhancements of existing mosques together with acoustical design of new generation mosques and the final group are the investigations on real or virtual mosques to develop acoustical design criteria for this specific building typology.

2.3.1. ASSESSMENT AND COMPARISON STUDIES OF MOSQUES

Assessment studies include single mosque cases, comparisons of mosques to other mosques and comparisons of mosques to churches. As a single case study, Sultan Hassan Mosque and Madrasa in Cairo are examined by field measurements and room acoustics simulations (El-Khateeb et al., 2007). The semi-open mosque is also a teaching center of Sunni rites so that the speech intelligibility is of great significance. Main *iwān*, sheltered by an enormous pointed vault reaching maximum height of 25 m, creates substantial volume. Originally, walls and vaults are covered with limestone and lower parts are of marble. In recent renovations walls and the vault are covered with cement mortar plaster. Although high RTs and echoes are observed in some specific locations due to vaulted geometry, field measurements in average reveal good STI values indicating that worshipers are able to hear and understand *imam*'s sermon. It is highly probable that the carpet floor finish and open back wall

to the courtyard are basic causes of lower RT values in compare to the mosques with similar volume which in result increases speech intelligibility characteristics of the Mosque.

Another case namely Kocatepe Mosque in Ankara is studied by Sü and Yilmazer (2008). The mosque having the formal language of 16th century mosques, mainly adapts materials and structural system of 20th century technology. The acoustical characteristics of the mosque are analyzed by computer simulation. With a reinforced concrete dome of 25.5 m diameter and an estimated acoustical volume of 68,696 m³, the mosque is in large size category. Marble, gold leaf, stained-glass and decorative tiles are major interior materials together with carpet floor finish. In contrast to what is expected from domed interiors, the focusing has not been observed as a major problem in the case of Kocatepe, due to the height of the dome base and its diameter enabling the focusing zone to lie much above the receiver surface. When all the studied parameters are considered, the results show that Kocatepe Mosque is a good place for reciting the musical version of the Holy Quran, as it creates a ritual and tranquil acoustical atmosphere. However, for the prayer mode, the mosque has inadequate intelligibility of speech by showing a tendency to keep and enhance the low frequency sound within the prayer area. The excessive bass accumulation within the mosque is due to the concrete skeleton that does not allow for the low frequency attenuation. In classical Ottoman period mosques some original interior decoration features such as embedded various sized clay pots within dome surfaces exposed to the interior space are thought to be applied for the control of reverberation tail of low frequency energy content. Use of reinforced concrete technology for dome structure, without application of cavity resonators as in Ottoman period mosques, are accused for the higher levels of reverberation especially in low frequency range in this newly adapted mosque prototype.

Acoustical characteristics of the Central Mosque of Lisbon are searched by in situ measurements by Carvalho and Freitas (2011). Results are compared with present

literature of other mosques and Catholic churches with similar volume. Sound reflective materials such as marble, tiles, bricks and painted plaster are major wall finish materials within the mosque, while floor is covered with carpet. The mosque has a volume of 6,040 m³. The windows with small openings permit the passage of outside noise. The average of measured RT values at mid frequencies is 2.8 s in the main prayer hall, which is higher than the recommended range per volume. Mosque of Lisbon is assessed to present the worst acoustical conditions within other mosques in the world with comparable volume, while found much appropriate for speech in comparison to the Catholic churches considering the analyzed parameters.

An extensive study is held by Abdou (2003a) on 21 representative mosques in Saudi Arabia. Field measurements are taken in mosques with different sizes and architectural features for assessing room acoustic parameters. The aim of that study is to document overall acoustical quality of different prototypes and how significant they deviate from optimal. Most of the mosques have concrete skeletal structures with flat roofs supported by columns on a regular grid. At some cases dome covers the central part of praying area. Interior finish materials for walls are out of plaster, marble tiles, and wainscot up to 1 m above ground. Concrete ceilings are painted with some decorations and floors are of heavy carpet. The average intelligibility for almost all mosques, when the sound reinforcement system (SRS) is not operated, lies in the range of Poor to Fair rating. Operating SRS improves intelligibility ratings especially at remote locations and provides a better distribution of STI. The results indicate that mosques are characterized by long sound decay at low frequencies. Almost all mosques have RT values greater than 1.0 s at mid frequencies, which is proposed to be the optimal upper limit for speech intelligibility in unoccupied condition. Considering all parameters author concludes that acoustical quality in the investigated mosques deviates from optimum conditions when unoccupied, while being closer to limit parameter values when fully occupied, except for the mosque with a volume greater than 10,000 m³.

Acoustical properties of Süleymaniye (completed in 1557), Rüstem Paşa (completed in 1561), Mihrimah Sultan (completed in 1560) and Cenabi Ahmet Paşa (completed in 1566) Mosques in Turkey are compared in the study of Topaktaş (2001; 2003). Computer simulations and interior field measurements are utilized in the analysis of energy decay curves. Mosque volumes range from 2,900 m³ to 85,300 m³. Diameters of the domes are in range between 14 m to 27 m. Simulation and field measurement results are found consistent. According to that, as volume per functional area increases, RT increases. C80 values are inversely proportional to volume per functional area, while D50 values are constant. Increasing values of RT corresponds to the decreasing values of clarity index. None of the mosques are appropriate for natural speech. Highest value of RT and lowest C80 is observed in Süleymaniye as it occupies the largest volume. Besides, in this mosque non-exponential decay is visually observed indicating probable acoustical coupling effect (Figure 1.1).

As part of the EU project CAHRISMA (Conservation of the Acoustical Heritage by the Revival and Identification of the Sinan's Mosques Acoustics) Weitze et al. (2002a) compare in-situ recordings and auralizations obtained from simulations carried out for Sokullu Mosque, Süleymaniye Mosque and Saint Irene Church. Monaural and binaural room impulse responses (BRIR) convolved with anechoic recordings are compared with simulated auralizations. According to field tests, T30 at 1000 Hz is 2.8 s for Sokullu, 4.2 s for Saint Irene and 5.9 s for Süleymaniye. Comparisons indicate that the signal from the auralization has a bit higher clarity than in-situ recording. Recorded BRIR signals have less high frequency energy due to the imperfections in the used loudspeakers having a frequency spectrum cut off at those frequencies. For the monaural in-situ recordings the 3D experience is lost, while there is still a good resemblance with auralizations for the perceived reverberation. This study emphasizes the possibility of creating realistic 3D acoustical environment of virtual spaces.

Within the same EU project context, authors (Weitze et al., 2002b) investigate the room acoustic differences of Hagia Sophia in three different time periods by generating different computer models with particular furnishings as reported in the historical archives. The main acoustic difference is the floor finish in the sense that the mosque scheme has floor with carpet, while the church and museum schemes have marble finish floor. T30 for empty mosque and church both peak at 250 Hz with a value of 8.9 s in mosque and 11.2 s in church scheme. Present museum configuration is very similar to mosque with the lack of altar and such Christian elements, but no carpet floor finish. T30 peaks at 500 Hz with a value of 10.6 s in the present museum state. All configurations have their lowest value around 2 s at 8 kHz. T30 values for low frequencies do not differ much between different configurations for both empty and occupied spaces. This is most probably owing to the fact that carpet floor finish does not present much different sound absorption performance in low frequencies when compared to marble. Empty rooms have the lowest C80 values and the parameter decreases with increasing distance to the source. When there is no direct sight to the sound source due to obstruction by walls or columns, C80 values are even lower. Large distances, due to the room dimensions and geometry, together with excessive reverberation and obstructed receiver locations are the major causes of uneven sound field.

The final review out of CAHRISMA project is Fausti et al. (2003)'s acoustical characteristics comparison of mosques including Süleymaniye, Selimiye, Sokullu to the Byzantine churches including St. Irene, St. Sofia, St. Sergius and St. Bacchus by field measurements. Results indicate that there is a strong correlation between RT and increase in volume of the enclosure, while the behavior of mosques and the byzantine churches are different when the volume is very large, particularly in mid frequencies. Sound levels in both types of religious/sacred spaces have a trend to decrease by the increase in volume. It can be stated that sound levels inside the Byzantine churches are higher than that in the mosques with a comparable volume. The acoustic field of Byzantine churches is extremely reverberant and reaching to the

upper limit of acceptability for typical liturgical music played with an organ. Authors state that in the unoccupied rooms RT values are very high depicting the room with a feeling of majesty. Both types of spaces are poorly suitable for musical performances or speech communication due to the excessive reverberation. Shorter reverberation times above 2 kHz improve speech communication inside the mosques, by additional sound absorption in the higher frequency range due to the carpet floor finish. Both in mosques and churches the positions close to the sound source are better in terms of intelligibility.

In Carvalho and Monteiro's study (2009) in order to characterize Catholic churches and mosques regarding to their main acoustical and architectural features 21 mosques in Saudi Arabia and 41 Roman Catholic churches in Portugal are assessed. The acoustic data and architectural information on churches and mosques are based on previous work and available literature. In mosques, major objective is defined to be intelligibility of speech. In Catholic churches, where music related activities as organ playing, choirs, congregation singing etc. take place, the sense of the musical environment should be supported by the reverberance of interior. The analyses indicate that RT average values increase with increasing size of architectural parameters. This is more radical in churches than in mosques. In both churches and mosques there is a decrease of C80 values with the increase of any of the architectural parameters. The majority of churches show Poor intelligibility rating, while the majority of mosques are classified as Fair. Lower RTs are due to the higher absorption within mosque interior that is highly associated with carpet floor finish. On the other hand, -according to the authors- larger RT average values in churches can be justified by their different acoustic objectives. Using sound reinforcement systems for improving acoustical parameter values are much satisfactory in mosques than in churches, however these devices in general are used for minor improvements in the acoustic outcome and do not provide a significant final solution in the acoustic performance of structures. All findings support the idea that *good architecture and design of a worship place are the key elements in their future acoustic performance.*

2.3.2. ACOUSTICAL RENOVATIONS AND ACOUSTICAL DESIGN OF MOSQUES

One of the first acoustical mosque renovation study is Abdelazeez et al.'s (1991) investigations on the acoustical properties of King Abdullah Mosque in the city of Amman in Jordan. Having a volume of 34,000 m³ the Mosque is a large structure with octagon plan layout. The hemispherical dome has a diameter about 38 m. Concrete and marble are main finish materials of interior wall surfaces together with the carpet floor surface. 20 s average of RT in mid-frequencies indicates excessive reverberance within the Mosque in its existing condition. The ambient noise level of 58 dBA, points out poor sound insulation characteristics due to eighty windows at the neck of the dome and on courtyard walls. Both excessive RT and high ambient noise results in poor intelligibility within the mosque in its original scheme. The first acoustical intervention proposed by authors is constructing an absorbent dome - perforated plywood with mineral wool backing- suspended underneath the original one. Following to that, vertical walls decorated with *mushrabiah* above are also backed by mineral wool and air gap behind. For minimizing outside noise the system of double glazing is applied for windows, and solid wooden doors are replaced with existing acoustically weak doors. After solving the main acoustical absorption problems electro-acoustic sound system is utilized for establishing uniform loudness distribution with reasonable sound levels throughout the mosque. Measurements after the application yields Good to Excellent STI values and RT is reduced from more than 18 s to less than 2 s at 1000 Hz.

In Hamadah and Hamouda's study (1998) acoustics of main prayer hall (MPH) of Kuwait State Mosque is discussed. The inner surfaces of the dome in its present form are lined with ceramic tiles. All the walls and pillars are covered by marble tiles. The floor is covered with 2 cm thick carpet. The measurements of the original setup of public announce system reveal Bad to Poor speech articulation over almost all area of the MPH. Poor speech intelligibility within the space is aimed to be treated with totally electronic approach rather than modifications on interior finish materials. A

modification to the original layout is made by grouping the fifty loudspeaker columns into four clusters and placing them equally on the right and left side of the *imam's* position at the front end of the MPH. Following to that the distance between microphones' locations and the new sound mixer are minimized by transferring the sound control room from the roof of the MPH to a control room at the corner of the MPH. Moreover, loudspeakers are installed within the chandeliers distributed all over the MPH and each loudspeaker is directed towards the carpet in order to avoid marble reflections. Field measurements taken after the electro-acoustic interventions reveal that an improvement in the MPH is achieved by enhancing intelligibility ratings from Fair to Good ratings.

An extensive research is held in transformation of Cordoba Mosque into a semi-Christian worship building (Su'arez et al., 2004). To open up longitudinal naves within the Islamic space, part of the Islamic aisles are eliminated and elevated for creating a chapel and a cathedral transept. Initial renovations without acoustical considerations end up with poor intelligibility indices. Architectural features have to be revised in accordance with redefined acoustical requirements. As a first acoustical intervention, a wooden platform acting as a stage is set to elevate the source plane, for both improving visibility from the nave and preventing direct sound being blocked by the spectators. Lateral glass panels are introduced in the neighborhood of platform for improving early reflections and direct sound in providing better clarity and intelligibility. Gothic space is separated from Islamic aisles by side curtains. These elements help the control of reverberation tail by high absorption coefficient values at high frequencies. Due to the air chamber behind the curtains, they also support the increase in absorption of low frequency sound. At the back of the nave, perforated wooden panel surfaces are applied to shut the nave off spatially and prevent access of sound entry from rear zones. Thin strips over the wooden panels are used to enhance diffusion and prevent possible strong reflections from back wall. After the acoustical interventions, intelligibility ratings are improved from Poor to

Fair rating. The resultant acoustical field is proper as a musical venue but intermediate for speech based activities.

In Su'arez et al.'s (2004) study specific factors as of the position of coupled space (Islamic aisles) in relation to the source or the direction from which sound penetrates to the coupled space, the volume ratios of main space (Christian transept) and the sound absorption characteristics of coupled spaces are found correlated with the effective absorption of coupling areas. Coupled Islamic aisles have RT averages greater than 2.5 s at mid frequencies. With acoustical interventions, cathedral is isolated from adjacent reverberant spaces only to some extent, as it is observed that the Christian spaces still reverberate with this additional energy flow in renovated state. Authors claim that *public eventually will become accustomed to this different acoustical experience and appreciate spatial quality of the music within cathedrals in compare to a classical concert hall.*

The design of a new-generation mosque namely Doğramacızade Ali Paşa Mosque in Ankara in Turkey is presented by Sü Gül and Çalışkan (2013a). The study aims to emphasize the importance of practicing acoustics of mosques as early as in the concept design stage. The edifice known as the technological mosque of its time and with its eclectic interpretation has a unique architectural style. The mosque has a square plan -22 m x 22 m from the perimeter of interior octagon-. The height of the dome from finish floor is 19.2 m. The upper structure dome is made of stained glass for providing natural light to the prayer zone. The radius of the dome section is 5.6 m, making a diameter of 11.2 m. In acoustical design of the mosque the scale of the glazed dome is intentionally adjusted to maintain certain geometrical limits in order to keep the unwanted reflections away from the receiver/prayer zone. The center of the dome is above the two thirds of the full height, so the possible sound focuses due to dome form falls much above the prayer area.

Apart from the geometrical development of the mosque dome, interior finish materials are studied in Sü Gül and Çalışkan's study (2013a). 10 mm thick, woven wool carpeted floor surface generates the largest absorptive area, which is effective on the absorption over the high end of the frequency range. Mid frequency range is optimized by the partial application (130 m² in total) of perforated wood on inclined *pendentive* surfaces, while the remainder are left as solid wood surface. Perforated wood boards have 200 mm air gap behind filled with 50 kg/m³ mineral wool. The remaining wall areas are of travertine and solid/unperforated wood (out of maple) boards. Stone wall surfaces are sandblasted for increasing the scattering characteristics and providing even distribution of sound.

In Sü Gül and Çalışkan (2013a)'s study computer simulation is applied as an acoustical design tool. Results are justified with real size field measurements inside the mosque and related objective acoustical parameters including reverberation time (RT or T30), clarity (C50 or C80), speech transmission index (STI) and A-weighted sound levels (SPL-A) are assessed. Average mid frequency T30 for unoccupied mosque with acoustical treatment on *pendentive* surfaces is 1.94 s and average low frequency T30 is 2.07 s. Average mid frequency T30 for occupied mosque is 1.34 s and average low frequency T30 is 1.86 s. Although speech is the leading activity in a mosque, the low frequency ratio and in relation the spiritual context of the male voice *-imam-* proves to be rather different than the ordinary speech. For that reason, it is advisable for a mosque to have a Bass Ratio (BR) that is closer to optima for music. In the case of Doğramacızade Ali Paşa Mosque, BR is 1.06 for unoccupied mosque and 1.38 for occupied mosque. Worshippers' corporeal presence attribute to further absorption in mid to high end frequency range of the occupied mosque space, creating a warm acoustical environment. Most of the prayer locations are satisfying Good intelligibility criteria. Within the mosque sound distribution throughout the usable prayer zone/floor is found to be clear of hot and dead spots. Distribution is even and parameter value drops/increases are consistent with the distance from the sound source. Evaluation of the space indicates that the optimized acoustical field is

proper for intended functions of use in a mosque and satisfies desired tranquil environment.

Another contemporary case is Sü Gül and Çalışkan (2013b)'s acoustical design study of the new Turkish Religious Affairs Mosque, further named as Ahmet Hamdi Akseki Mosque. With 5000 prayer capacity and 92,987 m³ volume, it is the largest classical-contemporary mosque project of the past decade built in Ankara, Turkey. Mosque has a neo-classical style with a single sheltering dome supported by 4 arches and *pendentives* as transitional elements. The dome sits on a square plan layout of 33 m x 33 m. Arches carrying the load from dome to ground have a maximum height of 18 m. The height of the dome from floor is 33 m. The mosque is also one of unique examples of its scale for which the room acoustic design is applied in its conceptual project phase. In the acoustical design of Ahmet Hamdi Akseki Mosque, for minimizing acoustical defects caused by domed geometry and large volume the dome is treated by an absorptive surface finishing. The absorption by the dome, composing one of the largest interior surfaces, is not only for reducing the effects of sound focusing but also for dropping the global reverberation times within the main prayer hall.

In Sü Gül and Çalışkan (2013b)'s study, the major intervention to the dome material design is application of perforated gypsum panels with mineral wool backing concealed behind surface carvings/reliefs out of molded gypsum. Attaining both sound absorption and scattering functions to the dome surface, aims to distract acoustical symmetry and consequently to provide much even distribution in interior sound field; that is free of sound foci and echoes. In addition to the absorption attained by the dome, walls are treated with micro-perforated wood panels, and cove ceilings are covered with perforated gypsum boards with mineral wool backing. For increasing diffusion and scattering characteristics in desired frequency ranges, specific surfaces such as stained glasses and marble wall claddings are either sand blasted and/or textured in special carvings. A final acoustical intervention is in

selection of carpet floor finish material, which composes the largest absorptive surface within a mosque prayer hall. Different alternatives are tested by impedance tube method for selecting the one that provides highest acoustical performance.

In Sü Gül and Çalışkan (2013b)'s acoustical design study computer simulations are utilized in assessment of objective acoustical parameters including RT, STI and SPL-A, with and without sound reinforcement systems for fully and partially occupied mosque conditions. Auralizations are held for *imam* and *müezzin* in different forms of religious call out to prayers. Field tests are performed specifically for tuning the installed sound reinforcement system. For fully occupied state of the mosque - indicating the maximum use of capacity in Friday's sermon- T30 average for mid-frequencies (average of 500 Hz and 1 kHz) is 1.97 s. The low frequency (average of 125 Hz and 250 Hz) T30 for the same condition is 2.51 s. STI distribution maps are obtained in operation of electro-acoustic enhancement and for NC-30. The range of STI over prayer zone is in between 0.42-0.70 in overall. The minimum values of STI are observed in side aisles or for spots that have architectural restrictions in the direct sound path, both of which are out of sight of imam situated in front of *mihrab*. For most receiver points STI indicates Good speech intelligibility within the mosque, for fully occupied condition with electro-acoustic enhancement. The mosque satisfies warmth and augmentation of male voice with BR values over 1.25. The balance of sound absorption over frequency ranges are obtained through the use of multiple types of sound absorptive materials applied in sufficient amounts and in proper locations. Considering all studied parameters, it could be stated that Ahmet Hamdi Akseki Mosque is an optimum space for mosque activities.

2.3.3. ACOUSTICAL INVESTIGATIONS ON VIRTUAL MOSQUES AND DESIGN CRITERIA DEVELOPMENT

Studies under this section aim either to propose specific architectural parameters/features that are effective on the acoustics of mosque typology or to specify acoustical parameter limits specifically for mosque function. To begin with,

Prodi and Marsilo (2003) developed a scale model with main features of a typical mosque for flat and domed ceiling alternatives. For different ceiling layouts the volume is kept constant by the use of movable floor plane. The relative importance of the ceiling with respect to the floor in providing sound absorption, reflective floor and absorptive floor alternatives are tested. Results indicate that if the floor is reflective there is an increase in RT for the flat ceiling configuration in compare to domed ceiling alternative for the same volume. The effect is limited by the upper limit of 500 Hz. The difference in RT is insignificant when the floor area is absorptive for both ceiling types. Domed ceiling increases the surface area exposed to the sound and introduces more absorption. For the absorptive or carpet floor finish the absorption caused by the floor masks the effect of the dome. When there is less absorption within the space the impact of the domed ceiling on reverberation time becomes more obvious.

Using computer simulation technique Abdou (2003b) investigates the acoustical impact of mosque forms and/or plan layouts, which are rectangular, trapezoidal, square, hexagon and octagon. The mosque's geometric parameters such as volume, floor area, walls and window areas and geometric ratios are kept constant, while different forms are compared. According to the simulation results trapezoidal and rectangular mosques both show Fair intelligibility on side walls expanding to the Kiblah wall. In the Hexagon mosque Fair intelligibility zones are concentrated in the middle and rear parts of the mosque. Author states that the octagon mosque geometry negatively impacts sound fields in the central zone of the floor area due to the cancellation of sound energy arriving from opposite directions. The octagon mosque has the highest RT values at all octave-band frequencies specifically at low frequencies. Global RT average of the hexagon prototype is the second highest. This is due to the general tendency of round enclosures or cylindrical forms; as reflected sound from boundaries add to the reverberant sound fields. In relation to that the square geometry results in the lowest RT values at mid frequency range. Excellent to Good STI rated zones are larger in the square mosque in compare to the other

geometry, while considering both the uniformity of distributions and intelligibility metrics octagonal mosque can be classified as worst among other basic mosque forms.

In search of dome effects on acoustics of mosques various domed ceiling configurations are studied by Utami (2005) by scale model and computer simulation techniques. Spherical and alternative onion shaped domes are combined with three different base structures providing six different principal models for the comparison study. Another evaluation is made in between the plaster painted concrete dome and a dome with highly absorptive ceiling finish material, namely BASWAphon. Results indicate that sound absorptive dome treatment significantly changes the intelligibility parameters. Different shaped domes and ring structure configurations beneath the domes do not create significant differences in the speech quality. This is partly due to the small geometrical proportion of the dome relative to the larger coupled rectangular room below it in studied case. Moreover, the base of the dome is high enough that the focusing occurs at points higher than the heights of the prayers seated or standing positions. This research is limited to a certain amount of dome and base configurations, while source is located only in front of the *mihrab* wall as in practical uses. According to the author this study should be extended with a wider range of dome sizes and shape configurations and by *alternative source positions especially one underneath the dome for enhanced analysis of dome and coupling effects*.

According to Orfali (2007) in assessing mosque acoustics specially developed parameters and limit values should be applied. Different than classical speech or music related halls, worship spaces serve for divine feelings. In a mosque, too high of a reverberation time distracts intelligibility while too low of it generates a dead space which is not appropriate for spiritual ceremonies. The attention of the worshiper should be taken with a live acoustic environment while keeping the intelligibility at maximum. Within this perspective author introduces newly defined

acoustical parameter values applicable for mosques for given volumes and introduce acoustical treatment recommendations for closed and open courtyard mosque typologies. Author redefines RT, STI and C50 limits with some correction factors in estimating volume dependent ranges for mosque acoustic parameters. As a result of this study authors present optimum ranges of RT over volume for mosque function (Figure 2.3). Other parameters are recalculated as a function of distance ratio (reverberation radius per critical distance) for different reverberation time values.

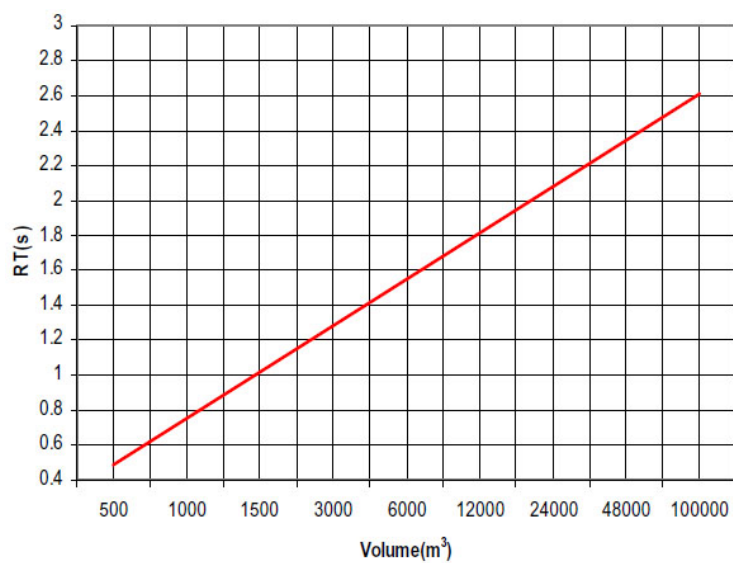


Figure 2.3. Recommended RT for different mosque volumes (Source: Orfali, 2007: 4)

Regarding to design issues, initially roof columns should be eliminated for minimizing acoustical shadows within prayer floor. If compulsory, larger columns should be subdivided into smaller ones to let the sound penetrate through them. Circular columns should be preferred instead of square ones. Domes are better than flat ceilings in terms of reducing shadow zones, however this time sound focusing is critical. In that case the ratio of speaker's height to the dome center over the dome radius should be more than 1.1 to prevent focusing at the height of listening plane of the worshippers. Concave surfaces must be avoided especially at the back wall and convex surfaces should be preferred on parallel walls to diminish the possibility of flutter echoes. Ornaments can be applied on parallel walls to scatter the sound waves.

The women's *mahfili* should be within the main structure rather than being a separate room with multiple columns joining surface. It is highly recommended to isolate the air conditioning units and locate them in a separate technical room for minimizing background noise levels. In closed structure mosques carpet covers large portion of the total surface area of a mosque. A minor change in its absorption behavior makes a considerable difference in reducing the total reverberation time. This can be done in various ways such as by increasing the thickness of the carpet or introducing an additional absorbing pad under the carpet to increase its absorbing behavior at low frequencies. In open courtyard models care should be taken to prevent the late arriving sound radiated from minaret (Orfali, 2007).

2.3.4. CONCLUDING REMARKS ON MOSQUE ACOUSTICS

All above cases on mosque acoustics reveal some common architectural features and corresponding acoustical outcomes. Mosques have all hard and reflective interior finishes including stone or plastered brick, ceramic tile, glass, wood, except for the carpet floor finish together with frequent use of prayer mats and rugs. In other words, most of traditional mosques in their current states are highly reverberant. Except for the use of voice in singing and chanting to emphasize the text's meaning, musical instruments are not employed in mosques. For that reason, speech and its intelligibility are the major acoustical considerations in the mosque design (Kleiner et al. 2010). On the other hand, in acoustical design of mosques the desired acoustical criteria must be incorporated with expected formal language which satisfies the spiritual aspects of worship.

According to previous research the expected acoustical qualities from a mosque can be summarized as follows:

- lower but controlled RTs for mid and high frequencies in compare to low frequencies for intelligibility of sermons
- higher but controlled RTs for low frequencies in compare to mid and high frequencies for enhancing the spiritual aspects of musical rites

- balanced sound absorption of interior surface materials over frequency range
- sufficient sound strength/level or loudness in prayer positions
- even sound distribution among prayer positions
- minimal acoustical defects such as sound glare, echoes and dead spots
- low background noise that does not mask speech intelligibility

It is known that very high RTs negatively affect speech intelligibility, while very short RTs cause a dead acoustical environment that would reduce the envelopment and spaciousness expected from a mosque. The basic challenge of mosque acoustics design is optimizing reverberance versus intelligibility. According to the very basic Sabine equation RT is proportional to volume and inversely proportional to the sound absorption area. The volume is dependent upon the prayer capacity, and typically cannot be revised in the acoustical design phase. RT is also a frequency dependent parameter, which means the selection of materials and their overall frequency response is highly influential on the acoustical characteristics of a mosque. In mosques the sound absorption is mostly provided by carpets which are effective sound absorbers in mid to high frequency range. On the other hand the presence of prayers also augment sound scattering and absorption.

As a function of acoustics in order to overcome the large sound attenuation of his voice over the rows of worshippers on the floor, *imam* delivers his sermon at *minbar* and *müezzin* delivers the commands of *namaz* from *müezzin's mahfili*. This scheme is specifically developed in the time of historical mosques when there were no sound reinforcement systems. It is a positive effect that the sound source is above the receiver locations for providing more sound strength to the audience, however if the space is highly reverberant than it means the problem is not totally solved. In that case, most of the sound from the *imam* at the top of the *minbar* feeds energy into the reverberant sound field. The worshippers are listening more to reverberation than to direct sound and leading to poor speech intelligibility. Speech intelligibility in a

mosque is hampered by reverberation and by echoes due to large sizes of traditional mosques.

To improve speech intelligibility, the reverberant sound can be reduced relative to the useful direct sound and possible early reflections either by using an appropriate reflector behind the imam, which is architecturally not common in the history of mosques, by using sound absorptive materials in proper locations to control RT and/or by applying a properly designed sound reinforcement system in new-generation mosques. Due to the sound absorption by the worshippers' clothing and the carpet surface, sound that reaches to the floor area is absorbed and is not reflected or scattered back to generate reverberation. For that reason, during the installation of any loudspeaker system in a mosque, it is important to take into account the time delays between the direct sound and the amplified sound from the speakers. *Imam's* voice should appear to come from the *imam* rather than the closest loudspeaker.

Echoes are foremost problems for *imam* (reciter) in mosques because the presence of echoes makes it more difficult to speak. For controlling acoustical defects as echoes and strong sound reflections in mosque design it is also important to consider the sound scattering/diffusion characteristics of interior surfaces in addition to their sound absorption capacities. Surfaces' form, geometry and/or dimensions are basic factors for sound scattering, and can be highly effective for providing homogenous sound diffusion within a space if properly designed. Even distribution of sound means an acoustical field clear of echoes, acoustical glares, late reflections, secondary source formations and dead spots.

The negative effect of domed mosque typology is proved in previous literature. The concave dome geometry is the primary reason for sound focusing and all relevant acoustical defects as of echoes, while causing dead spots in specific spots within the space so an uneven sound distribution. The inverse effect of dome is critical mostly when the center of the dome is at receiver/listener's ear height. For that reason

special effort is spend upon raising the focal zone of the dome to much above the prayer zone in mosques acoustical design studies. Another interesting finding is that when the floor finish is reflective, as in stone cladded Christian churches, dome represents a higher absorption in compare to a flat ceiling, specifically at low frequency band. However, this reduction is not obvious in carpet floor finished mosques, as the sound absorption performance of the carpet already dominates the flat or domed ceiling effect. In mosques together with the dome, the parallel reflective walls can also be an important factor for strong late sound reflections or even flutter echoes. For that reason, it is essential that surfaces to have some irregularities/ornamentations, inclinations and/or architectural volume fragmentations to distract the reflection patterns in between parallel walls.

One other parameter that affects speech intelligibility together with RT is the background noise. Background noise can be due to the environmental noise (traffic, industrial or human induced) that reaches to the interior through the exterior walls, glazing systems, doors, and upper shell structure or can already exist within the prayer zone due to the HVAC or other mechanical equipment. At this point increasing the sound insulation and isolation characteristics of exterior shell layers by a proper design of system and connection/point details of different architectural elements are fundamental. On the other hand, all mechanical equipment should be distantly located from the main prayer zone, or otherwise necessary precautions should be taken for minimizing the induction of airborne and structure borne mechanical noise. International standards on HVAC or background noise limits declare a maximum of 25-30 dBA or NC15-20 for noise sensitive spaces as of speech or music venues, which also applies for religious buildings (ASHRAE, 2013).

In reviewed literature most of the edifices have enclosures with poor sound insulation characteristics and located in a noisy city environment. Therefore all are suffering from noise intrusion which reduces the signal to noise ratio even more and worsens intelligibility. Intruding exterior noise due to low transmission loss of

exterior wall systems, glazing systems and doors commonly installed is a major sound insulation problem. For new generation mosques operating fans indicate very high background noise levels that cause interference with speech communication. Considering the conditions of historical mosques back then, less environmental noise as traffic and the absence of electro-mechanic systems depict the applied details to function their times.

Literature on the topic reveals the increasing interest on the worship space acoustics. Most of the current studies focus on the analysis of existing mosques using scale model and computer simulation techniques and/or site measurements. Some incorporate acoustical renovation studies for enhancing the acoustical qualities of pre-designed and built mosques' interior environment, while very few cases present cooperative, ground-up acoustical-architectural design. The sound field analysis is basically on the conformity of mosque function. Some studies recommend architectural modifications on geometry and materials in contrast to traditionally accepted. Almost none searches the sound field with a different perspective rather than the function of use, as can be expectable. In this research study for a deeper scientific understanding, the acoustics of mosques with their pre-well defined forms are aimed to be analyzed in relation to acoustical coupling. The focus is on the sound wave or energy density interactions due to the dominant architectural features as of domed geometries coupled to a rectangular or a square base, and distinctly separated absorptive (floor surfaces) versus reflective (upper shell and wall surfaces) zones of the familiar mosque typology.

2.4. REVIEW OF COUPLED SPACES

Theory on acoustical coupling has its roots back in 1931s (Eyring). In 2000s the investigations on the topic are sharply accelerated as specific features of acoustical coupling are adapted to be used as a design aid. Architectural acousticians have been increasingly interested in halls that incorporate coupled-volume systems because of

their potential for creating non-exponential sound energy decay. A coupled volume system is typically defined as two or more spaces that are joined by a common acoustically transparent surface, known as a coupling aperture. Or as Cremer and Müller (1978) define; coupled spaces are systems sharing a single air volume but subdivided architecturally into a number of smaller subspaces (Figure 2.4).

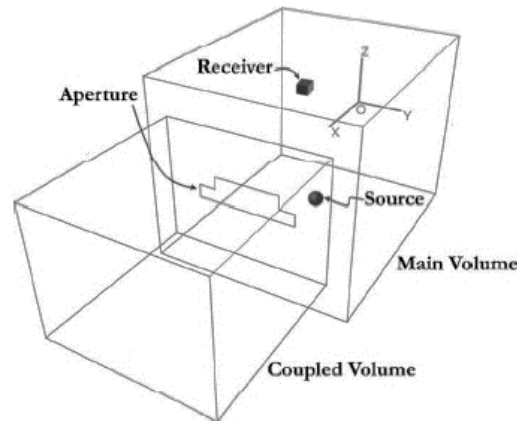


Figure 2.4. A typical coupled volume system (Source: anonymous)

In a coupled volume system, if the times required for sound decay in each space are unequal, there is an excess energy in one of the spaces during the decay process when compared to the other one. This leads to energy transfer from the energy surplus room to the energy deficient room, which can produce a sound decay proper for desired acoustic qualities within a space. Designers are attracted by the coupled volume concept, because it proposes a compromise between the competing acoustic conditions for both reverberance and clarity. Coupled room/volume concept also enables modification of sound field, in other words variable acoustics, in spaces that incorporate both music and speech related activities as of multi-function halls (Sü Gül and Çalışkan, 2010).

Coupled volumes can be regarded as design tools with different architectural and acoustical variables including geometric volume, form, materiality, coupling aperture size and shape, frequency and natural reverberation times of coupled rooms that is

dependent on the volume and absorption characteristics of each room. Location sensitivity is another physical parameter for coupling phenomenon occurrence. These variables are affecting the complex sound decay behavior of coupled volumes and necessitate an extensive analytical and experimental research.

There are mainly two types of acoustical coupling which are source-area coupling (stage house coupling) and distributed coupling (reverberation chambers) in a classical concert hall design case. In source-area coupling source is in the auxiliary room and auxiliary room is the stage tower above. Distributed coupling employs the volumes above ceiling or side walls and source is away from the room as it is on the stage. In this case, reverberation chambers envelope the side and back walls of the main hall or sometimes ceilings and provides energy feedback to the main hall when the coupling doors /apertures are open in desired ratios (Figure 2.5).

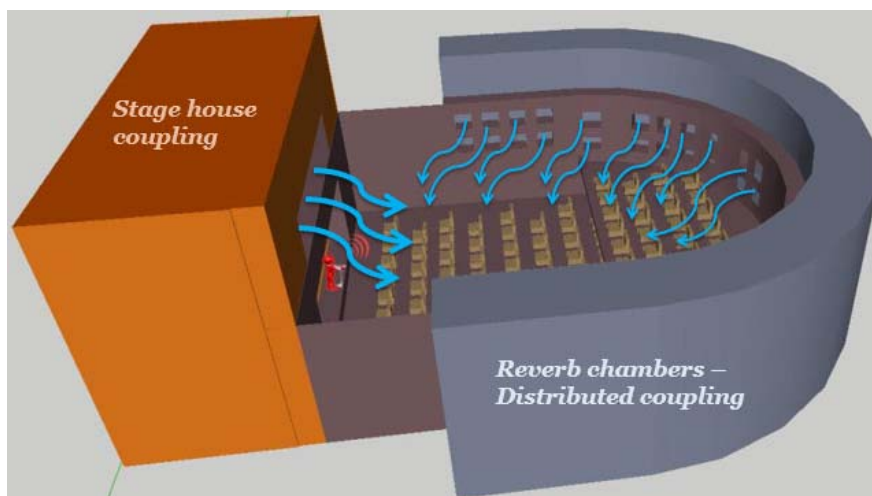


Figure 2.5. A schematic drawing for stage house and distributed coupling (Source: produced by the author)

Studies on the theory, rather than the applications of acoustical coupling on real cases, comprise the major academic research background on this specific field of interest. As it is paramount to understand the science behind coupled spaces or coupling outcomes in real architectural environments, in this section the theoretical

studies are reviewed and grouped under main headings namely geometrical room acoustics, statistical methods, diffusion equation model and wave theory. All cases depend upon data analysis collected by field tests, scale modelling or computer simulations. Decay parameter estimations aim to identify coupling quantifiers through different mathematical methods. Some authors have analyzed real cases of concert halls and churches, but none searched the concept over mosques or multi-domed single space superstructures. Typical acoustical parameters as decay rate/reverberation time, early decay time, clarity and sound pressure levels are investigated. Architectural parameters such as absorption ratio of materials, volume ratio of sub-rooms, aperture size and partition properties, source and receiver locations occupy the basic variables in effect of acoustical coupling.

2.4.1. GEOMETRICAL ROOM ACOUSTICS

In geometrical room acoustics (GA) the laws of sound propagation are studied on the basis of the concept of sound rays, which may be regarded as lines along which acoustic energy is propagated. If the dimensions of a room are large compared to the wavelength, then sound waves may be considered in much the same way as light rays are treated in optics. In a geometrical acoustics calculation the sound energy is assumed to travel from the source to the receiver like a beam or ray of light. Reflections from each surface are taken to be specular. The rays have the simplest form in a homogeneous medium in which they are straight lines (Long, 2006). The sound field to be analyzed in geometrical acoustics models (GA) is mostly restricted to frequencies of 500 Hz and above.

In one of the earliest studies of geometrical acoustics with a focus on acoustical coupling Nijs et al. (2002) investigate some problems related to the application of absorbing surfaces in coupled rooms, especially when they are modelled in a ray-tracing program. The accepted Sabine's and Eyring's laws for calculating reverberation times are for diffuse fields, where all directions have equal strength. When only the ceiling or the floor are highly absorbing, *the sound field splits up into*

a vertical field which decays very rapidly and a horizontal field where decay is very slow. Absorptive surface locations and attaining right values of absorption in a ray tracing software are highly important in the case of coupled spaces where the sound field is mostly not uniform.

Using scale model and computer model techniques, coupled rooms of the same geometry are tested for the accuracy of input parameters as absorption, reflection and diffusion coefficients. According to the results of scale model and computer models, big differences are observed due to the positioning of absorbing materials along the walls. One of main conditions to improve the accuracy of the results in a ray tracing simulation of coupled spaces is a proper modelling of wall reflections; as in a coupled system rays have preferential angles. Diffusion in computer modelling represents non-flat surfaces. In many acoustical model calculations in practice, diffusion is used to smooth fluctuating histograms. Values higher than 2% are not recommended in ray tracing programs as a diffusion factor for flat surfaces. Moreover, if absorption coefficients are to be used from measurements in a reverberation chamber, a correction has to be made as the chamber overestimates absorption. A 20% reduction is recommended over the results from the reverberation chamber as an input into a ray-tracing program for coupled space simulations (Nijs et al., 2002).

In Summers et al.'s (2004) research, the modelling techniques of statistical and geometrical acoustics are applied to systems of coupled rooms. The reverberant field in a system of coupled rooms is not well described by statistical models that have been developed for single-volume/exponential decay enclosures. Statistical acoustics (SA) models of coupled rooms are most accurate when applied to systems that are not strongly coupled, so resulting in an exponential decay. In Summers et al.'s study for a system of N coupled rooms; the reverberant field decay is defined as the linear combination of N exponential decays. Unlike prior models, the improved model by authors treat multiple sources distributed throughout the sub-rooms/coupled rooms or

sources that simultaneously radiate into more than one sub-room. It accounts for the nondiffuse transfer of energy due to radiation of the source into adjacent sub-rooms and radiation from apertures into adjacent apertures. SA and GA are compared for each studied room under a series of different conditions of the room surfaces by simulation technique. A simplified representation of a concert hall with an auxiliary coupled room is constructed by positioning the auxiliary volume, along the short side of the audience chamber. When loosely coupled, such a system displays strongly nonlinear decay curves typically associated with coupled rooms. Sabine and Eyring decay models used in the improved SA model under predict or over predict the decay rates, respectively. Improved model incorporates more accurate decay models as it accounts for the nondiffuse transfer of energy in between rooms and is less likely to overestimation than the prior SA models.

The first assumption of the statistical model, that there is an abrupt transition at the coupling aperture between unique diffuse sound fields, is found not to be quite accurate. Sound radiates from the coupling aperture with energy density that is distinct from the energy density of the reverberant field of the room into which it radiates. Therefore, it behaves, initially as a direct sound component. Only after undergoing reflection, it is the part of the reverberant field. Even in rooms/sub-rooms that do not contain a source, the aperture itself acts as a source, resulting in a spatial variation in the acoustical field. Results indicate that high levels of coupling cause large deviations between statistical predictions and computational values. Just in the case that all assumptions for single rooms, such as if a diffuse sound field with even distribution of absorption can be provided in the coupled system, then the theoretical and computational methods have stated to agree (Summers et al., 2004).

Bradley and Wang (2005) search for specific architectural parameters and their effects on non-exponential energy decay using simulation technique. Ways of quantifying the strength of non-exponential energy decay are investigated. Subjective relations of objective parameters are analyzed through psychoacoustic testing. Two

double slope effect quantifiers are defined. First is named to be decay ratio which is; Decay 2 ($T_{60,2}$, shallow late decay) / Decay 1 ($T_{60,1}$ steep early decay). Second parameter is named to be ΔdB that is the difference between the y intercepts of each of the two slopes. Architectural variables namely the volume ratio between coupled subspaces, the absorption ratio between the two spaces, and the aperture size are studied by modifying these variables through the use of computer simulation. Examining the existing halls three most common volume ratios are used, which are 20%, 35%, and 50%. The second parameter is the absorption ratio, which is the equivalent absorption area in the coupled volume as a percentage of the equivalent absorption area in the main volume. The final parameter is the aperture opening size that is the surface area of the opening between the main and coupled volumes, given as a percentage of the available aperture area.

According to the authors, defined coupling parameter results indicate that smaller volume ratio does not produce double slope effect. A non-exponential decay curve is observed at lower and higher aperture sizes, but there is no consistent fashion across the cases. Both decay ratio and ΔdB values peak at 10%–20% of the available aperture area for each absorption ratio. Results for largest volume ratio in all combinations of aperture size and absorption ratio depict some degree of non-exponential decay. Decay ratio and ΔdB do not show similar trend for all configurations, *which makes one to question the reliability of quantifiers*. Subjective testing -data from simulations- indicates that listeners generally perceive a higher reverberation as volume and aperture sizes are increased independently. *EDT increases as volume and aperture size are increased, which is another reason for the subjective perception of high reverberance*. There are no significant effects of architectural variables on perceived clarity. The simplified acoustical model geometry, which is lack of early reflections due to less diffuseness and density of the reflection diagram, is accused for the insignificant perceptual change in clarity across configurations.

In another study Ermann and Johnson (2005) investigate the thresholds of aperture openness between main space and coupled subspace for creating so called double-sloped decay acoustic conditions on a concert hall case. Another parameter that is searched in depth is the quantity of sound absorption present in the coupled volume and its effect on acoustic coupling. Double decay effect is studied to be a design tool instead of a phenomenon only. Coupling constant is defined as the ratio of T60 to T15 for evaluating the strength of acoustic coupling. Percentage of aperture indicates the portion of the available aperture that is exposed to the coupled volume. Results indicate that, coupling constant peaks at 4% of aperture size and drops rapidly as the aperture is opened further. It is claimed that to observe double decay the coupled room should be of hard, heavy, smooth and reflective surfaces. *Coupled volume should be at least five times as reverberant as the main hall.* Small variations in either aperture size or coupled volume sound absorption levels produce dramatic changes in the calculated sound decay of a space and accordingly the coupling constant.

In a later study Summers et al. (2005) investigate the weaknesses of existing geometrical acoustics prediction methods in depicting the sound fields of coupled systems. A method is introduced for more accurate and high speed predictions. From two primary methods of computational modelling of sound fields, the image-source model is flawed in all geometries due to the inability to model non-specular reflection, while its computational complexity allows for computing only low order reflections or reflections in simple geometries. Ray tracing method is computationally less demanding, but subject to systematic geometrical errors. Beam tracing is most often applied by tracing only the central axes of the beams, which offers the advantage of decreased computing time. The weakness of this final technique is that it can result in incorrect detections of energy arrivals at receivers in the late part of the decay. In beam tracing a growing detection sphere is susceptible to error in coupled rooms when the detection sphere extends into adjacent sub-rooms and an increasing number of geometrically valid reflections are undetected as time

increases. The error is anticipated in the cases for which the source and receiver are in the less reverberant of two rooms and is most severe for small coupling apertures and for receiver positions near boundaries between sub-rooms.

In Summers et al.'s (2005) newly developed methodology *tail-correction* assumes a quadratic growth rate of reflection density, in a single volume space allowing accurate results. However, the assumption of quadratic growth in reflection density can fail for certain systems of coupled rooms. In systems of coupled rooms reflection density is eventually quadratic in time, but is not described by a single quadratic function through time. A revised beam-axis ray-tracing algorithm is proposed by authors, which avoids possible error mechanisms by switching to ray tracing for the late part of the decay. The new algorithm behaves randomized tail-corrected cone-tracing (RTC) until any one of the expanding detector spheres contacts one of the surface boundaries. After that, rather than applying tail correction, the radius of each detection sphere is held fixed and the detection procedure at each receiver is altered to that of ray tracing. The new algorithm is first implemented as a user-selected option 'late part ray trace' in the CATT-Acoustic software. The revised algorithm uses a conventional ray-tracing algorithm for the late part of the decay, making tail-correction procedures unnecessary as ray tracing inherently compensates for the failure to detect certain paths by detecting geometrically invalid paths and preventing penetration of detector spheres into adjacent sub-rooms. Comparisons of computational geometric acoustics predictions with scale-model measurements indicate that the new algorithm, yields accurate predictions of decay curves in coupled rooms.

Another study based on a hybrid method computer modelling program namely ODEON (v.6.5), Bradley and Wang (2007) examine the accuracy of its use in estimations of sound energy decays of an existing coupled volume space. Tested concert hall is a multi-tiered 2000 seat concert hall in North America of a rounded shoebox shape with main volume of 24,000 m³. The hall is connected to a coupled

volume of 7,000 m³ through 70 concrete doors. Four different variables are investigated which are the height of the acoustical canopy, the aggregate aperture door opening area, the main hall absorption and the coupled space absorption. Seven configurations of these architectural variables are tested representing typical settings in which the hall is used for various performance types, including recital, classical, pop/variety and organ concerts. The comparison of the results indicates that the agreement in between computer simulation results and field measurements are mostly observed at 1 kHz octave band. The reliability of computer modelling is poor for C80 metric at lower frequencies (125-500 Hz) for all configurations and even for the non-coupled volume case. Computer modelling is much reliable for predicting C80 at higher frequency octave bands 1000-4000 Hz. According to the authors the reliability of the ray-tracing model is not a function of coupled volume geometry but rather a function of frequency or wavelength.

The acoustical design of 403 seat Kung Hsueh She (KHS) Concert Hall in Taipei metropolitan area is discussed by Chiang et al. (2009) using computer simulation, scale model and field test techniques. As for complying various scenarios of use including recitals, chamber music, theatre and amplified music, variable acoustics solutions are proposed within which coupled volume system is utilized. The hall has a volume of 3,228 m³. The average shell/canopy leaves a volume of 2,428 m³ for the coupled stage house. The primary volume and the coupled volumes are coupled with apertures at three locations. The first coupling is in between the moveable shell ceiling and a fixed extension of the shell ceiling. Second is in between the extension piece and the hall ceiling and the third one is in between the fixed shell rear wall and the shell side walls. The configuration of the stage with all coupling apertures being sealed are compared to three other configurations, which are the apertures open, with 300 mm gaps between individual shell ceiling pieces and with the shell size enlarged. It is observed that T30 averaged from 250 Hz through 2 kHz has increased by approximately 21% when the apertures are changed from sealed to open status. The 300 mm gaps provide little effect on both T30 and EDT. The double slope

characteristics can visually identified in the 125 Hz band for the configuration with the shell enlarged. In the presence of stage shell, the unoccupied mid frequency T30 varies in the range of 1.2 s to 1.7 s. In brief, coupling the stage space for music programs has provided longer reverberation as required, but double slope effect can only be attained at specific octave bands.

2.4.2. GEOMETRICAL STATISTICAL METHODS

In statistical acoustics (SA) instead of tracing the way of sound energy, statistically important characteristics of particular parts of the field are collected to form the basis for computations. In a room whose dimensions are large enough that there is a sufficient density of modes, the space is described in terms of a statistical model known as a diffuse field. A diffuse field is the one in which there is an equal energy density at all points in the room. That also implies that there is an equal probability that sound will arrive from any direction (Long, 2006).

The earliest study, which is also one of the first published investigations on acoustical coupling, is Eyring's (1931) corrections on statistical RT calculations. Classical RT formulas applied for diffuse fields where absorptive materials are evenly distributed for live (Sabine formula) rooms or dead rooms (Eyring formula) are not suitable for coupled rooms having non-exponential sound decay or even for single rooms with nondiffuse sound fields. Through experimental analysis live and dead rooms are coupled to each other in different configurations for different aperture sizes. According to the author, coupling should be considered for each unit area of open window rather than as a coefficient of absorption. A window which opens into the outdoors or its equivalent (large dead room) cannot be considered under certain conditions to have a coefficient of absorption of unity in calculations of RT. Reflection at the opening when its dimensions are not large as compared with the wavelength of the tone used, and the lack of a diffuse state of the sound waves are main causes of the apparent lowering of the coefficient of absorption attained to the opening. Author developed some correction factors to be applied for RT

calculations in studied dimensions of the aperture, *with a warning that those may not be safe for larger dimensions.*

Cremer and Müller (1978) discuss sound fields with an open coupling area and sound fields for coupling through a partition wall, for extreme cases. A quantifier namely coupling factor ($k=S/A$; S: coupling area, A: equivalent absorption area) is presented, which depends on the geometric conditions as the ratio of the coupling area to the total area of secondary room and the absorption coefficients of all surfaces in that room. If the boundary area covered with absorptive materials in secondary room exceeds the coupling area, the coupling area should be treated as an open window; otherwise secondary room should be treated as part of the primary room. Another discussion is on reverberation. The quantity which characterizes the rate of decay of the sound pressure in decoupled conditions of the rooms is called damping constant. The greater is the difference between damping constant of each room the greater the coupling constant is. If the coupling between rooms is provided by a partition wall or a door, coupling constant becomes too small and so negligible. According to their findings, when the source room is highly damped and the neighboring room is reverberant the longer reverberation of the secondary room can be heard from the source room after the sound level in the source room has decreased sufficiently. When the source room is highly reverberant and the neighboring room is damped, the longer reverberation in the source room predominates and the short decay in the secondary room is not heard.

According to Lyle's (1981) investigation, coupling lengthens the final RT in combined space relative to each space's natural RTs. In reverberation prediction of small coupling gaps the initial decay in the primary volume corresponds to the open window RT. For small coupling area the final slope is the decay rate of the more reverberant partial volume. If coupling coefficient ($\sqrt{Q_1*Q_2}$) is smaller than 0.25, then open window estimation can be used, where $Q_1=S/(S+A_1)$, $Q_2=S/(S+A_2)$, S is coupling gap size and A1, A2 are absorption areas of partial volumes. As the

coupling area increases the open window approximation underestimates the RT. Above maximum coupling gap size system tends to behave like a single volume. Dissimilar absorption coefficients in partial volumes cause the decay to be longer than in a single volume prediction.

A different branch of statistical methods is the statistical energy analysis (SEA), which is the notional division of a complex system into a small number of approximately homogeneous subsystems and the assumption of a diffusive flow of energy between subsystems. Wester and Mace (1998) investigate coupled rectangular room systems in quantifying the strength of acoustic coupling between the rooms. An improvement is made on the statistical energy analysis hypothesis of proportionality between coupling power and the difference in subsystem mean modal energies by the introduction of wave component decomposition. As the coupling strength increases, the directionally non-uniform flow of energy from both rooms and the interference between waves arriving from the two sides of the partition have increasing effect making the simple diffusive model inadequate. Coupling power is defined to be the energy flow from source room to the receiving room. When the coupling between rooms is 'weak', this power is greatest at frequencies for rooms' uncoupled room resonances. 'Weak' coupling is associated with small, heavy partitions and rooms of large equivalent absorption area. When the coupling is 'strong', maximum coupling power occurs close to global resonances which involve the coupled dynamics of both rooms. In strong coupling there is relatively free exchange of energy in between rooms. The energy density in the source room is considerably greater than that in the receiver room. According to the authors, 'strong' coupling is highly associated with the big aperture, light partitions and rooms of unequal absorption area, that involves relatively stronger reflections in the rooms and significant wave interference effects which are not accounted for in traditional theory. In 'very' strong coupling, the room which has the smaller attenuation parameter acts as a store of energy for the system, while the other acts as the primary dissipater of energy within the system.

In Andersons' investigation (2000) the process of sound reverberation in a system of coupled sub volumes is analyzed with a case of large public building namely St Paul's Cathedral. The space is divided into many coupled subspaces by columns and arches enabling a repetitive pattern for the energy balance equations. A numerical model of the space is constructed by dividing the interior space into 70 acoustical subspaces for each of which acoustic energy balance equations are formulated with initial conditions be reduced to the eigenvalue problem. Subspaces are coupled together by the interchange of sound energy. In each room sound field is assumed to be diffuse due to heavy ornamentation within the cathedral and characterized by a different value of the time averaged sound energy density. Impulse responses are obtained for occupied and unoccupied conditions of the Cathedral to verify theoretical model. Results depict the two stage structure of the decay due to the acoustic coupling. The duration of the early part of the sound energy decay, when the decay curve slope is changing in time, is called the equalization time.

According to Andersons' study (2000), for the large interiors considered with a repeatable pattern and with strong coupling between the rooms the rate of sound decay during the late stage is the same for all rooms and does not depend upon the distribution of sound sources. The duration of the early stage of sound decay depends on the distribution of sound sources throughout the space and the ratios of their powers. More uniform distribution of sound sources leads to a shortening of the equalization time. An interesting outcome is that the most governing coupling phenomena is observed for the cases in which *both the sound sources and the equivalent absorption areas of the rooms are asymmetrically distributed in space.*

A multi-volume church interior is investigated for testing acoustical coupling conditions by applying different statistical coupled room models (Sabine, Eyring, statistical energy analysis) by Magrini and Magnani (2005). In the historic center of the city of Genoa the acoustics of three churches, having a longitudinal plan with a nave and two aisles, divided by arches and columns are analyzed. When the field

measurements and models are both studied, it is observed that the absorption coefficient of the main volume plays a significant role in the determination of RT. A good knowledge of the absorption coefficient of the cavity or coupled subspace is equally important. The surface of the walls facing the coupled space has a significant influence on the spatial variation of the RT. For a given surface area and a given volume of the church, the mean value of the RT is not affected by the wideness of the connecting opening.

For cavities with large volume compared to the main volume, and wide internal surfaces compared to the ones of the main space, the opening seems to work more as a reflecting, than as an absorbing surface. It should also be noted that the coupling of rooms mainly influences the sound decay during the early stage of the process. This initial duration depends on the distribution of sound sources throughout the space and the ratios of their powers. An optimal distribution of sound sources leads to a minimization of the coupling effect. The most strong coupling phenomenon are observed for the cases in which both the sound sources and the absorption areas within the rooms are *asymmetrically distributed*, supporting Anderson and Anderson's study (2000).

By Chu and Mak (2009) two existing theoretical models (Barron's model and classical coupled-room model based on statistical energy analysis) are discussed to be used for energy decay analysis of different room systems. The classical model for coupled rooms is revised to derive a more accurate model for predicting the early sound energy decay performance with concentration on two churches in Hong Kong as case studies. The new model is named as delayed coupled-room model and its validity is tested by comparison with measurements. In the newly developed model it is assumed that diffuse sound fields in each of the subspaces do not become established instantaneously but only after a specific time delay following the production of sound. The new model takes into account that inner surfaces of church, such as ceilings, floors, side walls, carpets, curtains and even glass windows are not

flat and most surface reflections are scattered reflections. During the period between the sound impulse from the source reaching each subspace, the sound field of each subspace are not unified due to the reflection, scattering and diffraction associated with the energy absorption. The assumption is that no energy exchange occurs at any of the coupling areas between subspaces until the reflection density in subspaces is high enough. The predicted energy decay curves and energy parameters are found to agree well with the measured results indicating the model to be a more accurate description of early energy decay performance in churches.

2.4.2. DIFFUSION EQUATION MODEL (DEM)

The local acoustic energy density in rooms with perfectly diffuse reflecting walls is named to be diffusion model, which is based on the mathematical theory of diffusion of the sound field within an enclosed space. In this model physical analogy of the diffusion of particles in a medium by hitting spherical scattering objects is adopted (Picaut et al, 1997). Under this section basic diffusion equation model studies are presented. To be one of the data collection and analysis tools of this thesis research, detailed mathematical expressions of the model are given under Methodology section.

The numerical implementation of DEM in room acoustics predictions is initially studied by Valeau et al. (2006). With a focus on the source term and boundary conditions, they have applied the developed model to a cubic room, to a long room and a flat room. Results are then compared to statistical models and ray-tracing simulations. The conformity of the results indicates the possibility of this new model to be a solution of various room shapes. Besides in compare to previous models, DEM has the advantage of low computation time and availability of plotting spatial variations of acoustic density and sound flow vectors throughout the whole volume.

Billon et al. (2006), search for a new model for assessing spatial variations of the reverberant sound field both in terms of sound level and sound decay. A numerical

implementation of the diffusion model to the coupled room configuration is studied and results are compared with experimental data, statistical theory and a ray-based model. In this research the mean-free path of each coupled room is set to the value that as if the rooms are uncoupled. According to this approximation coupling aperture area is small compared to the area of the wall surfaces for each room, so that the mean-free path is not affected much by the open aperture. The reverberant field in each room is then calculated by using the diffusion model. Mean SPL of the reverberant field is obtained from the diffusion model, by averaging the stationary energy density over each room. The obtained solution allows the estimation of the sound decay and consequently the reverberation time at any location in the rooms.

Results of Billon et al.'s (2006) study indicate that when the receiving room is more reverberant than the source room, the diffusion model gives the typical double slope decay in the source room but not in the receiving room. When the receiving room is very reverberant, or when the rooms are not weakly coupled, the results given by the statistical theory are questionable. The main difference between the two theories is that the *diffusion model allows for modelling the spatial variation of the reverberant sound field, while the statistical model gives only one constant value for each room.* The statistical theory does not predict the true gradual transition through the coupling area, while the diffuse sound field at the coupling area is stepwise. The diffusion model takes the sound source location into account, while the statistical theory does not. The gradual sound attenuation due to the opening is well predicted both by the diffusion and ray based models. The major difference between ray based software and diffusion model is the computation time, which is much less in the later (Billon et al, 2006).

In 2007, Jing and Xiang has taken a step forward to extend DEM for high absorption cases meaning that some surfaces of room could be sound absorptive, whereas previous models are only for rooms with totally sound reflective (low absorptive) interior surfaces. By applying Eyring absorption coefficient for boundary conditions

(impedance terms), this new model provided much accurate results in rooms with non-homogenous surface characteristics. Later, Billon et al. (2008) also have applied the same coefficient (Eyring) for solving DEM within non-uniformly absorbing rooms. They have supported the argument (Eyring model) by experiments on real cases; specifically a reverberation chamber with sound absorptive patches of glass wool.

DEM is applied in coupled rooms in order to visualize sound flow directions (vectors) for transient sound energy cases by Jing and Xiang (2008a; 2008b). Finite element modelling software is used for numerical implementation. Depending on the size and the location of the coupling aperture, a reversal of flow is observed at specific time, supporting the turning point findings out of Schroeder decay analysis within Bayesian framework. The singularity problem of Eyring coefficient in DEM boundary terms, in rooms with surfaces having an absorption coefficient of 1, is improved by the modified boundary condition developed by Jing and Xiang (2008c). Simulations and scale model tests are held for comparisons and reliability analysis of the new boundary term.

Another study on diffusion model is held by Xiang et al. (2009) with a focus on sound pressure level distributions in coupled rooms. Authors proposed a new absorption term in to the model which can model high absorption for a small portion of surface just in case of a coupled system. For experimental verification, 1:8 scale model of a two room coupled system is constructed. Results indicate that when the natural reverberation time in the primary room is smaller than the secondary room, the sound-energy flows from the secondary room back to the primary room. The feedback energy dominates the decay process in the primary room but with a shallower decay rate indicating a double sloped energy decay. The energy flow direction turnaround is expressed as a dip on the energy flow decay curve, which correlates with the turning point on the double sloped sound energy decay extracted from the Bayesian analysis. For the condition that the primary room possesses same

or a higher natural reverberation time, then no energy flow is observed, indicating that the energy feedback is heavily depend on the decay rates of each room under consideration (Jing, 2009).

A shortage of DEM is stated to be the validity of the model only in later time components of impulse response (late reverberation). According to Escolano et al.'s (2010) study, direct sound and early reflections in initial time steps do not provide the diffuse field conditions, where DEM is not applicable. The very first time intervals should be taken out of the impulse data so as to hold reliable DEM analysis. Numerical experiments carried out to determine the initial cut of time from the impulse response. Results indicate that the diffusion equation model is *valid after two mean-free times*.

A final diffusion equation model application is carried out by Xiang et al. (2013) in search of aperture size and receiver location effects over the sound fields of coupled rooms. Scale model experiments are utilized for supporting DEM results by systematically changing architectural configurations. Basic findings of the study are as such: DEM is only valid to predict the reverberation in the later time instance (after the diffuse sound field is established, or at least two or three mean-free times); when the sound source is near the aperture; when the second decay slope is much shallower relative to the initial decay slope.

2.4.3. WAVE THEORY

Wave theory is based on the study of sound wave motion within three-dimensional enclosures. It requires the establishment of boundary conditions which describe mathematically the acoustical properties of the walls, ceiling and other surfaces in the room. In wave theory the room is considered as a complex resonator possessing many normal modes of vibration which are excited when a sound source is introduced to the room. The acoustic energy generated by the source excites these room modes with the resulting in the standing wave formation within the room. The

characteristic frequencies of these vibrations depend on the room size and shape, whereas the damping of the resulting waves depends upon the boundary conditions. Thus, every room imposes its own characteristics on to the sound source present (Long, 2006).

Statistical acoustics methods including the assumptions in deriving reverberation time by regarding diffuse distribution of the flow of sound in the rooms and continuous absorption of sound at the boundaries are not always valid for acoustically coupled rooms. Geometrical acoustics methods apply only to highly reverberant rooms whose characteristic dimensions are large compared to the wavelength. GA doesn't account for diffraction or interference of sounds, as straight lines is its main assumption. Wave theory is much reliable while it is limited to low frequencies in which the room dimensions are usually comparable with the sound wavelength. According to that, the response of a room can be understood in terms of its normal modes and the associated decay constant of each of these modes. An application of the wave theory to complex enclosure geometries such as coupled rooms is possible through numerical methods.

Within that perspective Harris and Feshbach (1950) experimented two cases of coupled room situations; first where the coupling area is comparable in size with the partition separating two rooms and second where the coupling area is very small in comparison to the partition separating two rooms. For the first case the window or coupling aperture is a constriction on the path of wave of interest. As wave attempts to maintain constant current flow it increases its velocity. This results in an effective increase in the wavelength of the standing wave. The shift in the resonant frequencies is dependent on the unperturbed normal particle velocity. The frequency shift is zero whenever the window is placed at a particle velocity node, and at this position the effect of the coupling partition is the least. In case two the area of the coupling window is small enough that the particle velocity over it is approximately constant. The effect of this hole in the partition is in the manner towards increasing

nodal lines and shortening the wavelength in the standing wave meaning an increase in frequency. When two rooms are acoustically coupled by an aperture, the normal frequencies and damping constants of the normal modes of vibration of the system depend on the position of the aperture. For instance, if the window is at a pressure node there is no excess pressure at this point meaning both sides of the coupling window are at the same pressure. In this condition there is no tendency for wave motion through the opening.

In principle of wave theory, for the low frequency range the acoustic field inside an irregularly shaped room is based on a solution of the wave equation with specified initial and boundary conditions. With that understanding the room can be treated as a resonator with characteristic acoustic normal modes determined by the eigen-functions. When a signal generator is switched off, the acoustic energy accumulated inside the room is dissipated on the walls and a reverberation, due to the common decay of eigen-modes, occurs. The computed eigen-functions represent the numerical solution of the wave equation in a two-dimensional area in the shape of the room's horizontal cross-section. In Meissner's (2007) research, the steady-state and time-dependent reverberant sound fields in a room consisting of two connected rectangular sub rooms are investigated considering the room dimensions are comparable with the sound wavelength, allowing a combination of a classical modal analysis with a numerical implementation. The results of the numerical study indicate that when the sound frequency is close to an eigen-frequency of the mode which is localized in one of sub-rooms, the highest values of the eigen-function occur in that room and values of modes are very small in the remaining sub-room. Because of this property a sound emitted by a source having a frequency of that specific eigen-mode is mainly absorbed in the first sub-room and weakly damped in the other.

When there is a large difference between absorption characteristics of two sub-rooms, the decay curve consists of two parts which refer to the rapid early decay and

the slow late decay. In such a situation, the time history of a pressure level characterizes a double slope effect. This occurs when a dominant acoustic mode is much more damped than neighboring modes. In brief, for large differences of sound damping in the sub rooms the acoustic pressure distribution and the reverberation time are strongly influenced by the phenomenon of eigen-mode localization. The location of absorbing material and the position of the sound source have a great influence on the distribution of the sound pressure and the reverberation time inside the sub-rooms (Meissner, 2007).

In a later paper Meissner (2012) presents the modal expansion method in predicting steady-state distributions of the potential and kinetic energy densities inside two coupled enclosures. An acoustic room response in a steady-state is described theoretically by means of a modal expansion of a sound pressure for a lightly damped room system. Space distribution of eigen-functions, modal frequencies and modal damping coefficients are calculated by the use of computer implementation searching the finite difference method. Calculation results indicate that the distribution of energetic quantities in coupled spaces is strongly influenced by the modal localization. *In low-frequency range coupled room systems have exhibited the concave double-sloped decay.* The degeneration of modes by the change in the coupling area and the modal localization have been detected through a concentration of acoustic energy in a small part of the room. It is also concluded that when the sound damping on room walls is negligible, there is only oscillatory sound energy flux inside a room.

2.4.4. ACOUSTICAL COUPLING QUANTIFIERS

Quantifying the degree of acoustical coupling has always been a challenging task. Different methods have been developed for defining coupling degree quantifiers. Some research findings rely on the visual inspection of the Schroeder decay function or the misleading observation of the energy time curve (ETC) (Figure 2.6). The problem with visual inspection can clearly be stated when the effects of upper limit

of integration (ULI) and background noise or signal to noise ratio changes are observed on energy decay curves (Xiang and Goggans, 2001).

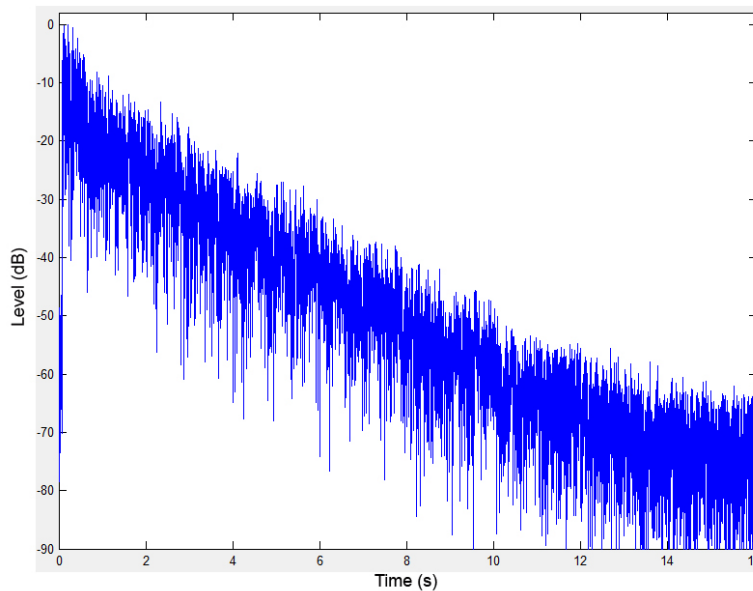


Figure 2.6. A typical appearance of energy time curve (Source: anonymous)

Some researches take a step forward and compared different portions of Schroeder decay function in defining some ratios namely coupling quantifiers. Coupling Coefficient is defined to be the ratio of two decay metrics: T_{30}/T_{15} (Bradley and Wang, 2005). The T_{15} decay measure represents the early portion of the decay, whereas T_{30} represents a larger portion of the decay in other words the first 30 dB drop. The possibility of turning point to occur outside of the T_{15} or T_{30} range depicts the quantifier ineffective in characterizing the double slope effect. Coupling Constant which is very similar to Coupling Coefficient is defined to be the ratio of decay metrics: T_{60}/T_{15} . The information is still limited to first 15 dB drop of the decay in this constant (Ermann, 2005). Decay Ratio is the ratio of natural reverberation times within each sub-room and ΔdB is the difference between the y-intercepts of each of the two decay lines (Bradley and Wang, 2005). These last two quantifiers do not behave in a consistent way for changes in auxiliary volume absorption coefficient, especially when the auxiliary volume is very large.

In a later study of Bradley and Wang (2009) a new quantifier is proposed namely Late Decay Time to Early Decay Time (LDT/EDT). For EDT the time of the first 10 dB drop is multiplied by a factor of 6 and for LDT the start and stop dB values are chosen to be -25 and -35 (Figure 2.7). According to the authors, since the numerator and denominator of LDT/EDT focus on different temporal portions of the decay, this ratio has a better potential for characterizing DSE in compare to previous ones.

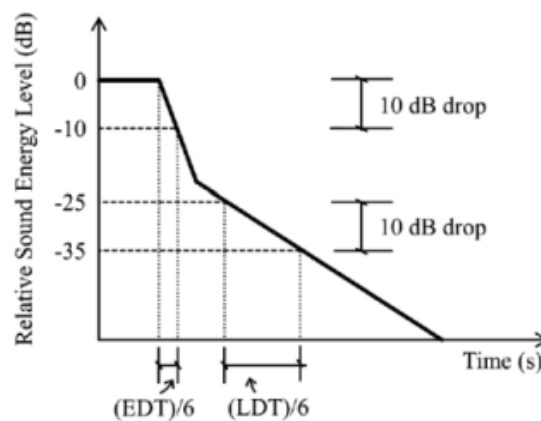


Figure 2.7. Coupling quantifiers based on EDT and LDT (Source: Bradley and Wang, 2009: 115)

In a later study using above mentioned quantifiers Bradley and Wang (2010) conduct subjective testing in order to examine the listener preference for different degrees of DSE on a concert hall case. In this study DSE is defined to be the phenomenon when the second slope is larger than the first, and dominates the decay profile during the late portion. The absorption in the coupled spaces and the aperture opening between the spaces are systematically varied to observe different effects. Absorption ratio is defined to be the equivalent absorption area in the secondary volume as a portion of the equivalent absorption area in the main volume. Aperture opening size is the percentage of the total surface area of the main volume. In general, the DSE values are much lower for the two larger aperture sizes, closely matching those for the single volume condition and indicating that the decays from these configurations behave like single slope decay. The four coupled configurations with the smallest aperture sizes indicate a significant non-linear decay.

Impulse responses having high DSE values are auralized to be used in subjective testing (Bradley and Wang, 2010). The results of psychoacoustic preference to sound fields in coupled volume spaces are compared with the objective scale of coupling degrees. Many of the coupled volume scenarios are preferred over the single main volume case. Hall configurations producing low and medium levels of DSE are most preferred by listeners, with the highest preference occurring at medium sized aperture opening with larger absorption ratios. The lowest preference value is for the highest DSE level. This final preference is even lower than preference for the single main volume case. In previous studies it is found that the perception is increased as the difference between the two slopes in the non-exponential decays are increased, in this study additionally the preference on perceived aural effects are presented.

Although Bradley and Wang's study (2005) aims to fill the gaps of previously defined quantifiers, it still depends on the proportion of some arbitrarily chosen sections of the decay curve. The interactive effects of the energy peaks and drops in every single point of the energy decay curve cannot be analyzed with such mathematical proportions of the visual decay curve, but by a more scientific statistical approach as discussed in following.

With an aim of obtaining better understanding and control of acoustics in coupled spaces Xiang and Goggans (2001) search for an efficient technique of determining decay times. The effort is especially on distinguishing different portions of simple exponentials having different decay rates. Using Schroeder's backward integration method, a decay function model is established. Then, the Bayesian parameter estimation is proposed for the evaluation of decay times. For experimentally verifying the model, room impulse responses are obtained from measurements in real halls and scale model coupled rooms. Schroeder integration is applied to all room impulse responses (RIR) after filtering by an octave band pass filter at a central frequency of 1 kHz. Comparison of decay time estimates from real and model decay

functions proves the validity of decay model. Besides, both the ULI and the signal to noise ratio are found not critical to the Bayesian decay time estimate provided that the former is sufficiently large in compare to the decay time and the latter is not less than a critical value as 40 dB.

In order to understand effects of coupling-aperture configuration and source and receiver locations on sound fields in coupled rooms, a systematic experimental study is carried out by Sü (2006) based on Bayesian parameter estimation technique developed by Xiang and Goggans (2001). A 1:8 acoustic scale model technique is used in collecting room impulse responses of a two-room coupled system for varying aperture configurations. Baseline behavior is established by alterations in aperture area, while holding coupling shape fixed. The effects of receiver location are systematically investigated by varying the distance of the receiver from the coupling aperture for a fixed aperture configuration. Schroeder decay-function decompositions by Bayesian analysis reveal sensitivities to receiver location and aperture configuration across different frequency bands. Based on a large number of data analysis from this study, it is concluded that acoustic coupling is a frequency dependent phenomenon, and very much sensitive from location to location. For the tested three cases of source, shape and aperture size configurations, the highest ratio of acoustic coupling is observed in 20% and 40% aperture opening sizes. In contrary to the common view that acoustic coupling should be observed mostly at aperture opening axis, the receiver locations with the strongest acoustic coupling throughout the main room are found to be the ones located in shadow zones to the coupled room.

A survey is carried out by Martellotta (2009) in St. Peter's Basilica in order to analyze and distinguish the proportionate effects of surface absorption and acoustical coupling on reverberation. Bayesian parameter estimation is used as an analysis tool, as indicated to be the most rigorous estimate of different decay constants that characterize multi rate decay processes while allowing more accurate comparisons with theoretical models. The basilica, having an approximate volume of 480,000 m³

is the sum of five large volumes joined together by means of the large openings of the crossing and by means of additional secondary volumes connected through smaller openings. Interior surfaces, which are richly decorated with deep carvings, are mostly of plaster, marble and stucco. The analysis of real size measurements shows that reverberation times measured in St. Peter's Basilica are shorter than generally observed in churches of even smaller dimensions. Geometrical acoustics is also applied by the use of CATT Acoustic software for further analysis of coupling mechanism. It is found that for having similar results in comparison to the measurements, coupled space model requires absorption coefficients greater than those applied to other spaces. According to the author the necessity to increase the sound absorption coefficient is not due to coupling effect, but mostly depends on the increased exposed surface due to the high degree of decoration. Both field measurements and geometrical acoustics analysis support that the basilica behave as a system of coupled volumes in which the acoustic conditions significantly vary from subspace to subspace, according to source and receiver placements.

As an extension of Xiang and Goggans' (2001) research in 2011 Xiang et al. present multi/ple-slope (2 or more slopes) energy decay analysis. According to the authors in coupled volume systems, even multiple-slope decays, beyond double-slope decays can occur. Bayesian analysis that is previously presented by authors is further developed to investigate multiple decays over sound fields of coupled systems. The number of decay times and decay rates are aimed to be identified. In that respect an approach based on Bayesian information criterion (BIC) to accomplish decay model selection is introduced. In order to experiment multiple slopes a one eighth-scale acoustic model of three coupled rooms are built. Interior surfaces are covered with pebbles in order to obtain a diffuse field in the region of 1 and 2 kHz. The natural RTs of each room/box is tuned to be sufficiently distinguishable from each other by proper sizing and adding of absorptive materials. RIRs are measured within the primary room at different locations. In coupled condition the sound energy decay processes in the primary room feature three decay-slopes. The experimental

investigations indicate that improved Bayesian formulation is capable of characterizing multiple-slope decays beyond single-slope and double-slope decays. The model based on Bayesian formation is presented in detail under Methodology section, as to be the basic coupling decay parameter, namely acoustical coupling quantifier, estimation method of this thesis research.

2.4.5. CONCLUDING REMARKS ON COUPLED SPACES

As so far discussed a coupled room system is traditionally defined as a collection of partial rooms separated by virtually non-transparent walls, where the only communication is through relatively small apertures embedded within these walls. In a typical coupled room system sound energy is assumed to exchange in between rooms through a coupling aperture. When the sound source is stopped, the sound in each room decays in its own rate. In condition that decay rates are unequal then there is an energy surplus in one room compared to the other/s leading to energy transfer from energy surplus room into the energy deficient room. This energy transfer in some conditions generates non-exponential energy decay which is quite different than an exponential decay of a typical single room in diffuse field state.

One of the conditions to satisfy the two slope profile decay curve is that the source to be in the room with lower decay rate. In such a scheme the steep early decay indicates the reverberation time of the comparatively dead room, while the shallow later decay designates the reverberation time of the relatively live room from which the energy transfers to the source room. In condition that the source is in live room, then the decay process of dead room would completely be masked by the decay of live room, causing the decay rates to be virtually same for both rooms. The reason that makes coupled space to be popular in recent concert hall designs is that the early steep decay provides definition to music, while the late slow decay increases the music's liveness and fullness of tone (Mehta et al., 1999). These two contradictory requirements namely clarity and reverberance are hard to satisfy with classical decay

properties of a single room while can be assured to some extent in a properly designed hall that adopts coupled space concept.

Case studies that incorporate acoustical coupling as a design aid are very few in academic literature. Most of the cases are selected specifically for understanding the ambiguous sound field due to different energy interactions between subspaces. Non-exponential or convexly curved decay curves are indicators of the presence of several energy stores, which are searched by experimental models (simulation or scale model) or in real-size measurements. Architectural variables such as coupling aperture, ratios of total absorption areas or volumes of sub-rooms are varied for creating non-exponential decays. Objective quantifiers are proposed to measure the level of coupling. Even subjective testing is held for understanding the psycho-acoustic effects of acoustical coupling.

Different models have different limitations. Statistical room acoustics quantifies the average properties of a sound field in a room, rather than properties associated with a specific frequency or location, and only when the field is diffuse. SA is useful when wave-based techniques become inefficient or when modes overlap significantly and cannot be studied individually. Geometrical room acoustics assumes that the dimensions of a room are large compared to the wavelength and applies only to reverberant rooms whose characteristic dimensions are large compared to the wavelength. For that reason GA is accurate for very short wavelengths, where the acoustic wavelength is much less than the dimensions of any surfaces and obstacles of interest in the room. In this method sound propagates in straight lines. For that reason, the geometrical acoustic models do not include wave phenomena, such as interferences and diffraction. The advantages of acoustic simulations are due to the presence of perfectly omnidirectional and impulsive sound source. Such an environment does not create any distortion problem, provides full control of the background noise, and a well-defined onset time of the impulse response (Christensen et al., 2010).

Diffusion equation model is more accurate than geometrical acoustics approaches, as it considers spatial distribution of sound energy throughout the space and enables sound flow/vector analysis. The computational speed of DEM as well is much faster than GA applications. On the other hand, the limitation to the diffuse field condition weakens its strength for spaces with very high absorption area. DEM is much more accurate for late reverberation tail and higher frequency range in comparison to the space dimensions in interest – so not much applicable for low frequencies over small rooms. Wave theory is generally limited to low frequency ranges, useful when the modes are well separated and can be studied individually. This theory has practical application for enclosures with dimensions comparable with the sound wavelength, such as recording studios. In literature different models are compared to each other and some corrections or modifications are made to existing models for improving their accuracy for coupling conditions.

Computations are for better understanding of acoustical properties of a room at its design phase. There is no single model that serves for a whole range of frequency or generic for all cases of architectural parameter configurations. The acoustical coupling field is still scientifically improving and it necessitates more input in form of real-size data for better understanding of the phenomenon. Field measurements still give the most accurate results, but the findings have limitation to be analyzed and quantified for the coupling effects in most of current studies. Interest in coupled room effects necessitates a reliable data analysis of non-exponential sound decay in such spaces. Among all other techniques the parametric model of the Schroeder decay function within Bayesian probabilistic interference proved to be a powerful tool in reliable estimations of multiple decay times which constitutes the basis of sound decay analysis of this proposal as explained in detail under Methodology section.

The variety of energy decay curves in a coupled system is far greater than it is in a single room. However, coupling effects are not restricted to some specific geometrical structure, as in the case of generally tested coupled rectangular boxes (Kuttruff, 2000). Although none of the previous studies has searched the phenomena deeply under single volume spaces without definitive aperture openings, there are implications on the non-exponential decay formation to even occur in single enclosures that are lack of sound field diffusion. Most specifically the mosque typology, adopting features of nondiffuse sound field with varying zones of absorption and reflection, encapsulated in some cases by a multi-domed upper shell structure with considerably large volumes has never been searched as a data source for coupling investigations. This research aims to find intersection points of coupling effects and single spaces with specific geometric attributes, as of superstructure religious spaces, that can inspire also future researches/rs in way of yielding extensive data accumulation for explaining the unknowns on this specific scientific field of interest.

CHAPTER 3

RESEARCH MATERIALS

In this investigation cases are selected in regards to the structures that can provide room acoustics coupling or more specifically non-exponential energy decay formation within their interior enclosures. Major criteria are for the structures to be monumental in size, to have up-scale volumes, and that they have multi-domed upper shell typology, which can augment sound energy accumulation underneath these forms. As being the inspiration to this study, due to some major motivations as discussed under Section 1.1., Süleymaniye Mosque in İstanbul is selected to be the major case for acoustical field analysis.

After the initial process of data collection through computer simulations and field measurements, data analysis is held for decay parameter estimations. Non-exponential energy decay formation within Süleymaniye Mosque is validated through DPE, DEM and energy flow vector analysis over real-size field and simulated data. Experimentation of different material use over floor (marble versus carpet) in Süleymaniye Mosque through DEM modeling, for highlighting the nondiffuse sound field formation in such an up-scale structure, has resulted in the significant effects of material change over non-exponential-energy decay. For that reason, in a multi-domed upper shell morphology, a real-size space has been necessitated for further real-size experiments in order to validate the DEM model findings over reflective versus absorptive floor.

In that respect, Hagia Sophia has come up to be an accessible monument for field-test measurements. Not only for the comparison of reflective versus absorptive floor,

but also for the comparison of some other specific geometric attributes, that distinguish Hagia Sophia from Süleymaniye Mosque, which are essential for further discussion over the non-exponential energy decay formations. Such as, the doubling of volume (in result higher RTs are expected for specific frequency ranges) and the basilican layout with side aisles separated by comparatively small arches (underneath side aisles depicting a coupled space scenario, instead of a single space). Specifically for underneath side aisle, where Hagia Sophia sub-spaces behave as virtually coupled volumes, more real-size data input are aimed to be collected for the benefit of acoustical coupling investigations, not only under the heading of single spaces but under the heading of the traditional coupled volume spaces.

As a result, it is presumed that, the volumetric and geometric effects together with the RT differences can illuminate the coupling phenomena in such mega-structures. Süleymaniye Mosque can be a prototype for later multi-domed superstructure investigations in search of acoustical coupling, not only within the boundaries of this research but as a sample case for future researchers on acoustical coupling under single space structures. Hagia Sophia, on the other hand, can be a supplementary case under single space heading as in this research, but fruitful in regards to data collection over multiple slope/decay (higher than double decay) formation in a real space/enclosed environment, which necessitates further future investigations and interpretation. The architectural details in relation to their origins, previous restorations, and as of today conditions for both monuments are discussed under following sections, out of which the material and geometric information are crucial in terms of assessing their acoustical field conditions either for today or over their historical time span.

3.1. CASE 1: SÜLEYMANIYE MOSQUE, İSTANBUL

Being the largest of the Ottoman building enterprises of the time, Süleymaniye Mosque and Complex is sponsored by Kanuni Sultan Süleyman in his ruling and designed by Mimar Sinan -the architect laureate of the Ottoman Empire-. The main construction is held in between 1550-1557, while the whole structure with the fine works of tombs is completed in 1568 (Cantay, 1989). The complex is currently located in the historical island of İstanbul, at the land of Old Palace which is completely destroyed in a fire in 1540 (Saatçi, 2007). Süleymaniye is built on a plan of three adjacent squares: the mosque itself, the courtyard with the last prayers section and backyard, where the tombs of Sultan and his wife Hürrem are located. Site plan of the complex takes its references from the topography. The complex is composed of 22 different structures with different functions surrounding an interior courtyard (T.R. Prime Ministry Directorate General of Foundations Archive, 2011; Yılmaz, 2008).

According to Necipoğlu-Kafadar (1985) Süleymaniye has a multilayered architectural discourse with interacting layers of meaning. Those layers are classified as functional, connotative (cultural associations and myths), formal (architectonic) and literal (its inscriptions). In the functional level besides medical and library facilities madrasas are rising as an important element for the socio-political and socio-religious being of the empire. Süleymaniye madrasas represent the growing political role of *ulema* under 'Süleyman's reign at the time in legitimizing the Süleyman's rule through the Sunni doctrine of the orthodox state'. Four Süleymaniye madrasas are dedicated to the four Sunni schools of law which have the vision of elevating matters of religion and religious sciences in order to strengthen the mechanism of worldly sovereignty and to reach happiness in the afterworld Necipoğlu-Kafadar (1985).



Figure 3.1. Süleymaniye complex - an old gravure (Source: anonymous)

Süleymaniye Mosque which is the central figure of the whole complex (Figure 3.1) has always been an inspiration source for many fields including architectural aesthetics, structure and construction, acoustics and material science. The acoustics of the mosque in this respect is an important subject of research.

3.1.1. ARCHITECTURAL FEATURES

Süleymaniye Mosque's main structural elements are domes, arches and flying buttresses. The mosque is covered centrally by a single dome which is supported on two sides by semi domes. The two semi domes align with the direction of the *mihrab*. Side aisles are sheltered by five smaller domes which complete the upper structure. The load from dome to footings is being transferred to half domes through the arches and *pendentives*. The arch walls and dome rim are pierced with number of windows, which also lighten the weight of the structure.

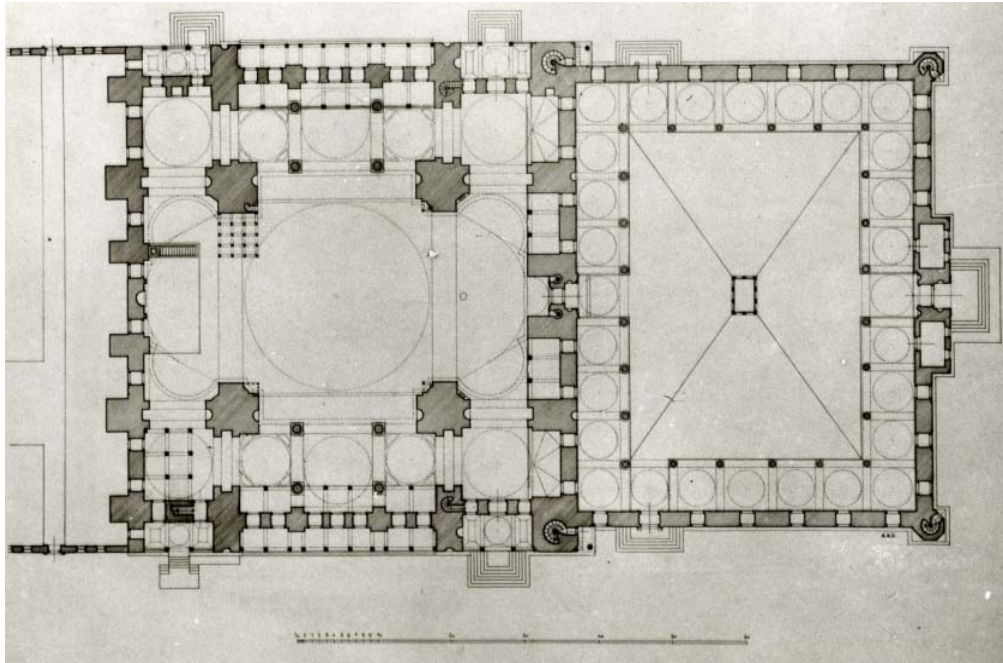


Figure 3.2. Süleymaniye Mosque plan view (Source: T.R. Prime Ministry Directorate General of Foundations Archive, 2011)

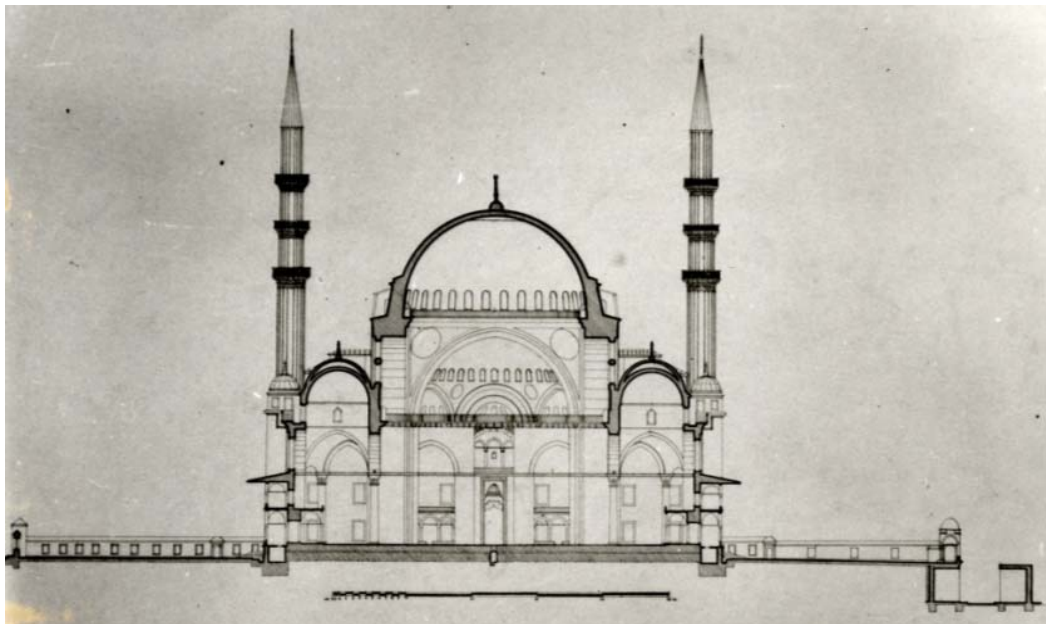


Figure 3.3. Süleymaniye Mosque central section, looking towards mihrab (Source: T.R. Prime Ministry Directorate General of Foundations Archive, 2011)

The inner plan of the mosque is a rectangle measuring approximately 63 by 69 m (Figure 3.2). Main dome rests on 4 elephant feet and 32 footings on a circular wheel with a diameter of 26.20 m (Figure 3.3). The height from the foundation to the

impost is 33.70 m. The inner rise of the dome is 14.05 m, and thus the height of the dome from the ground to the keystone is 47.75 m (Mungan, 2007). The middle and corner smaller domes on aisles have a diameter of 9.90 m and the middle ones have a diameter of 7.20 m. Except for the elephant feet, there are eight columns carrying secondary arches. Corner domes are supported by arches in between elephant feet and exterior shell walls. The other three side domes sit on arches, each of which is supported by two columns on two rows. *Pendentives* are utilized to smooth the central dome, secondary half dome and arch connections. *Muqarnases* are located in half dome skirting's and side dome arch transitions (Kuban, 2010).

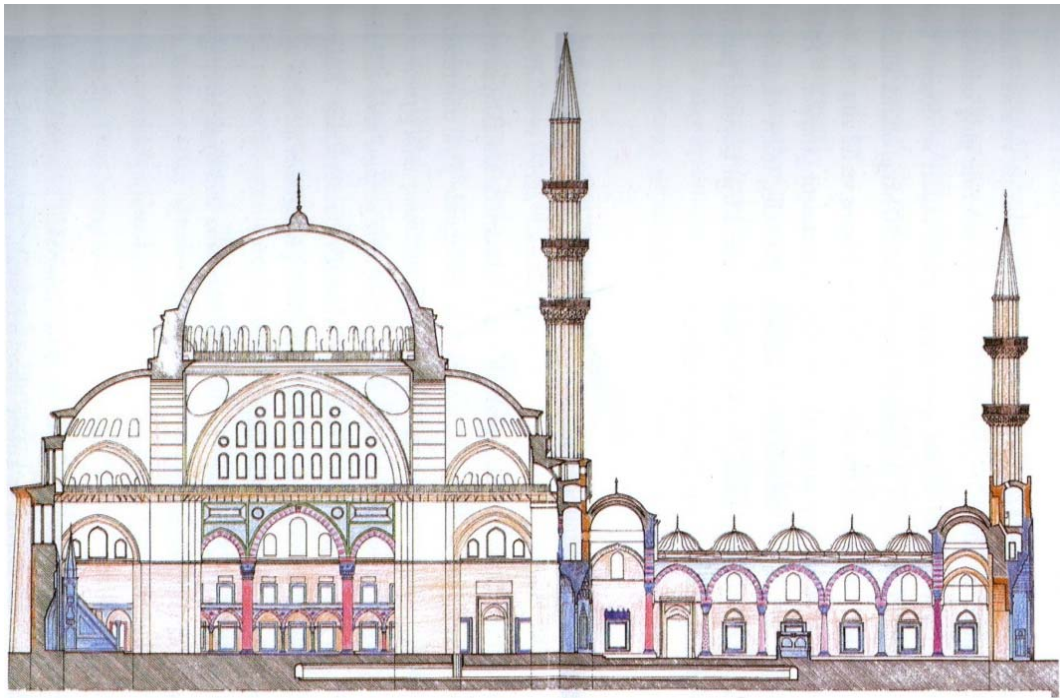


Figure 3.4. Süleymaniye Mosque, section view (Source: Çelik, 2009: 37)

The richness of materials applied within Süleymaniye Mosque, with different regions of material source and construction techniques, has always been an extensive research subject). In Süleymaniye there is an abundant source of stone supplies including Constantinople (İstanbul), Chrysopolis (Üsküdar), Chalcedon (Kadıköy), Perinthos (Ereğli), Viza (Vize), Adrianople (Edirne), Nicomedia (Kocaeli), Nicaea (İzmit), Cius (Gemlik), Cape Triton (Bozburun), Myrlea (Mudanya), Miletopolis and

Lopadion (Mihaliç), Cyzicus (Aydincık), Alexandria Troas (Eski İstanbulluk), Neandria (Ezine), Pitane (Candarlu), Miletos (Balat), Mytilene (Midilli), Chios (Sakız), Tenedos (Bozcaada), Thessaloniki (Selanik), Coracesion (Alanya), Cilicia (Mersin), Seleucia (Silifke), Danisancclus (Mud), Celendis (Selendi), Tarsus, Adana, Misis (Kozan), Alexandria (İskenderiye), Ascalon and Heliopolis. The uniqueness of the building complex comes from different types of stones delivered from various ruins of ancient cities all over the world (Necipoğlu-Kafadar, 1985; Kolay and Çelik, 2006).

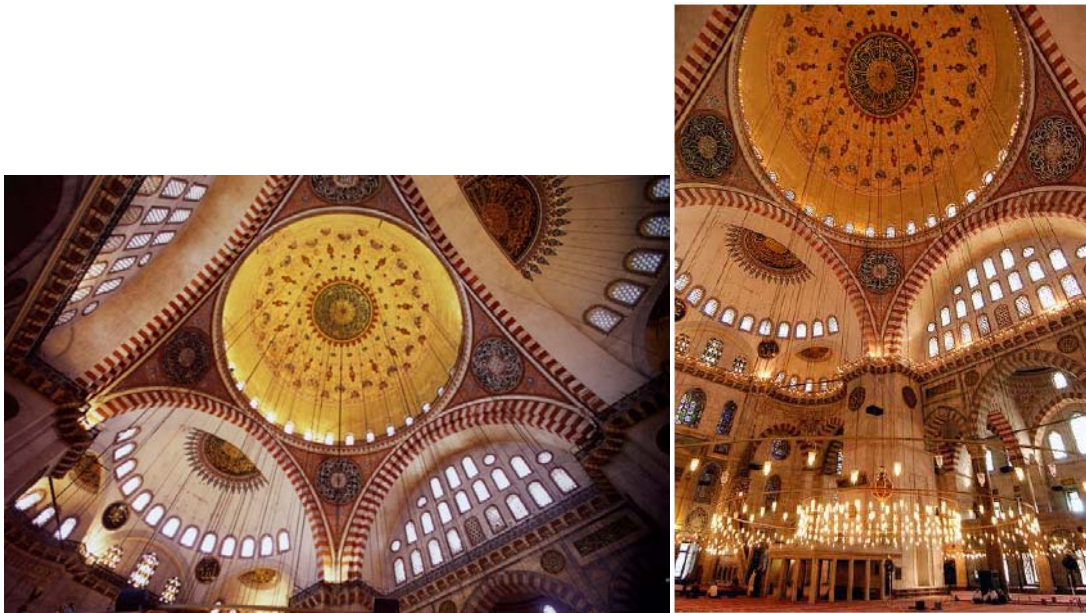


Figure 3.5. Interior view of domes and *pendentives* in Süleymaniye Mosque (*Source: anonymous*)

For its original state other basic interior materials -together with stone- are brick, tile, ceramic pots, plaster, paint, glass, wood and carpet. The interior walls are faced with stone revetments. The ceilings of the pulpits and the royal box, the domical superstructure, and the *pendentives* are painted (Figure 3.5). In contrast to lavishly painted domes and *pendentives* in lower zones the stone revetments left relatively bare. The prominent architectural features of the interior are historical columns, marble panels, porphyry discs, great arches, the *mihrab*, *minbar* and royal box, stained glass windows and inscriptions.

Limestone appears to be the main structural stone as well as the facing stone for interior walls and wall footings. Piers carrying the main dome and suspension arches are of cut limestone while the inner faces are painted as of Hereke conglomerate and Proconnesian marble. Columns are of Egyptian porphyry (red sparrow eye). Differently brick is utilized as the core material of domes due to its lightness. Painted brick domes are then decorated with gold foiled pen paintings. The *mihrab* and the *minbar* (pulpit) are of carved white marble and have stained glass windows on the sides (İrteş, 2007).

Lime, horasan, fine sand, gypsum, linen and straw are the basic ingredients of plaster layers and seams. Linen is applied in dome plasters. In accounting registers of Süleymaniye Mosque construction (account book number 108), it is declared that for plaster finish of dome (Beray-i siva-i kubbeha-i cami'-i şerif) 134 kantar of linen is purchased (Barkan, 1972). This is a significant information in terms of acoustical assessment that is detailed in following chapters.

Floor finish of the mosque is carpet with straw backing -which are collected from the finest straws grown in Nile delta- as stated in original documents (Barkan, 1972). Carpets had originally been woven in Egypt and Aydın-Tire. Wood in interior is mostly used for flat ceilings, doors, window frames and furniture. Only the two windows on each side of *mihrab* have '*kündekari*' wooden work shutters (Çelik, 2009).

One of the most important inventions of Sinan, applied in Süleymaniye Mosque, are the functional spaces namely fume rooms. These rooms acting as chimneys provide natural ventilation (Figure 3.6). From the four square hole/vent at the floor, smoke of the burnt chandeliers within the mosque are transferred to the fume rooms. The collected fume is then used in form of ink, which is then utilized in pen wall paintings ('*nakış*') of the Mosque (Acar, 2000).



Figure 3.6. Süleymaniye Mosque fume room (Source: Neftçi, 2007: 112)

Another feature of Süleymaniye Mosque in its original state is the use of *Sebu*'s, that are believed to be applied for the function of cavity resonators for the control of excessive low frequency sound content. In accounting registers of Süleymaniye Mosque construction (account book number 88, paper 19/a), it is declared that each for 2 akçe's (Ottoman coin) 255 "*Sebu*"s (clay pots in function of a cavity resonator) are purchased (Baha-i Sebu, beray-ı kubbe-i cami'-i şerif) (Barkan, 1972). According to the previous investigations the lengths of *Sebu* voids are 50 cm, whereas the neck widths vary in between 2-6 cm (Kayılı, 1988a; Kayılı 198b). The probable effects of *Sebu* application on the original state of Süleymaniye Mosque are discussed in following sections.



Figure 3.7. Openings for resonators within the dome of Süleymaniye Mosque (Source: Acar, 2000: 112)

As a final acoustical point, within the mosque *muqarnas*/stalactites are used as a transition element in column heads, in the skirting of half domes and such spots where the load encounters with the load-bearing structure. These elements do not have any structural function and are out of gypsum. *Muqarnas* helps to enhance the sound diffusion in mostly curvilinear and concave transition planes by fragmenting the surfaces into much smaller pieces (Figure 3.8).



Figure 3.8. *Muqarnas* detail - highlighted with pen paintings (Source: İrteş, 2007: 303)

The mosque has recently undergone some restorations, and currently only its existing sound field could be assessed through real-size field measurements. As pre-recent restoration conditions have already been documented by some researchers, the acoustical tests are not only to provide the data source for acoustical coupling investigations, but also to compare the declared acoustically problematic field conditions in present/post-restoration state and pre-restoration conditions of the Mosque.

3.1.2. RESTORATION WORKS

The architectural form and material information for the original state of Süleymaniye Mosque is detailed in previous sections. Until recently, the Mosque has gone through many restoration works. Since 16th century, Süleymaniye Mosque hasn't gone through major structural or special architectural changes. Besides for some small extensions, the structure in whole keeps its integrity and original form. However, there has been couple of major interior material modifications.

The initial restorations are held in 19th century successively in 1840, 1844, 1845, 1847, 1870 and 1873. In these interventions basically pen-carved paintings and plasters are modified, which ended up in a totally different (in terms of chemical and physical ingredients) interior finish characteristics (Kütükoğlu, 2000; Ersen et al., 2011; Cantay, 2011). At 1840's and 1880's restorations, held by Italian experts and Fossati-, it is recorded that the clay pots are covered/closed and the original dome plasters are modified with gypsum plaster (Kayılı, 1988b).

Since 1958, the restorations are allowed to be held within the control of 'T.R. Grand Commission of Memorial' (T.R. Prime Ministry Directorate General of Foundations Archive, 2011). For 1959 -1969 restorations basic interventions are; the renewal of oil paints on elephant feet, removal of wooden cabinets at some locations, painting of door and window jambs, renewal of dome and arch paintings. In these restorations some of the 19th century paintings are removed in order to uncover the original

paintings (Eyüpgiller, 2007; T.R. Prime Ministry Directorate General of Foundations Archive, 2011).

Prior to 2007-2011 restorations, on stone and wooden surfaces different types of material deteriorations are detected. Particularly the pen-paintings on dome facings and on ceilings of exterior side galleries are corroded due to moisture (Eyüpgiller, 2007). Damage report prior to 2007-2011 restorations also include structural damage, the damages due to cement based plastering or seam fills, and damages due to some other inappropriate use of material (Ersen et al., 2011; Cantay, 2011). The cement-based plasters and application of pen wall paintings on these plasters are significant in assessing the changes in acoustical field of the Mosque.

During 2011 restorations the samples of original horasan plasters in dome are collected. Tests and analysis are held for obtaining cement free plasters that are compatible with original ones. These are then applied on renewed plastering and pen-wall paintings ('nakış'). The paintings within the Mosque has taken its final shape after 1957-1959 and 2007-2011 restorations (Eyüpgiller, 2007; Ersen et al., 2011; Cantay, 2011). Besides, it is also declared in press that the mouths of 15 cm width and 45 cm length 256 *Sebu's* are opened and cavities are repaired (<http://www.radikal.com.tr/>, 2013). This section is a brief for the architectural and material modifications of the mosque in different restoration works as mentioned in the relevant literature. The detailed interpretation of the acoustical field for Süleymaniye Mosque's original state and acoustical field comparisons out of different renovations are given under Discussion section.

3.2. CASE 2: HAGIA SOPHIA, İSTANBUL

Hagia Sophia, the Holy Wisdom of Christ, is constructed as a church in between 532-537 in İstanbul (Constantinople) in the ruling of Justinian -the emperor of Byzantine at the time-. Anthemios of Tralles and Isidore of Miletus, foremost architects and engineers of Byzantine of its time, planned and consulted the construction of the church. Hagia Sophia was both the center of the religious life and had been a legend for the new wave of church building in the West in twelfth and thirteenth centuries. After the Ottoman conquest in 1453, in the ruling of Mehmet II, it was converted from church to mosque (Figure 3.9). In 1932 upon order from Atatürk, Hagia Sophia has started to function as a museum and is still one of the most inspiring architectural achievements of all time (Klenbauer, 2004; Oyhon and Etingü, 1999).



Figure 3.9. Hagia Sophia exterior view - an old painting (Source: Kahler and Mango, 1967: 250)

Hagia Sophia is a masterpiece of not only Byzantine art but also of world's historical heritage. Its architectural success and carried messages affected both the Ottoman Empire and architects as of Sinan. The influences of the form have revitalized in

many other domed spaces both in churches and mosques. On the other hand, the building physics aspects as of structure and materials has grounded in many researches (Mark and Çakmak, 1992).

The interior sound field of such an immense monumental building has also inspired many acousticians. In some acoustical studies on Hagia Sophia, the room acoustical parameters are analyzed for its existing condition (CAHRISMA, 2001). By some other researchers the acoustical history of the structure is virtually generated for different time periods and activity patterns (Weitze et al., 2002a; Weitze et al., 2002b). One study focuses on recreating Hagia Sophia's acoustics within other venues by the use of electronic architecture, or more specifically the so called artificial reverberance (Abel et al., 2013).

Hagia Sophia is a large space with many coupled sub-spaces. High reverberance within such a large interior, lends unique properties to the music and demands suitable repertoire and singing ability in terms of liturgical music. The acoustics of such a volume with dominating geometric and material attributes also inspired this study in terms of acoustical coupling investigations.

3.2.1. BASIC REPAIRS AND ALTERATIONS

Over the 1400 years of its existence, Hagia Sophia has suffered much damage essentially due to major earthquakes. Three main phases of structural repair and strengthening are recorded. The first repairing phase was in 1317, in the reign of Andronicus Palaeologus; the second was in 1573 under the architect Sinan; and the third repair was in 1847 under the Swiss architect Gaspare Fossati, assisted by his brother Giuseppe. The principal work undertaken in 1317 was the construction of new buttresses. In 1573, Sinan built a new minaret in place of one that was to be demolished. In 1847 major works were the rectification of a number of columns in the gallery exedra, the installation of new ties for critical locations, and other repairment at the level of the dome base (Mainstone, 1988).

Hagia Sophia has also undergone many alterations due to changes in its activity patterns. In conversion from church to mosque, some Christian elements are removed and Islamic additions are introduced. Since pictorial representations are traditionally not permitted in Islam, after 1453 the mosaics were gradually covered up, whitewashed or plastered over and hence preserved. After Ottoman conquest all the Christian furnishings were swept away (Mainstone, 1988). In 1847 the sultan commissioned a pair of Swiss architects, Gaspare and Giuseppe Fossati, to restore both the fabric and the decoration of the building. During these works all the surviving mosaics were uncovered, and copied in order to provide visual record. Unfortunately, many of the mosaics recorded by Fossati's had disappeared by this date, most probably lost in the great earthquake of 1894 (Klenbauer, 2004). The original altar, screen and ambo badly damaged in the first collapse, and rebuilt in the subsequent restoration. Other damages are engaged to the 14th century collapse. Damage by crusaders in 12th century in the form of robbery should also be included in the history. Today some of these stolen items are on display in San Marco Church in Venice.

Among the Islamic additions four minarets complementing the exterior mass of Hagia Sophia were built for Islamic prayer function. A mihrab was added on the kiblah axis (the church is oriented to the east), about ten degrees further to the south (Figure 3.10). The minbar was constructed in the same direction. Prayer carpets and banners of victory were hung on the walls flanking the mihrab during the mosque period. The *Müezzin's mahfili* (Figure 3.11) in the center of the structure and four more galleries in the narthex were added. On the left side of the central nave there still is the preaching pulpit. Imperial Pavilion and Imperial Loge are some other additions (Figure 3.12) which did not exist during the Christian period. As another significant addition, huge disks of inscriptions/ calligraphies over wooden roundels with diameter of 7.6 m, are acknowledged to be largest inscriptions in the entire Islamic world (Eyice, 1984, vol.3).

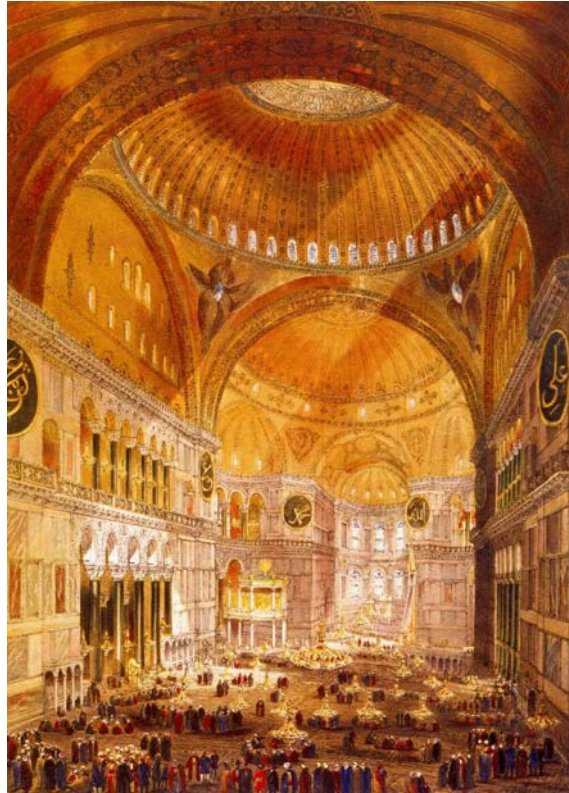


Figure 3.10. Hagia Sophia interior view - an old painting (Source: Akgündüz et. al, 2006: 284)

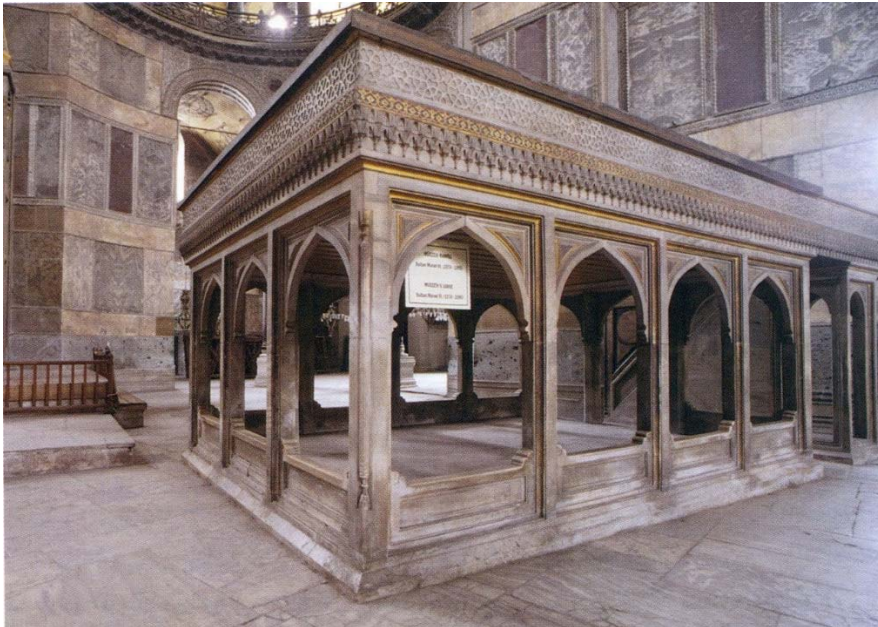


Figure 3.11. Muezzin's mahfili, Hagia Sophia (Source: Akgündüz et. al, 2006: p.179)



Figure 3.12. Imperial Pavilion and Loge - on the left, preaching pulpit – on the right (Source: Akgündüz et. al, 2006: 176, 180)

As Hagia Sophia ended up to be a mosque, and later become a museum, initially all the carpets on the floor were removed. In 1932 upon order from Atatürk, Prof. Thomas Whittemore -founder of the Byzantine Institute of America- had been given the permission to uncover and clean the mosaics (Oyhon and Etingü, 1999). In 1992, a major restoration and consolidation of the mosaics in the dome was started by the Central Laboratory for Restoration and Conservation of İstanbul in collaboration with an international team of experts funded by UNESCO (Klenbauer, 2004). Not all listed here but many other Hagia Sophia restoration works has taken in its lifespan. Even today the scaffoldings cover a huge space within the interior space for observable mosaic damages currently due to the water leakage and humidity at the central dome.

In this section it is aimed to brief and highlight some significant changes within the interior space of Hagia Sophia that would as well have affected its acoustical field. In the context of this study, multi-slope investigations over the sound decays of

collected impulse responses rely on the *current condition* of Hagia Sophia as detailed in the following section.

3.2.2. ARCHITECTURAL FEATURES AS OF TODAY

The major figure of Hagia Sophia is an expanded dome basilica: a rectangular building covered by a central dome between two half domes and integrating longitudinal and centralized planning (Figure 3.13 and Figure 3.14). This structure has an interior length of 73.5 m and a width of 69.5 m, excluding the narthex and the apse. The length of the entire interior from the exonarthex to the edge of the apse is 92.25 m. The central space of the Hagia Sophia, the naos, is divided on both sides from the side aisles by four big piers and the columns between them. The central nave is built on east-west axis, and a large dome is constructed right in the center to cover up the space. In overall with an approximate volume of 200.000 m³, Hagia Sophia has an outstanding interior volume that creates outstanding virtual and acoustical environments.

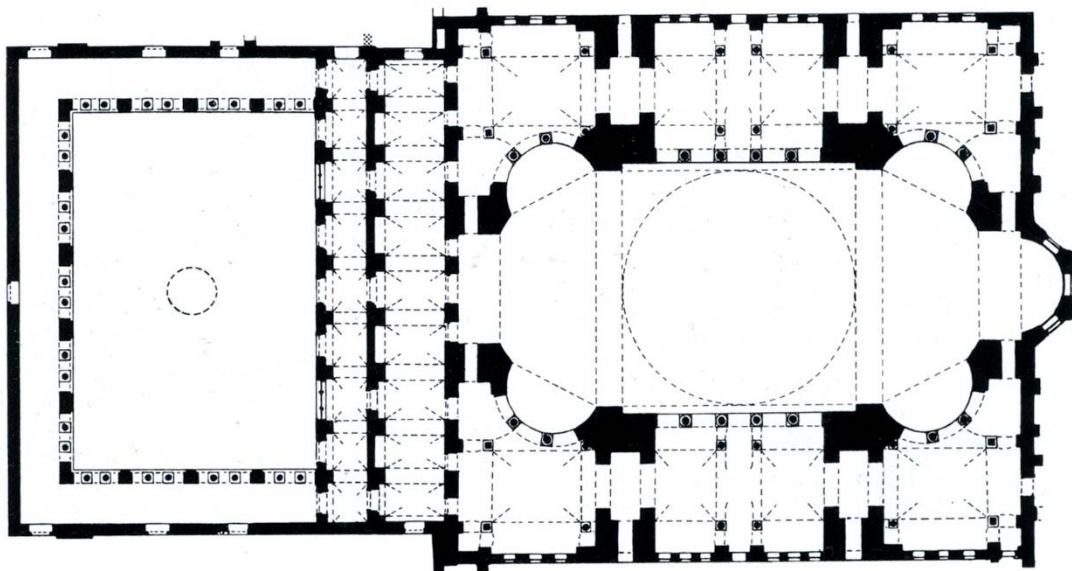


Figure 3.13. Plan view of Hagia Sophia (Source: Mainstone, 1988: p.250)



Figure 3.14. Section view from the central axis by Salzenberg, Hagia Sophia (Source: Akgündüz et. al, 2006: p.280)

The central dome that rises 55 m above the pavement of the nave is not exactly round but slightly elliptical today, with a diameter of 31.24 m on one axis and 32.81 m on the other. In order to keep the basilica design on both sides of the central nave, rather than semi domes there are columns, arches and vaults. From the crown of each of the main pier and between the four great arches, the pendentives fan out on the interior and rise to a roughly circular projecting cornice. The central nave of the Hagia Sophia is lighted by the dome windows together with the windows in the upper walls (tympana) that fill the space between the large arches on either side (Klenbauer, 2004; Eyice, 1984, vol.1).

The domed center space is skirted by two large hemicycles covered by half domes to the east and west. The diameter of these half-domes roughly equals to that of the central dome. The base of each half-dome is fenestrated with a ring of five windows, providing another source of natural illumination. These core spaces are separated from one aisle to the north and another to the south by superposed colonnades, with galleries over the side aisles and inner narthex, creating a U-shape that reinforces centralizing tendency of this expanded dome basilica. Curved columnar exedra rise up in both storeys at the diagonals of the hemicycles toward the corners of the aisles and galleries, and each of the exedra is covered by a semi dome again pierced by a

ring of windows. This central oval vessel of enclosed space is further expanded by barrel-vaulted spaces that terminate along the building's longitudinal axis at the east and the west ends of its nave (Klenbauer, 2004).



Figure 3.15. Interior view from south gallery, Hagia Sophia (Source: Akgündüz et. al, 2006: p.91)

Stone, brick and mortar make up all the main elements of the above-ground structure -the piers, columns, arches, vaults and dome-. Stone is either limestone or green stone -local granite-. Four main piers and the four secondary piers are constructed out of stone up to springing's of the gallery vault. Above the springing level of the gallery vaults most of the piers are built of brick. The surfaces of all the walls as well as the large supportive piers are covered with polished slabs of veined marble and other colored stone -bordered by long narrow strips of marble of wider sculptured moldings-. The spandrels and soffits of the colonnades on the ground floor are faced with white marble. Internally most of the original marble revetment of the walls remains in place at ground level (Klenbauer, 2004; Mainstone, 1988).

Most of the original non-figural mosaic decoration of the vaults has remained undamaged at ground level. Some of the non-figural decoration in the galleries and above distinguished partly by a much greater use of tesserae cut from natural stones and terracotta. All surviving figural mosaics are of later date; the survivals are

however only a small fraction of what was once there. The floor of this broad space is paved today with large rectangular marble slabs -not the original one which are crushed in 1346- (Mainstone, 1988; Eyice, 1984, vol.1).

CHAPTER 4

METHODOLOGY

In the extent of this research, sound fields within multiple dome superstructures are investigated by the use of ray-tracing based room acoustics simulations, field measurements including classical room acoustics measurements and 3-D sound intensity measurements and finite element solvers with diffusion equation model application for acoustical data collection. These data collection methods and data analysis approaches, specifically decay parameter estimation within Bayesian formation, are detailed under this section. Room acoustics simulations, diffusion equation modeling and intensity probe measurements are held over the major case of Süleymaniye Mosque. Field measurement and decay parameter estimations are held for both Süleymaniye Mosque and Hagia Sophia.

4.1. ROOM ACOUSTICS SIMULATIONS

Technological developments provide new opportunities for acoustical design and assessment of a space in the design phase that used to be done with scale-models. It is now possible to use computer simulation to analyze acoustical properties prior to the actual construction of a building in testing different alternatives in a short time span, while acoustical design can become an integral part of the architectural design process (Schmidt and Kirkegaard, 2004). Computational modelling has also been a considerable part of theoretical experimentations and has proven to be a viable tool in single space enclosures. Moreover, some pioneer room acoustics software developers have recently been developing algorithms to improve the products

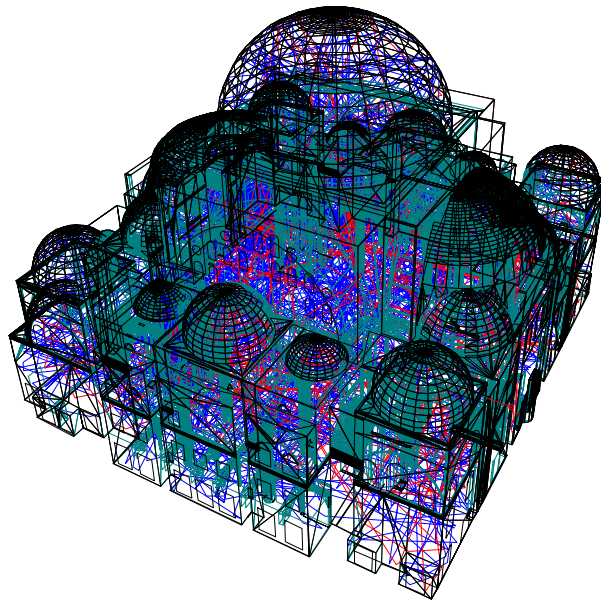
(simulation software) for acoustical coupling cases as discussed in the literature review.

As a pilot case ray-tracing simulations of Süleymaniye Mosque are held both before and after field measurements. Aim of pre-simulation studies is to provide initial guess and aid source and receiver location selections for field tests. Aim of post-simulation studies is to adjust model in lieu with field test results for following experimental study. Moreover, simulations are employed in order to assess and compare the occupied state with unoccupied state of the Mosque, as a practical cause field tests can only be held when the facility is not in use. This method is also utilized to compare interior finish material usage (specifically to compare historical plasters to cement based plasters) for different states/times of the Mosque.

Different phases of simulations is carried by ODEON Room Acoustics software version 12.12 which is originally released by the Technical University of Denmark (Naylor, 1993). The calculation method of this software is based on prediction algorithms including hybrid models of the image-source method, ray tracing and classical diffusion/scattering models. The ODEON Room Acoustics program also takes into account the statistical properties of the room geometry and absorption characteristics of surface materials (Rindel, 2000). Ray tracing model computations form the base of real-size experiments, which in result can provide the grounds to discuss the correlation of simulations and field measurements in acoustical coupling investigations.

The 3D acoustical model of Süleymaniye Mosque that reflects its current status is generated by joint use of AutoCAD-2D and SketchUp-3D modelling software; in reference with the latest *röleve*'s obtained from T.R. Prime Ministry Directorate General of Foundations Archive (2011). In the process of modification of the geometry the graphical model is preserved in great detail in order to maximize the effects of domes and scattering surfaces, while keeping the limits of minimum

surface dimensions dictated by the theory behind the software. The simplified model of Süleymaniye Mosque made up of 3-D face elements is comprised of 38,478 plane surfaces. Acoustical model is then imported into ODEON. Visualization of ray tracing is used majorly in sound path analysis and for checking waterproofness of the model (Figure 4.1). In calculation parameters number of late rays is defined to be 329,283 and the impulse response length is set to 15,000 ms. Estimated acoustical volume of the mosque is approximately 129,000m³.



Odeon©1985-2013 Licensed to: MEZZO Studio, Turkey

Figure 4.1. Süleymaniye Mosque, ODEON ray tracing view

Materials are defined with associated sound absorption and scattering coefficients of the interior surface materials. Dark colors in 3D-OpenGL view indicate absorptive materials, while light color scheme stands for the sound reflective surfaces (Figure 4.3). In pre-field simulations initial guess of the materials are made in accordance with previous acoustical field tests (Topaktaş, 2003; CAHRISMA, 2001; CAHRISMA, 2003). Sound absorption coefficients of materials in post-field simulations are adjusted according to the field test results held in 2013 within the context of this thesis research. The sound absorption coefficient data of people on

prayer area applied in simulations -reflecting occupied state of the mosque- are taken from previous laboratory tests on mosque congregation (Ahnert et al., 2013).

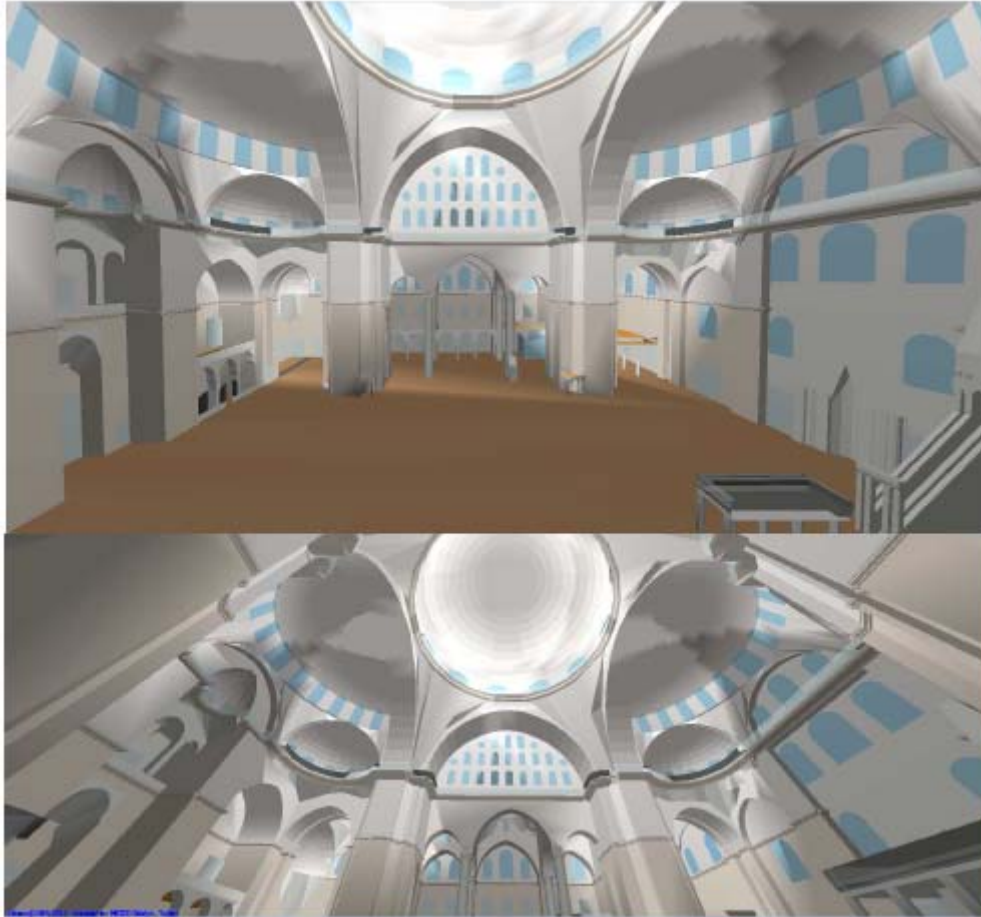


Figure 4.2. 3D-OpenGL view of modelled Süleymaniye Mosque

The source and receiver locations are integral part of the investigation, as coupling is highly dependent on these variables. Simulations are able to give clues on the most appropriate placing of sources and receivers for following field experiments that augments non-exponential decay formation. Omni-directional sound source is initially attained in simulations as in classical reverberation time estimations/measurements; in front of *mihrab* at 1.50 m depicting standing imam. Twenty two receivers are distributed throughout the prayer zone as of standing prayer positions (Figure 4.4). Three different source locations are tested which are one at *minbar*, one above *müezin's mahfili*, one underneath central main dome and

one underneath side corner dome. Impulse responses are obtained for each receiver position for different source locations, which are then exported from ODEON in *.wav format to be analyzed by the decay parameter estimation method as discussed in following sections.

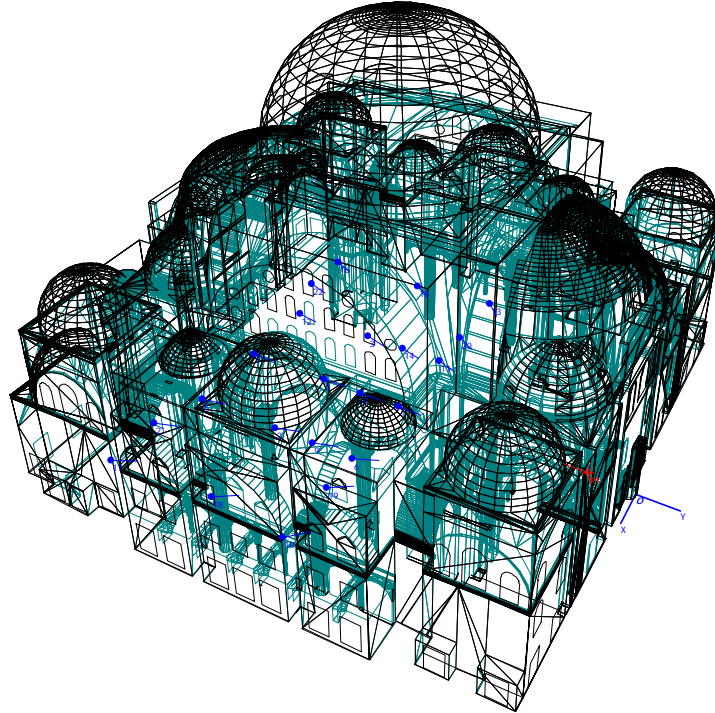


Figure 4.3. Süleymaniye Mosque ODEON acoustical model with source (red) and receiver (blue) positions

4.2. ROOM ACOUSTICS MEASUREMENTS

In assessing room acoustic parameters acoustical field measurements are held in accordance with ISO 3382-1 (2009). B&K (Type 4292-L) standard dodecahedron omni-power sound source is used in acoustical signal generation with B&K (Type 2734-A) power amplifier. The impulse responses at various measurement points are captured by B&K (Type 4190ZC-0032) microphone, incorporated into the hand held analyzer (B&K-Type 2250-A). Sampling frequency of the recorded multi-spectrum impulse is 48 kHz, covering the interval of interest between 100 Hz to 8000 Hz. The

height of the omni-power sound source and microphone heights are adjusted by light-weight tripods B&K Type UA-0801. DIRAC Room Acoustics Software Type 7841 v.4.1 is used for both generating different noise signals and for post processing of the measured impulse response data for each receiver position. The general set-up for room acoustic measurements is given in Figure 4.4.

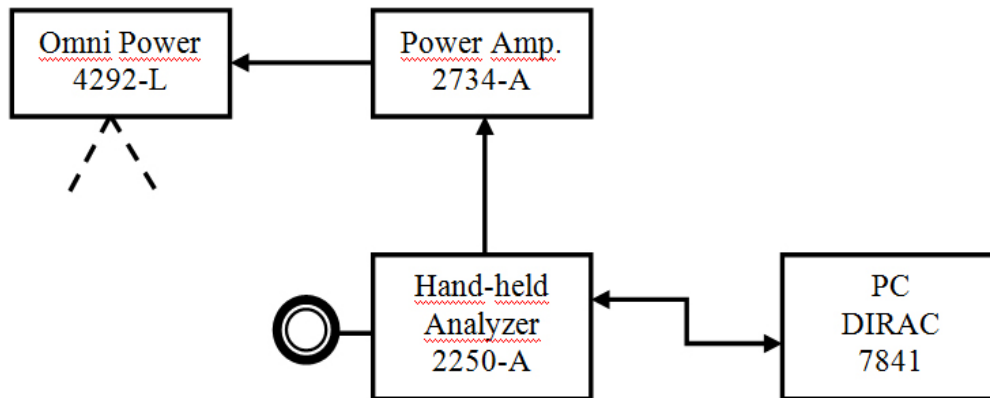


Figure 4.4. Measurement set-up of field tests (Source: produced by the author)

4.2.1. SÜLEYMANIYE MOSQUE MEASUREMENTS

Süleymaniye Mosque field tests are held in 23rd February 2013, hours in between 19.30(pm) - 3.00(am) (Sü Gül et al., 2013d), when the Mosque is unoccupied and there exists the minimum background noise (environmental, traffic etc.) within the main prayer hall. For estimating the basic features of sound field the impulse responses are collected. The major intention is to get the Schroeder decay curves, which are the logarithmic expression of impulse responses, from which many of acoustical parameters can be estimated (Schroeder, 1965) including classical RT, EDT or C80 parameters as well as the decay rates for coupling investigations.

When measuring an impulse response the dynamic range is limited by background noise. If the background noise is high in the environment where the impulse is collected, then within the signal the sound decay interval that includes clues on important acoustical features could be lost or distorted. For that reason, the time or

environment of collected impulses are so crucial in these noise sensitive measurements. This fact can significantly influence all parameters that can be derived from the impulse responses, especially if the noise level is not low enough to be compensated for. This level of reliable decay range is highly important in multi slope decay analysis. For that reason in Süleymaniye Mosque field tests it is aimed to get signal that is at least 50 dB higher than the noise in all octaves (Impulse to Noise Ratio - INR > 50 dB).

For the same reason; in obtaining the purest signal (least distortion) and highest INR, at each source-receiver configuration tests are repeated multiple times with different types of signals (e-sweep & MLS, MLSpink) and for different pre-averaging values (2-5). The length of impulse is set to be 21.8 s, which is the highest allowable range of DIRAC software. The length of impulse is also important in terms of not biasing the data in multi-slope analysis. In other words, if the data to be cut earlier than some probable later decays, the analysis result could indicate less slope numbers than the actual.

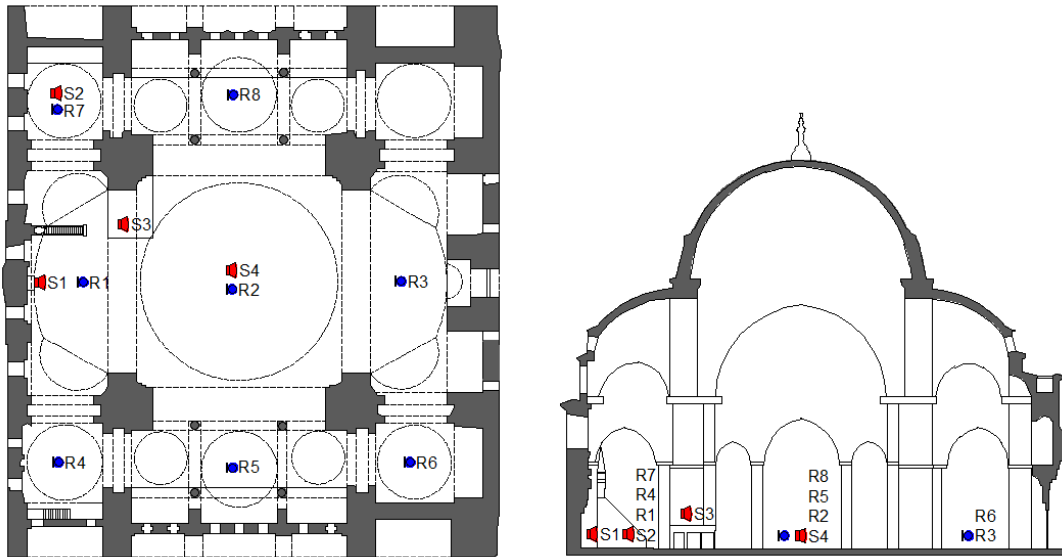


Figure 4.5. Süleymaniye Mosque field tests source(S) and receiver(R) locations; plan view (on left), section view (on right)

Source and receiver locations are selected in accordance with the simulation results yielding most probable coupling configurations. Major source locations are one in front of *mihrab* (S1) and one at *müezzin mahfili* (S3) as part of classical acoustic parameter calculations to assess the acoustics for traditional uses of mosque. *Minbar* location could not be tested due to the proximity of the source to the closest surface (*mihrab* wall), which is not applicable according to the standards (ISO 3382-1, 2009). For coupling search, additional source locations such as one underneath the main dome (S4) and one underneath side corner dome (S2) are tested (Figure 4.5 and Figure 4.6). Eight receiver locations (R1-R8) are coupled with four source locations (S1-S4) providing measured source-receiver configuration spots.

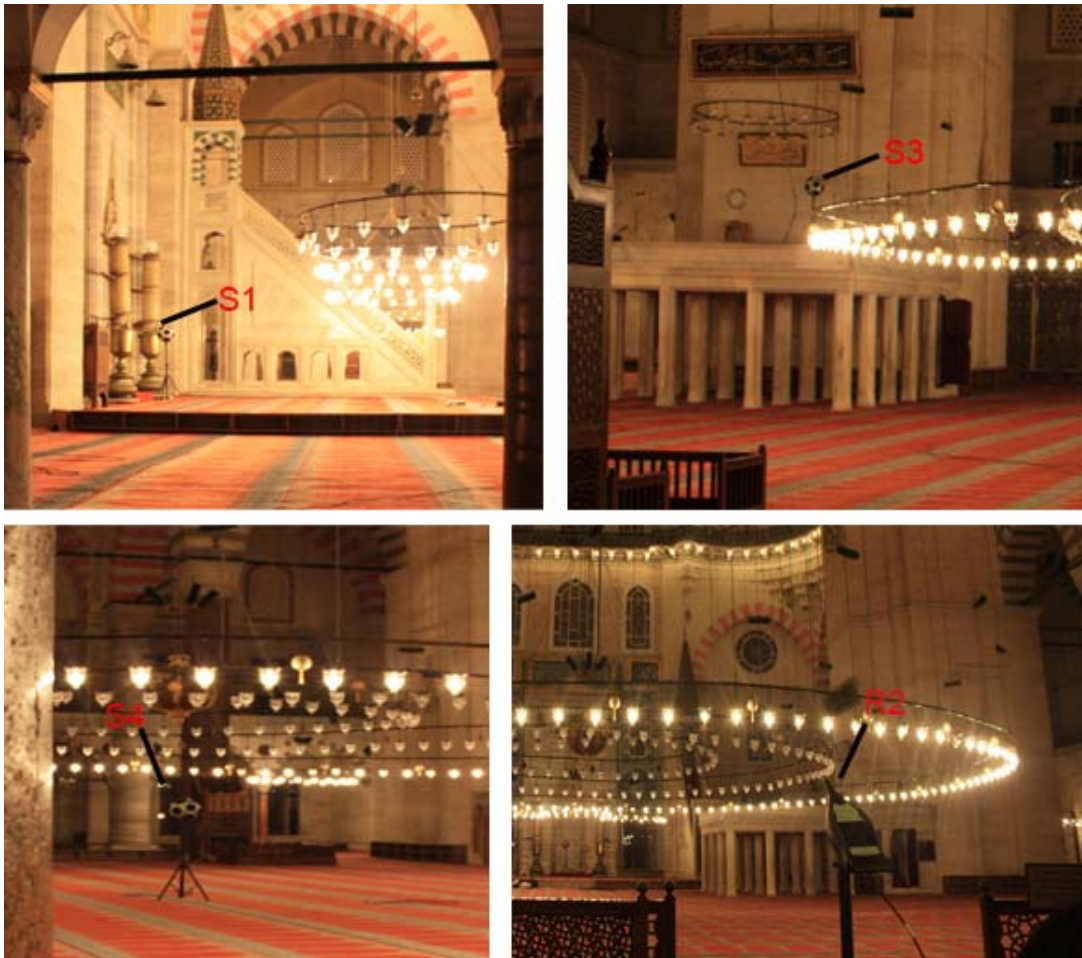


Figure 4.6. Süleymaniye Mosque field measurement photographs, 23rd February 2013

For each microphone-source configuration, with multiple signal and pre-average tests, in total 83 impulse responses in *.wav format are obtained. Files are then post-processed with DIRAC for room acoustics parameter estimations (T20, T30, EDT, C80). Separately, impulse responses (*.wav) are computed by Bayesian decay parameter estimation approach for multi-decay curves formation analysis, which is detailed in following sections.

4.2.2. HAGIA SOPHIA MEASUREMENTS

Hagia Sophia field measurements are held in 25th August 2014, hours in between 09.00 -12.00 at ground floor, as for permitted. For estimating the basic features of sound field, the impulse responses are collected at different source and receiver positions. For reliable decay parameter estimations during the post-processing of collected impulses, it is aimed to get signal that is at least 50 dB higher than the noise in all octaves (Impulse to Noise Ratio-INR > 50 dB). The usable impulse response range has been an important issue not only for this study, but it is a problematic for many other room acoustics measurements. For that reason, some researchers are in the process of developing new techniques (artificial) for extending room impulse responses beyond their noise floor in the phase of post-processing (Bryan and Abel, 2010).

An impulse response can be obtained directly by recording the response to hand-clapping, popping of a balloon/paper-bag, a gunshot or even with a hard footstep. By some researcher's balloon pop measurements, to be used in auralizations, has been previously applied in Hagia Sophia, as it is a compact solution and desires no electric power. However the overall spectrum of the impulse density has not been found dense enough, so different techniques over balloon pop signals are proposed to overcome this disadvantage (Abel et al., 2010).

A more technologically developed/modern method is the impulse obtained indirectly by producing a Maximum Length Sequence (MLS) or a sweep signal using an

electro acoustic source. The excitation by these later cases provide substantial amount of energy that in return allowing superior signal to noise ratio (S/R). Reproducibility is also easier to be controlled by electro-acoustic stimuli, due to uniform radiation (Christensen et al., 2013).

In Hagia Sophia measurements for obtaining the purest signal (least distortion) and highest INR, at each source-receiver configuration tests are repeated multiple times with different types of signals. Three major source signal types that are repeated for each measurement position are e-sweep, balloon pop and wood clap. The reason for testing different source signals is to identify the type that provides highest INR values throughout the frequency spectrum, as high INR values are directly related to multi-slope observation/detection in a decay curve.

The duration for collecting impulses should also be long enough, so that the decay can provide its all probable multi-slope patterns. For that reason, the length of impulses are set to be 21.8 s, which is the highest allowable range in DIRAC software. It is also acknowledged that the signal to noise ratio (S/N, INR) increases by 3 dB per doubling of sweep length (Christensen et al., 2013). However, the long sweep signals is also under discussion in terms of their liability to distortion.

In order to compare multi-slope decay formation for different locations considering the effects of architectural/spatial variations (such as main central space versus underneath side galleries) within Hagia Sophia, three source (S1 - S3) and six receiver (R1 – R6) positions are tested in various configurations (Figure 4.7 and Figure 4.8). Total of 33 impulse responses are gathered and reliable data are selected for future DPE analysis considering INR, and excluding data with distortions, echoes/flutter echoes and deviations from overall range.

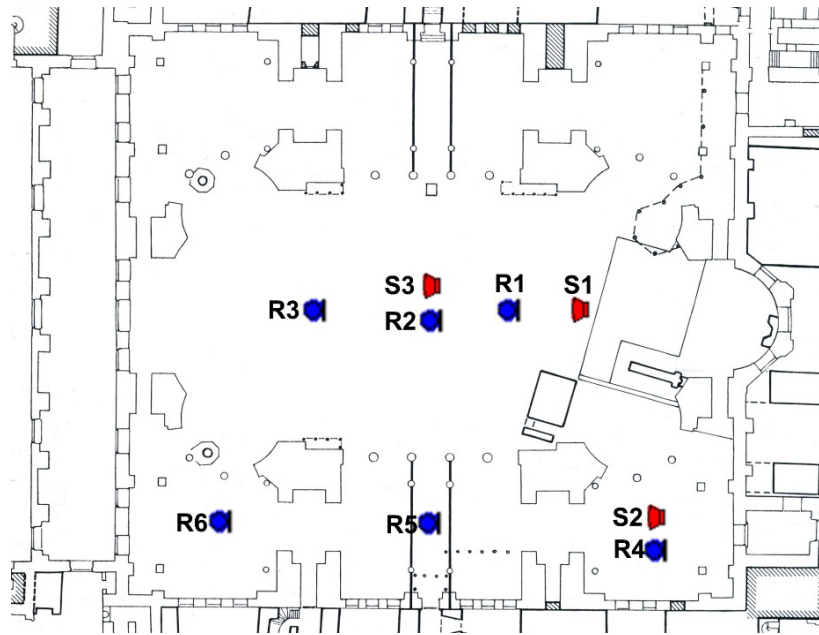


Figure 4.7. Hagia Sophia field tests source(S) and receiver(R) locations; plan view

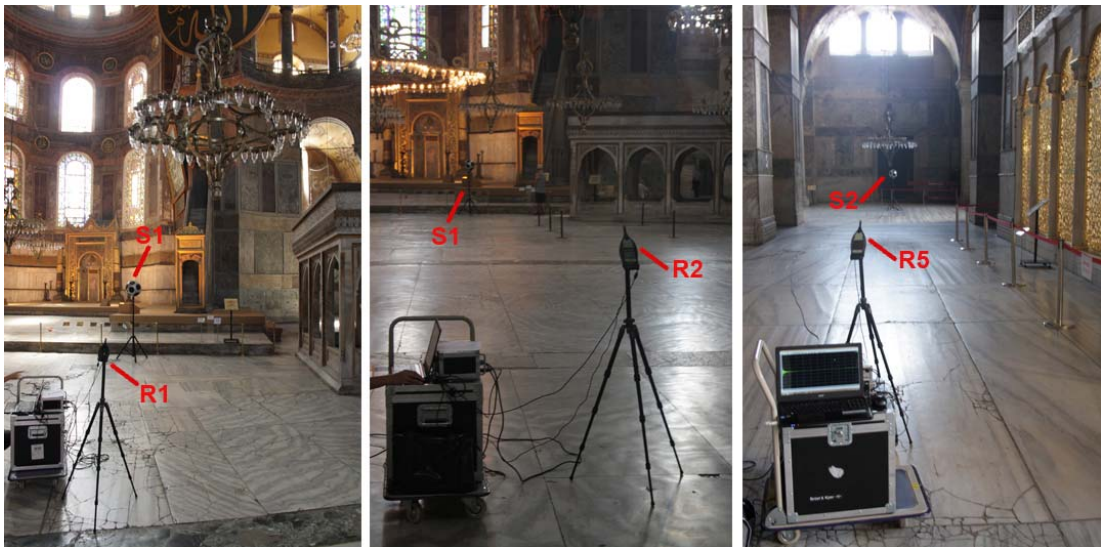


Figure 4.8. Hagia Sophia field measurement photographs, 25th August 2014

4.3. DECAY PARAMETER ESTIMATIONS (DPE)

Decay parameter estimations (DPE) of the acoustical data in this research basically relies on the analysis of real and simulated impulse responses. The reliability of data analysis is of priority, considering the fact that most of some previous research

findings, as detailed in literature review, are questionable or have limitations to specific cases. The method for final data computation should be scientifically approved and be applicable for generalized case conditions.

Decay rate and decay order estimations of multiple slopes have always been a challenging task. Methods for identifying double-slope decays and the degree of coupling are proposed. Visual inspection, comparisons of linear-fits of different portions of logarithmic decay functions or applying ratio based quantifiers without considering their absolute values are proved to be scientifically ineffective by some recent studies especially when the decay profile has more than two slopes.

The computational analysis methodology of this study employs Bayesian probabilistic inference as an efficient tool. Bayesian analysis has long been applied by researchers (Xiang and Goggans, 2001; Xiang and Goggans, 2003; Xiang et al. 2005; Xiang et al. 2010; Xiang et al. 2011) and reliable methods in characterizing sound energy decays consisting of one or two slopes has been presented. Bayesian probability theory is a quantitative theory of inference that includes valid rules of statistics for relating and manipulating probabilities. It considers all the given information on the data input and determines local extremes. The parameters that are out of interest can be incorporated and averaged over or marginalized. Marginalization reduces the dimensionality of the parameter space enabling a better handling of the parameter.

The analysis method starts with data collection in form of impulse responses. Out of these collected sound files energy decay curves can be obtained. Schroeder's backward integration, which defines Schroeder decay function, is also the essence of reverberation time calculations. It gives a smoother shape to the energy decay curves, making it easier and reliable to compute many other objective acoustical parameters. Bayesian model-based parameter estimation, relying on the model approximation of real-data out of Schroeder curve, is used to produce an algorithm

for the evaluation of multi-rate decay functions. It allows for the estimation of the number of decay rates without requiring an initial guess on the number of slopes inherent in the decay. The analysis method is used to determine the parameters of the decay profile, namely the slopes of the decays and ordinate intercepts of those slopes.

Bayesian model based parameter estimation is founded on the Schroeder decay model, which is a generalized linear model consisting of linear combinations of a number of nonlinear terms or exponential terms. Schroeder decay functions are obtained through Schroeder backward integration. Parametric model describing Schroeder decay function is as follows;

$$H_s(A, T, t_k) = A_0(t_K - t_k) + \sum_{s=1}^S A_s \left(e^{\frac{-13.8 \times t_k}{T_s}} - e^{\frac{-13.8 \times t_K}{T_s}} \right) \quad (5.3-1)$$

where $1 \leq t_k \leq K$

Parametric model describing Schroeder decay function contains decay parameters of A_s and T_s , where A_s is the linear amplitude parameter and related to the level of individual exponential decay terms, T_s is the decay time associated with the logarithmic decay slope of individual exponential decay terms, with $s = 1, 2, \dots, S$, and S is the maximum number of exponential decay terms, also termed as the decay order, $A_0(t_K - t_k)$ is the noise term, and t_k is the upper limit of integration (Xiang et al., 2011).

The question of how many decay slopes are in the energy decay data has always been challenging. Evaluating degrees of the curve fitting leads to over-parameterized models, since increased decay orders always improve curve fitting. As a scientifically rigorous solution Xiang et al. (2011) propose to evaluate the Bayesian evidence which automatically encapsulates the principle of parsimony and

quantitatively implements Ockham's razor. Bayesian evidence prefers simpler models and penalizes over-fitting, so that it offers effective tools to conduct model selection and comparison going beyond traditional parameter estimation methods. The quantifier is defined to be Bayesian Information Criterion (BIC), which subtracts the penalty of over-parameterized models from the degree of the model fit to the data. Bayesian model selection is a scientifically rigorous approach to ruling out wrong models, or competing unnecessary models. In the scope of the energy decay analysis among a set of decay models, the model yielding the largest BIC value is considered to be the most concise model providing the best fit to the decay function data and at the same time capturing the important exponentially decaying features evident in the data. Applying BIC for ranking the competing decay models, such as double-slope, triple-slope, and even quadruple-slope decay models, is found appropriate for data analysis in this study.

To sum up, it could be clearly stated that visual interpretation is the roughest way of searching for multiple decays in a room impulse response. Moreover, visual inspection is subjective and may differ according to one's own way of look, which consequently is far away from being scientific. The term double-slope decay often vaguely characterizes decay functions which consist of a single or multiple decay components. Successful application of Bayesian analysis to the characterization of the Schroeder decay model of sound-energy decays demonstrates that methods for characterizing non-exponential decays through visual inspection, through comparisons of linear-fits of logarithmic decay functions on an arbitrarily chosen portion or applying ratio based quantifiers without considering their absolute values fail to capture important aspects of the system. Those quantifiers cannot generally provide a unique description for a non-exponential decay consisting of a linear combination of exponential decay functions and are scientifically questionable. For all that reason, Bayesian decay parameter estimation as described in this section has been found to be the most reliable analysis approach for coupling investigations on

either architecturally/visually coupled rooms or virtually coupled rooms in form of a single space with specific geometric attributes as of multi-domed superstructures.

4.4. DIFFUSION EQUATION MODEL (DEM) ANALYSIS

Diffusion equation model (DEM) theory for room acoustics applications have recently been investigated by many researchers as discussed previously in literature review. Due to its computational efficiency and provided advantages as of spatial energy density and flow vector analysis, it is chosen to be a viable tool for explaining or understanding the multi-slope formation in multi-domed single shell space superstructures, specifically Süleymaniye Mosque. In this section the governing and boundary DEM equations that fits most properly to this case study/s are presented.

4.4.1. INTERIOR DIFFUSION EQUATION

In a finite medium a source with an infinitely small dimension is considered to be emitting q particles per second omni-directionally. In a time interval dt , this source emits qdt particles. After a time t , all particles are located within a spherical shell of thickness cdt and radius ct , with enclosed volume $4\pi(ct)^2cdt$. The concentration of particles $w(r)$ at a distance r from the source is then;

$$w(r = ct) = \frac{qdt}{4\pi(ct)^2cdt} = \frac{q}{c4\pi r^2} \quad (5.4.1-1)$$

The acoustic energy density at a distance r from a source of power P emitting omni-directionally is $P/(c4\pi r^2)$ and c is the sound speed. In an infinite medium, the quantity or particle density q is analogous to the acoustical power P . By this analogy the model for the diffusion of particles in a medium containing spherical scattering obstacles can be used for modelling the scattering of the sound in enclosed spaces (Picaut, 1997; Valeau et al., 2006).

Assuming that a room has a volume of V , surface area of S , and an average surface absorption coefficient of $\bar{\alpha}$. The probability $P(x)$ of a particle to cover a distance x without any collision with a scatterer is described by an exponential distribution;

$$P(x) = Qne^{-Qnx} \quad (5.4.1-2)$$

where, n is the density or the number of scattering particles per volume unit, Q is the particle scattering cross-section. $\bar{\alpha}$ (between 0 and 1) is the probability for a scatterer to absorb a particle after a collision. The mean free path (λ) between two collisions is;

$$\lambda = \int_0^{\infty} xP(x)dx = \frac{1}{Qn} \quad (5.4.1-3)$$

In room acoustics, the analytical expression for the mean free path (between two collisions) in a room with diffusively reflecting boundaries is;

$$\lambda = 4V/S \quad (5.4.1-4)$$

A change of the sound energy density per unit time is associated with changes in the sound energy flow vector. In diffusion phenomena, the local particle-density flux $J(r, t)$ is approximated as the gradient of the particle density;

$$J(r, t) = -D \nabla w(r, t) \quad (5.4.1-5)$$

In the presence of an omni-directional sound source within a room or region/domain (V) with time-dependent energy density $q(r, t)$, the particle density or the acoustic energy density (w) at a position (r) and time (t) is;

$$\frac{\partial w(r, t)}{\partial t} - D\nabla^2 w(r, t) + cmw(r, t) = q(r, t), \quad \in V \quad (5.4.1-6)$$

where, ∇^2 is the Laplace operator, D is the ‘diffusion coefficient’, c is the speed of sound and m is the coefficient of air absorption. The diffusion coefficient D used in this equation is different from its definition in room acoustics, which is the proportion of diffuse reflections at the room surfaces. The diffusion coefficient D in Eq. (5.4.1-7) is a term that takes into account the room morphology through its mean free path which is;

$$D = \frac{\lambda c}{3} = \frac{4Vc}{3S} \quad (5.4.1-7)$$

where, λ is the mean free path, c is the speed of sound, V is the volume of the room and S is the total surface area of the room (Valeau et. al, 2006).

In Eq. (5.4.1-8) the source term $q(r, t)$ is zero for any subdomain where no source is present. In the theory of the diffusion of particles by scatterers, a point source emitting q particles per second is modelled by a source term equal to $q\delta(r - r_s)$, where r_s denotes the position of the source. Similarly, in a room-acoustics problem, for time-dependent solutions a point source with an arbitrary acoustic power of $P(t)$ can be modelled as follows;

$$q(r_s, t) = P(t)\delta(r - r_s) \quad (5.4.1-8)$$

Or can be modelled as an impulsive sound source as follows;

$$q(r_s, t) = E_0\delta(r - r_s)\delta(t - t_0) \quad (5.4.1-9)$$

where, δ is the Dirac-delta function and E_0 is the total acoustic energy at t_0 ($E_0 \approx P\Delta t$).

Above given equations are presented and applied by different researchers (Valeau, 2006; Billon et al., 2008; Xiang et al., 2009; Escolano, 2013). The algorithms have been the base for domain partial differential equations of Süleymaniye Mosque DEM application through a finite element solution.

4.4.2. BOUNDARY CONDITIONS

The diffusion equation is defined for ‘inside the domain (V)’ in previous section. The effects of enclosing room surfaces can analytically be expressed by boundary equations defined for ‘on the domain (V)’. If it is considered that in an enclosure/domain (V) the sound energy cannot escape from bounded surfaces (S), then the boundary condition equation is as follows;

$$J(r, t) \cdot n = -Dw(r, t) \cdot n = 0, \text{ on } V \quad (5.4.2-1)$$

where, n is the surface outgoing normal, D is the ‘diffusion coefficient’ and $w(r, t)$ is the acoustic energy density at a position (r) and time (t). Eq. (5.4.2-1) solves the so-called homogeneous Neumann boundary condition, which considers only an overall mean absorption coefficient $\bar{\alpha}$ of the enclosure under investigation (Valeau et al., 2006). The boundary condition that is established to include the energy exchanges on enclosing surfaces is as follows;

$$J(r, t) \cdot n = -Dw(r, t) \cdot n = A_X cw(r, t), \text{ on } S \quad (5.4.2-2)$$

where, c is the speed of sound, A_X is an exchange coefficient or the so called *absorption factor*. Assuming the sound energy density is uniform in a proportionate room while the energy density only varies along the long dimension in a disproportionated room, the absorption factor is expressed as follows;

$$A_X = A_S = \frac{\alpha}{4} \quad (5.4.2-3)$$

where, α is the absorption coefficient of the specific surface/boundary. The subscript S of A_S is used to denote Sabine absorption (Valeau et al., 2006). The diffusion equation model with this boundary condition is accurate only for modelling rooms with low absorption. To improve the accuracy of mixed boundary conditions associated with high absorption for specific room surfaces, the Sabine absorption coefficient in the absorption factor is replaced by the Eyring absorption coefficient as in follows (Billon et al., 2008);

$$A_X = A_E = \frac{-\log(1 - \alpha)}{4} \quad (5.4.2-4)$$

The subscript E of A_E is used to denote Eyring absorption. There exists a singularity within the diffusion-Eyring model given in Eq. (5.4.2-4), when the absorption coefficient for a surface in frequency of interest becomes 1.0. For resolving the singularity problem of the Eyring model a modified boundary condition is introduced (Jing and Xiang, 2008c). This final absorption factor term can be applied for mixed boundary conditions or more specifically for modelling the local effects of the sound fields that have comparatively higher absorption on specific surfaces, as given in following;

$$A_X = A_M = \frac{\alpha}{2(2 - \alpha)} \quad (5.4.2-5)$$

In Süleymaniye Mosque case given the fact that the room has an absorptive carpet floor -for specific octave bands- versus a low absorptive/reflective upper shell, its boundary condition fits best to the modified mixed boundary model. Thus, combining Eq. (5.4.2-2) and Eq. (5.4.2-5) gives the resulting system of boundary equation, as follows;

$$-D \frac{\partial w(r, t)}{\partial n} = \frac{c\alpha}{2(2 - \alpha)} w(r, t), \quad \text{on } S \quad (5.4.2-6)$$

In application of DEM analysis on Süleymaniye Mosque, initially the solid geometry of the space is re-generated using AutoCAD. The model is imported in a commercial finite element solver software, namely, COMSOL Multi-physics v4.03. Eqs. (5.4.1-6), (5.4.1-7), (5.4.1-9) and (5.4.2-6) are solved for total of 124,788 linear Lagrange-type mesh elements (Figure 4.9). The mean free path (MFP) of the room is estimated to be 18.26 m, and accordingly the mean free time (MFT) of the room is 0.053 s (53 ms). Maximum mesh element sizes are selected to be much smaller than the mean free path. In a time-dependent solution, resultant $w(r, t)$'s after relevant logarithmic scaling, in other words after conversion of sound energy into decibels, are used for spatial sound energy density distribution and sound energy flow vector analysis.

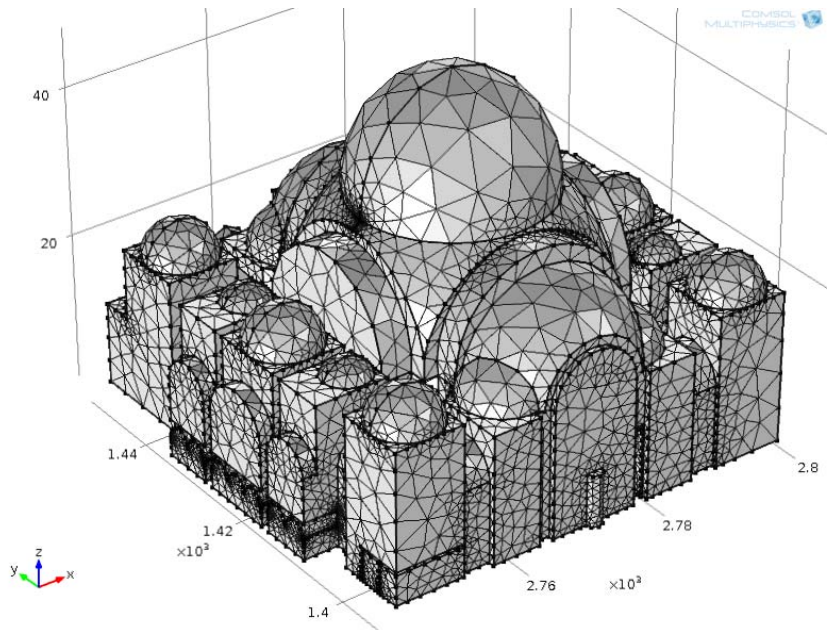


Figure 4.9. Süleymaniye Mosque solid mesh model

4.5. INTENSITY PROBE IMPULSE RESPONSE MEASUREMENTS

In order to support and validate findings out of DPE and DEM analysis, recording of three dimensional impulse responses, specifically for intensity vector analysis, of Süleymaniye Mosque case are found necessary. Thus, a final group of field test are taken with a different equipment set-up (in compare to classical room acoustics measurements) in Süleymaniye Mosque on 19th of December 2014, hours in between 20.00 (pm) - 00.00 (am). These hours are specifically preferred for minimum background noise and unoccupied state of the Mosque.

The basic component for collecting 3D impulse responses is the intensity probe. Conventionally, room acoustic measurements are based upon sound pressure microphones. By the invention of the Microflown sensor in 1994 (Bree et al., 1994), acoustic particle velocity has become a measurable quantity. Together with a regular sound pressure sensor, acoustic vector -acoustic pressure multiplied by particle velocity- can be measured. Intensity probes combine both sound pressure and particle velocity sensors; coupled with a pressure microphone, these probes can measure both kinetic and potential energy. Possible applications of such measurements via particle velocity and pressure incorporated probes, in relation to this research, are the mapping of the direction of incoming reflections versus time. With a sound pressure microphone a scalar quantity can be obtained, which does not provide directional information. Additionally, if the particle velocity can be measured in three directions the 3D intensity can be calculated (Tijds et al., 2009). Intensity is a vector indicating the direction of energy flow, thus it is instrumental for explaining and validating the energy flows and energy flow returns in relation to multi-slope energy formation.

In Süleymaniye Mosque measurements Microflown mini USP (1 pressure sensor and 3 orthogonally placed particle velocity sensors built in a single enclosure) is utilized. B&K (Type 4292-L) standard dodecahedron omni-power sound source and balloon pops are used for acoustical signal generation. The height of the omni-power sound

source (1.5 m above floor) and microphone heights (1.2 m above floor) are adjusted by light-weight tripods B&K Type UA-0801. Microflown 4 channel signal conditioner MFSC4 and Microflown data acquisition kit Scout 422 USB complete the measurement set-up. Microflown Velo 2.A Analyser is used for both generating e-sweep signals and for post processing of the measured impulse response data for each receiver position. The general set-up for room acoustic measurements is given in Figure 4.10.

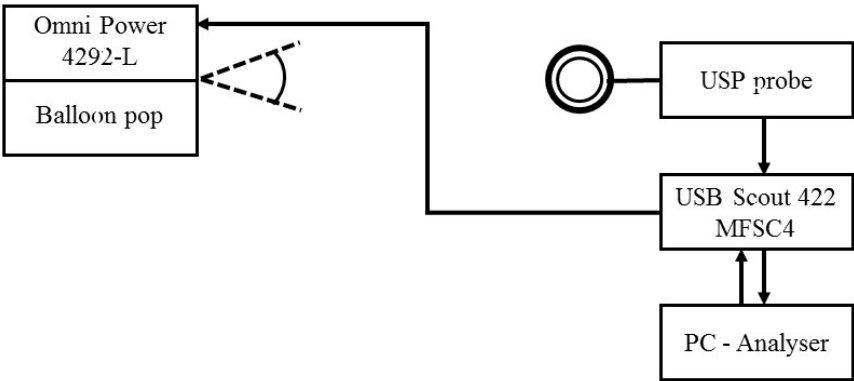


Figure 4.10. Measurement set-up for probe measurements (Source: produced by the author)

In this set-up using both e-sweep and balloon pops, total of 37 3D-impulse responses are collected for 4 source and 14 receiver locations (Figure 4.11). The time-averaged intensities are then calculated in three Cartesian coordinate directions from the pressure and velocity signals. The three-dimensional intensity vectors are then used to show the direction of the windowed reflection or energy flow. The instantaneous intensities are analyzed over different time windows for different source-receiver configurations and for different frequency ranges of interest. Critical outcomes are presented under Results section.

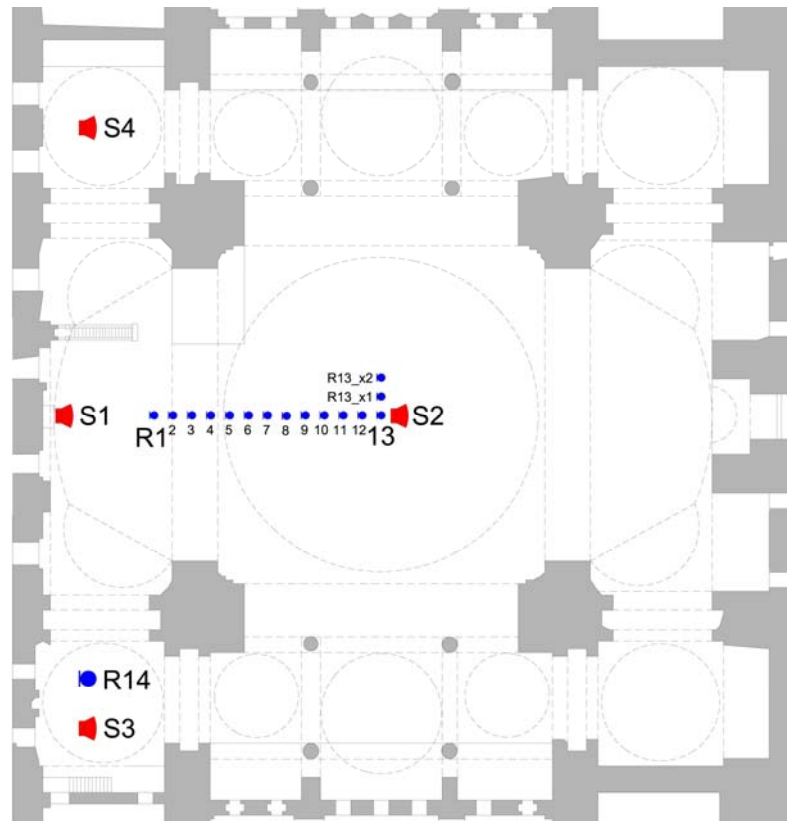


Figure 4.11. Plan layout of Süleymaniye Mosque probe measurements; source(S) and receiver(R)

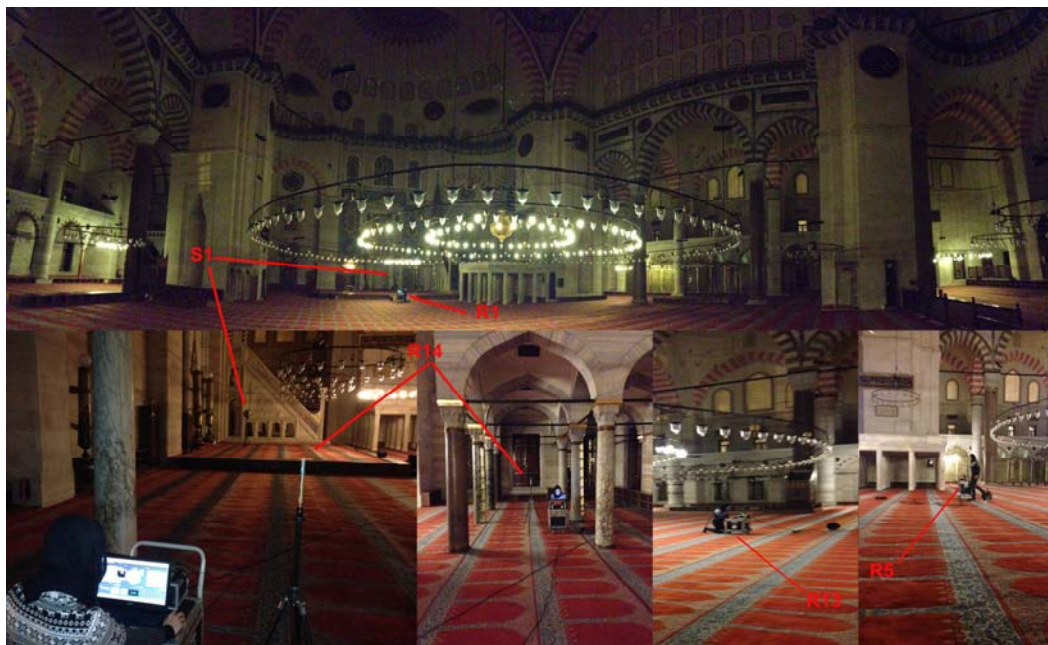


Figure 4.12. Süleymaniye Mosque probe measurement photographs, 19th December 2014

CHAPTER 5

RESULTS

Under this section findings out of field tests, room acoustic simulations, decay parameter estimations (DPE) and diffusion equation model (DEM) solutions are presented. Estimated or measured classical room acoustics parameters, more specific multi-slope decay parameters, and spatial sound energy distributions are analyzed. Detailed arguments on results comparison of different methods and different cases are given under Discussion section.

5.1. SIMULATION AND FIELD MEASUREMENT DATA

5.1.1. SÜLEYMANIYE MOSQUE FIELD DATA

In this section Süleymaniye Mosque room acoustics parameter field test results are presented. Out of collected total 83 impulse responses, for each receiver-source configuration the impulse with the highest INR and least distortion is included in post-processing. Source and receiver locations are previously illustrated in Figure 4.5. For 17 source-receiver configurations, Süleymaniye Mosque T30 results for 1/3 octave bands are presented in Table 5.1. The field test results, averaged over measurement positions for 1/3 octave bands are given for decay rates; T20, T30 and EDT in Figure 5.1, and for decay ratio; C80 in Figure 5.2.

Table 5.1. Süleymaniye Mosque overall T30 (s) field test results in 1/3 octaves

Location	Frequency (Hz)																	
	100	125	160	200	250	315	400	500	630	800	1000	1250	1600	2000	2500	3150	4000	5000
S1R1	19,3	17,0	14,7	11,2	6,8	4,9	5,7	6,6	6,5	6,3	5,9	5,1	4,3	3,7	3,0	2,7	2,2	1,6
S1R2	20,1	17,3	14,6	11,3	6,9	4,8	5,8	6,5	6,7	6,4	6,0	5,1	4,4	3,8	3,2	2,7	2,2	1,8
S1R3	19,7	17,1	15,1	11,9	7,1	4,5	6,2	6,9	6,9	6,6	6,1	5,1	4,4	3,8	3,2	2,7	2,3	1,8
S1R4	20,0	17,6	15,0	12,2	8,2	4,8	6,0	6,7	7,0	6,4	5,9	4,9	4,4	3,6	3,2	2,7	2,2	1,6
S1R5	20,0	17,3	15,3	11,8	7,5	4,7	6,2	6,7	6,6	6,4	5,9	5,1	4,5	3,8	3,2	2,8	2,3	1,8
S1R6	19,2	17,2	14,3	12,6	8,1	4,8	6,1	6,3	6,9	6,4	6,0	5,1	4,5	3,8	3,3	2,8	2,3	1,8
S2R1	20,3	17,6	14,6	11,7	8,0	4,8	6,3	6,8	6,5	6,5	5,8	5,2	4,5	3,8	3,2	2,6	2,2	1,7
S2R2	20,0	17,6	15,4	11,9	8,5	5,0	6,3	6,3	6,9	6,5	6,0	5,1	4,5	3,8	3,2	2,7	2,3	1,8
S2R4	19,8	16,9	14,8	10,4	8,5	4,6	5,8	6,9	6,6	6,5	5,9	5,0	4,4	3,8	3,2	2,7	2,2	1,8
S2R6	20,5	16,8	14,7	11,9	8,6	4,9	6,3	6,7	7,1	6,6	6,0	5,1	4,4	3,8	3,3	2,8	2,4	1,8
S2R8	19,8	14,8	14,1	11,5	8,4	4,5	6,0	6,6	6,8	6,4	5,7	4,8	4,2	3,6	3,0	2,5	2,0	1,6
S3R2	20,2	17,2	14,7	11,2	7,7	4,9	6,0	6,6	6,6	6,6	5,9	5,1	4,5	3,7	3,2	2,7	2,2	1,7
S3R5	20,7	17,6	14,1	11,5	8,7	4,8	6,1	6,7	6,9	6,6	6,1	5,2	4,5	3,7	3,3	2,7	2,3	1,8
S3R7	19,8	18,6	15,2	12,1	8,1	4,9	6,2	6,8	6,7	6,5	6,0	5,2	4,4	3,7	3,1	2,7	2,3	1,8
S4R3	20,2	16,0	14,4	11,1	8,1	4,9	5,9	6,8	6,8	6,4	5,9	4,9	4,5	3,8	3,2	2,7	2,2	1,7
S4R5	19,7	17,6	14,3	11,9	8,1	4,8	6,2	6,8	6,9	6,7	5,8	5,1	4,4	3,8	3,2	2,6	2,2	1,8
S4R6	19,6	15,3	14,9	11,7	8,8	5,0	6,0	6,8	6,7	6,7	5,8	5,1	4,5	3,8	3,2	2,7	2,2	1,8

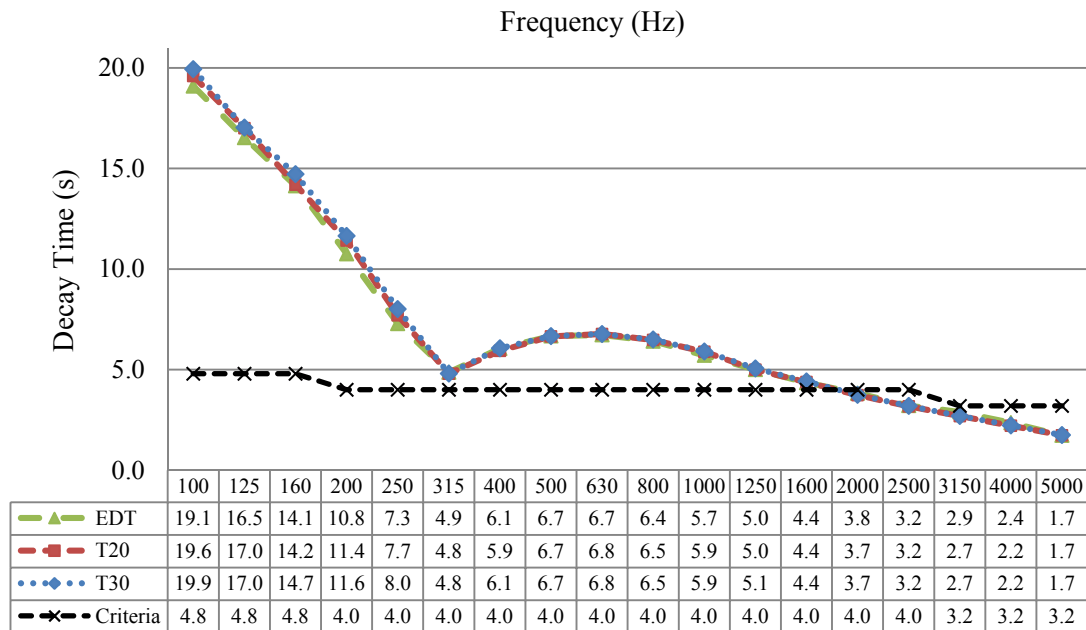


Figure 5.1. Süleymaniye Mosque average EDT, T20, T30 field test results in 1/3 octave bands and their comparison with upper limit of criteria for mosques in similar volume

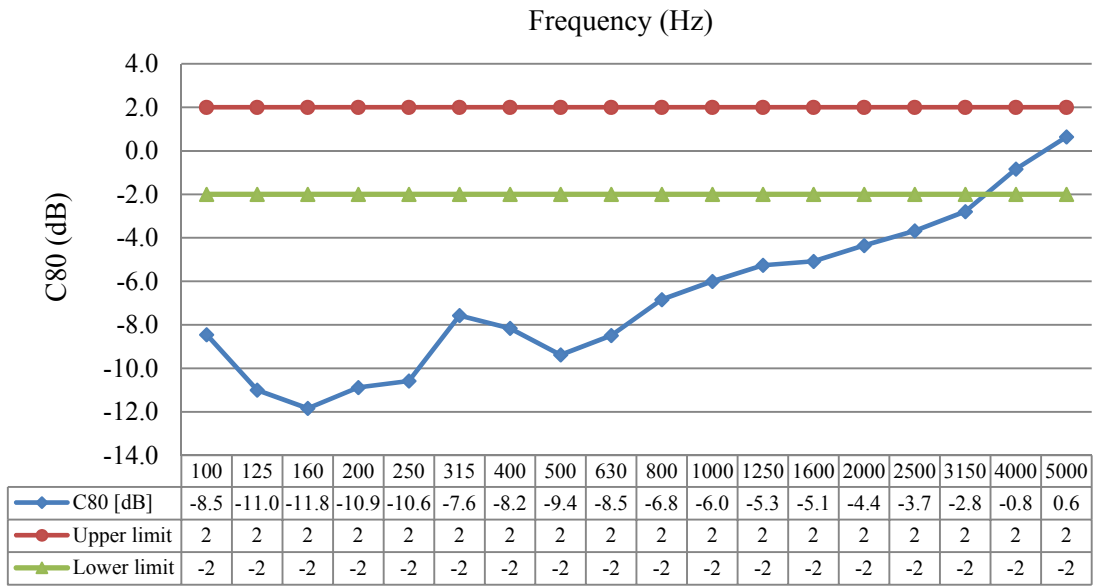


Figure 5.2. Süleymaniye Mosque average C80 field test results in 1/3 octave bands and their comparison with upper and lower limit of criteria for mosques in similar volume

Z-weighted equivalent background noise levels (Leq) measured during field tests and their comparisons with Noise Criterion curves (Beranek, 1971) are presented in Figure 5.3.

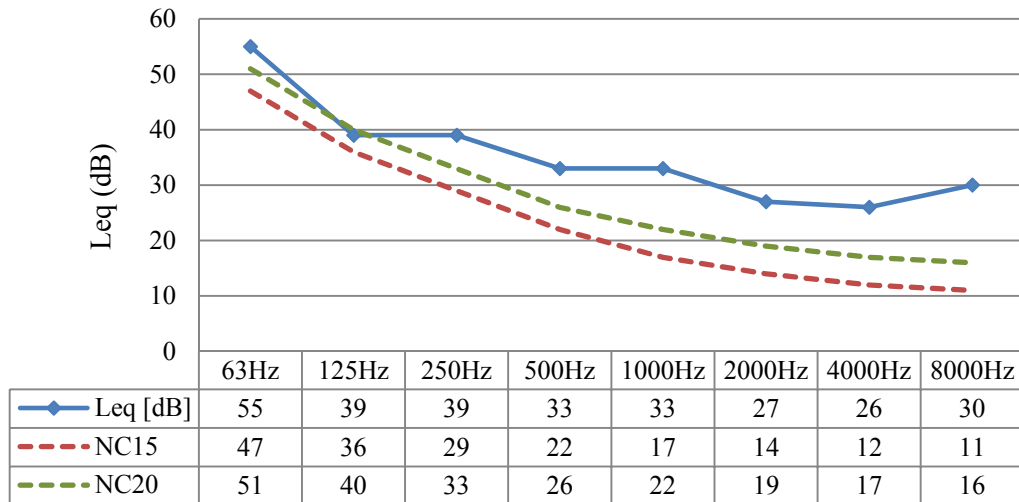


Figure 5.3. Süleymaniye Mosque background noise levels (Leq) in 1/1 octave bands and their comparison with NC15 and NC20 noise curves

5.1.2. SÜLEYMANİYE MOSQUE SIMULATION DATA

The purpose of acoustical simulations in different phases within this research are as follows;

- pre-field simulations: to provide initial guess and aid source and receiver location selections for 2013 field tests. The reference for material selection and acoustical adjustment of pre-field simulations are Topaktaş (2003) and CAHRISMA (2001) field measurement data.
- post-field simulations: by adjusting acoustical model in lieu with field test results experimental studies could be held in order to;
 - gather data for use in DPE analysis in coupling investigations,
 - assess and compare the occupied state with unoccupied state of the Mosque,
 - experiment with interior finish materials, specifically historical lime-based plasters, to highlight acoustical conditions in original state of the Mosque.

In this section initially simulated reverberation time parameter results (T30) of Süleymaniye Mosque for different cases are presented. The comparisons of T30 results of pre and post simulations over 1/1 octave bands are presented in Figure 5.4. T30 results of post-simulations representing the current state of the Mosque for its unoccupied condition (field test approximated model) and occupied condition (full occupancy representing Friday's sermon) are given in Figure 5.5.

For post-field tuned model, representing the current state of the Mosque, simulations are also held for plotting T30 results for the overall ground floor prayer zone. While in field tests it is practical to held measurements on some limited amount of receiver locations, ray-tracing simulation has an advantage for providing mapping of a complete zone under consideration. 2 m x 2 m grids are defined for the main prayer hall of Süleymaniye Mosque, while source is defined in front of mihrab wall

presenting *imam*'s position in classical use. Distribution maps are obtained for T30, C80, STI and SPLA. Results are presented in Appendix A.

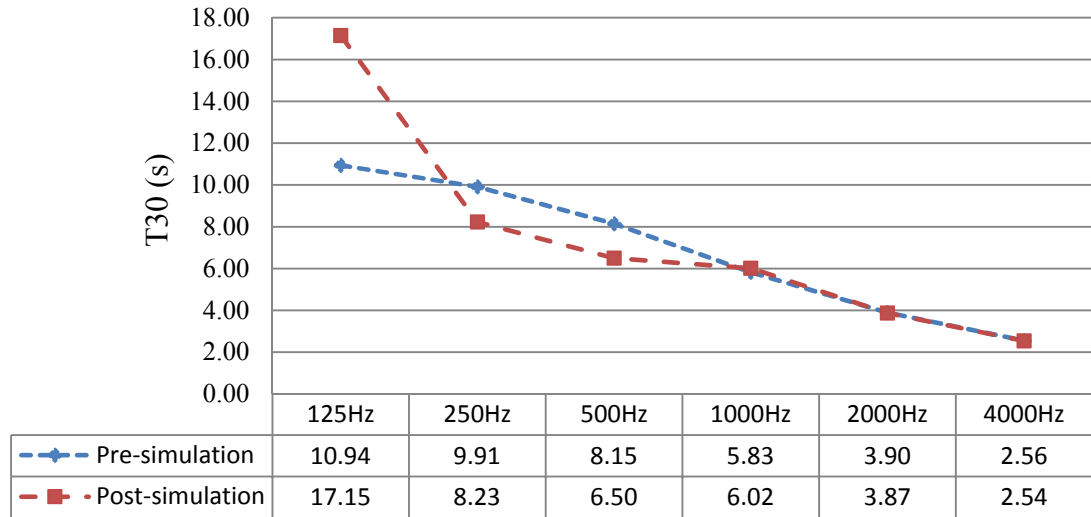


Figure 5.4. Comparison of T30 results for pre and post-field simulations, Süleymaniye Mosque

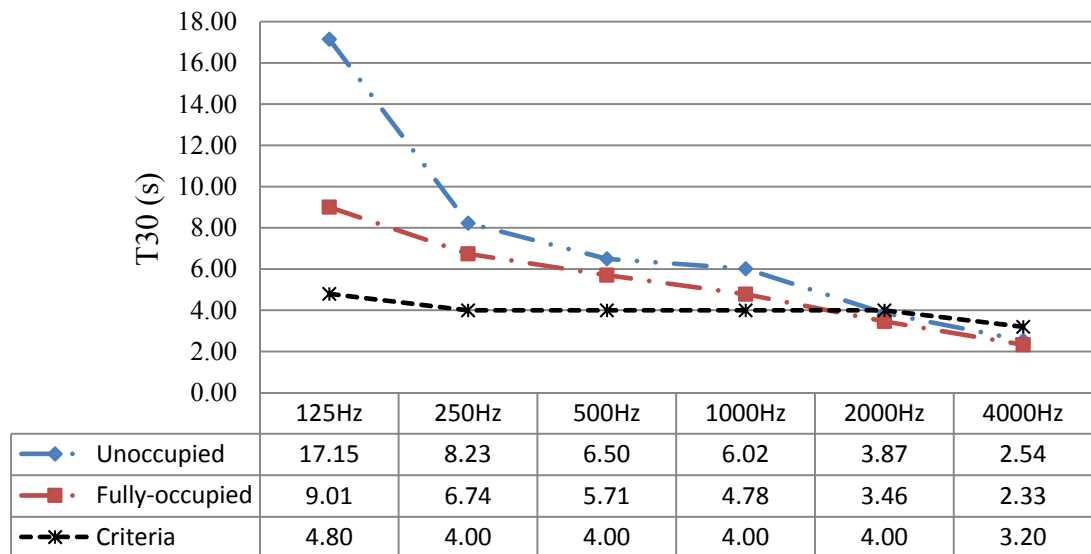


Figure 5.5. Comparison of T30 results for full and unoccupied Mosque in 1/1 octave bands and their comparison with upper limit of criteria for mosques in similar volume

As a pilot study the present plaster material input of the Mosque in field-tuned model is replaced with an historical lime based plaster, the sound absorption performance of which have been tested and presented in previous researches (Tavukçuoğlu et al.,

2011; Aydın, 2008). Comparison of T30 results of the Mosque with adjusted plasters and current state is given in Figure 5.6 for unoccupied state. Finally, the occupied and unoccupied states are compared for the case of historical plaster application, as for an approximation to the original state of Süleymaniye Mosque in Figure 5.7.

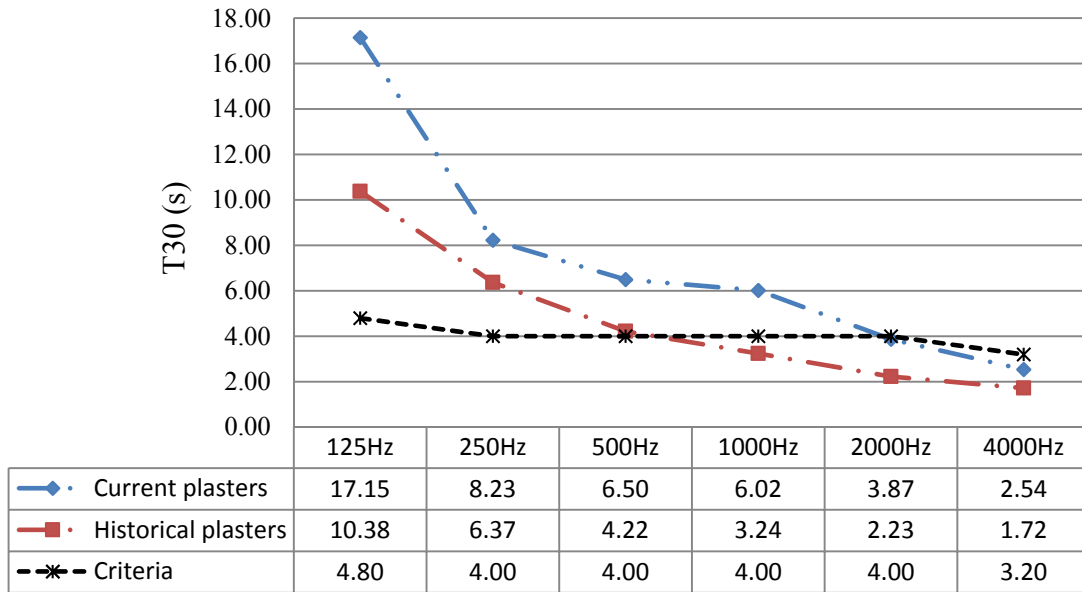


Figure 5.6. Unoccupied state of the Mosque, comparison of plasters; T30 results for current status of plasters and adjusted model with historical lime based plasters, and their comparison with upper limit of criteria for mosques in similar volume

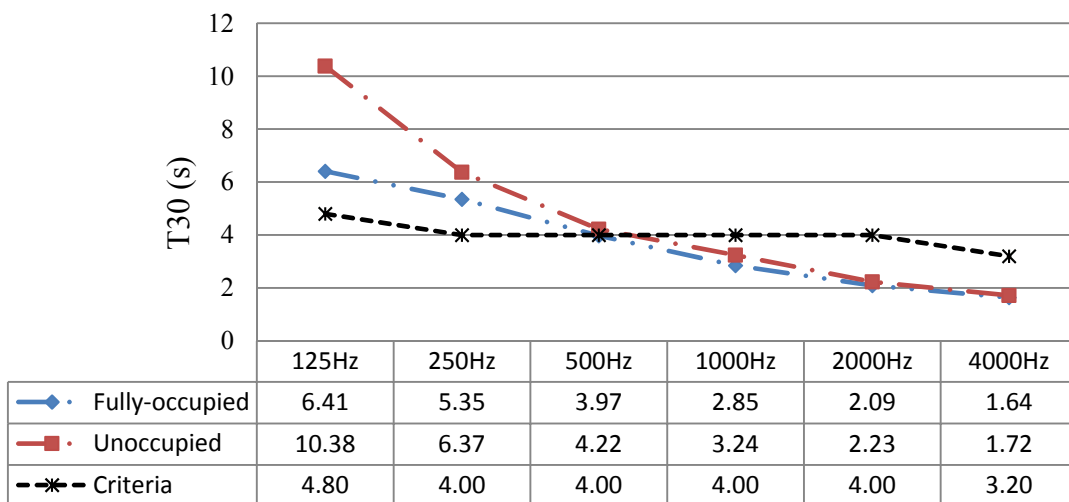


Figure 5.7. Occupied state of the Mosque, comparison of plasters; T30 results for adjusted model with historical lime based plasters (approximation for original state), and their comparison with upper limit of criteria for mosques in similar volume

5.1.3. HAGIA SOPHIA FIELD DATA

In this section Hagia Sophia room acoustics parameter field test results are presented. Two basic metrics for multi-slope investigation out of collected impulse responses including decay rates, specifically T30, and background noise indicator, specifically INR, are evaluated. Due to the long decay rates of the space, the e-sweep source signal lengths necessitated for Hagia Sophia tests are around 20 s. Although it is accepted that longer the sweep signals higher the INR, it is also under discussion in terms of their liability to distortion (Christensen et al., 2013). Thus, within the process of impulse response selection initially the INR values are compared for e-sweep, balloon pop and wood clap. Another reason for testing these different source signals is to relatively test the adequacy of e-sweep for both low frequency and high frequency range analysis.

Among the many available measurement methods the preferred/recommended one today is the e-sweep (or swept sine) method that uses comparatively long exponential sweep. This method can produce impulse responses with very good dynamic range and minimized harmonic distortion by the loudspeaker. There can still be some influence from non-harmonic distortion (Christensen et al., 2013), which can easily be truncated/cropped out of the full range impulse. This outcome of previous studies is also supported out of Hagia Sophia measurements within the context of this study as detailed in the following.

Hagia Sophia has resulted to be too large to be excited with either balloon pop or wood clap in overall frequency spectrum. Using alternative excitation signals such as wood claps or popping of a balloon have not provided the sufficient signal to noise ratio, and neither of those source signals are perfectly omni-directional. As can be observed from Figure 5.8, providing higher signal to noise ratios, e-sweep is more reliable to be used in multi-slope investigations in compare to balloon pop and wood clap both in low and high frequency ranges. Deviation is mostly at lower octaves, where wood clap has the lowest INR values in compare to both balloon pop and e-

sweep. High octaves are much identical for balloon pop and wood clap, where e-sweep still has a significant raise, almost 10 dB higher, in signal to noise ratios. For that reason in decay parameter estimations, presented in following sections, only the e-sweep generated impulses are analyzed.

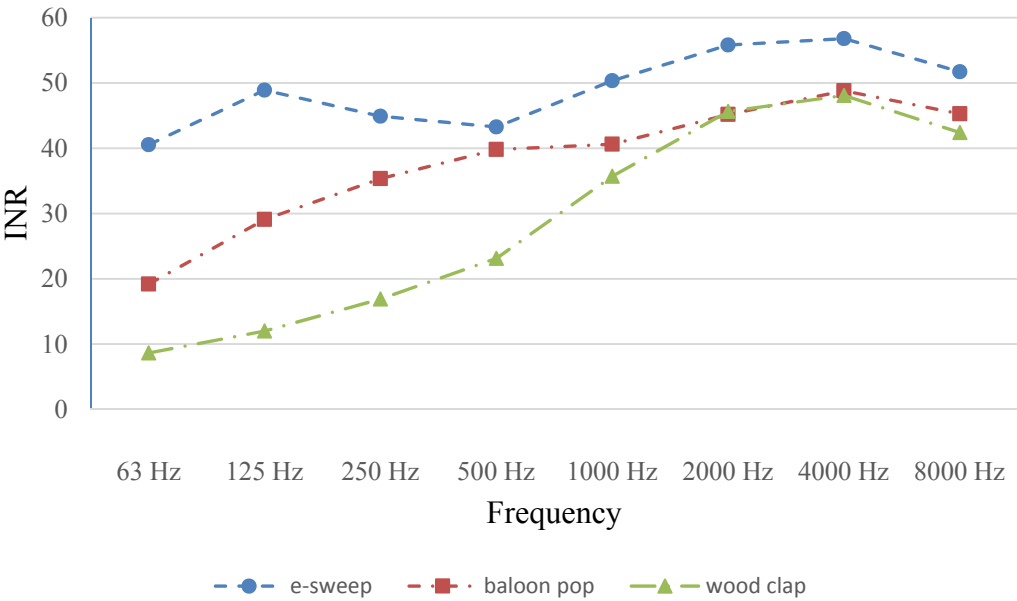


Figure 5.8. Hagia Sophia INR measurements in 1/1 octave bands, comparison of e-sweep, balloon pop and wood clap source signals

The ISO 3382-1 parameters except for T30 have limited accuracy in a large space as of Hagia Sophia. For instance, acoustical parameter evaluation of C80 in coupled spaces such as Hagia Sofia where the buildup of the squared impulse response far exceeds the 80 milliseconds time limit used for the C80 parameter, cannot provide the anticipated results (Christensen et al., 2013). As a result of this outcome as well as the fact that decay rates being the focus of multi-slope investigations, energy fraction metrics as of C80, D50 are extracted from the scope of this study. Specifically, T30 and INR results for 11 source-receiver configurations are evaluated and listed in Table 5.2.

Table 5.2. Hagia Sophia INR and T30 (s) field test results in 1/1 octaves, for e-sweep, balloon pop and wood clap source signals

Location	Source		Frequency (Hz)							
			63	125	250	500	1000	2000	4000	8000
S1 R1	e-sweep	INR	40	47	46	45	48	54	59	57
	e-sweep	T30	7.77	8.52	9.89	9.53	7.81	6.19	4.32	2.69
	balloon	INR	22	25	27	33	37	42	47	48
	balloon	T30	1.12*	7.12*	9.14	9.64	19**	6.04	4.02	2.51
	wood	INR	14	21	23	20	34	40	48	52
	wood	T30	0.00*	0.11*	0.10*	13.8*	8.12	6.70	4.62	2.68
S1 R2	e-sweep	INR	41	48	45	39	46	51	54	54
	e-sweep	T30	8.25	8.96	9.80	12**	8.85	10**	5.9**	2.80
	balloon	INR	18	23	28	26	27	39	43	44
	balloon	T30	5.88*	6.22*	8.32	7.35	6.50	5.41	4.54	2.75
	wood	INR	13	10	29	21	34	46	54	52
	wood	T30	0.01*	0.07*	0.14*	9.91*	7.95	6.28	4.48	2.78
S1 R3	e-sweep	INR	39	49	43	42	48	53	56	52
	e-sweep	T30	8.03	8.81	9.89	10.0	8.34	6.45	4.61	2.85
	balloon	INR	22	28	34	40	42	47	48	44
	balloon	T30	5.15*	9.56*	12**	9.74	8.70	6.38	4.75	2.77
	wood	INR	6	20	17	24	36	47	52	51
	wood	T30	--	0.04*	4.97*	8.77*	7.60	6.33	4.65	2.85
S1 R4	e-sweep	INR	43	50	57	40	55	60	61	55
	e-sweep	T30	8.36	8.43	9.88	9.70	8.19	6.23	4.45	2.69
	balloon	INR	21	33	40	46	44	50	51	49
	balloon	T30	4.96*	7.92*	9.72	9.75	8.36	6.12	4.70	2.45
	wood	INR	8	7	23	34	48	58	57	50
	wood	T30	2.29*	0.02*	6.87*	8.95*	7.37	6.47	4.55	2.70
S1 R5	e-sweep	INR	44	49	38	39	53	58	56	50
	e-sweep	T30	8.24	8.91	9.83	9.78	8.22	6.43	4.67	2.85
	balloon	INR	20	30	36	39	40	49	52	48
	balloon	T30	5.41*	10.9*	10.4	10.8	8.33	6.31	4.76	2.69
	wood	INR	10	13	15	22	37	49	55	49
	wood	T3	9.21*	2.05*	8.92*	14.0*	8.47	8.78	4.62	2.92
S2 R1	e-sweep	INR	41	51	44	45	51	55	55	51
	e-sweep	T30	9.75	8.88	9.89	9.45	8.18	6.46	4.63	2.85
	balloon	INR	18	27	36	41	41	41	39	27
	balloon	T30	8.24*	7.28*	10.3	9.67	8.80	6.64	4.78	3.85
	wood	INR	8	10	19	26	36	45	47	38
	wood	T30	--	--	4.24*	7.60*	7.46	6.43	4.74	3.09

Table 5.2. (continued)

S2 R2	e-sweep	INR	36	46	42	43	50	55	55	47
	e-sweep	T30	8.24	8.92	9.94	10.1	8.52	6.43	4.66	2.90
	balloon	INR	17	28	37	44	45	43	49	46
	balloon	T30	9.88*	8.10*	9.95	9.54	8.66	6.58	4.36	2.77
	wood	INR	9	10	17	26	36	48	50	40
	wood	T30	1.49*	6.37*	18.7*	8.16*	7.87	6.14	4.65	3.02
S2 R3	e-sweep	INR	37	48	39	41	46	55	53	46
	e-sweep	T30	8.20	8.97	10.0	9.64	8.15	6.52	4.77	2.93
	balloon	INR	16	31	38	44	45	43	42	33
	balloon	T30	1.19*	8.18*	10.1	9.63	8.61	6.51	4.83	3.19
	wood	INR	8	13	6	20	34	47	47	39
	wood	T30	1.13*	26.0*	1.19*	5.68*	7.44	6.52	4.78	3.09
S2 R5	e-sweep	INR	42	55	46	43	48	54	57	55
	e-sweep	T30	6.93	8.19	8.99	9.07	7.71	5.89	3.91	2.29
	balloon	INR	21	31	36	41	43	47	56	55
	balloon	T30	9.21*	7.89*	8.57	9.18	8.54	5.29	3.83	2.06
	wood	INR	11	19	19	25	40	57	60	55
	wood	T30	0.09*	0.02*	2.75*	5.93*	7.30	5.96	4.23	2.35
S2 R6	e-sweep	INR	38	49	38	45	54	57	57	50
	e-sweep	T30	8.11	8.55	9.74	9.19	8.04	6.26	4.34	2.64
	balloon	INR	17	32	41	44	45	49	50	45
	balloon	T30	1.21*	8.37*	9.52	9.40	8.38	6.33	4.54	2.55
	wood	INR	9	14	17	24	39	50	53	46
	wood	T3	10.2*	0.86*	7.09*	7.25*	7.31	6.08	4.40	2.71
S3 R1	e-sweep	INR	45	46	56	54	55	62	62	52
	e-sweep	T30	7.7	8.8	9.9	9.6	8.0	6.2	4.4	2.4
	balloon	INR	19	32	36	40	38	47	60	59
	balloon	T30	4.22*	6.94*	9.89	9.57	8.92	6.39	4.08	2.54
	wood	INR	12	9	15	23	33	49	50	44
	wood	T30	23.1*	--	11.8*	7.9*	8.4	6.3	4.6	3.1

* results in blue indicates unreliable T30 as a result of inadequate INR, thus the data is excluded from analysis

** results in red indicates deviations from overall T30, indicating echo or flutter echo formation for that specific location and octave band, thus the data is excluded in the averaging of results

From Figure 5.8 and Table 5.2 it can easily be observed that wood clap has the lowest INR, so the resulting T30 values over collected impulse are much below or higher than expected, indicating unreliable data. Balloon pop is better than wood

clap, but still unsatisfactory specifically for lower octaves. E-sweep excitation has the highest INR and provide the most dependable data even in high frequency range in compare to other source signals. T30 averages for 11 measurement set-up over 1/1 octave bands for all three tested source-signal types with included reliable data are compared in Figure 5.9.

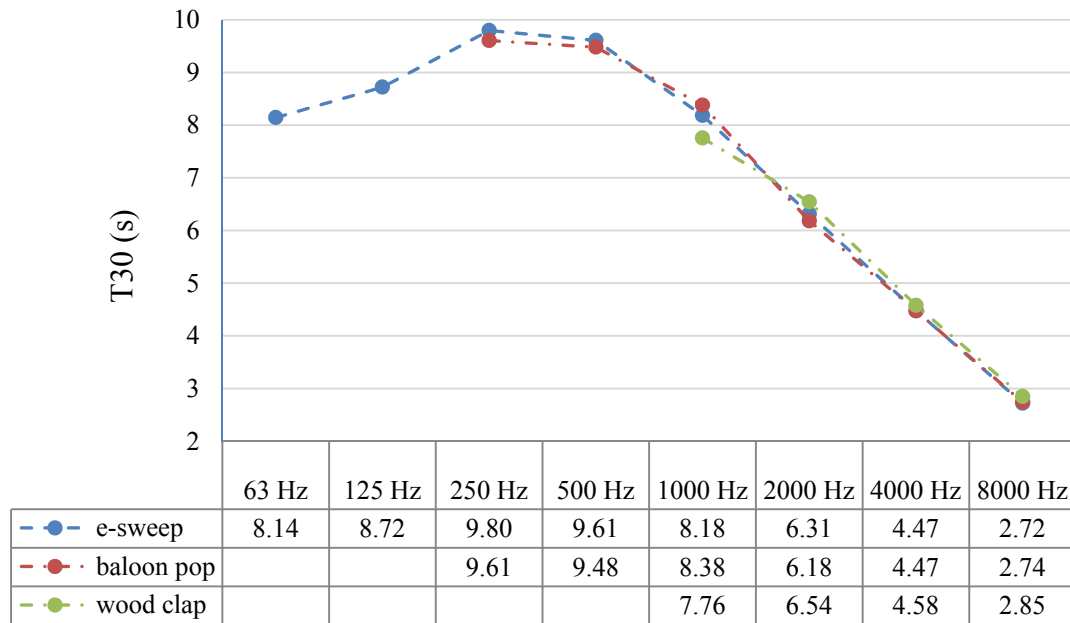


Figure 5.9. Hagia Sophia T30 measurements in 1/1 octave bands, comparison of e-sweep, balloon pop and wood clap source signals

Results support very high reverberation within the super-structure. Mid and low frequency average of T30 around 9 s and high frequency of around 5 s are even much higher than the recommended highest value of 2.5 s for liturgical music. This superb and extraordinary aural environment is unique and has the potential to provide acoustical field conditions in relation to coupled spaces for specific locations. Further investigations are held in order to enlighten the formal/architectural relations and their contribution to acoustical coupling; more scientifically multiple non-exponential energy decays.

5.2. DPE DATA

Multi-slope decay formation analysis within domed superstructures basically relies on decay parameter estimation within Bayesian formation as discussed under the State of the Art and Methodology sections. In this section the DPE analysis results of collected data (impulse responses) out of field tests and simulations are presented.

5.2.1. SÜLEYMANIYE MOSQUE PRE-FIELD SIMULATION DPE

The initial DPE analysis is processed before field tests using the impulses out of raw acoustical model (pre-adjustment of materials) (Sü Gül et al., 2012). As the major aim is to aid following field tests, many number of source and receiver configurations are tested. Specifically, 6 omni-directional source (at h: 1.5 m) and 32 receiver (at h: 1.2 m) and in total 76 different source-receiver configuration jobs are run in simulations. Thus, the source and receiver configurations and number of analyzed data, which are same for field tests and post-field simulations, are different and greater in number for pre-field simulations. Source and receiver locations for this phase are separately presented in Figure 5.10. The main advantage of pre-field simulation DPE is to pre-practice with high number of data until the confidence to the Bayesian analysis is established. As T30 results out of pre-field simulation data change at specific octave bands, in compare to field and post-field simulation, it is expected that the DPE results also would differ in specific octave bands as from 125 Hz to 500 Hz.

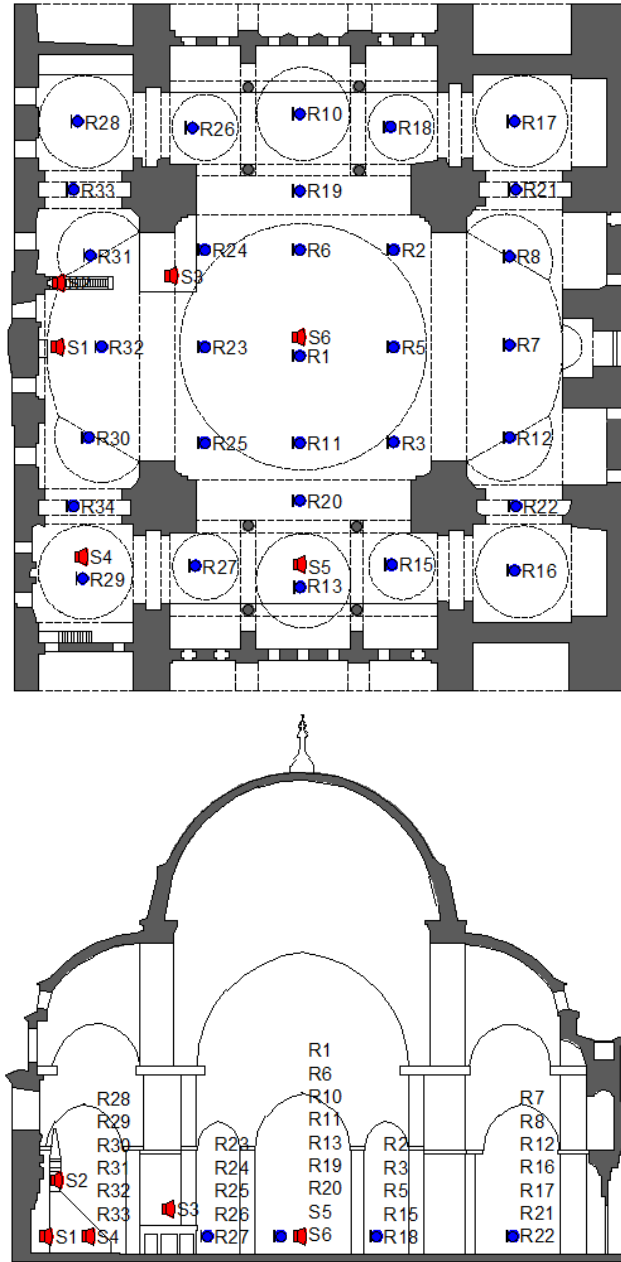


Figure 5.10. Pre-field simulations source(S) and receiver(R) locations, plan view (above), section view (below), Süleymaniye Mosque

The acquired impulse responses or the raw *.wav data are analyzed for estimating decay parameters. The analysis results for pre-field simulations are summarized in Table 5.3 including decay times and number of exponential decay terms out of Bayesian analysis for each source-receiver configuration. As previously defined T_s (T_1, T_2, T_3, \dots) is the decay time associated with the logarithmic decay slope of

individual exponential decay terms, with $s = 1, 2, \dots, S$, and S is the maximum number of exponential decay terms. Couple of representative cases is included within Table 5.3 and the whole analysis results are presented under Appendix B.

Table 5.3. Süleymaniye Mosque multi-slope analysis, typical pre-field simulation data; number of decay/slope, decay rates (s) over frequency for different source-receiver configurations

Receiver Source #		Frequency (Hz)						
		125	250	500	1000	2000	4000	8000
R1 S1	# of slope (S)	1	1	1	2	2	3	4
	decay rates (s)	T1:9.8	T1:9.2	T1:8.3	T1:5.3 T2:7.8	T1:3.9 T2:7.4	T1:2.4 T2:4.7 T3:9.0	T1:1.2 T2:2.3 T3:4.4 T4:9.8
R1 S2	# of slope (S)	1	1	1	2	2	3	4
	decay rates (s)	T1:9.6	T1:9.1	T1:8.3	T1:4.6 T2:7.8	T1:3.86 T2:7.5	T1:2.6 T2:4.7 T3:9	T1:1.17 T2:2.37 T3:4.57 T4:10
R1 S3	# of slope (S)	1	1	1	2	2	3	3
	decay rates (s)	T1:9.6	T1:9	T1:8.1	T1:5.4 T2:8.6	T1:3.76 T2:6.88	T1:2.5 T2:4.4 T3:8.5	T1:1.4 T2:2.8 T3:8
R1 S4	# of slope (S)	1	1	1	2	2	3	4
	decay rates (s)	T1:9.8	T1:9.47	T1:8.2	T1:5.26 T2:8.67	T1:4.15 T2:7.09	T1:2.97 T2:4.75 T3:9.03	T1:1.65 T2:2.9 T3:5.6 T4:9.7
R1 S5	# of slope (S)	1	1	1	2	2	3	4
	decay rates (s)	T1:9.9	T1:9.4	T1:8.2	T1:5.32 T2:8.4	T1:4 T2:7.09	T1:2.9 T2:4.8 T3:9.13	T1:1.62 T2:2.69 T3:6.04 T4:11.9
R7 S6	# of slope (S)	1	1	1	2	2	3	4
	decay rates (s)	T1:9.7	T1:9.3	T1:8.4	T1:5.23 T2:8.4	T1:3.85 T2:6.89	T1:2.56 T2:4.65 T3:9.02	T1:1.40 T2:2.65 T3:5.74 T4:12.3

A sample quadruple decay case is selected in order to give more information on estimated decay parameters (Table 5.4). The decay model comparisons of impulse response collected at R₃S₁ and filtered for 8 kHz is presented in Figure 5.11 with relevant decay slopes and turning points indicated on the graph.

Table 5.4. Decay parameters for impulse response collected at R₃S₁, filtered for 8 kHz, at pre-simulation, Süleymaniye Mosque

Decay parameters	R ₃ S ₁ 8 kHz
A_0 (dB)	-157
A_1 (dB)	-5.95
T_1 (s)	1.28
A_2 (dB)	-12.79
T_2 (s)	2.73
A_3 (dB)	-30.09
T_3 (s)	7.49
A_4 (dB)	-39.34
T_4 (s)	14.01
BIC (Neper)	14756

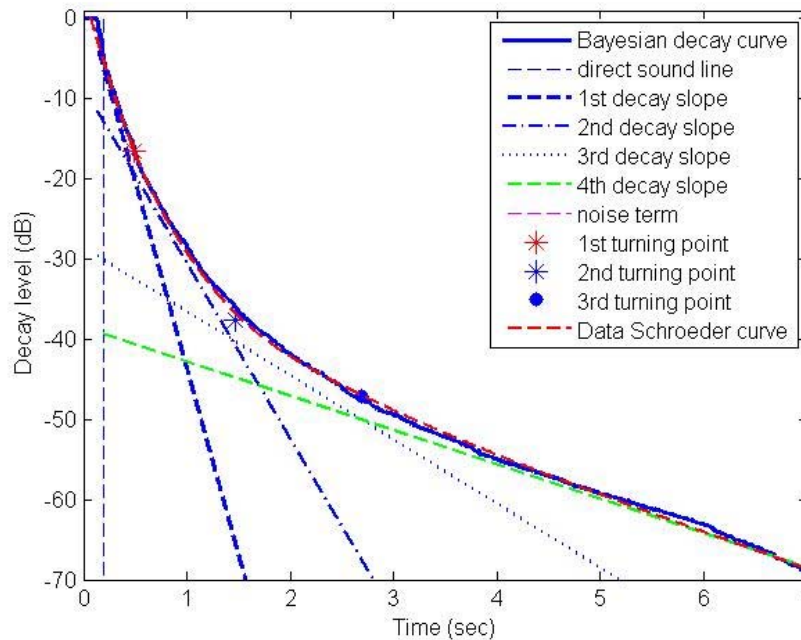


Figure 5.11. Comparison of Schroeder curve and the model curve for R₃S₁; a quadruple-slope model derived from the room impulse response, band pass-filtered at 8 kHz, at pre-simulation; four decomposed decay slope lines and three turning points, Süleymaniye Mosque

5.2.2. SÜLEYMANIYE MOSQUE FIELD DPE

For different source-receiver configurations out of 83 impulse responses collected at field measurements 17 best (highest INR - least distortion) *.wav data are analyzed for estimating decay parameters. The analysis results for field measurements are summarized in Table 5.5 including decay times and number of exponential decay terms out of Bayesian analysis for each source-receiver configuration. Couple of representative cases is included within Table 5.5 and the whole analysis results are presented under Appendix B.

Table 5.5. Süleymaniye Mosque multi-slope analysis results, typical field measurement data; number of decay/slope, decay rates (s) over frequency for different source-receiver configurations

Source Receiver #		Frequency (Hz)							
		63	125	250	500	1000	2000	4000	8000
S1 R1	# of slope (S)	2	2	2	2	2	2	2	2
	decay rates (s)	T1:11 T2:22	T1:12 T2:20	T1:7.7 T2:14	T1:5.8 T2:9.0	T1:5.3 T2:7.8	T1:3.6 T2:7.0	T1:2.3 T2:3.8	T1:1.3 T2:2.3
S2 R1	# of slope (S)	1	2	2	2	2	2	2	2
	decay rates (s)	T1:19	T1:15 T2:18	T1:10 T2:15	T1:6.2 T2:10	T1:5.5 T2:8	T1:4 T2:6.5	T1:2.5 T2:4.1	T1:1.55 T2:2.23
S3 R2	# of slope (S)	1	2	2	2	2	2	2	2
	decay rates (s)	T1:19	T1:14 T2:21	T1:8.6 T2:15	T1:6.0 T2:9.6	T1:5.4 T2:7.9	T1:3.8 T2:5.7	T1:2.5 T2:3.8	T1:1.51 T2:2.24
S6 R3	# of slope (S)	2	2	2	2	2	2	2	2
	decay rates (s)	T1:14 T2:21	T1:13 T2:18	T1:10 T2:15	T1:6.1 T2:9.9	T1:5.3 T2:7.8	T1:4.1 T2:5.9	T1:2.5 T2:4.1	T1:1.55 T2:2.22

A sample triple decay case is selected in order to give more information on estimated decay parameters (Table 5.6). BIC values are compared for two and three slope cases of this sample impulse, which implies a higher ranking for three slopes. The decay model comparisons of impulse response collected at S₃R₇ and filtered for 250 Hz is presented in Figure 5.12 with relevant decay slopes and turning points indicated on the graph.

Table 5.6. Decay parameters for impulse response collected at S₃R₇, filtered for 250 Hz, at field tests, Süleymaniye Mosque

Decay parameters	S ₃ R ₇ 250 Hz
A_0 (dB)	-85.86
A_1 (dB)	-8.92
T_1 (s)	2.3
A_2 (dB)	-13.54
T_2 (s)	4.0
A_3 (dB)	-17.13
T_3 (s)	8.1
BIC (Neper)	15829 (3 slopes)
BIC (Neper)	9700 (2 slopes)

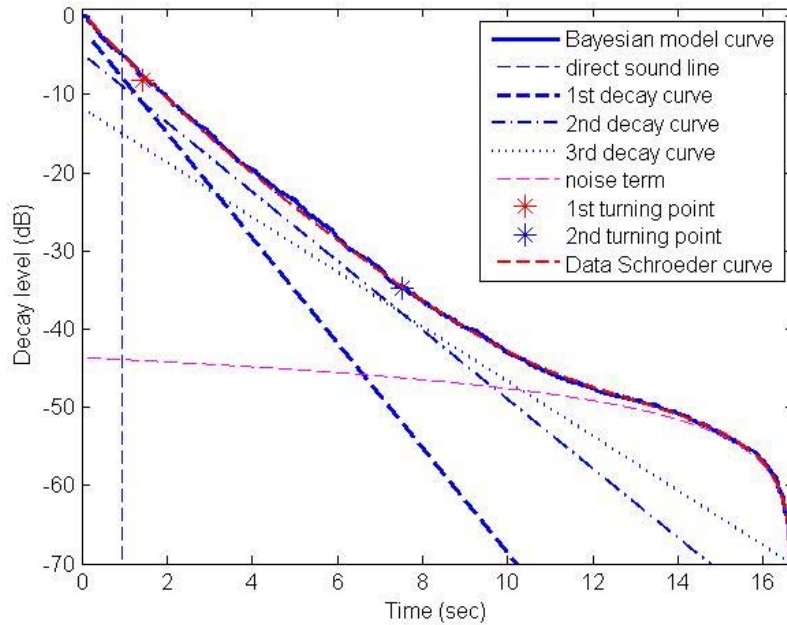


Figure 5.12. Comparison between Schroeder curve and the model curve, S₃R₇, a triple-slope model derived from the room impulse response, band pass-filtered at 250 Hz, at field tests; three decomposed decay slope lines and two turning points, Süleymaniye Mosque

5.2.3. SÜLEYMANIYE MOSQUE POST-FIELD SIMULATION DPE

In order to provide data for comparison studies of field and simulation results, in post-simulation decay parameter estimations 17 *.wav files are collected and analyzed for source-receiver configurations corresponding to field test locations. The analysis results for post-simulation data are summarized in Table 5.7 including decay times and number of exponential decay terms out of Bayesian analysis for each source-receiver configuration. Couple of representative cases is included within Table 5.7 and the whole analysis results are presented under Appendix B.

Table 5.7. Süleymaniye Mosque multi-slope analysis results, typical post-field simulation data; number of decay/slope, decay rates (s) over frequency for different source-receiver configurations

Source Receiver #		Frequency (Hz)						
		125	250	500	1000	2000	4000	8000
S1 R1	# of slope (S)	2	1//2	2//3	2	2	2//3	3
	decay rates (s)	T1:10.3 T2:16.6	T1:8.42 T2:12.62	T1:5.35 T2:10	T1:4.64 T2:8.54	T1:3.76 T2:7.52	T1:2.32 T2:5.04	T1:1.18 T2:2.39 T3:5.90
S2 R1	# of slope (S)	2	1//2	2	2	2	3	3
	decay rates (s)	T1:10.1 T2:19.2	T1:9.46 T2:15.82	T1:7.19 T2:14.2	T1:5.2 T2:10.8	T1:4 T2:8	T1:2.46 T2:4.53 T3:10.5	T1:1.29 T2:2.99 T3:10.22
S3 R2	# of slope (S)	1	1	2	2	2	2	3
	decay rates (s)	T1:14	T1:11.6	T1:6.02 T2:10.8	T1:5.4 T2:10.4	T1:4 T2:7.8	T1:3.05 T2:7.2	T1:1.35 T2:2.9 T3:8.8
S4 R5	# of slope (S)	2	1//2	2//3	2	2	2	3
	decay rates (s)	T1:12.2 T2:20.1	T1:8.2 T2:14.2	T1:6.9 T2:13.2	T1:5.3 T2:10.1	T1:4.04 T2:8.3	T1:3.05 T2:7	T1:1.5 T2:2.99 T3:9.6

**// indicates impulses that are weak cases of the higher number of slope*

A sample triple decay case is selected in order to give more information on estimated decay parameters (Table 5.8). BIC values are compared for two and three slope cases

of this sample impulse, which implies a higher ranking for three slopes. The decay model comparisons of impulse response collected at S₂R₂ and filtered for 4 kHz is presented in Figure 5.13 with relevant decay slopes and turning points indicated on the graph.

Table 5.8. Decay parameters for impulse response collected at S₂R₂, filtered for 4 kHz, at post-simulation, Süleymaniye Mosque

Decay parameters	S ₂ R ₂ 4 kHz
A_0 (dB)	-100.61
A_1 (dB)	-5.96
T_1 (s)	2.57
A_2 (dB)	-11.53
T_2 (s)	4.55
A_3 (dB)	-24.24
T_3 (s)	11.10
BIC (Neper)	41549 (3 slopes)
BIC (Neper)	16398 (2 slopes)

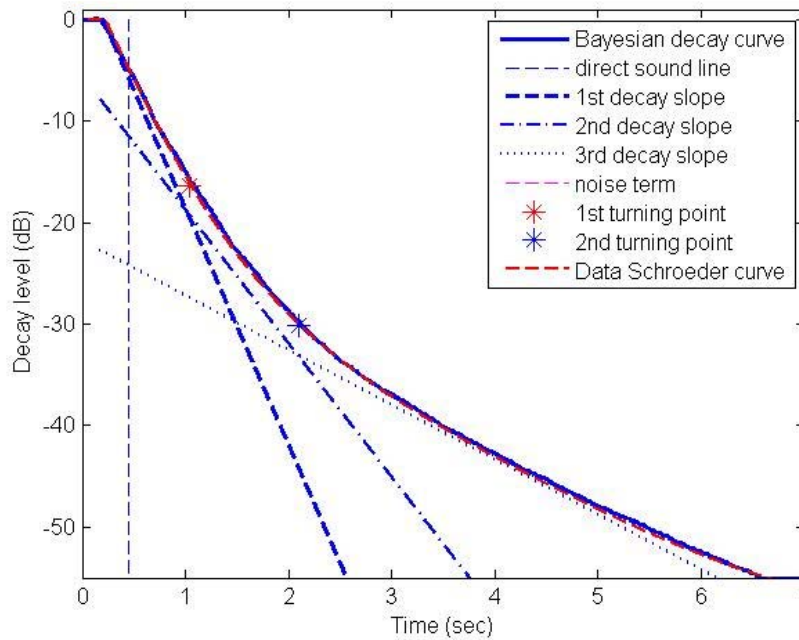


Figure 5.13. Comparison between Schroeder curve and the model curve, S₂R₂, triple-slope model derived from the room impulse response, band pass-filtered at 4 kHz, at post-simulation; three decomposed decay slope lines and two turning points, Süleymaniye Mosque

5.2.4. HAGIA SOPHIA FIELD DPE

Under this section DPE analysis results are presented for Hagia Sophia, as of a multi-domed superstructure with a basilican plan layout, with comparatively higher volume to Süleymaniye Mosque and differently with reflective floor surface due to marble cladding. For different source-receiver configurations out of 68 impulse responses collected at field measurements, 11 best (highest INR - least distortion) *.wav data - all comprising the e-sweep source signals- are analyzed for estimating decay parameters. The analysis results for field measurements are summarized in Table 5.9 including decay times and number of exponential decay terms out of Bayesian analysis for each source-receiver configuration. DIRAC post-processed T30 results are also included within the table for comparison. Couple of representative cases is included within Table 5.9 and the whole analysis results are presented under Appendix B.

Table 5.9. Hagia Sophia multi-slope analysis results, typical field data; number of decay/slope, decay rates (s) over frequency for different source-receiver configurations versus DIRAC post-processed T30 data

Source Receiver #		Frequency (Hz)							
		63	125	250	500	1000	2000	4000	8000
S1 R1	T30 (s)	7.77	8.52	9.89	9.53	7.81	6.19	4.32	2.69
	# of slope (S)	1/2	1	1	1	1/2	2	2	2
	decay rates (s)	T1:7 T2:12	T1:8.6	T1:10	T1:9.3	T1:6.61 T2:8.89	T1:5.4 T2:7.6	T1:2.9 T2:5.3	T1:2.4 T2:3.3
S2 R1	T30 (s)	9.75	8.88	9.89	9.45	8.18	6.46	4.63	2.85
	# of slope (S)	1	2	1/2	1	2	2	2	2
	decay rates (s)	T1:8.6	T1:7.7 T2:10	T1:8.5 T2:10	T1:9.4	T1:6.90 T2:9.34	T1:5.7 T2:8.0	T1:3.5 T2:5.6	T1:2.0 T2:3.6
S3 R1	T30 (s)	7.7	8.8	9.9	9.6	8.0	6.2	4.4	2.4
	# of slope (S)	2	1	1	1/2	2	2	2/3	2
	decay rates (s)	T1:7.4 T2:12	T1:8.8	T1:9.8	T1:9.59	T1:6.61 T2:9.10	T1:5.3 T2:7.4	T1:3.0 T2:5.3	T1:2.1 T2:3.7

Average number of exponential decay terms (# of slopes) out of Bayesian analysis for Hagia Sophia field tests are compared over octave bands in Figure 5.14, compared over source locations in Figure 5.15, compared over receiver locations in Figure 5.16 and the total number of slopes are compared over source-receiver locations in Figure 5.17.

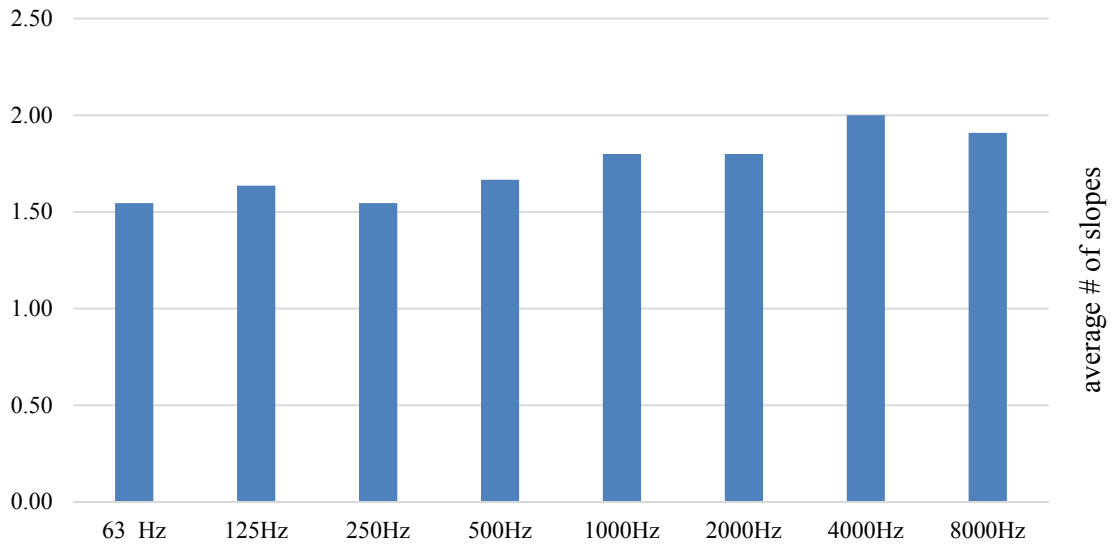


Figure 5.14. Average # of slopes per 1/1 octave bands, Hagia Sophia

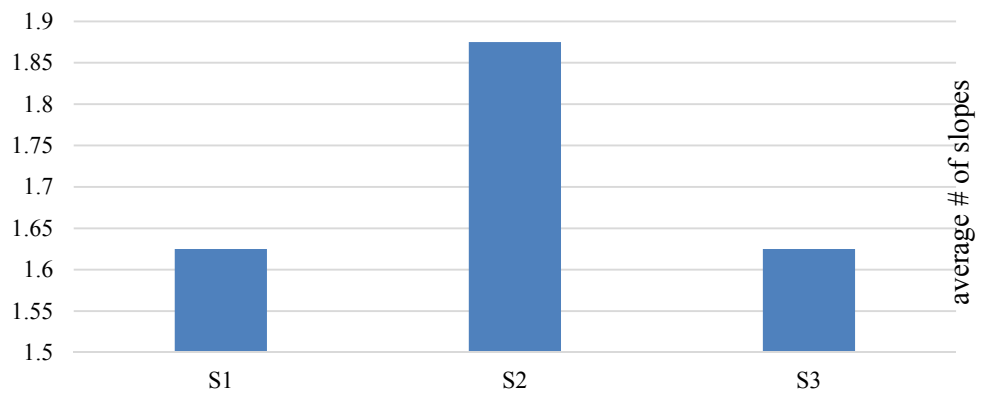


Figure 5.15. Average # of slopes per source locations, Hagia Sophia

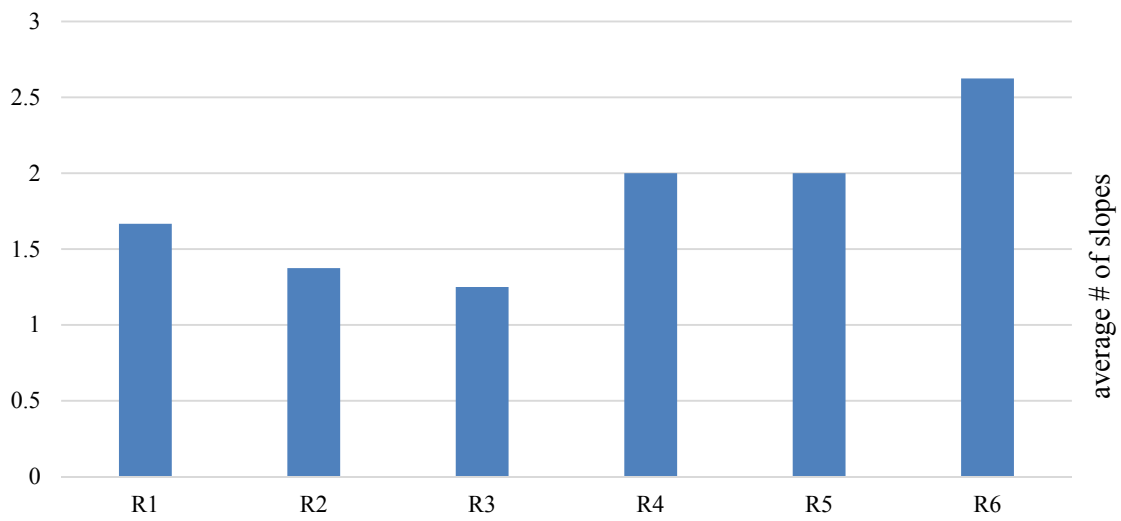


Figure 5.16. Average # of slopes per receiver locations, Hagia Sophia

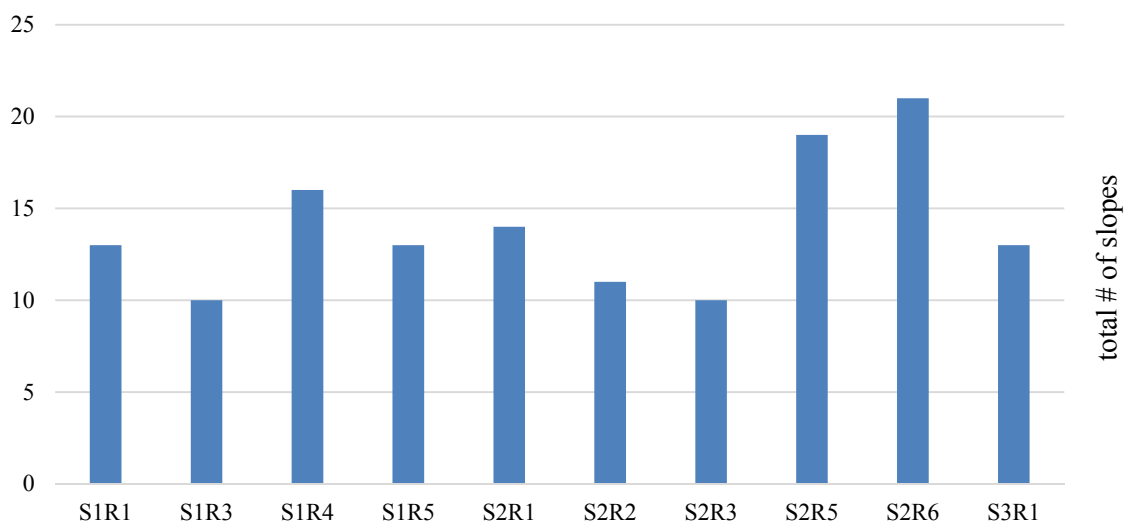


Figure 5.17. Total # of slopes per source-receiver configurations, Hagia Sophia

A sample triple decay case is selected in order to give more information on estimated decay parameters (Table 5.10). The decay model comparisons of impulse response collected at S₂S₆ and filtered for 500 Hz is presented in Figure 5.18 with relevant decay slopes and turning points indicated on the graph.

Table 5.10. Decay parameters for impulse response collected at S₂R₆, filtered for 500 Hz, at field tests, Hagia Sophia

Decay parameters	S ₂ R ₆ 500 Hz
A_0 (dB)	-79.2
A_1 (dB)	-7.34
T_1 (s)	6.7
A_2 (dB)	-10.35
T_2 (s)	10.3
A_3 (dB)	-14.80
T_3 (s)	13.3
BIC (Neper)	20882 (3 slopes)

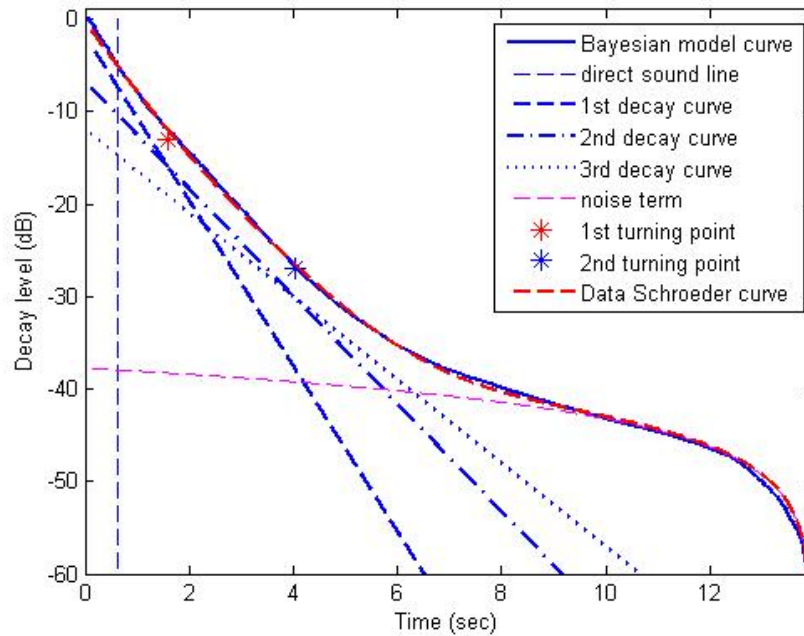


Figure 5.18. Comparison between Schroeder curve and the model curve, S₂R₆, a triple-slope model derived from the room impulse response, band pass-filtered at 4000 Hz, at field tests; three decomposed decay slope lines and two turning points, Hagia Sophia

Results indicate that there is an increasing trend of multiple slopes towards high frequencies. As all the surfaces within the room are in reflective range, air absorption may cause this energy divergence within the space that can augment the nondiffuse sound field formation at those frequencies. Measurements for source and receiver locations underneath the side gallery have provided higher number of decay slopes.

Specifically the measurement set-up when the source and the receiver are both underneath gallery (side aisle) with enough separation in between (S_2R_6) has resulted in the maximum number of decays in overall octave bands. This result is expected, as of in a typical coupled volume space. When it is considered that underneath gallery volume (side aisle) -with its lower natural reverberation- is coupled to the main space with higher natural reverberation time, the energy flow should be observed towards main volume with higher RT to subsidiary space - in this case side aisles- with lower RT. In other words, the source is within the energy deficient room (side aisles) and the energy surplus room which is the central volume of Hagia Sophia sheltered by the main dome is coupled to the aisle space as of a reverberation chamber. Detailed discussion on this topic is presented under Section 6.5.

5.3. DEM DATA (SÜLEYMANIYE MOSQUE)

Diffusion Equation Model (DEM) of Süleymaniye Mosque is initially fine-tuned with field test results considering reverberation time (T_{30}) as a basic indicator of the acoustical field. Tuning process over sound absorption coefficient data of current state materials in DEM is similar to that of ray-tracing model as to get the best overlap in T_{30} results over post-processed impulse responses with field test impulse responses. Point responses are collected for receiver locations in DEM solution and compared to field test results for the same locations.

In Figure 5.19, T_{30} result of S_1R_4 for 1 kHz is compared to T_1 (first decay rate) of point response solution of DEM. Both impulses are analyzed for their decay parameters using multi-slopes code. Both T_{30} and T_1 results are in good agreement for field collected and DEM solved impulses. An important finding is that neither of field or DEM data is a single slope case, but instead indicates a double slope formation as shown in Figure 5.20. The difference in later decay shapes is a result of noise term (background noise) that is present in field tests, whereas there is no noise to interfere with the impulse in DEM simulated data.

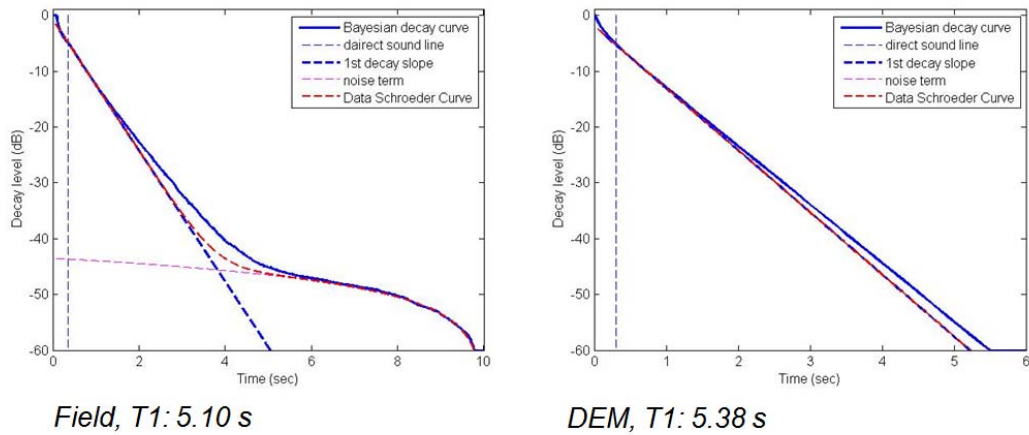


Figure 5.19. Field versus DEM results for S₁R₄, 1 kHz, 1 slope, Süleymaniye Mosque

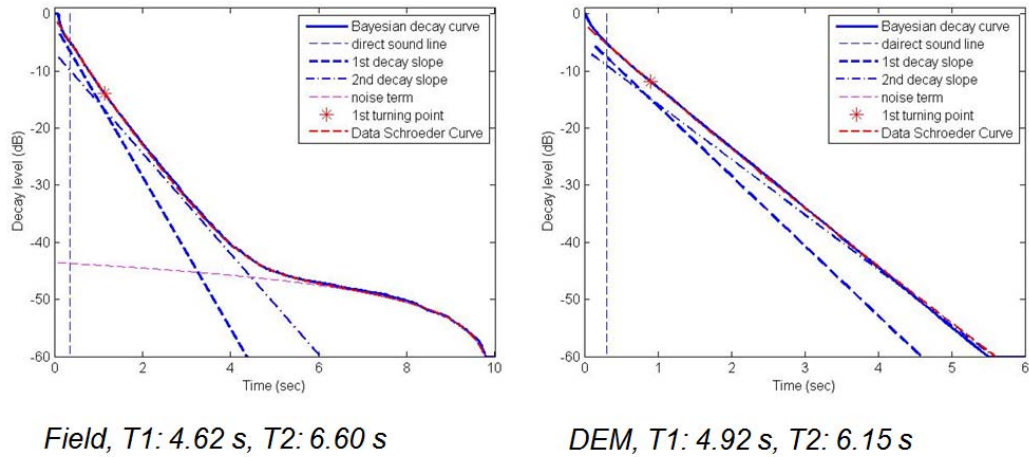


Figure 5.20. Field versus DEM results for S₁R₄, 1 kHz, 2 slopes, Süleymaniye Mosque

Following up the tuning of DEM model by the comparison with field test results, the model has also supported the argument on multi-slope formation for specific data at certain receiver locations and frequencies. For highlighting the probable reasons of multi-slope formation, time dependent DEM solutions of Süleymaniye Mosque for its current state is presented under this section. Source is defined in front of *mihrab* wall (standing *imam* position) as a representative case for common use of mosque prayer function. In a time dependent solution spatial sound energy distributions (in dB) and sound energy flow vector analysis results are summarized for chosen cases of octave bands; for 250 Hz (Figure 5.21 to Figure 5.27) and for 1000 Hz (Figure

5.28 to Figure 5.34) over axonometric, plan and section views. In order to prevent unnecessary repetition of data, specific times are selected for illustration of the common trend, as other time intervals are either identical or very close to the prior/following time steps. Higher resolution plots of selected cases for Süleymaniye Mosque DEM solution for floor with carpet are presented under Appendix C.

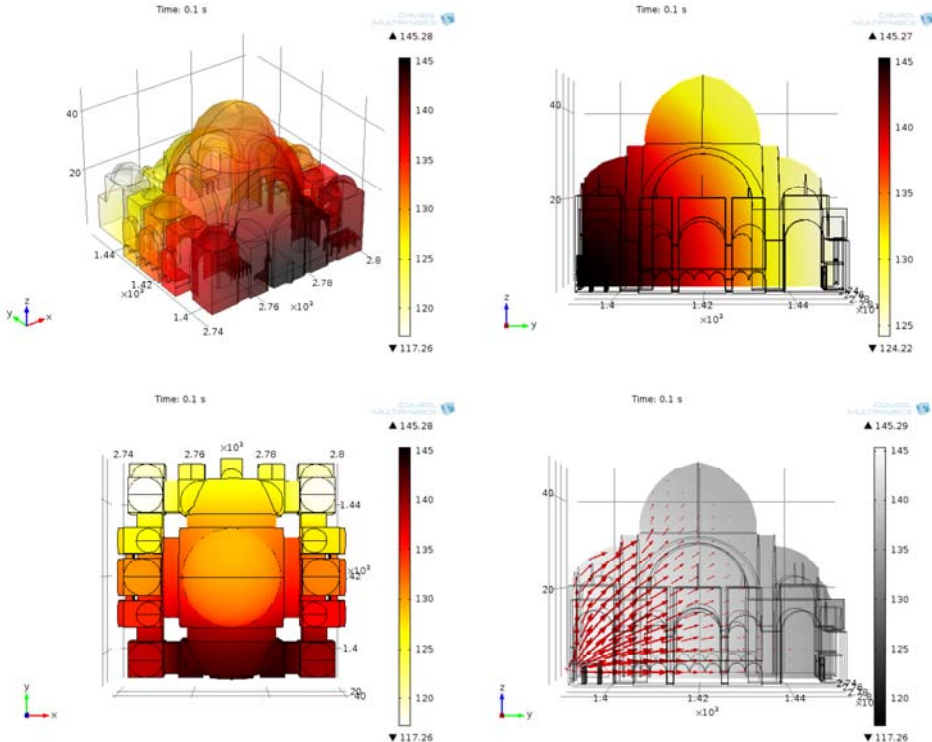


Figure 5.21. Süleymaniye Mosque DEM results, spatial sound energy distributions and flow vectors for 250 Hz, time: 0.1s

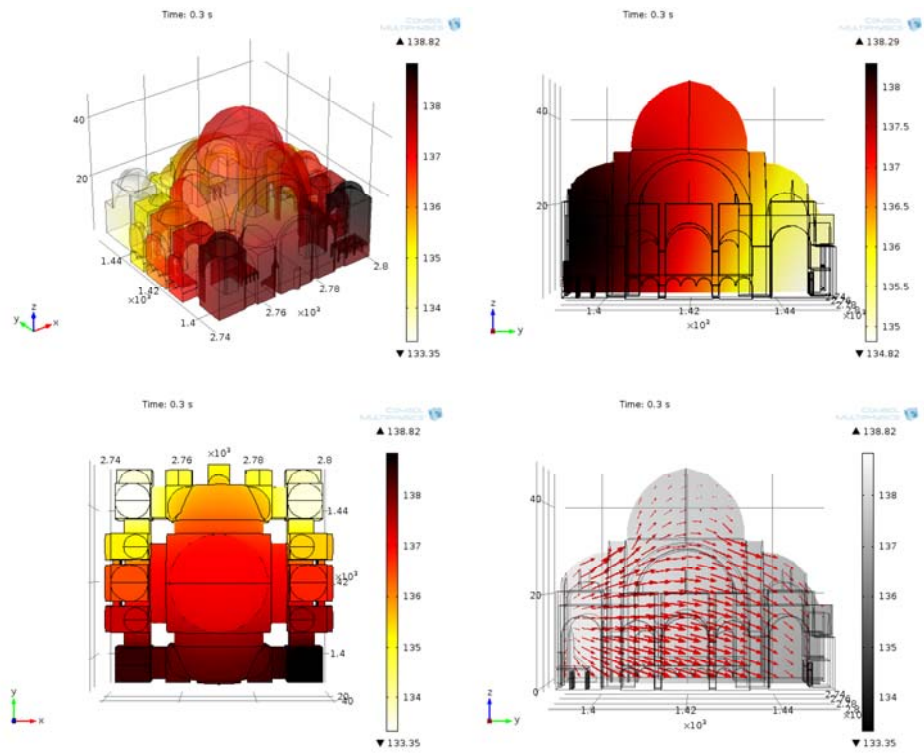


Figure 5.22. Süleymaniye Mosque DEM results, spatial sound energy distributions and flow vectors for 250 Hz, time: 0.3s

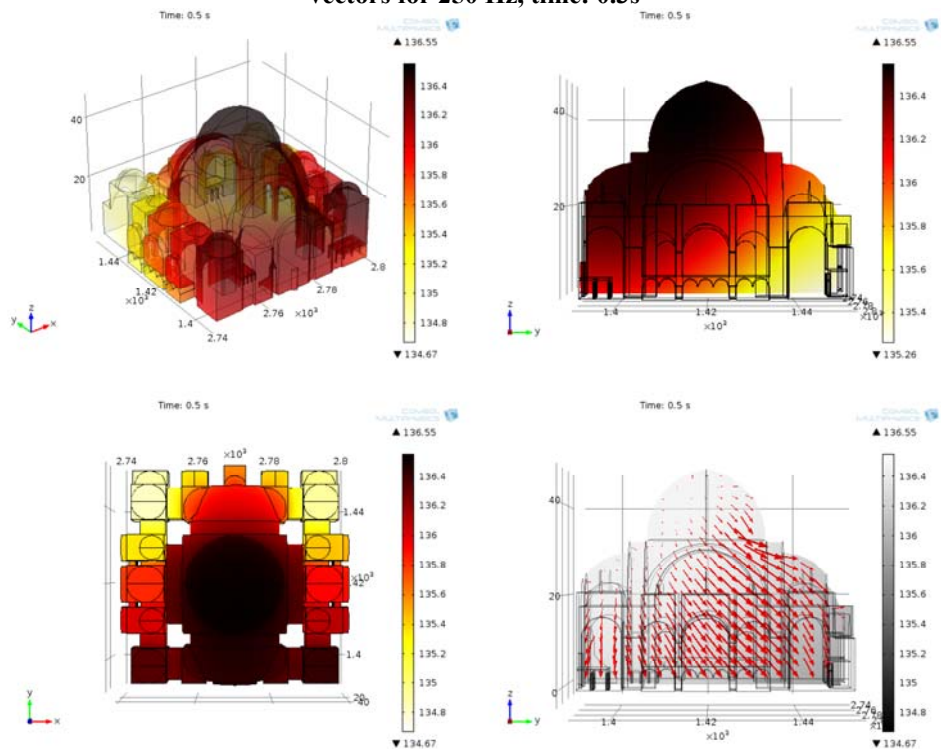


Figure 5.23. Süleymaniye Mosque DEM results, spatial sound energy distributions and flow vectors for 250 Hz, time: 0.5s

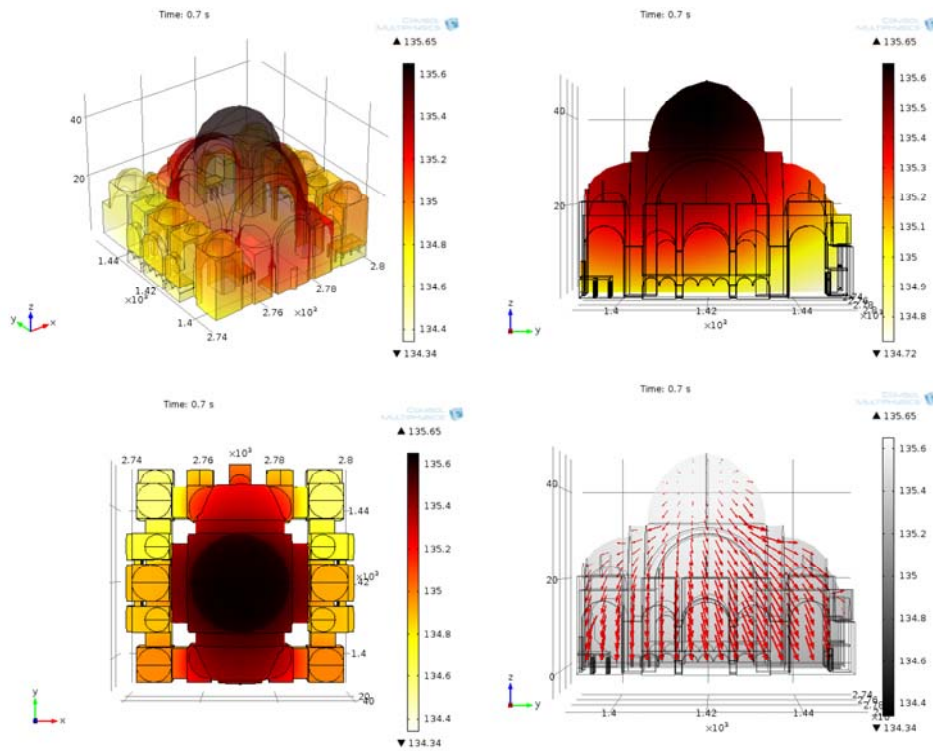


Figure 5.24. Süleymaniye Mosque DEM results, spatial sound energy distributions and flow vectors for 250 Hz, time: 0.7s

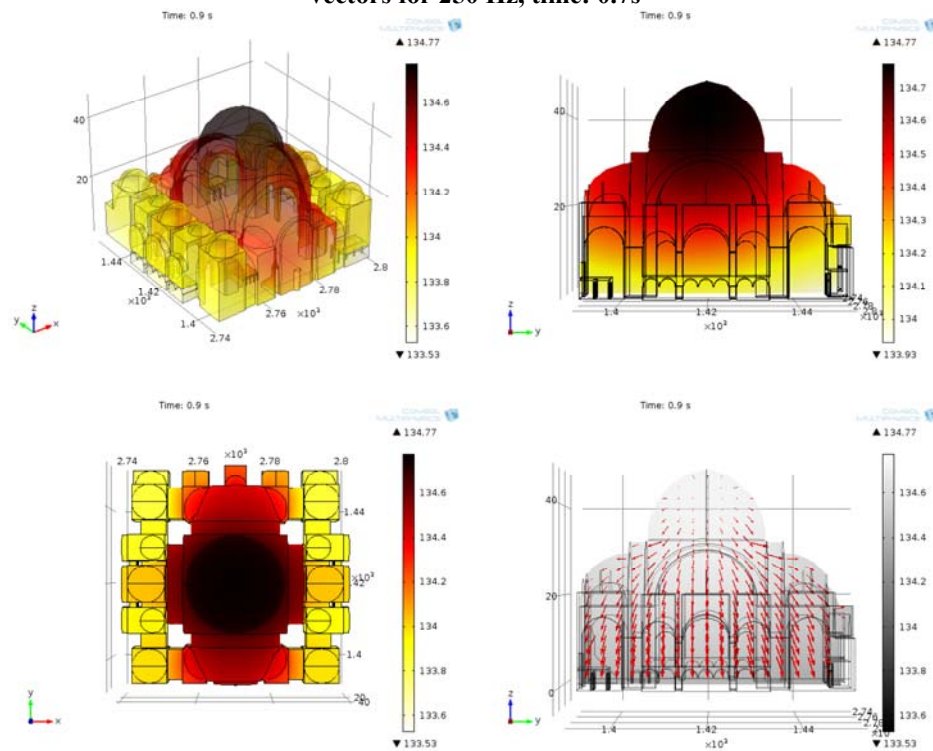


Figure 5.25. Süleymaniye Mosque DEM results, spatial sound energy distributions and flow vectors for 250 Hz, time: 0.9s

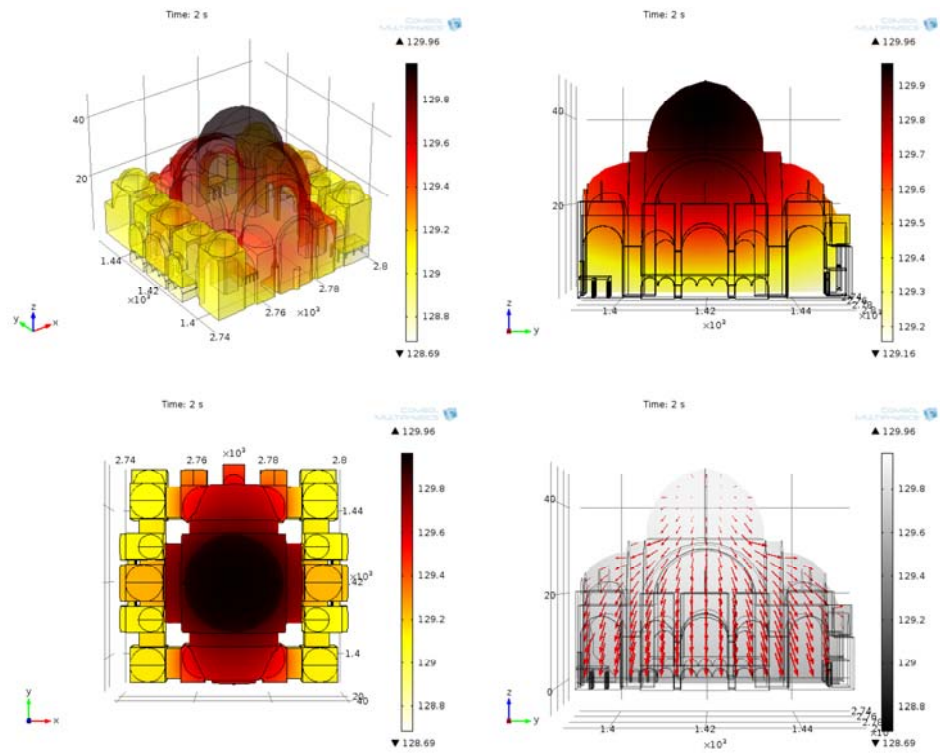


Figure 5.26. Süleymaniye Mosque DEM results, spatial sound energy distributions and flow vectors for 250 Hz, time: 2s

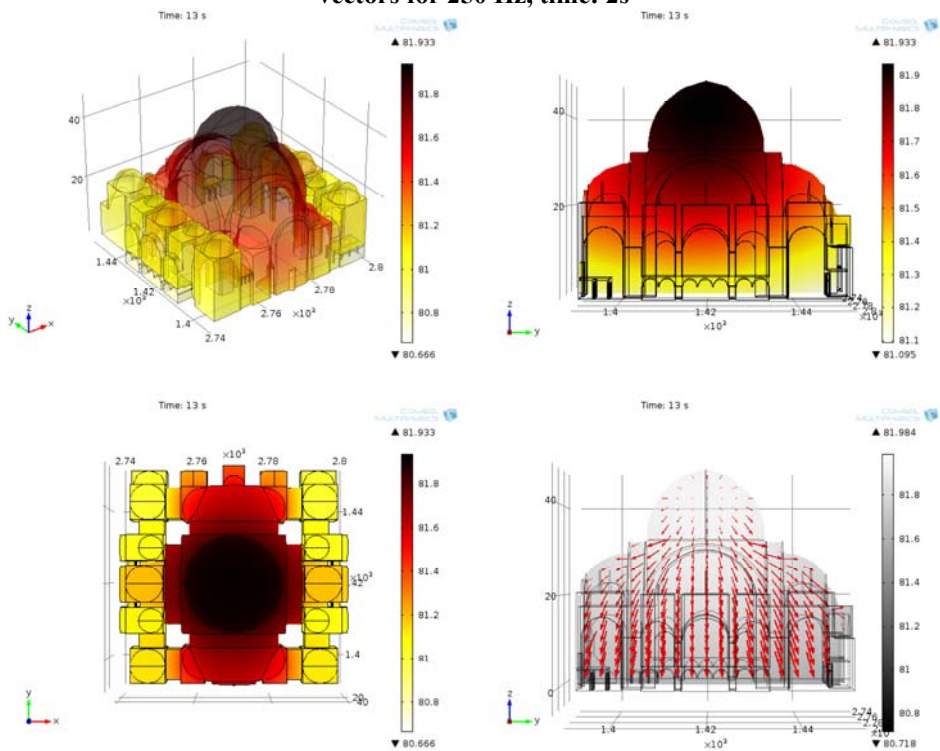


Figure 5.27. Süleymaniye Mosque DEM results, , spatial sound energy distributions and flow vectors for 250 Hz, time: 13s

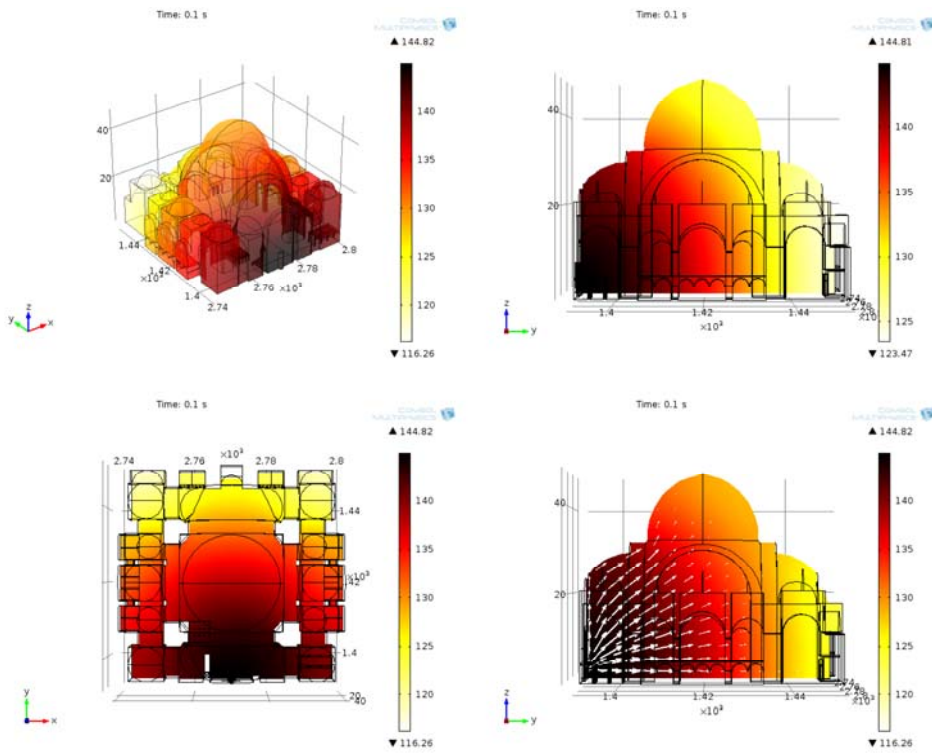


Figure 5.28. Süleymaniye Mosque DEM results, spatial sound energy distributions and flow vectors for 1 kHz, time: 0.1s

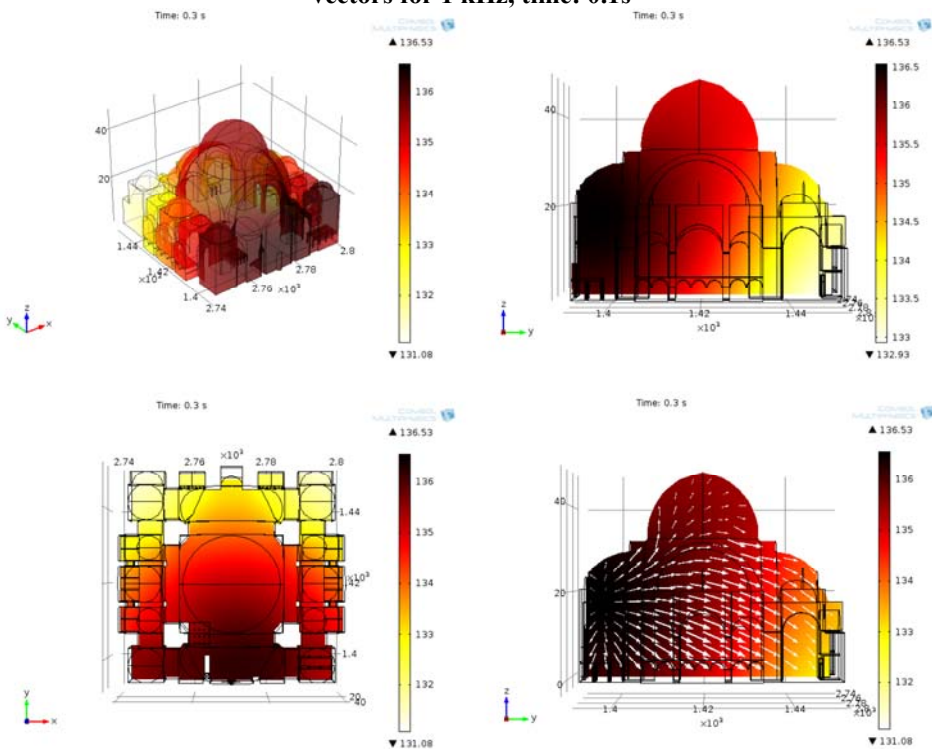


Figure 5.29. Süleymaniye Mosque DEM results, spatial sound energy distributions and flow vectors for 1 kHz, time: 0.3s

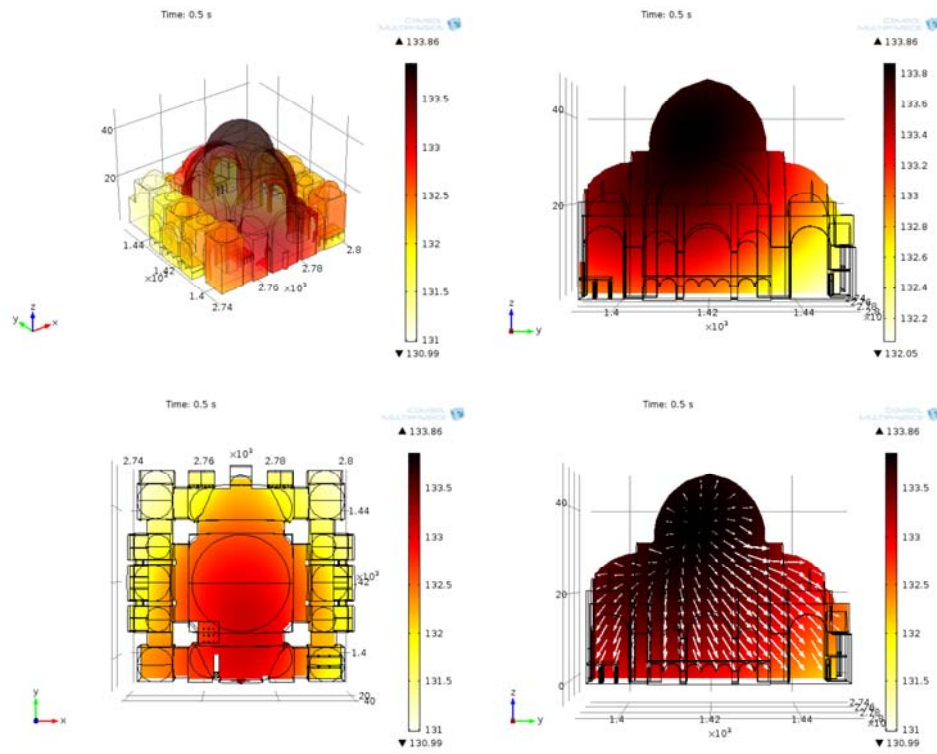


Figure 5.30. Süleymaniye Mosque DEM results, spatial sound energy distributions and flow vectors for 1 kHz, time: 0.5s

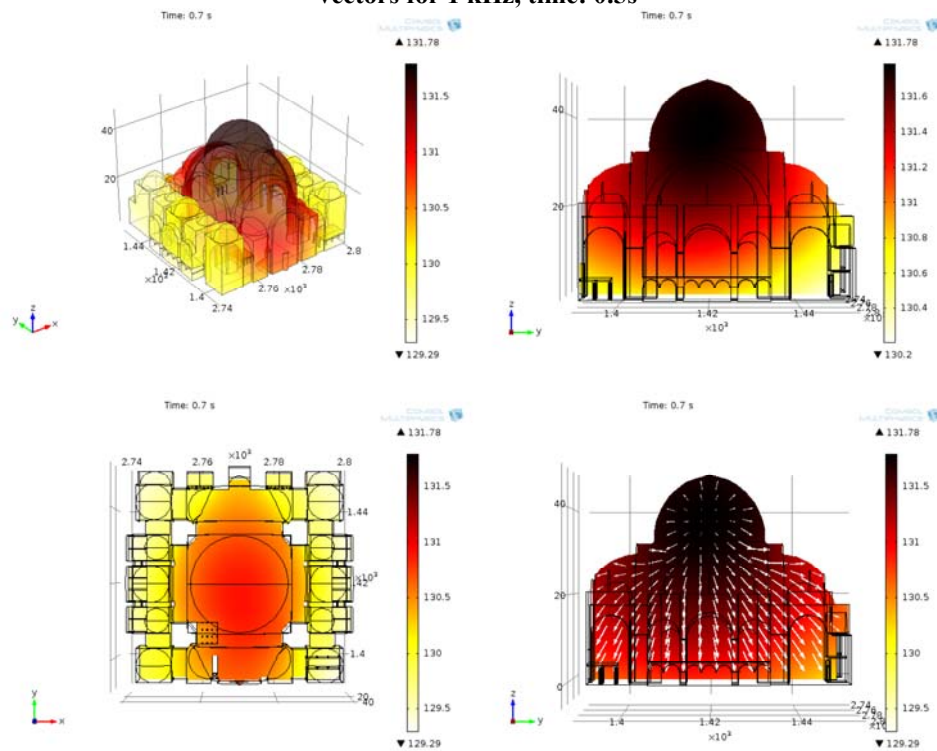


Figure 5.31. Süleymaniye Mosque DEM results, spatial sound energy distributions and flow vectors for 1 kHz, time: 0.7s

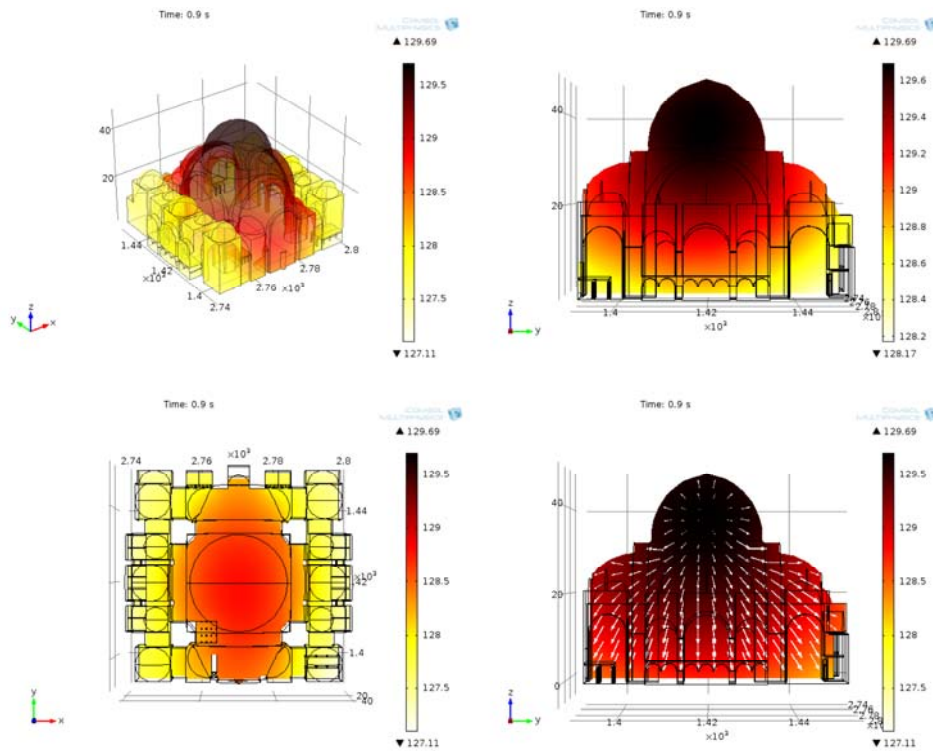


Figure 5.32. Süleymaniye Mosque DEM results, spatial sound energy distributions and flow vectors for 1 kHz, time: 0.9s

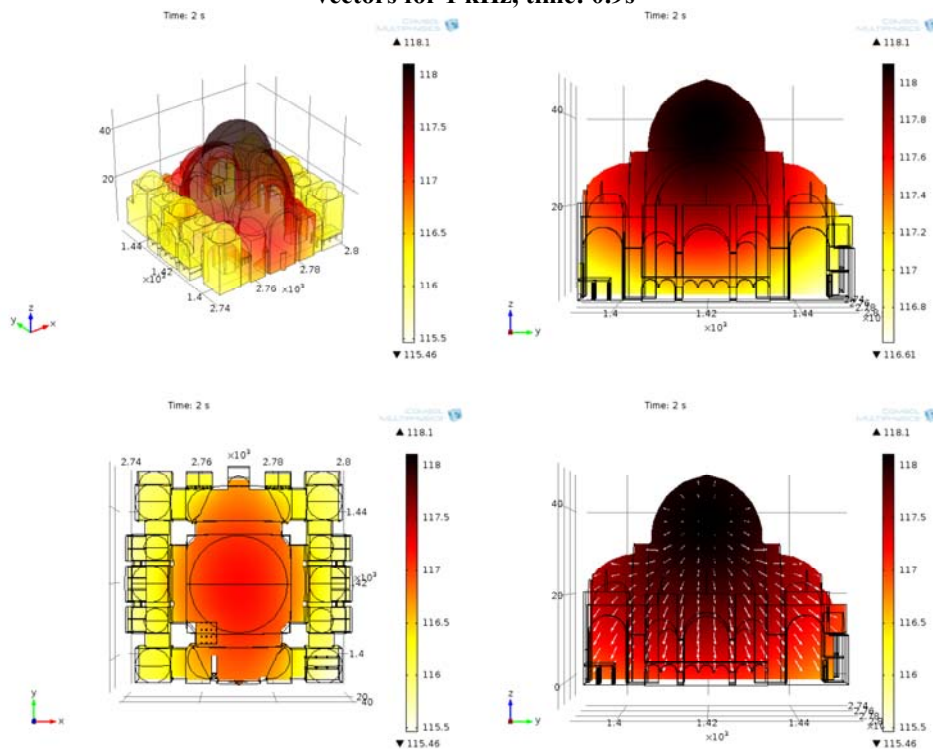


Figure 5.33. Süleymaniye Mosque DEM results, spatial sound energy distributions and flow vectors for 1 kHz, time: 2s

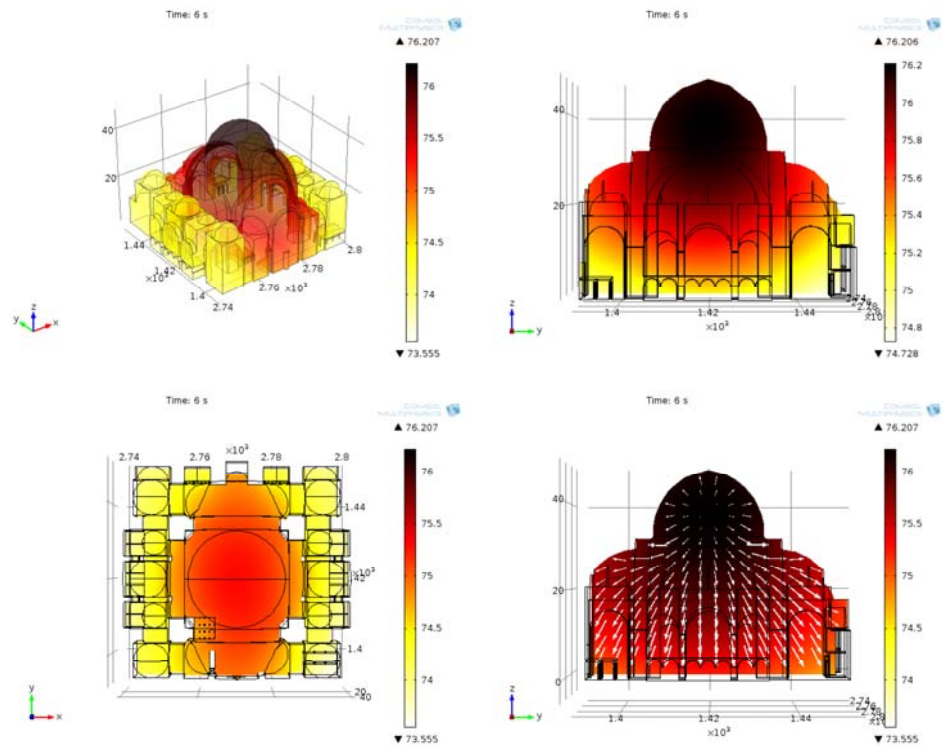


Figure 5.34. Süleymaniye Mosque DEM results, spatial sound energy distributions and flow vectors for 1 kHz, time: 6s

Following the case that represents the present condition of the Mosque with current materials, the effects of absorptive floor versus reflective upper shell structure on non-exponential energy decay formation is searched by replacing carpet floor with marble (Sü Gül et al., 2014c). Another group of DEM solution results are presented for Süleymaniye Mosque in a virtual case of floor with marble (see Figure 5.35 to Figure 5.41). 1000 Hz is chosen as a representative higher 1/1 octave band, in which there is a significant difference in between sound absorption coefficients of carpet (~ 0.40) and marble (~ 0.01). Higher resolution plots of selected cases for Süleymaniye Mosque DEM solution for floor with marble are presented under Appendix C. Detailed interpretation of Süleymaniye Mosque marbled floor DEM results and their relation to coupling investigations are presented under Section 6.4.

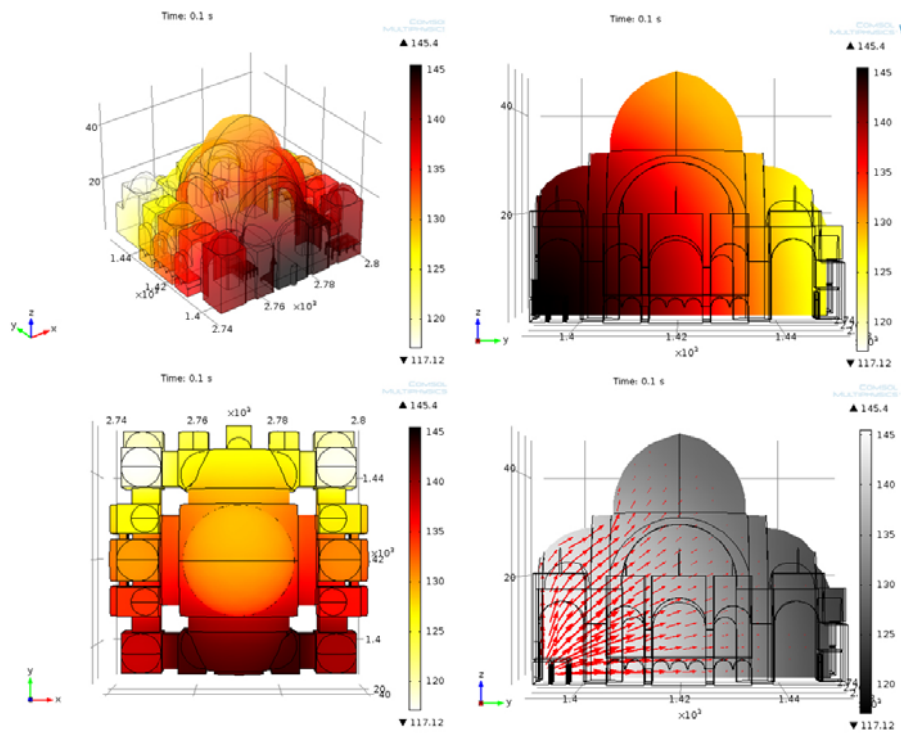


Figure 5.35. Süleymaniye Mosque DEM results, spatial sound energy distributions and flow vectors for 1 kHz, time: 0.1s; marble floor

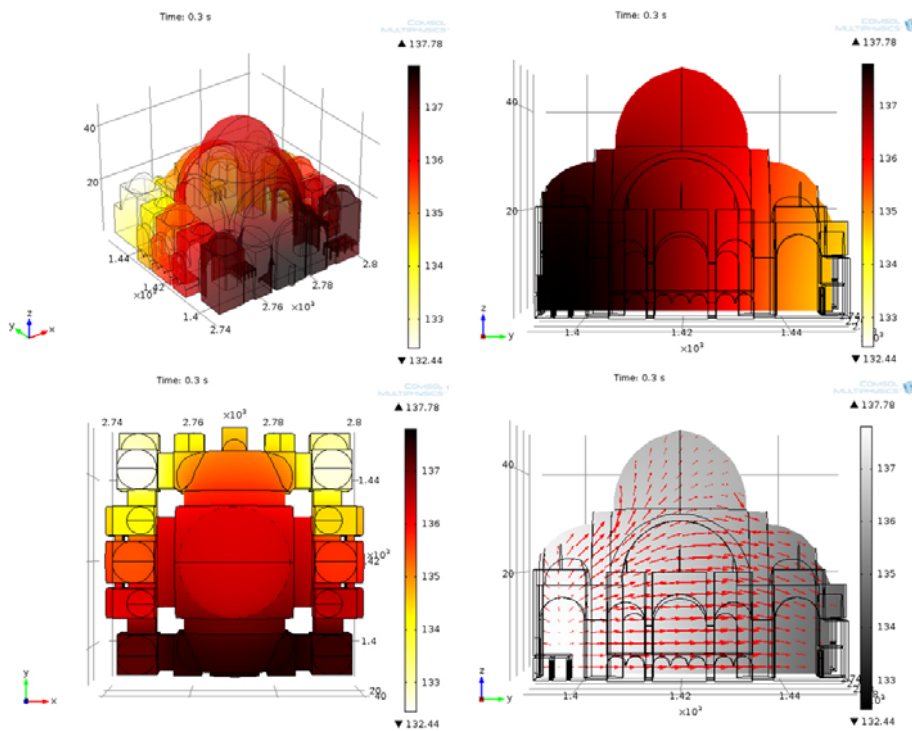


Figure 5.36. Süleymaniye Mosque DEM results, spatial sound energy distributions and flow vectors for 1 kHz, time: 0.3s; marble floor

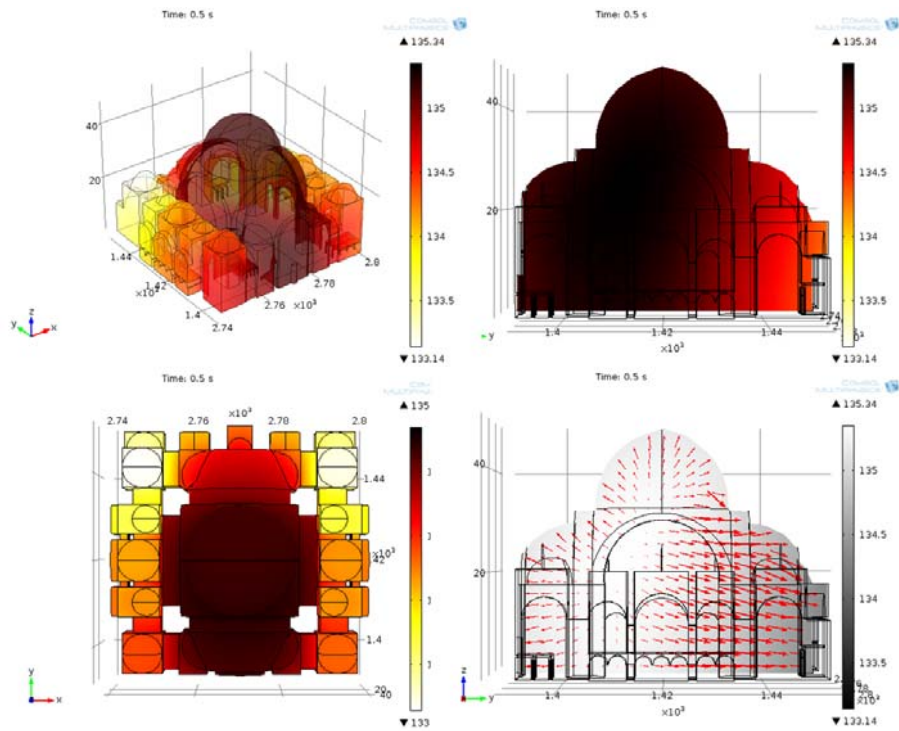


Figure 5.37. Süleymaniye Mosque DEM results, spatial sound energy distributions and flow vectors for 1 kHz, time: 0.5s; marble floor

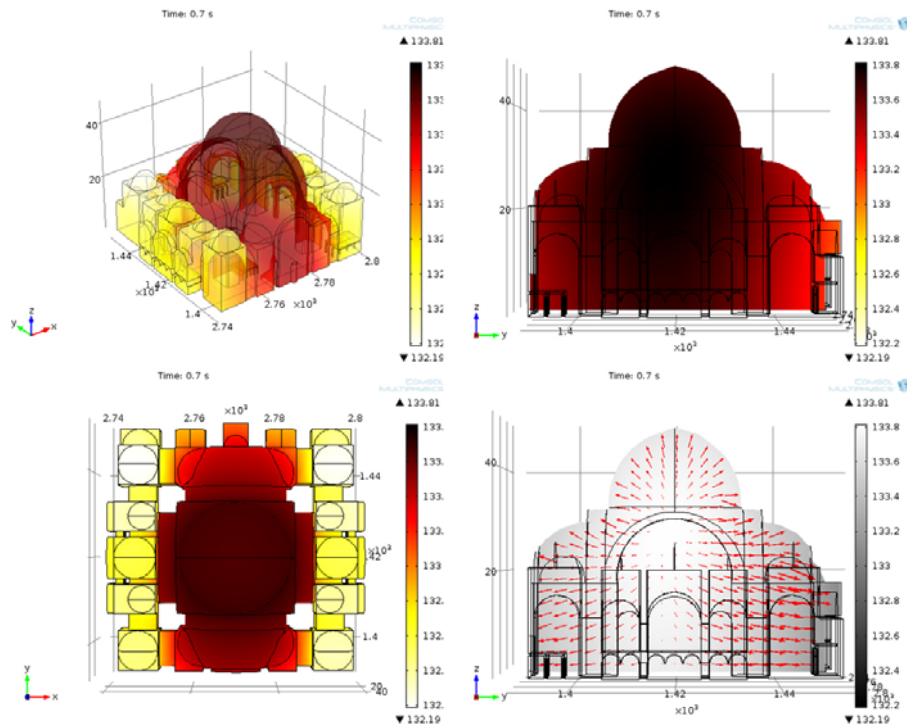


Figure 5.38. Süleymaniye Mosque DEM results, spatial sound energy distributions and flow vectors for 1 kHz, time: 0.7s; marble floor

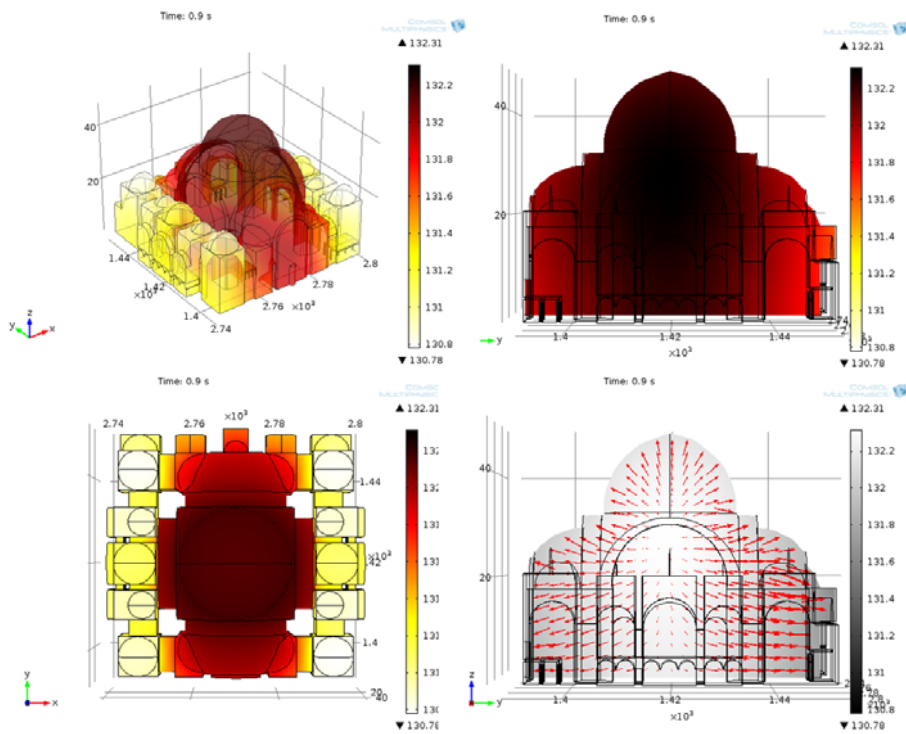


Figure 5.39. Süleymaniye Mosque DEM results, spatial sound energy distributions and flow vectors for 1 kHz, time: 0.9s; marble floor

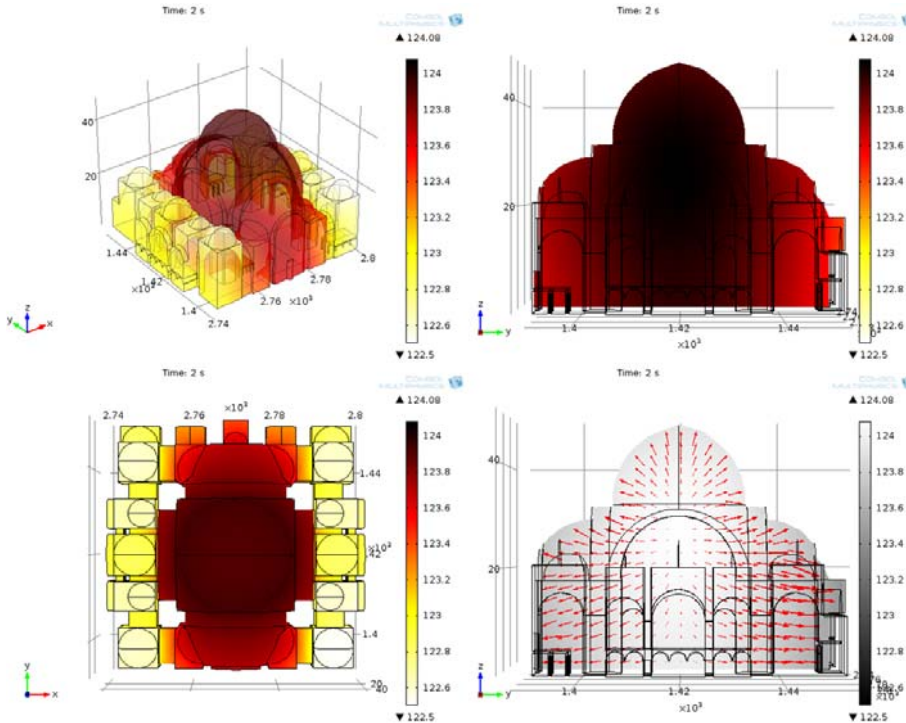


Figure 5.40. Süleymaniye Mosque DEM results, spatial sound energy distributions and flow vectors for 1 kHz, time: 2s; marble floor

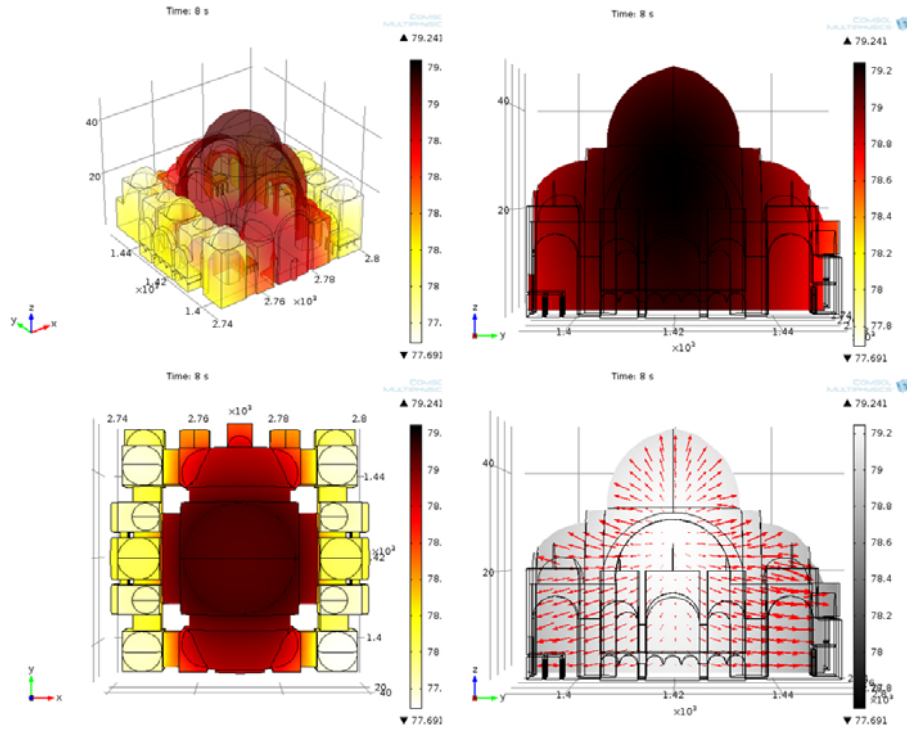


Figure 5.41. Süleymaniye Mosque DEM results, spatial sound energy distributions and flow vectors for 1 kHz, time: 8s; marble floor

5.4. INTENSITY PROBE DATA (SÜLEYMANIYE MOSQUE)

Within Süleymaniye Mosque’s main prayer hall via intensity probe measurements total of 37 3D-impulse responses are collected. These data are initially evaluated for their usability by checking the acceptable INR values and dependable T30 values in compare to previous DIRAC post-processed T30 and Multi-Slope analyzed decay rate values. Results of T30 and INR values over octave bands through 63 Hz to 8 kHz are summarized in Table 5.11. The T30 results out of probe measurements are also compared to DIRAC T30 results in Table 5.11 for different sound-receiver configurations. Reliable data for future intensity vector analysis are highlighted. USP indicates the results out of intensity probe as in this case the Microflown mini USP and P indicates the results out of regular pressure microphone as in this case the B&K type hand-held analyzer (DIRAC results). S indicates e-sweep measurements, B indicates balloon pop and W indicates wood clap measurements. The total signal generation and recording durations are indicated in seconds (s).

Table 5.11. Süleymaniye Mosque intensity probe field measurement data and comparison of T30 results of probe measurements (USP) to T30 results of pressure microphone (P)

Location	Frequency								
		63	125	250	500	1000	2000	4000	8000
S1R1_S_35s	INR [dB]	18	25	27	25	21	32	62	50
	T30 [s] USP	16.71	12.22	18.77	4.67	4.37	2.44	1.76	1.79
	T30 [s] P	17.93	16.59	10.89	6.36	5.72	3.91	2.35	1.42
S1R1_S_40s	INR [dB]	16	26	28	27	23	30	60	49
	T30 [s] USP	31.32	15.29	11.87	4.74	5.20	3.75	1.80	1.81
	T30 [s] P	17.93	16.59	10.89	6.36	5.72	3.91	2.35	1.42
S1R1_B_10s	INR [dB]	22	31	41	45	49	59	58	55
	T30 [s] USP	10.25	17.54	9.59	6.35	5.63	3.77	2.65	1.34
	T30 [s] P	17.93	16.59	10.89	6.36	5.72	3.91	2.35	1.42
S1R1_B_15s	INR [dB]	25	35	43	49	51	58	64	60
	T30 [s] USP	13.94	14.23	9.63	6.26	5.51	3.65	2.34	1.47
	T30 [s] P	17.93	16.59	10.89	6.36	5.72	3.91	2.35	1.42
S1R1_B_20s	INR [dB]	28	34	45	50	49	60	63	59
	T30 [s] USP	12.47	14.50	9.57	6.12	5.88	3.39	2.47	1.45
	T30 [s] P	17.93	16.59	10.89	6.36	5.72	3.91	2.35	1.42
S1R2_S_35s	INR [dB]	16	27	28	25	22	30	61	50
	T30 [s] USP	11.94	13.74	9.55	6.21	3.54	3.72	1.77	1.77
S1R2_S_40s	INR [dB]	18	25	28	26	21.00	31	62	50
	T30 [s] USP	7.52	10.65	13.30	8.51	10.62	3.30	1.77	1.79
S1R3_S_40s	INR [dB]	18	29	28	25	21	31	61	49
	T30 [s] USP	6.49	26.50	15.96	6.86	5.28	3.44	1.78	1.82
S1R3_S_30s	INR [dB]	15	28	28	25	21	30	60	49
	T30 [s] USP	NA	21.46	13.53	4.69	3.87	3.13	1.76	1.78
S1R4_S_40s	INR [dB]	20	29	28	25	22	29	58	48
	T30 [s] USP	21.32	12.99	12.31	6.73	3.74	4.97	1.83	1.81
S1R4_B_20s_r1	INR [dB]	21	32	41	49	49	54	61	58
	T30 [s] USP	11.26	13.53	8.80	6.28	6.09	3.65	2.28	1.42
S1R4_B_20s_r2	INR [dB]	24	36	43	53	53	54	58	58
	T30 [s] USP	13.37	14.46	9.81	6.35	5.86	4.07	2.34	1.38
S1R4_W_20s	INR [dB]	33	20	25	37	45	56	59	57
	T30 [s] USP	0.08	13.05	6.17	6.31	5.39	3.67	2.35	1.41
S1R5_S_40s	INR [dB]	19	31	31	27	25	36	67	56
	T30 [s] USP	5.91	16.75	11.65	6.81	4.76	3.18	1.76	1.75
S1R6_S_40s	INR [dB]	17	27	26	23	22	27	57	47
	T30 [s] USP	13.79	15.12	10.10	4.97	3.72	3.85	1.86	1.85
S1R7_S_40s	INR [dB]	35	48	39	37	26	31	46	44
	T30 [s] USP	0.27	0.25	13.28	0.78	5.00	3.03	1.74	1.71

Table 5.12 (continued)

S1R8_S_40s	INR [dB]		15	27	26	23	21	27	57	47
	T30 [s]	USP	14.97	17.06	14.30	7.27	4.69	4.46	1.87	1.85
S1R9_S_40s	INR [dB]		15	27	27	23	21	26	55	44
	T30 [s]	USP	27.62	15.01	16.64	5.38	5.85	4.05	1.89	1.85
S1R10_S_40s	INR [dB]		19	45	53	36	28	30	54	44
	T30 [s]	USP	39.09	14.65	7.49	5.95	4.20	3.95	1.88	1.85
S1R11_S_40s	INR [dB]		18	24	26	24	21	30	59	46
	T30 [s]	USP	3.30	11.46	10.20	5.06	4.81	4.02	1.90	1.84
S1R12_S_40s	INR [dB]		11	26	26	22	19	29	58	46
	T30 [s]	USP	5.90	12.04	11.50	5.96	5.82	4.22	1.86	1.83
S1R13_S_40s	INR [dB]		22.00	32.00	29.00	25.00	22.00	34.00	65.00	55.00
	T30 [s]	USP	14	16.52	13.16	10.80	3.91	3.90	1.83	1.83
S1R13_S_40s	INR [dB]		18.00	27	25	22	21	28	58	47
	T30 [s]	USP	29.60	14.32	16.80	4.93	11.26	4.16	1.83	1.82
S1R13_B_20s_r1	INR [dB]		17	31	39	44	44	55	52	46
	T30 [s]	USP	7.70	19.77	11.46	6.59	5.75	3.91	2.68	1.51
	T30 [s]	P	20.12	16.83	11.42	6.45	5.85	4.10	2.56	1.55
S1R13_B_20s_r2	INR [dB]		21	32	39	42	36	36	34	23
	T30 [s]	USP	14.49	16.66	11.60	6.52	5.94	4.47	2.67	2.83
	T30 [s]	P	20.12	16.83	11.42	6.45	5.85	4.10	2.56	1.55
S1R13x1_S_40s	INR [dB]		14	26	25	22	21	26	56	45
	T30 [s]	USP	25.94	14.97	9.76	12.71	8.65	3.01	1.78	1.78
S1R13x2_S_40s	INR [dB]		16	27	24	23	20	27	57	46
	T30 [s]	USP	4.29	17.11	10.14	7.18	9.42	4.55	1.79	1.76
S1R13x2_B_20s	INR [dB]		21	33	41	49	50	52	57	56
	T30 [s]	USP	12.33	14.72	10.19	6.54	6.11	4.08	2.35	1.58
S1R14_S_40s	INR [dB]		16	27	27	25	22	30	58	46
	T30 [s]	USP	7.37	17.87	11.71	5.19	4.59	3.28	1.83	1.95
	T30 [s]	P	21.46	17.06	12.48	6.62	5.74	4.08	2.52	1.39
S1R14_B_20s_r1	INR [dB]		27	39	45	53	53	60	64	59
	T30 [s]	USP	13.97	15.42	9.81	6.47	6.09	3.74	2.35	1.43
	T30 [s]	P	21.46	17.06	12.48	6.62	5.74	4.08	2.52	1.39
S1R14_B_20s_r2	INR [dB]		24	39	45	52	52	59	62	58
	T30 [s]	USP	16.57	17.14	9.34	6.45	6.03	3.69	2.34	1.45
	T30 [s]	P	21.46	17.06	12.48	6.62	5.74	4.08	2.52	1.39
S2R4_B_20s	INR [dB]		22	32	40	50	52	53	59	59
	T30 [s]	USP	11.47	12.90	9.91	6.51	6.03	3.98	2.29	1.43
S2R13x2_B_20s	INR [dB]		24	31	41	49	53	61	67	64
	T30 [s]	USP	12.65	12.29	9.35	6.74	5.53	3.23	2.26	1.33

Table 5.13 (continued)

S3R14_B_20s	INR [dB]		25	34	42	52	50	51	53	49
	T30 [s]	USP	19.22	16.05	10.26	6.27	6.00	4.10	2.24	1.45
S4R14_B_10s	INR [dB]		18	27	36	45	42	44	48	42
	T30 [s]	USP	12.05	17.56	10.73	6.45	6.06	4.18	2.46	1.65
	T30 [s]	P	21.61	16.95	12.53	6.77	6.00	4.13	2.56	1.56
S4R14_B_20s	INR [dB]		20	31	39	47	46	48	51	46
	T30 [s]	USP	14.98	15.25	9.96	6.57	6.13	4.00	2.43	1.63
	T30 [s]	P	21.61	16.95	12.53	6.77	6.00	4.13	2.56	1.56

**values in green indicate reliable data considering INR values, values in red indicate reliable data for analysis considering T30 values*

As highlighted in Table 5.11, balloon pop measurements are found more reliable in overall intensity vector analysis. Out of these data representative cases for 1 kHz for S₁R₄, S₁R₄ and S₁R₁₃ are summarized under this section. These source-receiver configurations are also important for comparison with DEM results on the longitudinal section of the Mosque, where energy exchanges are dominantly observed. Intensity vector plots for three receiver (R1, R4, R13) positions, when source is in front of mihrab wall (S1) are plotted together in longitudinal section (XZ coordinate; Figure 5.42 to Figure 5.48) and axon (3D; Figure 5.49 to Figure 5.55) views. First image under each group (Figure 5.42 and Figure 5.49) is a full size image (full section and full axon views) for time 0 millisecond (right after the source is stopped or the balloon is popped) to express the approximate location of vector plots and other images are close-up images for better use of space. Vectors in all plots indicate the flow direction meaning from energy surplus location to energy deficient location. Data are exported in general for 25 ms to 50 ms time intervals. Detailed analysis is held for critical time spans as flow return occurrence for critical locations. Individual outputs for typical as well as shorter time windows, where necessary, are presented under Appendix D and detailed interpretation of the results are presented under Discussion section by comparison with DEM results.

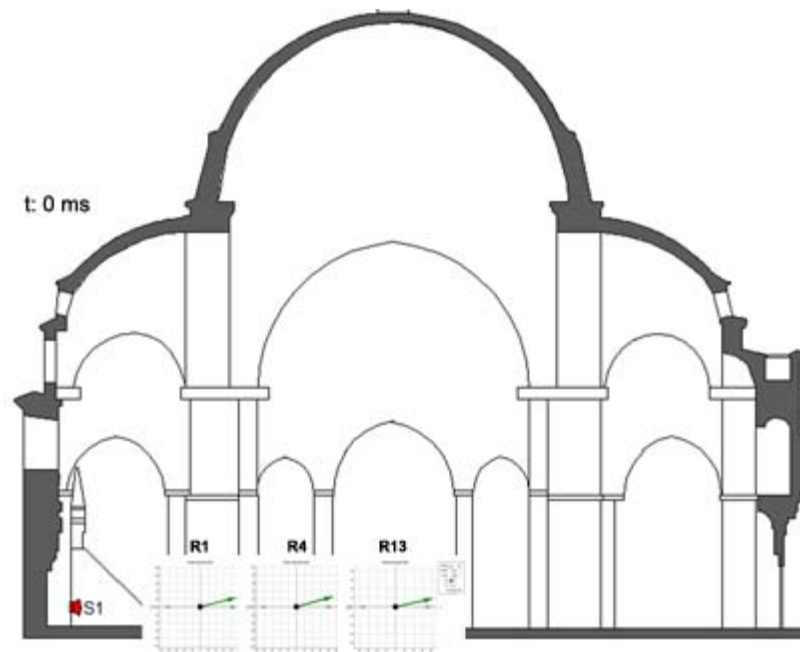


Figure 5.42. Intensity vectors, 1kHz, t: 0 ms, full section view (XZ axis), Süleymaniye Mosque

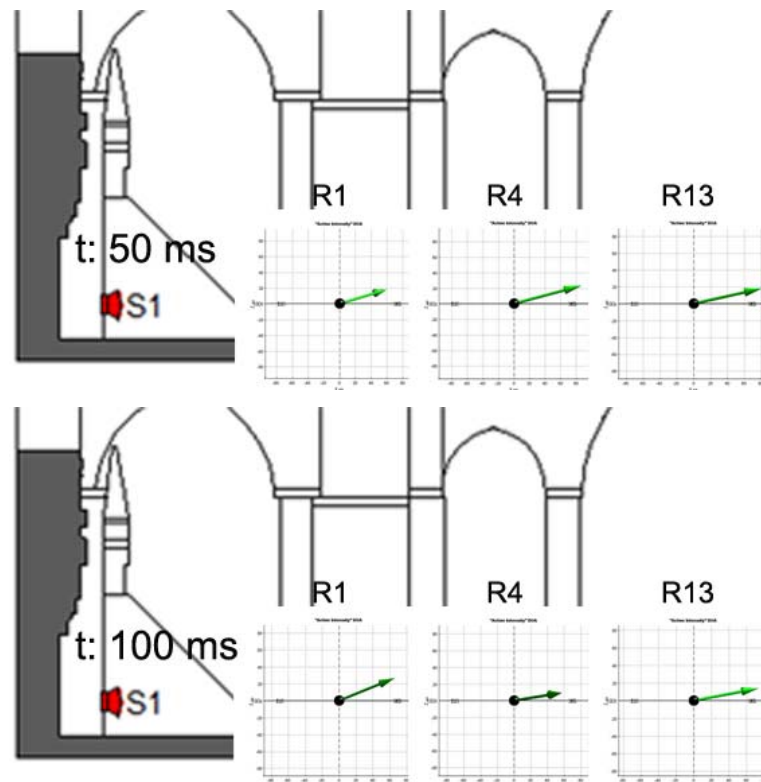


Figure 5.43. Intensity vectors, 1kHz, t: 50 and 100ms, section view, Süleymaniye Mosque

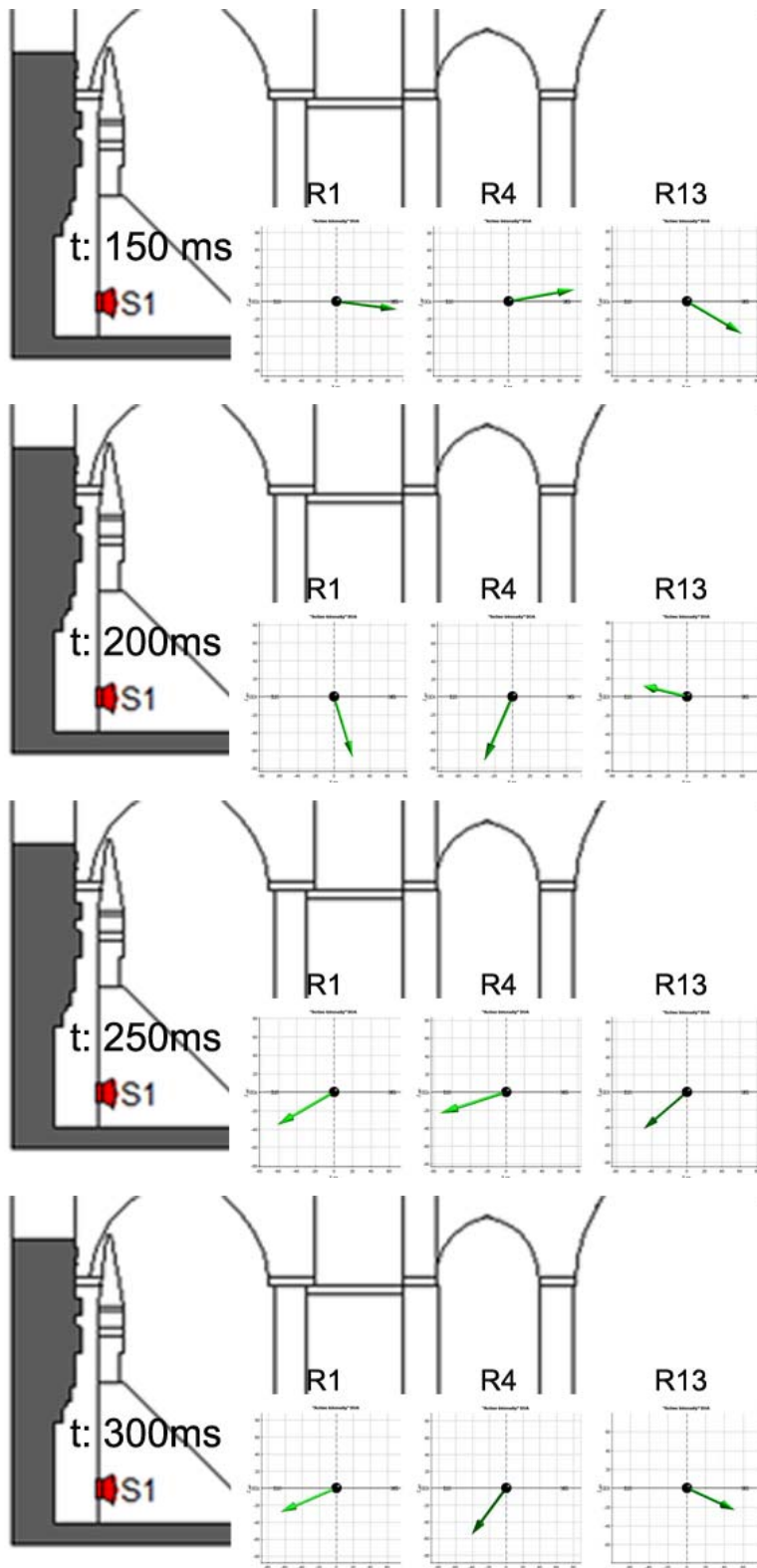


Figure 5.44. Intensity vectors, 1kHz, t: 150, 200, 250 and 300ms, section view, Süleymaniye Mosque

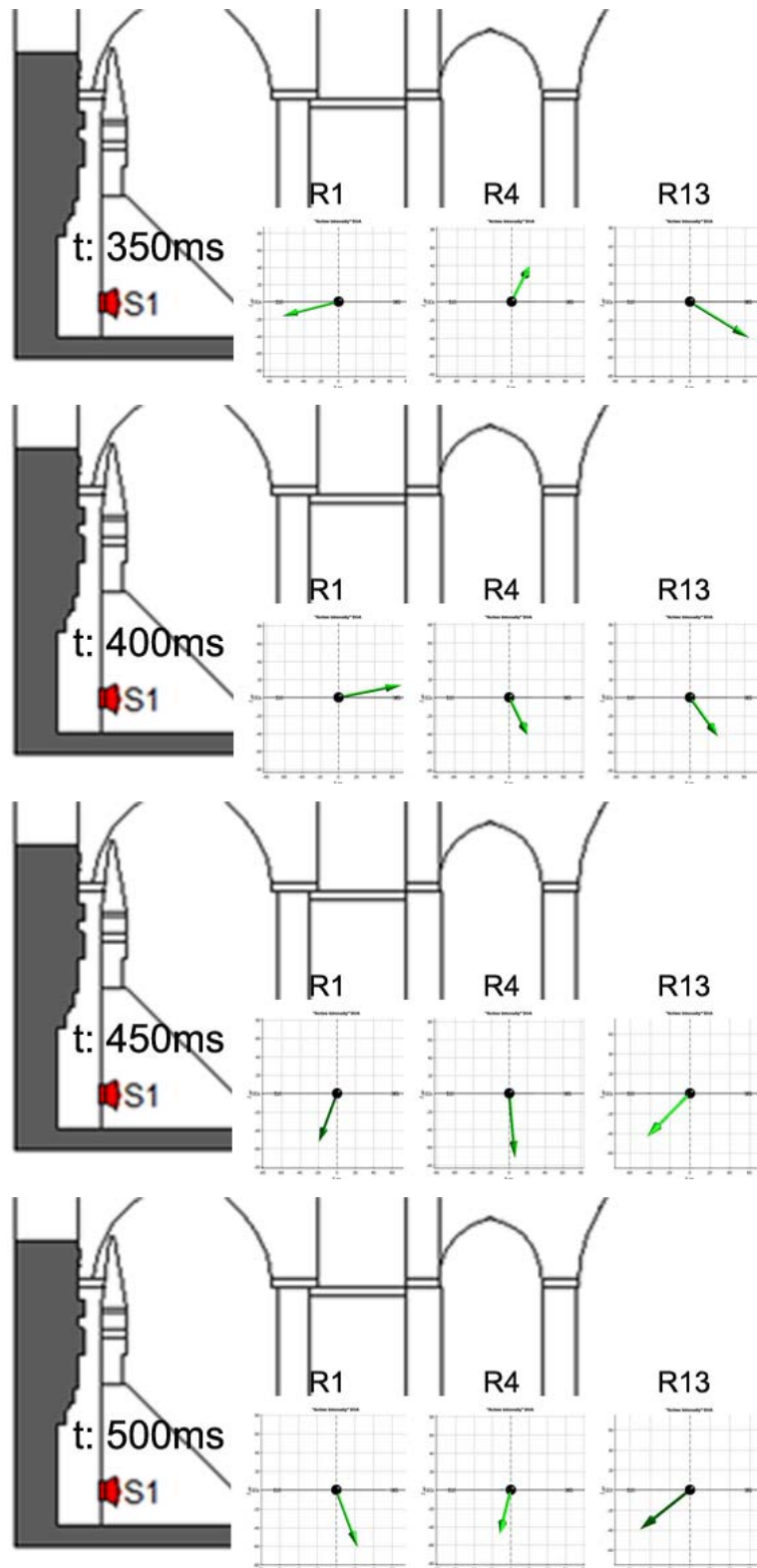


Figure 5.45. Intensity vectors, 1kHz, t: 350, 400, 450 and 500ms, section view, Süleymaniye Mosque

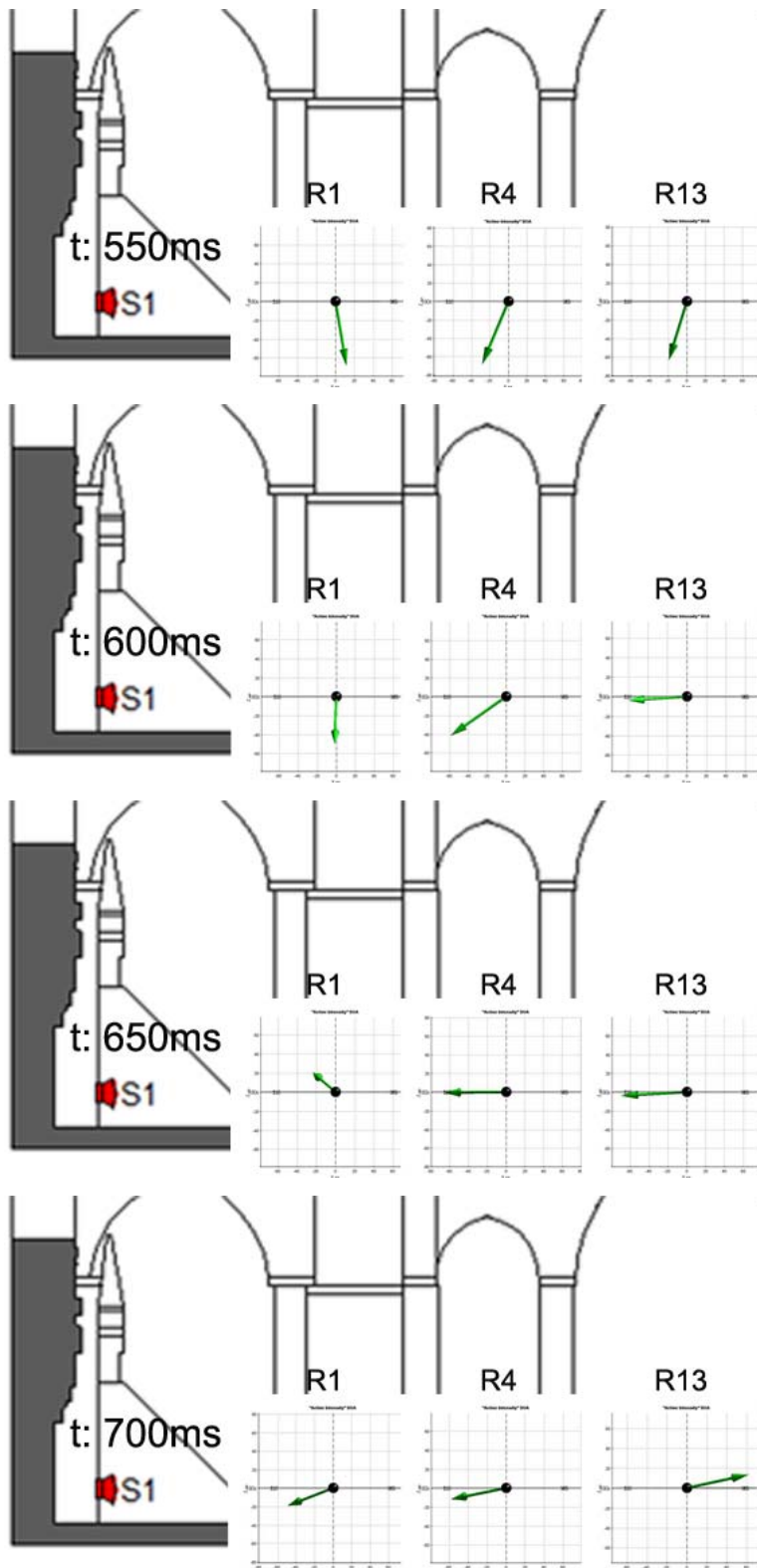


Figure 5.46. Intensity vectors, 1kHz, t: 550, 600, 650 and 700ms, section view, Süleymaniye Mosque

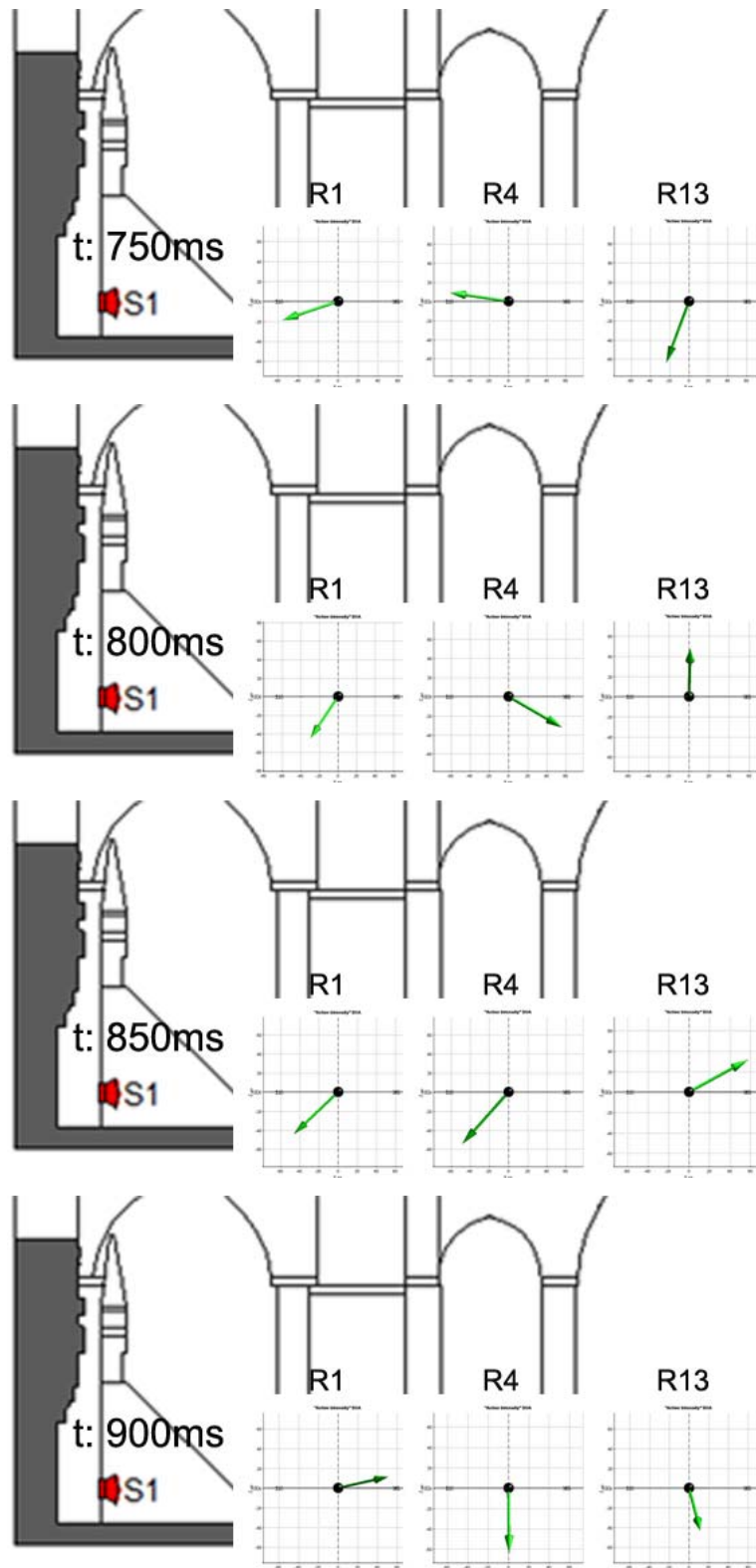


Figure 5.47. Intensity vectors, 1kHz, t: 750, 800, 850 and 900ms, section view, Süleymaniye Mosque

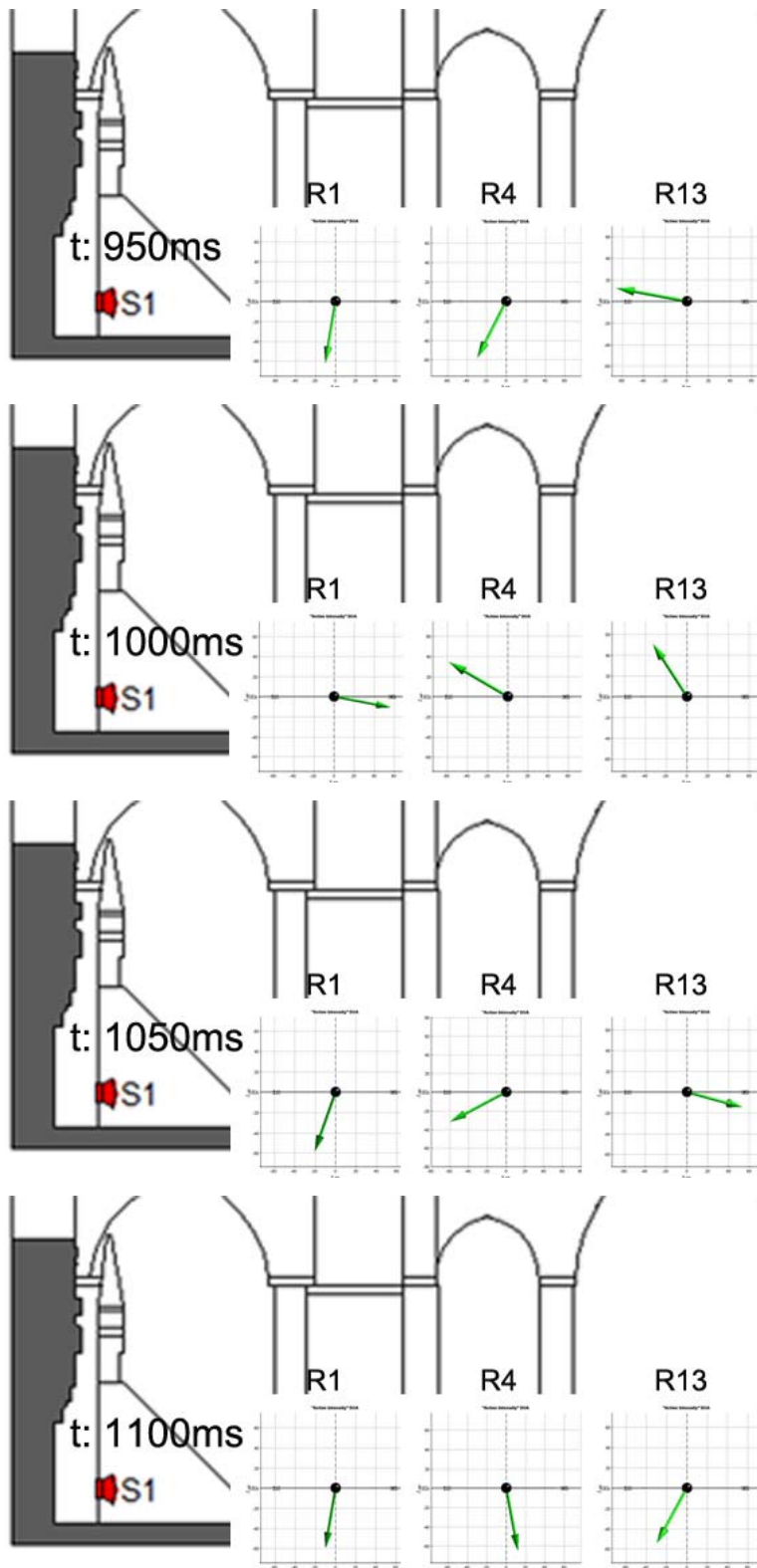


Figure 5.48. Intensity vectors, 1kHz, t: 950, 1000, 1150 and 1100ms, section view, Süleymaniye Mosque

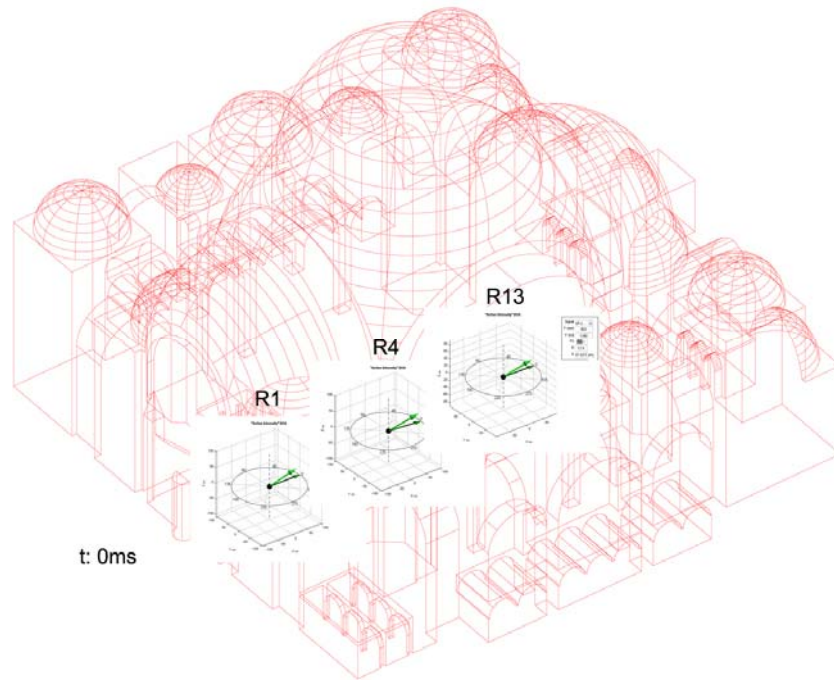


Figure 5.49. Intensity vectors, 1kHz, t: 0 ms, full axon view, Süleymaniye Mosque

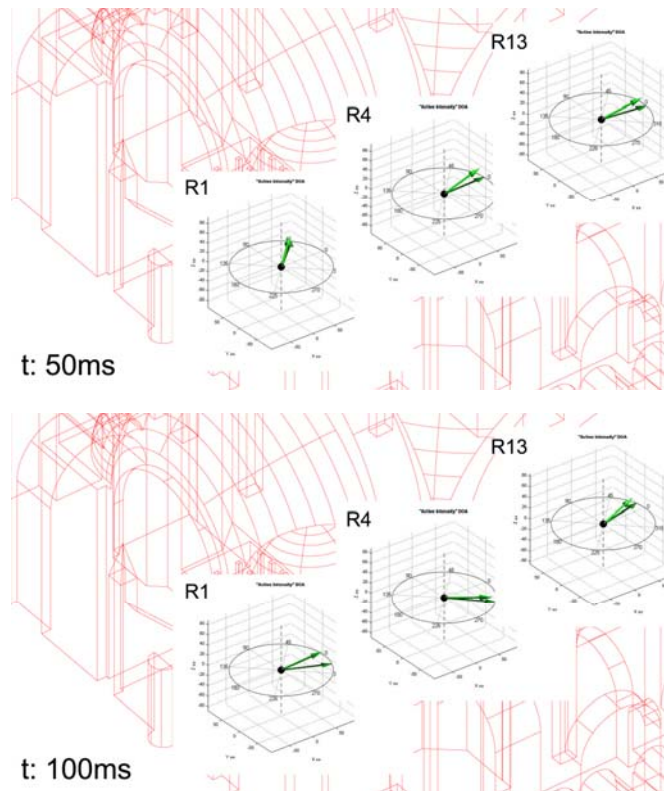


Figure 5.50. Intensity vectors, 1kHz, t: 50 and 100ms, axon view, Süleymaniye Mosque

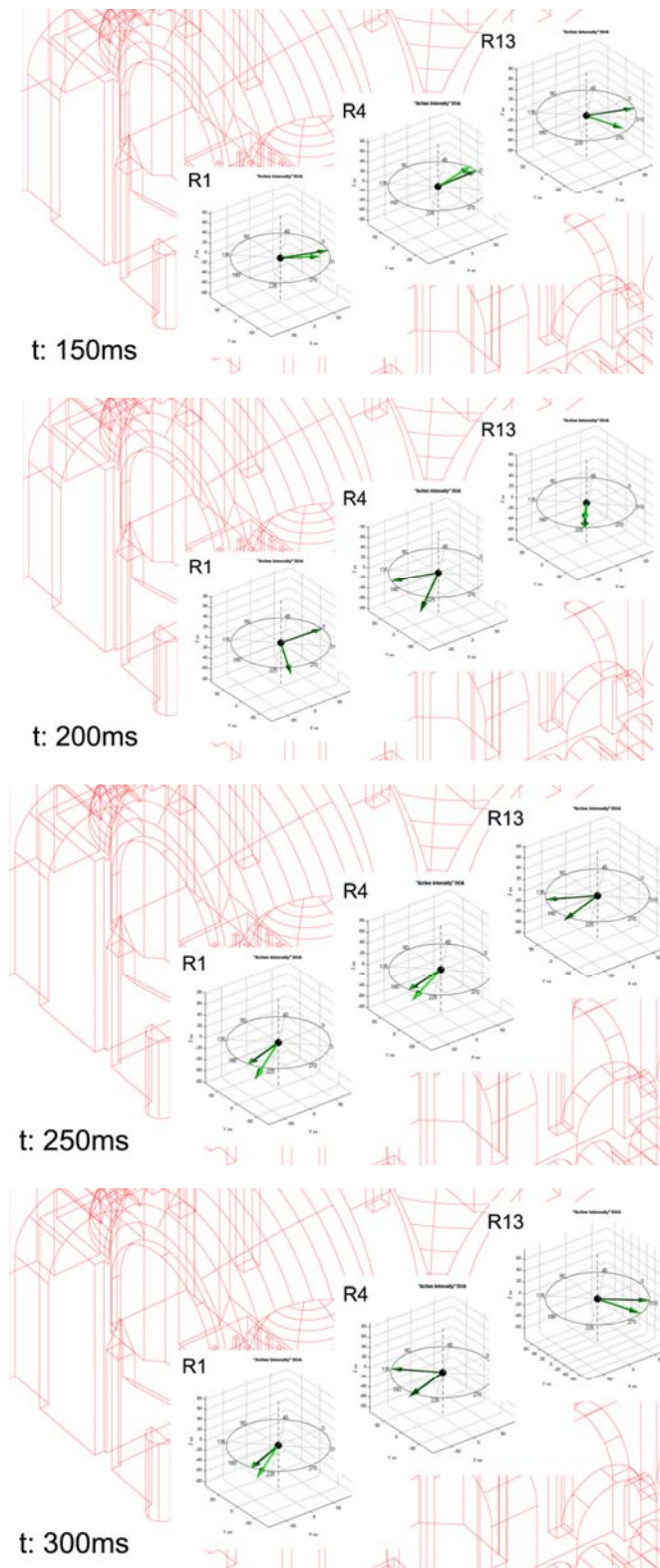


Figure 5.51. Intensity vectors, 1kHz, t: 150, 200, 250 and 300ms, axon view, Süleymaniye Mosque

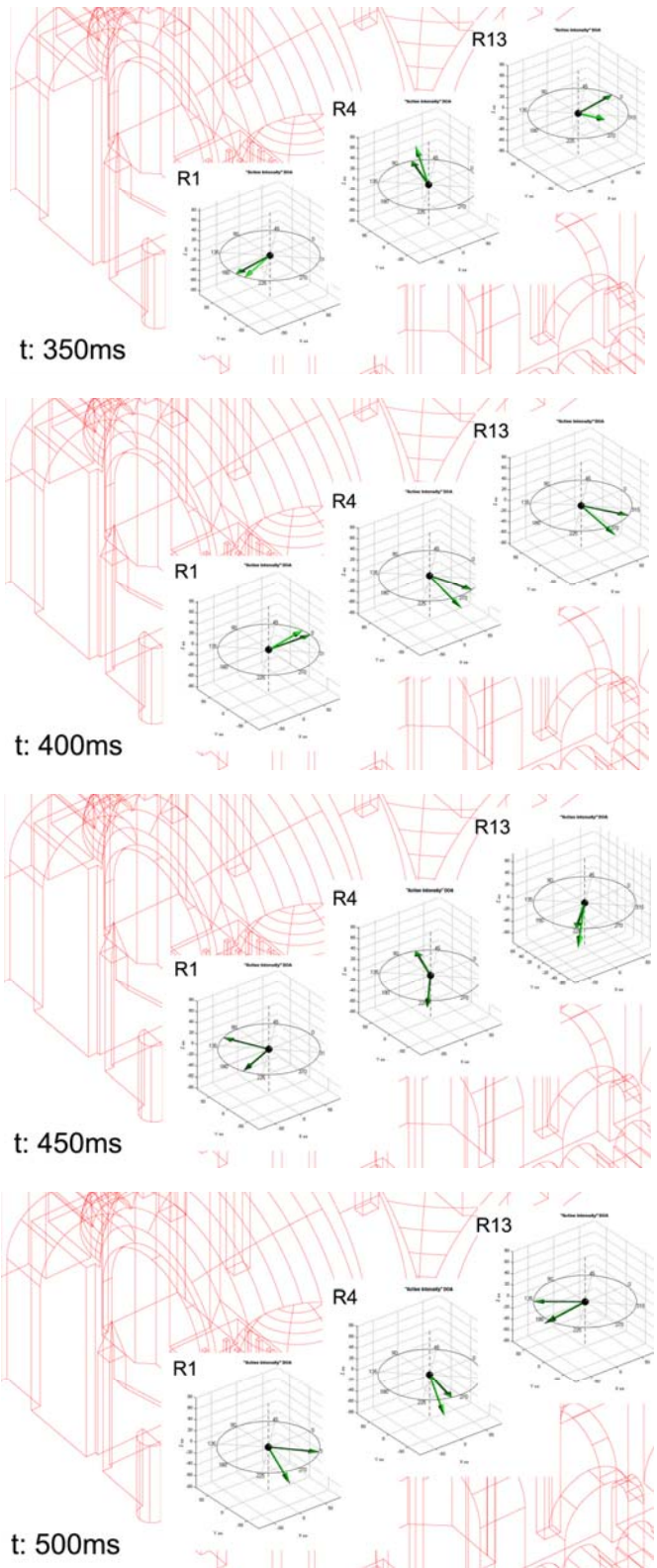


Figure 5.52. Intensity vectors, 1kHz, t: 350, 400, 450 and 500ms, axon view, Süleymaniye Mosque
163

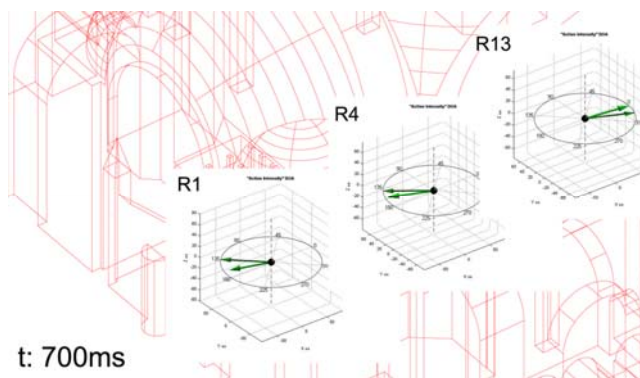
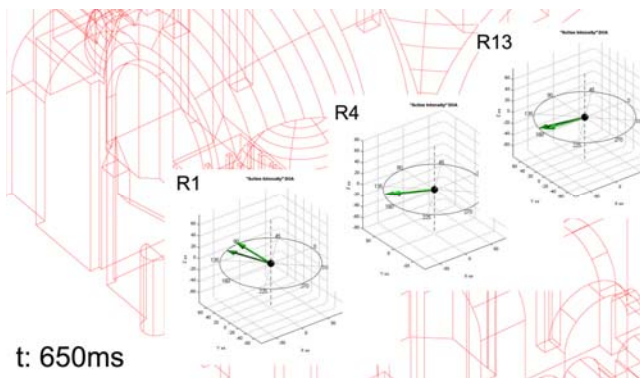
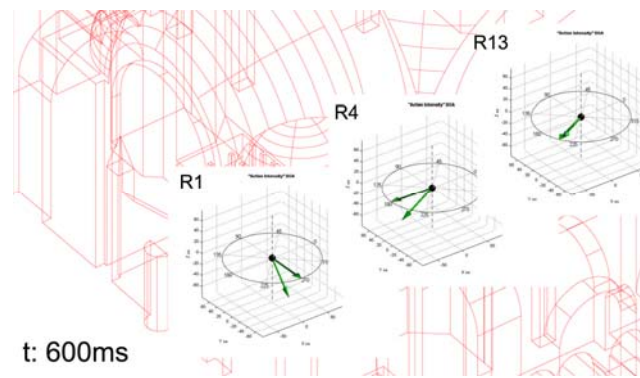
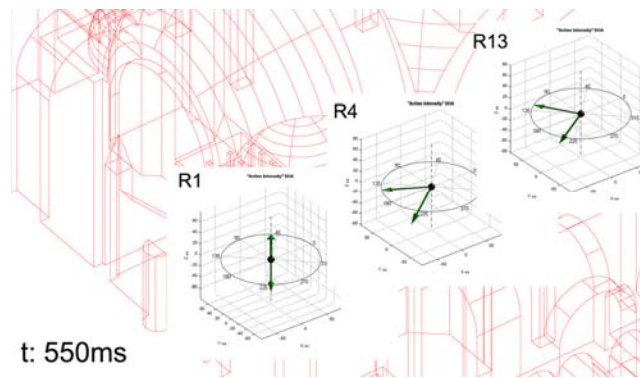


Figure 5.53. Intensity vectors, 1kHz, t: 550, 600, 650 and 700ms, axon view, Süleymaniye Mosque

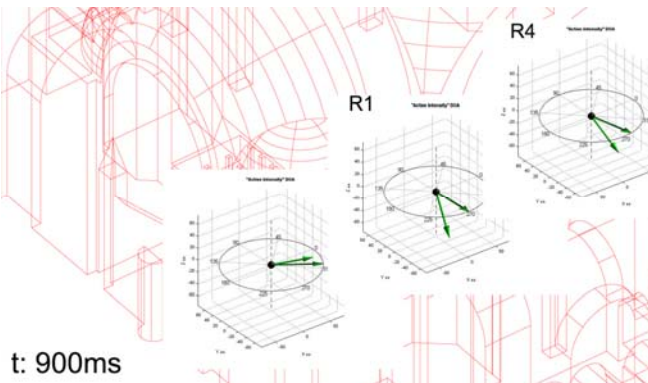
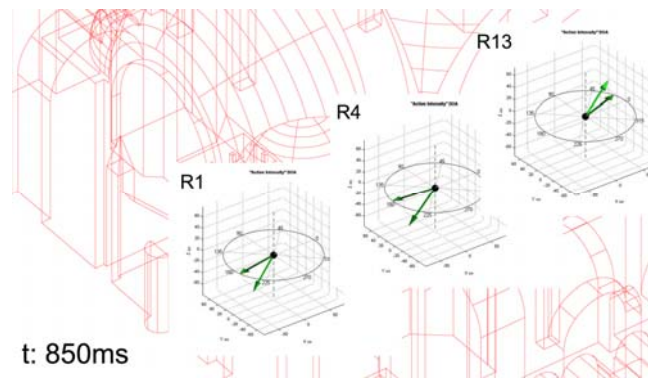
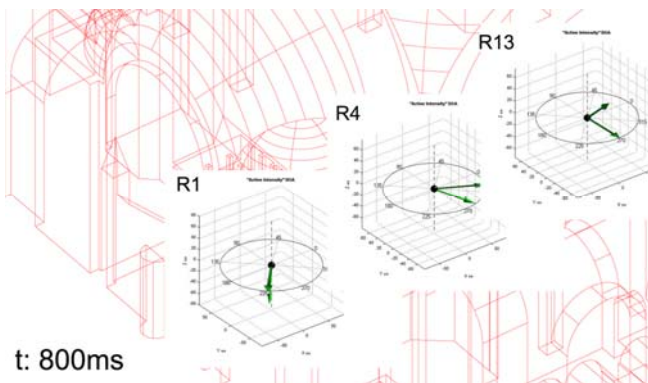
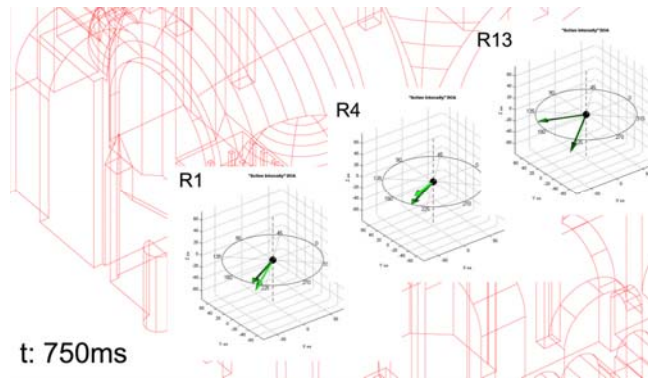


Figure 5.54. Intensity vectors, 1kHz, t: 750, 800, 900 and 950ms, axon view, Süleymaniye Mosque

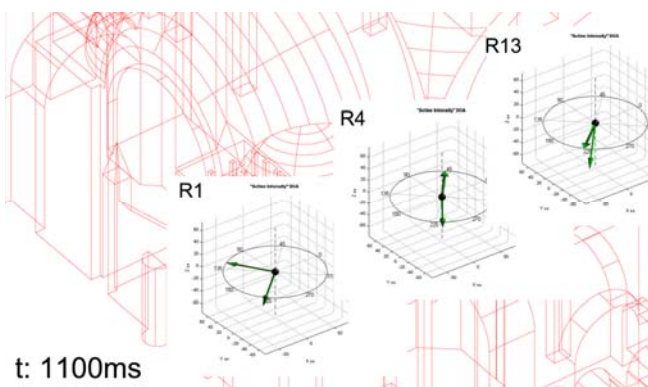
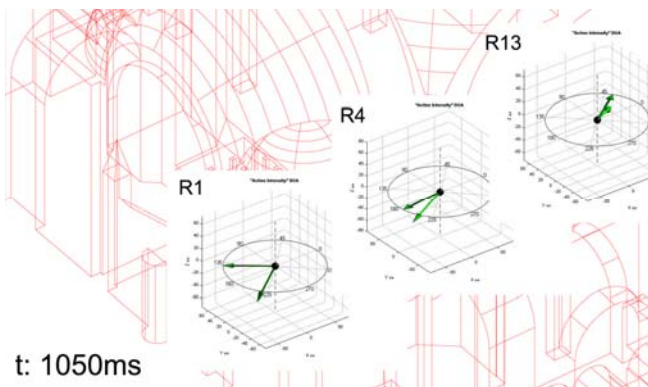
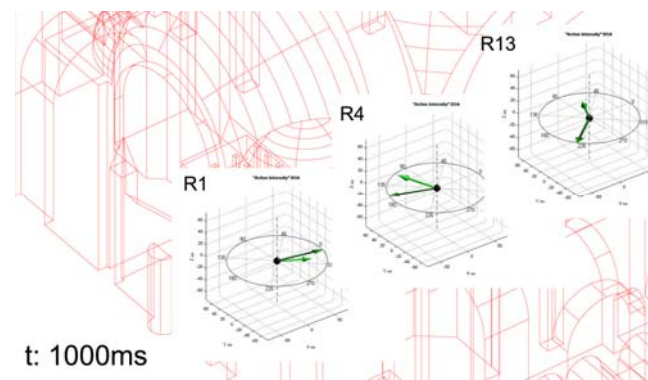
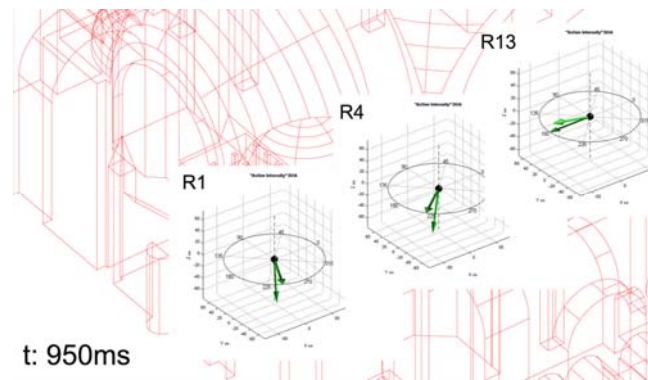


Figure 5.55. Intensity vectors, 1kHz, t: 950, 1000, 1050 and 1100ms, axon view, Süleymaniye Mosque

CHAPTER 6

DISCUSSIONS

6.1. ACOUSTICAL FIELD COMPARISON OF SÜLEYMANİYE MOSQUE FOR BEFORE AND AFTER 2007-2011 RESTORATIONS

The architectural/material modifications over Süleymaniye Mosque in different time periods are briefed in Research Materials section. With an aim of assessing the acoustical effects of previous restoration works the field measurements taken in 2013 within the context of this thesis research are compared with previous field test data (Sü Gül et al., 2013d). The common acoustical parameter measured and assessed in all field tests is the reverberation time (T30). Thus, measured T30s over octave bands are the basis of comparisons.

The first set of measurement after 1959-1969 restorations was held by Gazi University in 1988 (GÜ-1988). The measurements are taken in 1/3 octaves for the frequency spectrum in between 100 Hz to 8 kHz (Kayılı, 1988a). Following field tests were taken by Middle East Technical University (METU) in 1996 (ODTÜ-1996). Broadband noise signal was emitted at two source locations including one in front of *mihrab* and one over *müezzin's mahfili*. Impulse responses were collected for six receiver locations at the prayer's area (Topaktaş, 2003). The final group of measurements after 1959-1969 restorations, as can be find in the academic literature, were held in 2000 within the program of EA project namely CAHRISMA (Karabiber, 2000). Ferrara University (UNIFE-2000) and Denmark Technical University (DTU-2000) hold two different measurements in the context of EU

project. Sweep signal was used as a source signal, and impulse responses were collected for different configurations of three source and six receiver locations. UNIFE used test signal possessing 80 Hz to 18000 Hz spectrum range and DTU used test signal possessing 35 Hz to 11500 Hz spectrum range. DTU recorded impulses for 10 seconds of capture length (CAHRISMA, 2001).

The first measurements after 1959-1969 restorations are held within the context of this thesis research (Sü Gül et al., 2013) and abbreviated as ODTÜ-2013 (or METU-2013) in following discussion for the ease of comparisons. The final field tests held in 2013 are coordinated by Atılım University (AÜ-2013). 1/3 octaves are used in collecting data in between 100 Hz to 8 kHz frequency spectrum in this final set of measurement (Eröz, 2013). T30 results of all field tests summarized above are compared in 1/1 octaves for frequency range in between 125 Hz to 4 kHz (Figure 6.1).

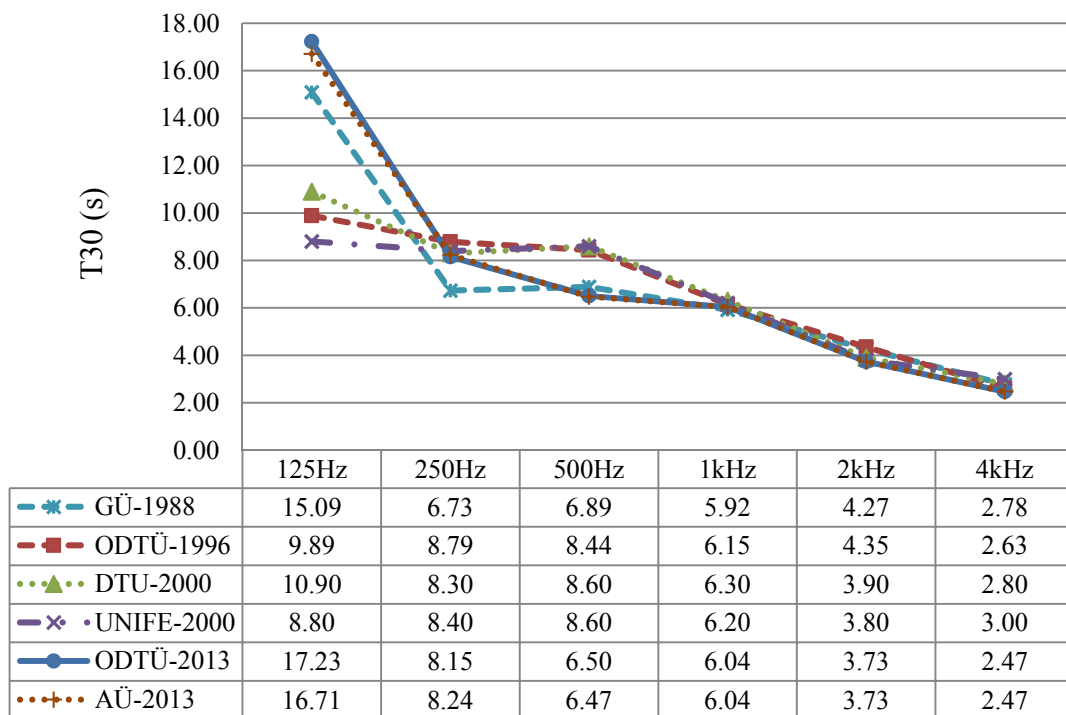


Figure 6.1. Comparison of T30 for field tests held in 1988, 1996, 2000, 2013; for 125 Hz to 4000 Hz, in 1/1 octaves bands

All of the field tests indicate very long reverberation times within the Mosque in its unoccupied condition. For speech frequencies (500Hz, 1000Hz, 2000Hz) the recommended 4.8 s limit, and in broadband 2.8 s limit for mosques with similar volume are not satisfied (Orfali, 2007; CAHRISMA 2003). Especially 125 Hz is very problematic considering the intelligibility of speech; which will be even worse when electro-acoustic system is on. On the other hand, the T30 values in different locations, as given in Table 5.1, do not deviate much. This indicates an even distribution of sound within the prayer area as a positive result of interior surfaces' scattering features.

Apart from 125 Hz, T30 results of ODTÜ-2013 (or METU-2013) and AÜ-2013 field tests in 1/1 octave bands are almost identical. Considering the minor differences in measurement set-up including high and low cut of frequency and source-receiver configurations, it can easily be stated that these two measurement results held in 2013 support each other. In ODTÜ-2013 measurements below 100 Hz, reverberation times reaching 20 seconds are observed. The 1/1 octave band results in Figure 6.1 are calculated from 1/3 octave bands meaning; 125 Hz T30 result is the mean value of T30's at 100 Hz, 125 Hz and 160 Hz making an average of 17.23 s. On the other hand, AÜ-2013 measurements are not taken for below 125 Hz in one-third octave bands; excluding a higher value of decay time in 100 Hz. Thus, it is logical that T30 for 125 Hz in AÜ-2013 measurements are slightly lower than that of ODTÜ-2013 measurements. It is also noted that there are some measurement spots reaching 20 s at 125 Hz in GÜ-1988 measurements that are excluded from the average considered to be the highest deviation (Kayılı, 1988a). In 1996 and 2000 field tests, measured 9 to 11 seconds of T30s at 125 Hz, which are comparatively lower than 2013 measurements, are thought to be caused by the insufficient capture/impulse response lengths. For instance DTU-2000 measurement set-up uses 10 seconds of impulse response length, in the real case which could easily have missed the chance of estimate for a longer reverberation time. On the contrary, both of the first

measurements taken by GÜ-1988 with analog equipment and the final measurements taken by ODTÜ-2013 with digital equipment indicate 15 to 17 seconds of T30 values at 125 Hz. Thus, it could be stated that 2007-2011 renovations have not significantly affected the T30 values at 125 Hz, which are still very high and above the acceptable limits for Mosque function.

According to 2013 measurements, reverberation times for octave bands in between 250 Hz to 4000 Hz have been lowered by different ratios in compare to previous years' results. Especially 2 seconds of drop at 500 Hz is striking. Similarly, at 4000 Hz there is a reduction at T30 by 0.20 to 0.50 seconds. When T30 values at 250 Hz and 500 Hz are compared for 1988 measurements and 1996-2000 measurements, an increase of 1.5 to 2 seconds are observed in the later. In order to be able to explain this increase, the probable undocumented minor-restorations or material changes in between the years of 1988-1996 should have known if any survey was undergone during that time.

The comparative analysis of field test results indicate that the 2007-2011 restorations resulted in positive decreases in reverberation times, specifically at 500 Hz and above, whereas in overall the values are still higher than the recommended ranges. The attempts for removing cement based plasters, and application of plasters that are compatible with historical/original plasters, as so declared, are constructive but not yet efficient acoustical interventions; especially in control of low frequency sound content. The effects of so stated intrusion on *Sebu* voids -opening the mouths and repair of inside cracks- are still vague. In order to be able to scientifically comment on acoustical effects of *Sebu* changes, the present geometrical and dimensional properties of these elements should be identified, which can only be possible by their systematic inspection on site.

Reverberation time (RT, T30, T20) is one of the parameters affecting intelligibility of sound/speech. Another important acoustical parameter that affects intelligibility is

the level of background noise. High background noise can mask the speech subjectively and can drastically lower the speech transmission index values (STI). Background noise is a frequency dependent parameter so its spectrum differs for different noise sources. As given in Figure 5.3, high noise levels are observed in ODTÜ-2013 measurements within prayer hall of the mosque. Measured A-weighted equivalent sound level (LAeq) of 39.3 dBA corresponds to Noise Criteria-NC33, which is higher than the NC15-20 (25-30dBA) upper limit of background noise levels recommended for religious spaces (Beranek, 1971; ASHRAE, 2013). These background noise data are utilized in room acoustics simulations of Süleymaniye Mosque and for natural speech levels the intelligibility values are estimated for overall main prayer zone. As can be observed in distribution maps given in Appendix A (Figure A.27 and Figure A.28), average STI value for the main prayer area is around 0.3 indicating POOR to FAIR intelligibility class.

ODTÜ-2013 measurements are taken at night time hours, when the Mosque is closed for visit or prayer and intriguing environmental/traffic noise is at minimum. The high background noise levels are found to be caused by the cooling fan units of electrical panels located within the mosque at the first level right across the *mihrab* wall. It is evident that one of the basic reasons behind the claims for acoustical or intelligibility problems within Süleymaniye Mosque after final restorations is the presence of fan noise, which can easily distract speech related activities such as *hutbe's* by *imam* (Sü Gül et al., 2014d).

6.2. INTERPRETATION OF SÜLEYMANIYE MOSQUE'S ACOUSTICS FOR ITS ORIGINAL STATE

Süleymaniye Mosque has gone through various restorations in years, and the acoustical conditions within the Mosque after specific restorations are compared and assessed in previous section by the data out of field tests. However, none of the field test results reflect the acoustical conditions of the mosque in its original state. On the

other hand, the acoustical expectations from the mosque in the years of its construction and expectations from a mosque in these contemporary years are quite different. All of the historical mosques today incorporate the use of sound-reinforcement systems. For historical mosques, designed for natural sound in their time, it is evident that problems would occur in application of electro-acoustic systems unless necessary precautions are taken.

The basic parameters in room acoustics affecting natural speech/sound are the volume of the main space and its geometry. It is known that, the dimensions and basic geometrical features of Süleymaniye Mosque have not been altered until today. The dominating form of the Mosque is the central dome which is supported by two semi-side domes. Acoustical focusing effects of dome can be prevented to some extent, in the case that the lower end of the diameter/circumference of the dome section is located at much higher than the receiver/prayer ear height. In Süleymaniye Mosque even the focusing zone of the biggest central dome is located 20 m above the prayer plane/floor. This indicates that Süleymaniye Mosque domes are designed so delicately that the first order high reflections and/or acoustical foci and echoes are minimized. Still, the dome form may cause sound foci at its focal points and so negatively affect the sound scattering.

Sinan in his mosques applied *Sebu* (clay pot) technique, which enables acoustical asymmetry within the dome by scattering the sound and enlarging dome reflection zone. By that, much even distribution of sound within the prayer zone could be provided. *Sebu* forms are similar to that of amphoras, which have a short neck and a backing volume. *Sebu* technique in statics enables to lessen the weight of the dome, while in acoustics they function as Helmholtz resonators. These elements can scatter sound to some extent and especially at low frequencies (63 Hz - 250 Hz) they are narrow band volume absorbers (Long, 2006, p.203).

In the account books (D.88. Yp. 19/a) of Süleymaniye Mosque's construction work, it is recorded that each for 2 akçe's 255 '*Sebu*' (Baha-i Sebu, beray-ı kubbe-i cami'-i şerif) are purchased (Barkan, 1972). In several investigations it is stated that 64 of these pots are located on a circular disk at the central dome, which have a length of 50 cm and neck width of 2 to 6 cm (Acar, 2000; Kayılı 1988a-b, Kayılı, 2002). On the other hand, in 2007-2011 restorations it is declared -in press- that 256 pots with 45 cm length and 15 cm mouth, open towards the interior space are detected (<http://www.radikal.com.tr/>, 2013).

The numerous applications of these pots with various sizes would widen the frequency bandwidth that they are effective. Thus, it could be predicted that such an application in the original state of the Mosque, to some extent, have healed the excessive low frequency sound content. Together with *Sebu* voids, the fragmentation of parallel surfaces in both section and plan scheme of the Mosque by architectural elements such as *mahfil*'s, niche's and surface treatments such as *muqarnas*, *kündekari* and glazed ceramics have provided sound scattering in a wide frequency spectrum, so that an even distribution of sound throughout the prayer zone is obtained.

In spaces with excessive volume as in Süleymaniye Mosque, the expected long reverberation times have to be controlled by increasing the sound absorptive surface area. As absorption increases, reverberation time decreases ($RT_{\text{sabine}} = 0.163 * [\text{volume}/\text{absorption area}]$) (Egan, 1988). The absorption area of the overall space for each frequency is calculated, firstly, by the multiplication of sound absorption coefficient of each interior finishing surface at a certain frequency (octave band) and the corresponding surface area, and then, by summing up all individual absorption area.

In Süleymaniye Mosque shiny and tight stone wall, column and elephant feet surfaces compose the reflective area. The absorptive carpet floor surface is not

sufficient to tolerate the long reverberations that occur in this large volume; so additional absorptive surfaces are required. The sound absorption coefficients of applied stones within Süleymaniye Mosque can be predicted for the current and original states as given in the range of 0.01-0.10 in the literature (CAHRISMA, 2003). The unknown is the sound absorption coefficient data of original/historical plasters with or without paintings that are renewed in several restorations. These plasters are applied at dome, arch and mostly upper wall surfaces, and compose a very large surface area of approximately 19,000 m². The influence of these plasters on reverberation times would be noteworthy.

In the account books (D.108) of Süleymaniye Mosque's construction work (Barkan, 1972), it is recorded that 134 scale linen is purchased for to be used in plastering of dome (Beray-i sıva-i kubbeha-i cami'-i şerif). At some other account books it is also recorded that 524 kantars of linen are purchased for plastering of the structure in general (Beray-i sıva-i bina-i şerif) (Barkan, 1972). Use of linen within the composition of interior surface plasters in Süleymaniye Mosque is an important acoustical factor. Linen is commonly used to improve the tensile strength of mortar and/or plaster material; on the other hand in acoustical terms it can as well increase the sound absorption performance of the plaster at low frequency range. Linen would also augment the mechanical strength of plasters (Bos et al., 2002; Dalmay et al., 2010). It can be predicted that by the use of linen Sinan has increased sound absorption area serviced by plastered surfaces, which then has provided a more controlled reverberation within the mosque in both low and mid frequencies.

In support of above argument, in 15th - 16th century structures, the techniques of multi-layered plasters, which function for the benefit of many different building physics aspects, are previously investigated by some researchers (Esen et al., 2004). Another research on Sinan's mosques highlights the acoustical significance of porous and soft horasan mortar with linen and hemp fiber ingredients that are applied on dome and wall surfaces (Kayılı, 1988a). The replacement of historical mortar and

plasters, which are good absorbers at low to mid frequency range, with tight and stiff cement based plasters in specific restorations are accused for excessive reverberation times observed especially at low to mid frequencies at most of the historical mosques (Kayılı, 1988a). The use of natural fibers as an ingredient in historical plasters, in fact, is considered to be significant information in terms of acoustical performance of historical plasters, and need to be investigated with further studies.

In another research the historical Turkish Baths', of the same era, are investigated in terms of acoustical performances of interior surface finishes. The sound absorption coefficients of historical multi-layered puzolonic lime plasters are tested by impedance tube method (Aydın, 2008; Tavukçuoğlu et al., 2011). According to that, historical Turkish Bath plasters at dry air have 8.5 times higher sound absorption capacity (for 500 Hz – 1000 Hz) than that of today's cement based plasters. Moreover, noise reduction coefficient (NRC), which is the average alpha of 250 Hz, 500 Hz, 1000Hz and 2000 Hz, of historical lime plasters are 14 times higher than that of cement based plasters.

In Süleymaniye Mosque the current plastered surface area is approximately 19,000 m², which is a significantly large amount that should have a drastic impact on sound absorption area for different materials. For testing this argument, the acoustical model of Süleymaniye Mosque is utilized in a preliminary simulation study that compares today's plasters with historical lime based plasters, the results of which are presented in Figure 5.6 and Figure 5.7. Recent research on mosque acoustics reveals that super-structure mosques with high volumes as of Süleymaniye Mosque, should have RT mid frequency average below 4 s in prayer zones closer to the *mihrab* and *minbar* and should have RT below 4.6 s in distant prayer locations (CAHRISMA, 2003). A rise of 0.2 s is expected per octave band below 250 Hz, and a rise by 0.2 s is considered optimum above 2000 Hz per octave band (Orfali, 2007). According to the simulation results for unoccupied condition, the replacement of cement based repair plasters with historical ones ended up with a drop of 2 s in T30

value at 500 Hz and a drop of 7 s in T30 value at 125 Hz. The fully-occupied state of the mosque with the application of historical plasters, as shown in Figure 5.7, provided the upper limit of criteria above 500 Hz, and it is much closer to the limits below that frequency. Although there are some recent attempts in removing cement based plasters (2007-2011 restorations), the 2013 field measurements indicate that the problems are not thoroughly solved. Results indicate that if the historical plasters could have been survived till now or if the Mosque underwent repairs with the plasters totally compatible with the historical ones, the acoustical conditions would be much suitable for the function of the Mosque in today (Sü Gül et al., 2014a).

For an even distribution of reverberation over frequency, the sound absorption performance of materials in over frequency spectrum should be well balanced. Carpet is an absorptive material only after mid frequency range (1000 Hz to 8000 Hz), unless it has at least 5-10 cm height platform underneath. In records of construction documents of Süleymaniye Mosque such a platform is not mentioned (Barkan, 1972). This means the original carpet's sound absorption performance would be similar to that of today's carpet for low frequencies, and not much of a difference is expected from high frequencies in reference to some other research on carpet effects (Sü Gül and Çalışkan, 2013b).

Carpet is still significant in terms of providing positive absorption area for intelligibility (of consonants). One other significant information is that in its original state straw is laid underneath carpet of Süleymaniye Mosque (Barkan, 1972; Çelik, 2009), which would provide an improvement in absorption of mid frequency sound content. Apart from those, in prayer scenario the presence of people and their compactness should have improved sound absorption as well as scattering within the Mosque, as observed in full-occupancy simulation results (Figure 5.5 and Figure 5.7).

Being located in a courtyard of a big complex (*külliye*) surrounded by walls together with a thick and strong exterior shell of domes and walls, Süleymaniye Mosque is very well isolated from any environmental noise that might be present in its time. It is also hard to talk about any traffic or industrial noise as in today's, and any noise sourced from mechanical equipment that were not existent in the past. Thus, the intelligibility of speech within the Mosque should have been least masked or distorted in its original state. As a conclusion of all these assessments on different aspects above, it can be stated that Sinan has taken many delicate precautions for the sake of acoustics of Süleymaniye Mosque considering the site location, volume, geometry, interior surface forms and materials.

6.3. COUPLING TREND INVESTIGATIONS OF SÜLEYMANIYE MOSQUE BY COMPARISON OF FIELD AND SIMULATION DPE

The results of field tests and pre - post field simulations decay parameter estimation analysis are given under Section 6.2. In this chapter the comparison studies of DPE results are presented. Number of exponential decay terms (# of slopes) out of Bayesian analysis for pre-field simulation, field test and post-field simulations are compared over octave bands in Figure 6.2, compared over source locations in Figure 6.3, compared over receiver locations in Figure 6.4 and compared over source-receiver locations in Figure 6.5.

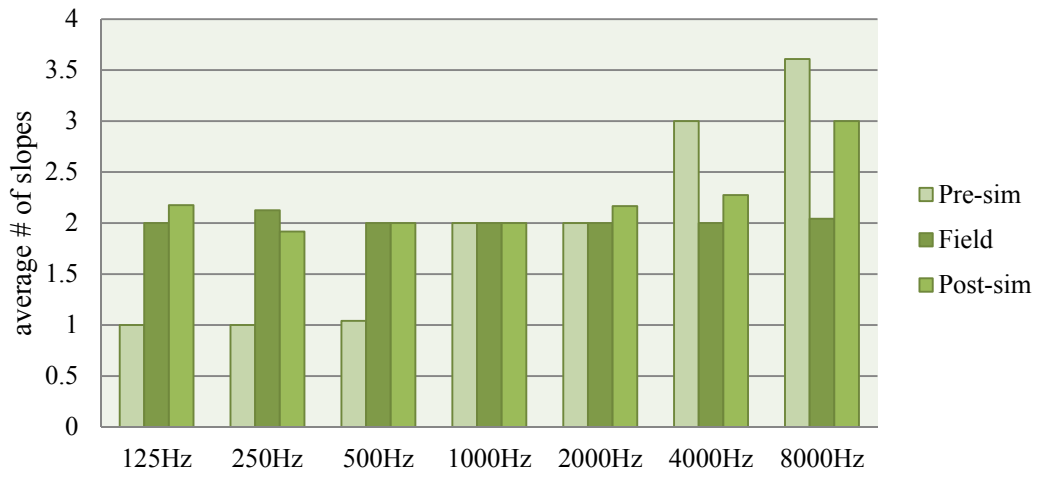


Figure 6.2. Average # of slopes per 1/1 octave bands, Süleymaniye Mosque

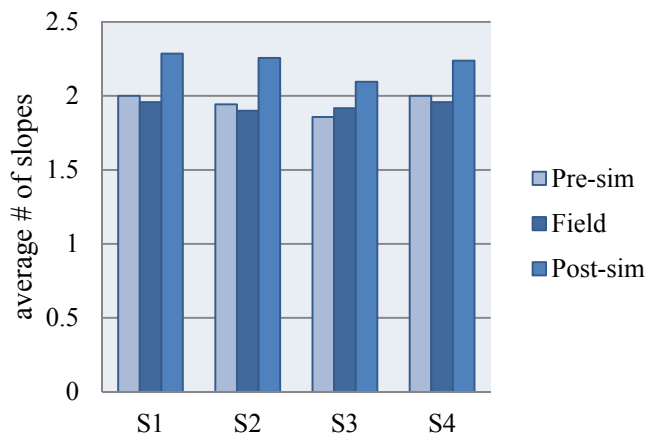


Figure 6.3. Average # of slopes per source locations, Süleymaniye Mosque

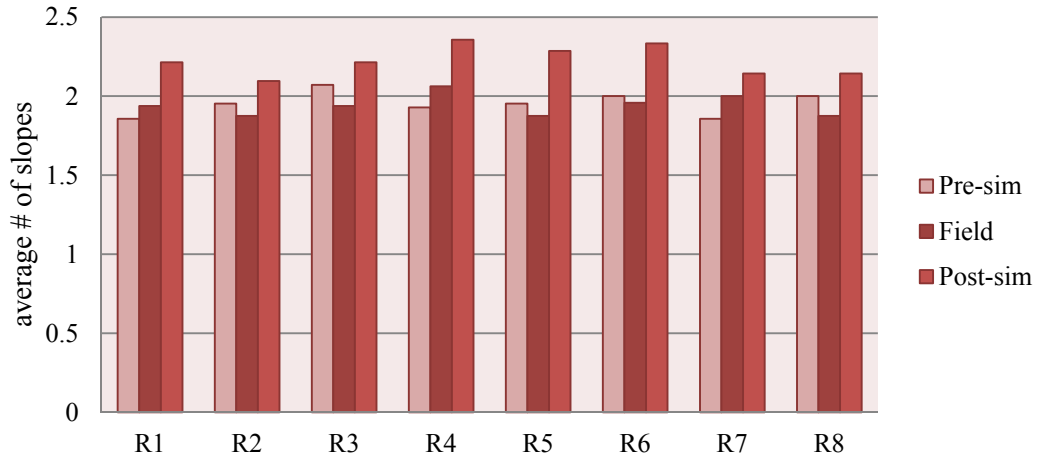


Figure 6.4. Average # of slopes per receiver locations, Süleymaniye Mosque

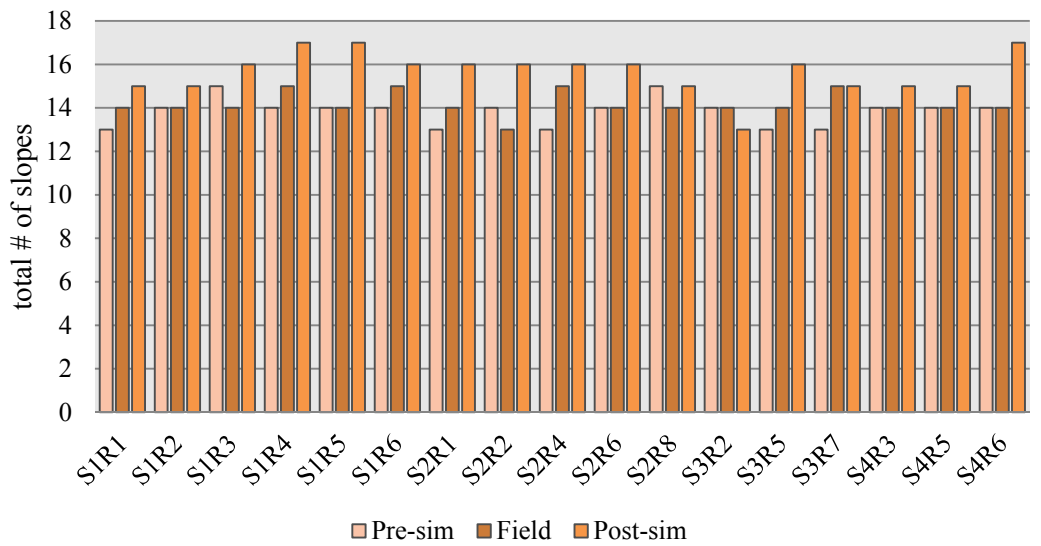


Figure 6.5. Total # of slopes per source-receiver configurations, Süleymaniye Mosque

For all cases the decay order selection is based on BIC comparison of models that fit well with the Schroeder decay curve. Estimated number of decay slopes and decay times for different source-receiver configurations are presented in Table B.1 for pre-simulations, in Table B.2 for field tests and in

Table B.3 for post-simulations (Appendix B). In pre-field simulations with the un-adjusted model double, triple and quadruple decays are observed with increasing

number of decay rates above 2 kHz. Increasing trend over frequency is also observed at post-simulations with adjusted model, while in field results average of two slopes are observed in between 125 Hz and 8 kHz. The higher number of decay rates in frequencies over 2 kHz in simulations are due to the absence (or weakness) of noise term in compare to real-size field tests with accompanying background noise.

In initial studies under pre-simulation DPE analysis multiple slopes are not observed in low and mid frequency ranges. Preliminary assumption for this outcome was as such:

- the sound field is much diffuse in mid to low frequency range in compare to higher frequencies. According to that, the high frequency content of sound scattered from highly reflective wall and ceiling/dome surfaces has encountered with the absorption on the floor. As a result of the large area it covers, the carpet floor finish composes the highest Sabine at frequencies over 2 kHz. The concentration of sound absorption at specific locations – mainly on the floor surface-, in other words the uneven distribution of absorption coefficients, creates the nondiffuse field at corresponding ranges of the frequency spectrum.

However, the occurrence of multiple slopes in low and mid frequency range -where there is no significant difference in sound absorption coefficients of carpet and plaster surfaces- in both field tests and post-simulations, has weaken the strength of above statement/hypothesis. On the other hand, DEM study for floor with marble instead of carpet, as discussed more in detail under Section 6.4., highlights that if the floor would be a reflective one rather than an absorptive surface the energy concentration/focal point will be at the center of the total height rather than at the center of the upper central dome. This outcome (observed out of sound energy flow vectors) indicates a much even/diffuse sound field in compare to floor with carpet, and in that case multiple slopes could not be observed. For all that reason it should be noted that the absorptive floor finish is not the only reason for nondiffuse acoustical

field, and it is supported by the geometrical attributes. The basic geometrical attribute that affects the energy fragmentation (so the nondiffuse acoustical environment) is the main central dome, with its excessive size and height from the ground.

The major reason of changes in pre and post simulations is that the materials' sound absorption coefficients are adjusted/tuned, and accordingly the sound field for different locations has differed. The same acoustical model of the mosque with the same volume but with different ratios of sound absorption on specific surfaces, radically effected the occurrence of multiple decays, indicating that the phenomena is very susceptible even to very low reverberation time differences and material (absorption) changes.

The comparison of real-size measurements and simulations in a DPE analysis could only be made for controlled/similar architectural environments. In that sense, the mosque model in post-simulations is approximated to field test conditions. The increasing trend in high frequencies in simulations in compare to field tests is due to the absence of noise. By that, it is more possible to observe additional decays (non-exponential energy flow) in later shallower decay end as pointed out above. There is no significant deviation in average number of slopes per source locations, and the trend for both field and simulation results are similar.

In overall, number of decay slopes are slightly higher for receivers underneath side corner domes and slightly higher for source in front of *mihrab* and underneath central dome. It is hard to discuss about a trend (maxima and minima) for source-receiver configurations when comparing simulations with field tests. The variations are statistically insignificant due to the even distribution of sound throughout the Mosque, which is still a single space enclosure with no real aperture as in coupled spaces.

The field test results, which provide the most realistic data for multi-slope investigations within such single space enclosures, indicate multiple slopes (specifically double slopes) in all octave bands except for 63 Hz. Triple slopes have been mostly observed at 250 Hz, which is a very critical band when 1/3 octave bands are observed. As shown in Table 5.1, the sharp decrease of decay time (T30) from 200 Hz to 250 Hz, indicating an excessive absorption within these frequency ranges, might probably be caused by the multiple uses of narrow-band volume absorbers, *in this case specifically Sebu voids*.

The DPE investigations in Süleymaniye Mosque out of real and simulated impulse response data have proved the hypothesis of even a single space with particular geometrical features can provide the circumstances for multiple-slope decay formation. The answers of the mechanism of why multi-slope decay may occur in such an architectural scheme are discussed in further under following section by comparison of advanced analysis and measurement results; the application of diffusion equation model (DEM) theory in room acoustics by FEM and the intensity probe field measurements held for the validation of DEM study.

6.4. COUPLING TREND INVESTIGATIONS OF SÜLEYMANIYE MOSQUE BY THE ANALYSIS OF SIMULATED DEM AND INTENSITY PROBE FIELD DATA

Results of DEM solution for Süleymaniye Mosque are given under Section 5.3. In order to highlight some important aspects in relation to acoustical coupling, findings are summarized for specific cases in this section. Besides, coupling trend formation is supported through decay parameter estimations out of single point response data. Intensity probe measurement results, providing 3D impulse responses for intensity vector analysis, are given under Section 5.4. Intensity vectors out of field measurements with intensity probe indicate the real condition, and are used for

comparison with DEM results as well as for validation of the mechanism in multi-slope decay formation.

In Figure 6.6, spatial sound energy level distributions out of DEM are given for volume and slice plots, for 1 kHz and time 0.1 s, indicating the ignition of the sound source and direct sound effect. In Figure 6.7, the same conditions are given for time 2 s, indicating a sample period after steady-state condition where reverberation tail is in drop. Two and three-dimensional mapping of impulse-response derived sound-energy flow vectors are illustrated in Figure 6.8 and Figure 6.9 for 250 Hz, for initial time decay periods.

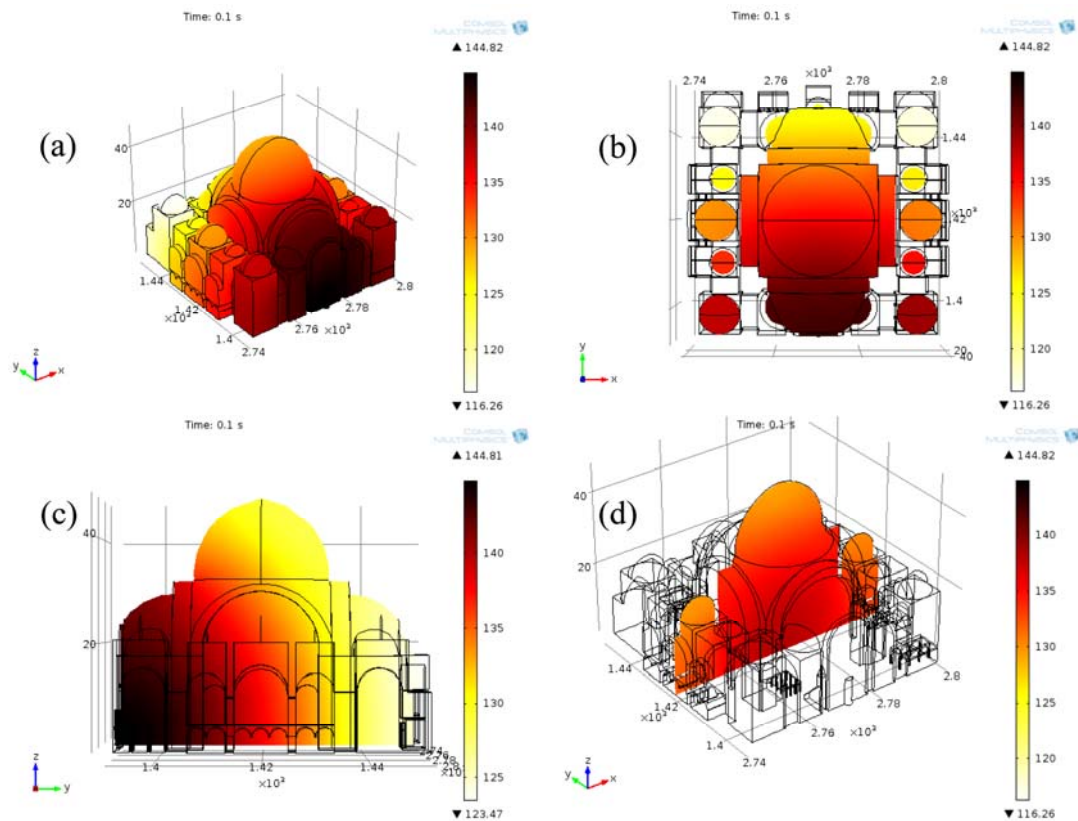


Figure 6.6. Spatial sound energy level (dB) distribution, time: 0.1s, 1 kHz; volume and slice plots of Süleymaniye Mosque DEM solution, a) axonometric view, b) plan view, c) section through the *mihrab* wall, central axis, d) section parallel to the *mihrab* wall, central axis

In Figure 6.6, the sound energy density distribution in between time periods of excitation and termination of the sound source can be observed. The solution for this case is taken for 1 kHz, which is defined by the relevant sound absorption coefficient data (impedance term within DEM solution) of surface materials for interior boundary layers. The concentration of sound energy density is at the front part of the *mihrab* wall, where the point source is defined, as can be seen from axonometric, plan and *mihrab* wall section views. The energy starts to flow from *mihrab* wall towards the back of prayer hall, while, at this point the central dome and back wall aisles have not been completely filled with the sound energy. The inverse section (Figure 6.6-d) indicates a more even distribution and an average sound level. The zones closer to the floor (receiver/prayer heights) underneath the central dome at that direct sound period get more energy in compare to prayer locations in front of the back wall and get least underneath back wall corner domes and upper back half of the central dome.

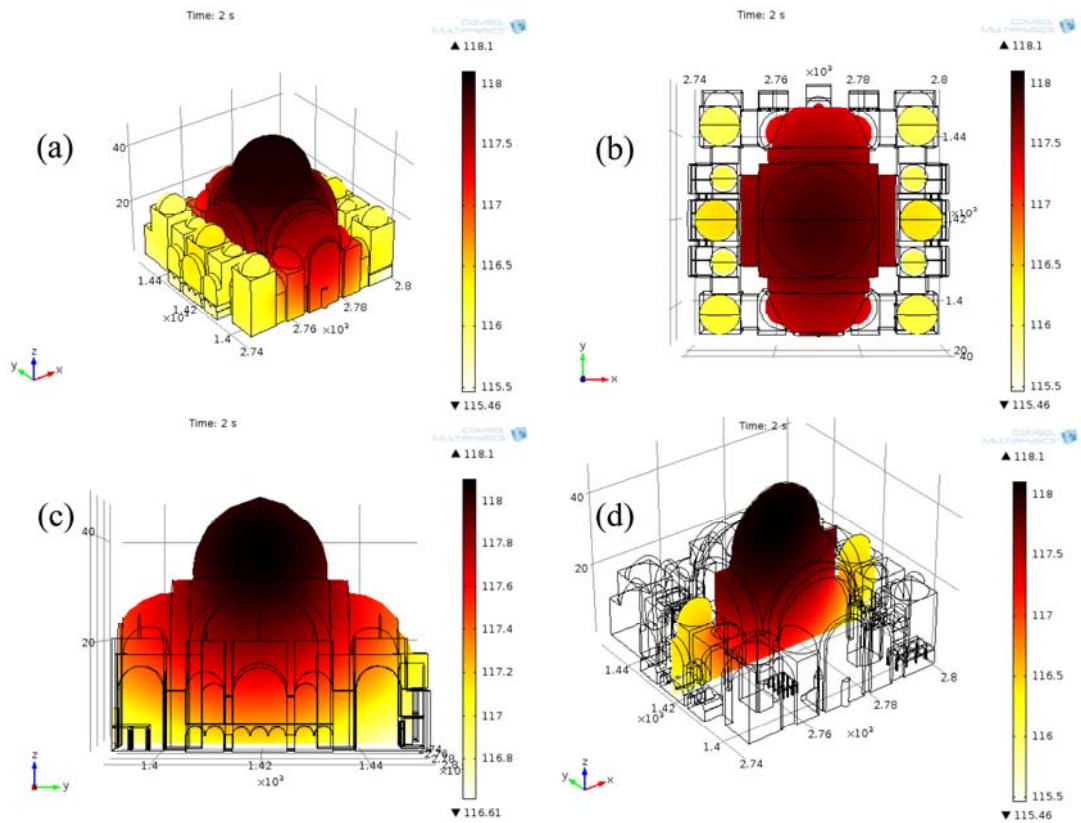


Figure 6.7. Spatial sound energy level (dB) distribution, time: 2s, 1 kHz; volume and slice plots of Süleymaniye Mosque DEM solution, a) axonometric view, b) plan view, c) section through the *mihrab* wall, central axis, d) section parallel to the *mihrab* wall, central axis

In Figure 6.7, the sound energy density distribution at a time after the steady-state can be observed. As all-time intervals closer before and after this time shows a similar trend, solution for 2 s of 1 kHz case is selected to be representative. From all of the plots it can be clearly observed that at this state sound is concentrated at the central axis underneath the main dome and semi-domes. From this point out, the energy center is the central dome, with its comparatively reflective surfaces and focusing geometry. In architectural acoustics terms, it is beneficial that the dome focusing area is completed much above the receiver height. On the other hand, this energy accumulation center keeps feeding energy back to the floor area, as can be seen from following Figures of flow vectors (Figure 6.8 and Figure 6.9). Another point is that, the side aisles underneath secondary domes gets less energy in compare to the *mihrab* wall section (Figure 6.7-c). This energy fragmentation indicates the

zone underneath the main and secondary domes to work as of a reverberation chamber, while the aisles are fairly dead areas that get later energy feedback from the central zone.

In Figure 6.8, arrow surface plots of Süleymaniye Mosque DEM solution crossing centrally the *mihrab* wall, for the time dependent solution of 250 Hz are presented. Times in between 0.1 s to 0.8 s with a time step of 0.1 s are analyzed. The frequency is selective in the boundary definition, where the absorptive carpet and reflective upper shell structure -including walls-, together with the dominant geometrical features cause the main energy flow characteristics. The initial part of the decay after the shut off time of the sound source, which is from 0.1 s to 0.8 s in this case, is trivial in terms of many acoustical parameters such as of EDT, C80, D50, LF and ITDG. On the other hand the flow patterns also include some clues on the acoustical coupling trends.

Figure 6.9, involves supportive arrow volume plots of three-dimensional impulse-response derived sound-energy flow vectors, for 250 Hz. In this case the interval between 0.1 s to 2 s are selected for specific time zones. In both Figure 6.8 and Figure 6.9 the flow return around 0.7 s can be observed. After 1 s, the energy is stabilized at the central upper zone (main dome) as indicated above, and starts feeding back the rest of the mosque's prayer zones. The acoustical coupling, in other words multi-slope decay formation, is estimated to be primarily the result of this energy division in between upper central zone of the mosque -in between the four elephant feet in plan, and approximately where the *pendentives* of the main dome are started at the section on the boundaries-, and the side aisles underneath the secondary dome structures.

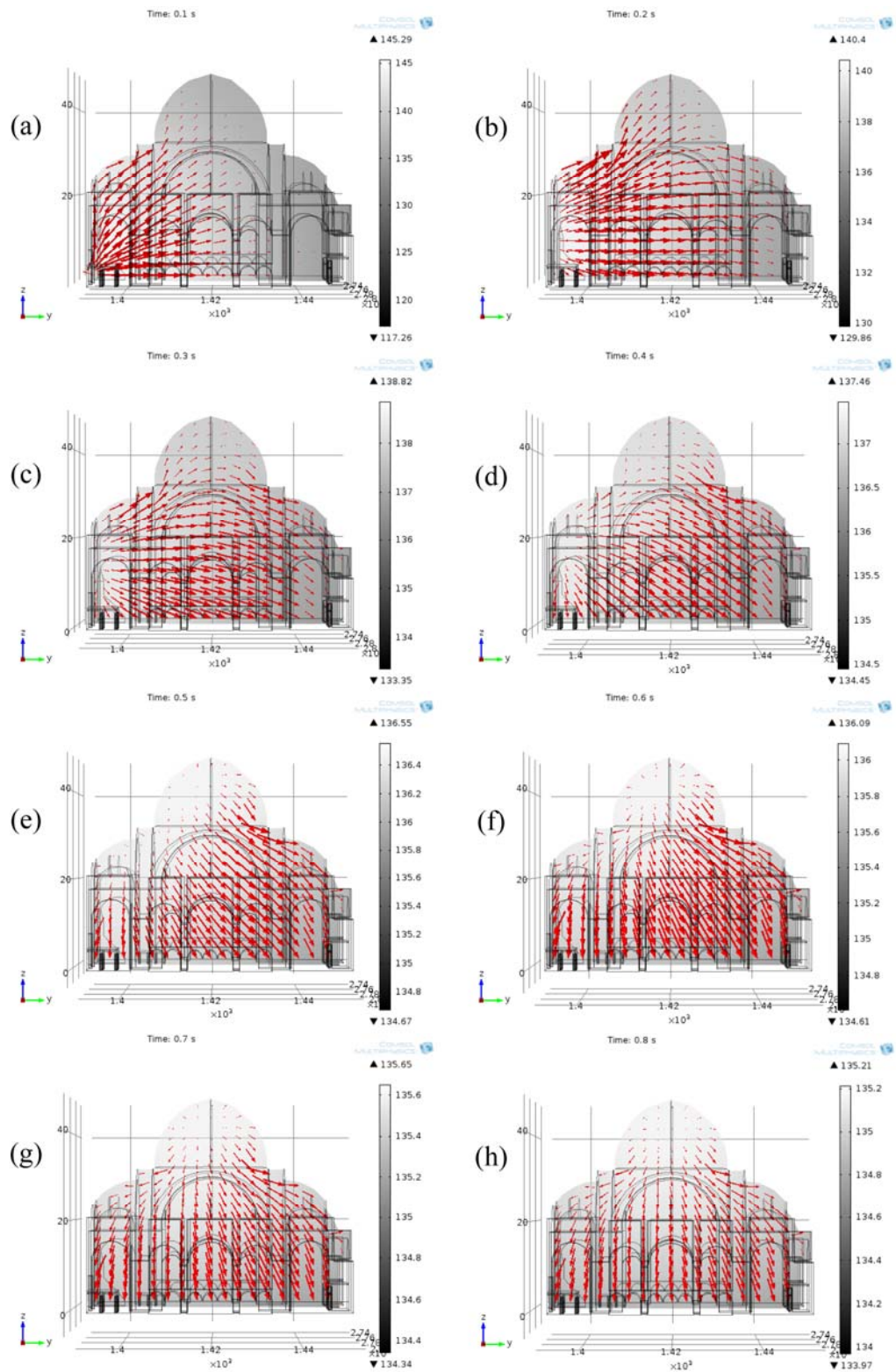


Figure 6.8. Two-dimensional mapping of sound-energy flow vectors (arrow surface plots), for 250 Hz. a) time: 0.1s, b) time: 0.2s, c) time: 0.3s, d) time: 0.4s, e) time: 0.5s, f) time: 0.6s, g) time: 0.7s, h) time: 0.8s, Süleymaniye Mosque

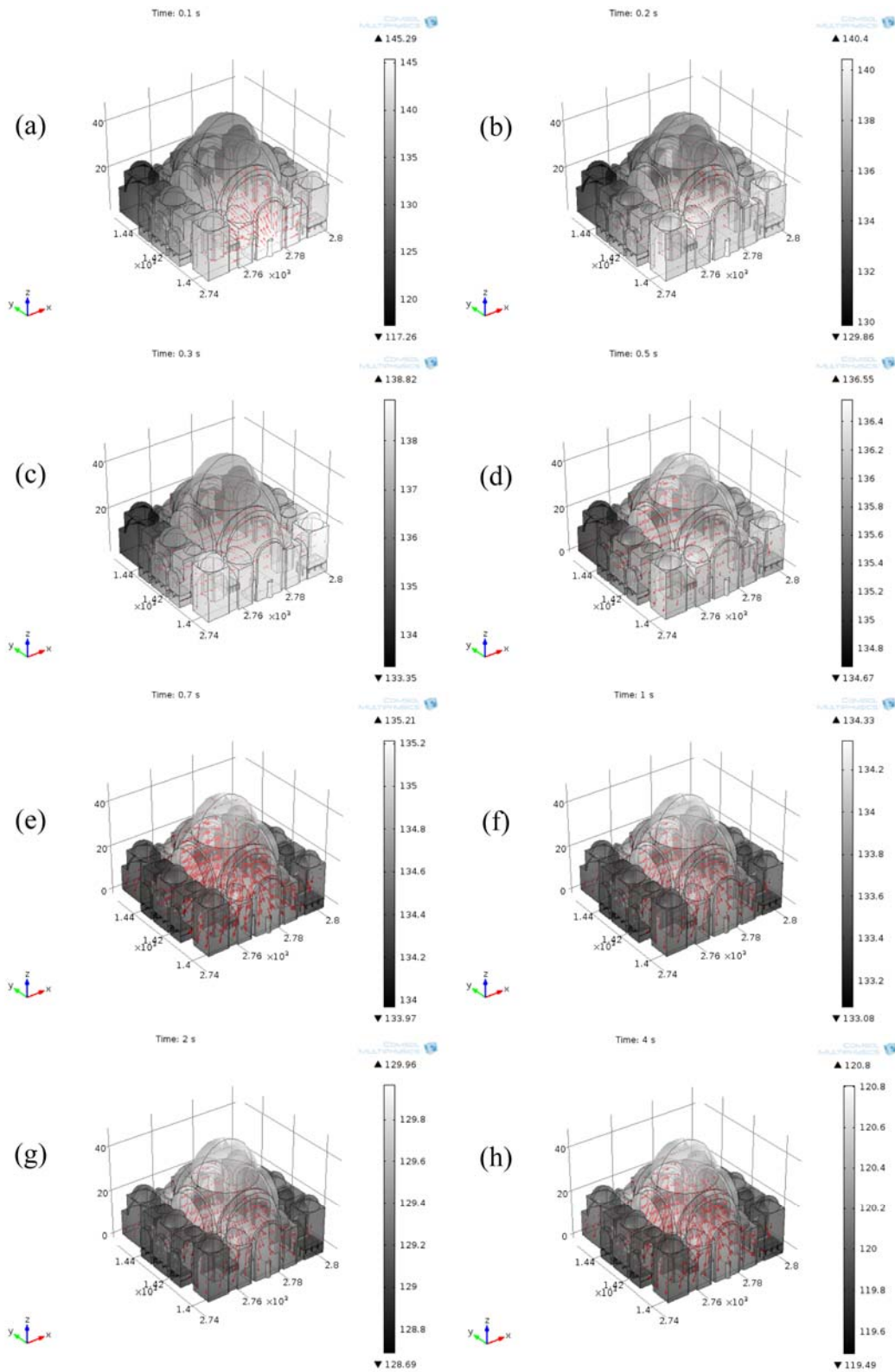


Figure 6.9. Three-dimensional mapping of sound-energy flow vectors, 250 Hz; DEM solution for the time dependent solution, a) time: 0.1s, b) time: 0.2s, c) time: 0.3s, d) time: 0.5s, e) time: 0.7s, f) time: 1s, g) time: 2s, h) time: 4s, of Süleymaniye Mosque

Above given simulated DEM results are further examined by real-size field measurements with the use of intensity probe for gathering 3D impulse responses for specific source and receiver configurations as detailed under Methodology -Section 4.5. The intensity probe results in general are given under Section 5.4. In this section the initial sound decay is compared for DEM and probe results (Figure 6.10 to Figure 6.12), for better understanding/interpreting the real field in compare to simulated field over sound energy intensity flow vectors.

Below figures highlight that around 100 ms (0.1 s) to 900 ms (0.9 s) the energy flow return is complete out of DEM solution. From that time span out the behavior of the space are similar as discussed in previous sections. Both DEM and field results indicate that the major shifts occur within 0 to 1s. DEM results rest after 0.9 s in form of the dominating energy flow from the central dome to floor. The general tendency in field results are similar in terms of the energy directed towards the central dome to floor and side walls (back-front walls and side walls), however in the real case there is energy turnaround from central dome axis to mihrab wall and back wall due to dominant reflections from close-by reflective surfaces. For R₁₃ (which is right underneath the central dome) in the real case there are back and forth movements from dome to floor due to the focusing effect of the dome, which ends up in the clear vertical shifts of the vector –from dome to floor and vice-versa.

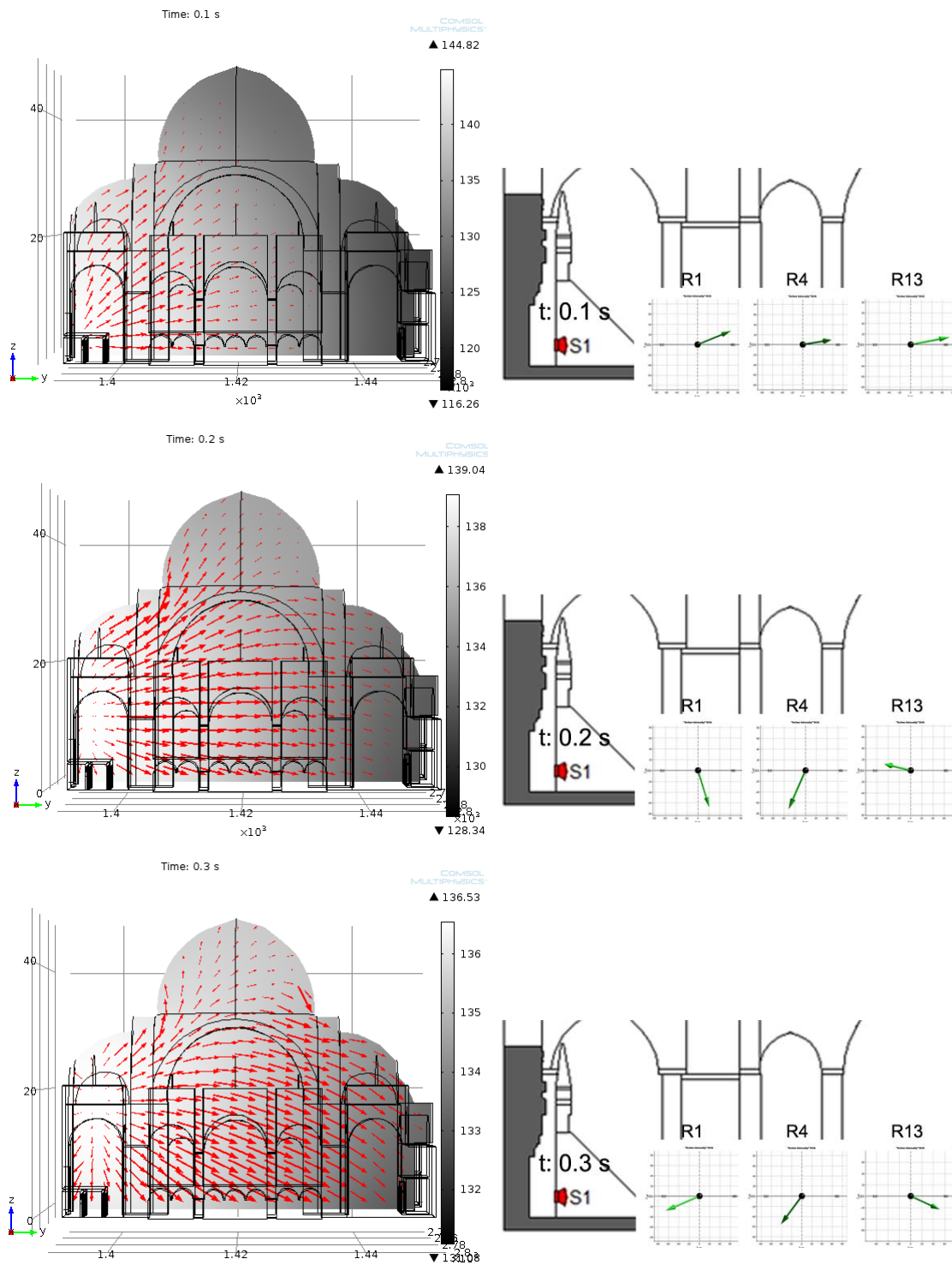


Figure 6.10. Flow vectors (DEM) versus intensity vectors (field), t: 0.1 to 0.3s, 1 kHz, mihrab wall section, Süleymaniye Mosque

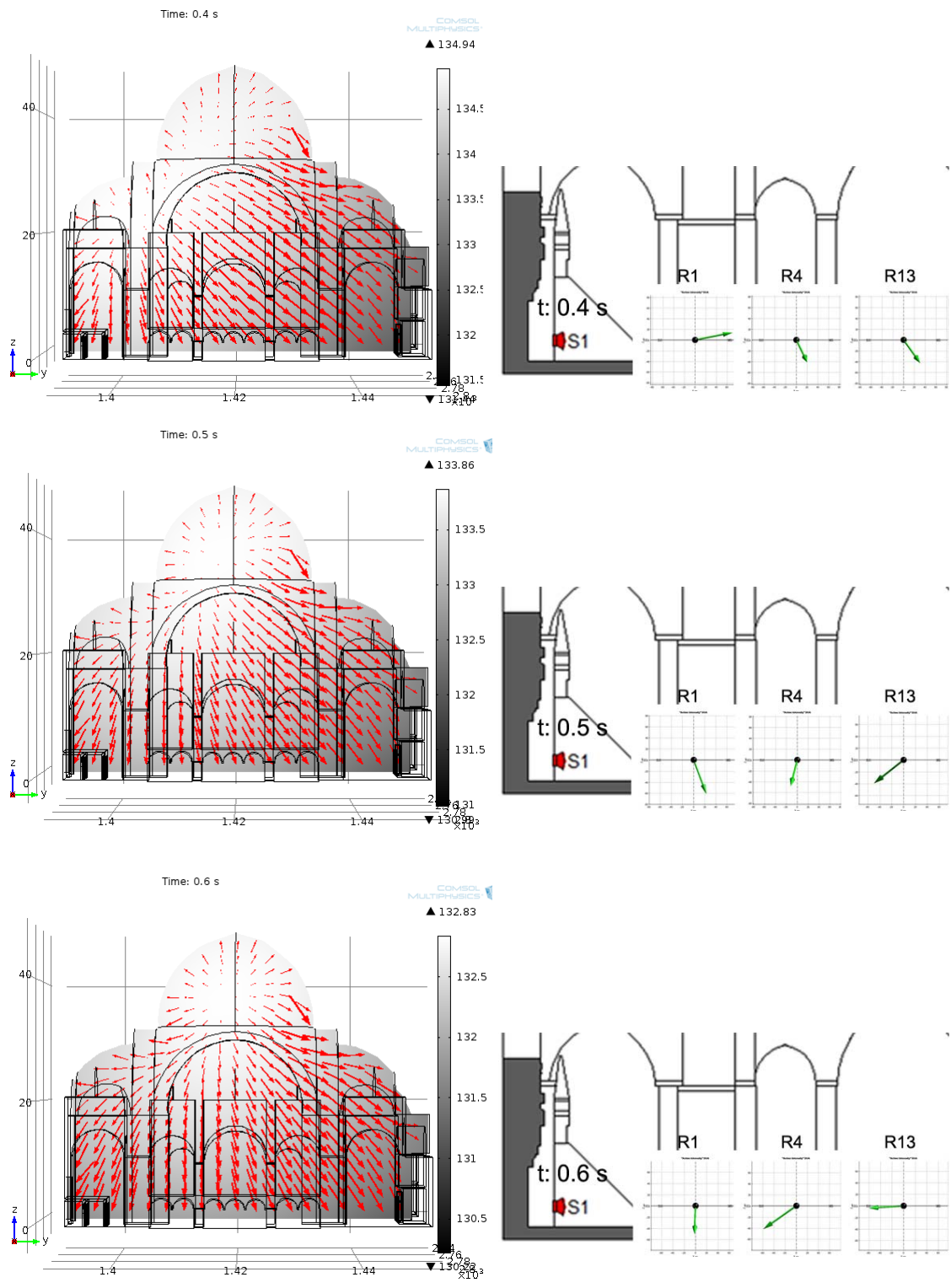


Figure 6.11. Flow vectors (DEM) versus intensity vectors (field), t : 0.4 to 0.6s, 1 kHz, *mihrab* wall section, Süleymaniye Mosque

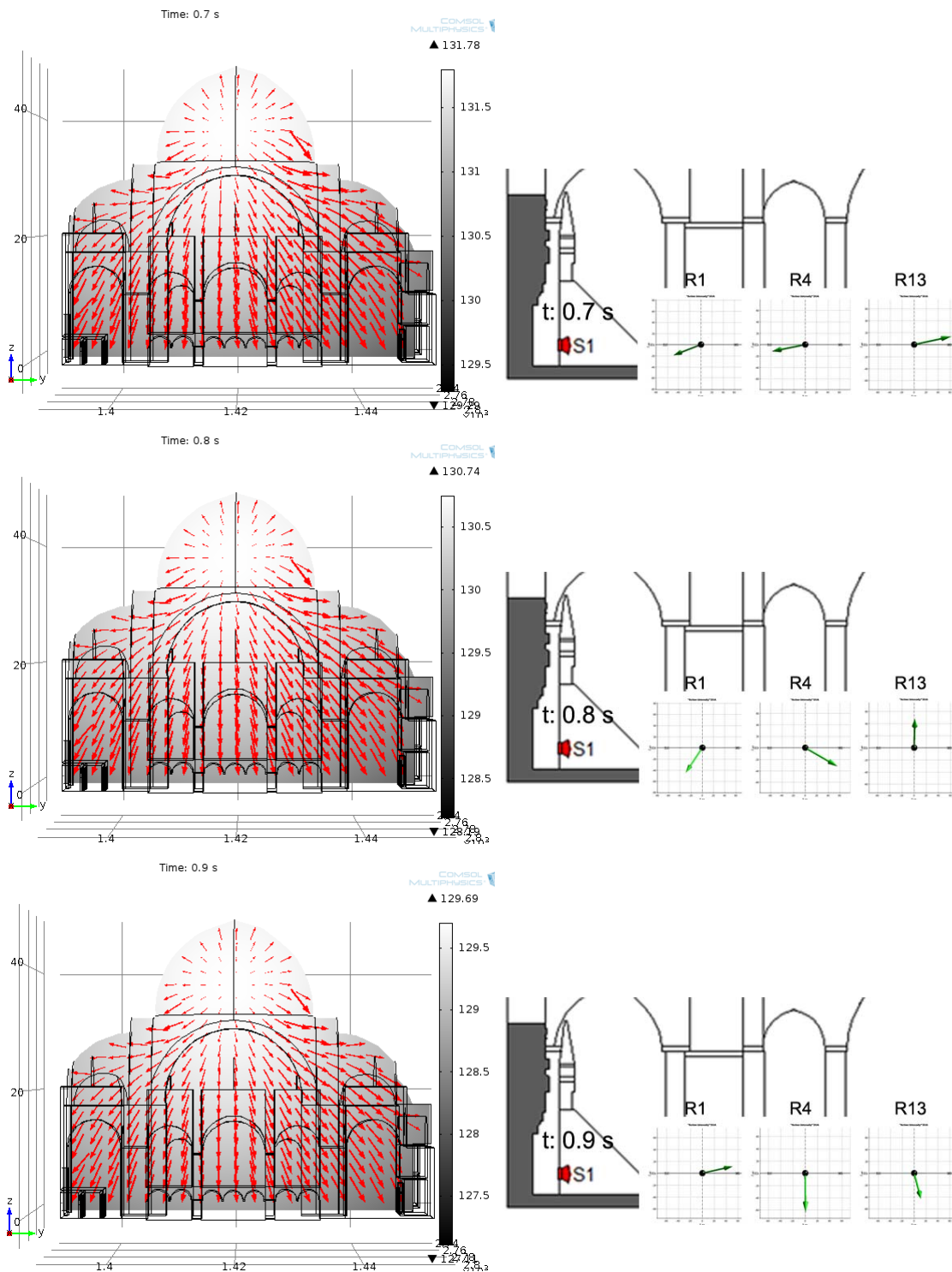


Figure 6.12. Flow vectors (DEM) versus intensity vectors (field), t: 0.7 to 0.9s, 1 kHz, mihrab wall section, Süleymaniye Mosque

It is worth observing that the real data out of a nondiffuse sound field, in compare to the simulated data within the perspective of a diffuse sound field (DEM) support each other in general (larger time window frame), but have dissimilarities for shorter time windows. This outcome is due to the fact that for smaller time windows the real data is more susceptible to individual reflections from close-by reflective surfaces. The real size field probe measurements have also revealed the specific times for sound energy returns. Corresponding close-by time interval energy flow return around 0.7 s to 1.1 s with real-size intensity vectors, in support of DEM results and multi-slope energy decay formation are given for S₁R₁ for 1 kHz in Figure 6.22. Similar flow returns are observed throughout the time solution of 3D impulse responses for different source-receiver configurations and frequencies, validating DEM results as well as multi-slope decay formation mechanism.

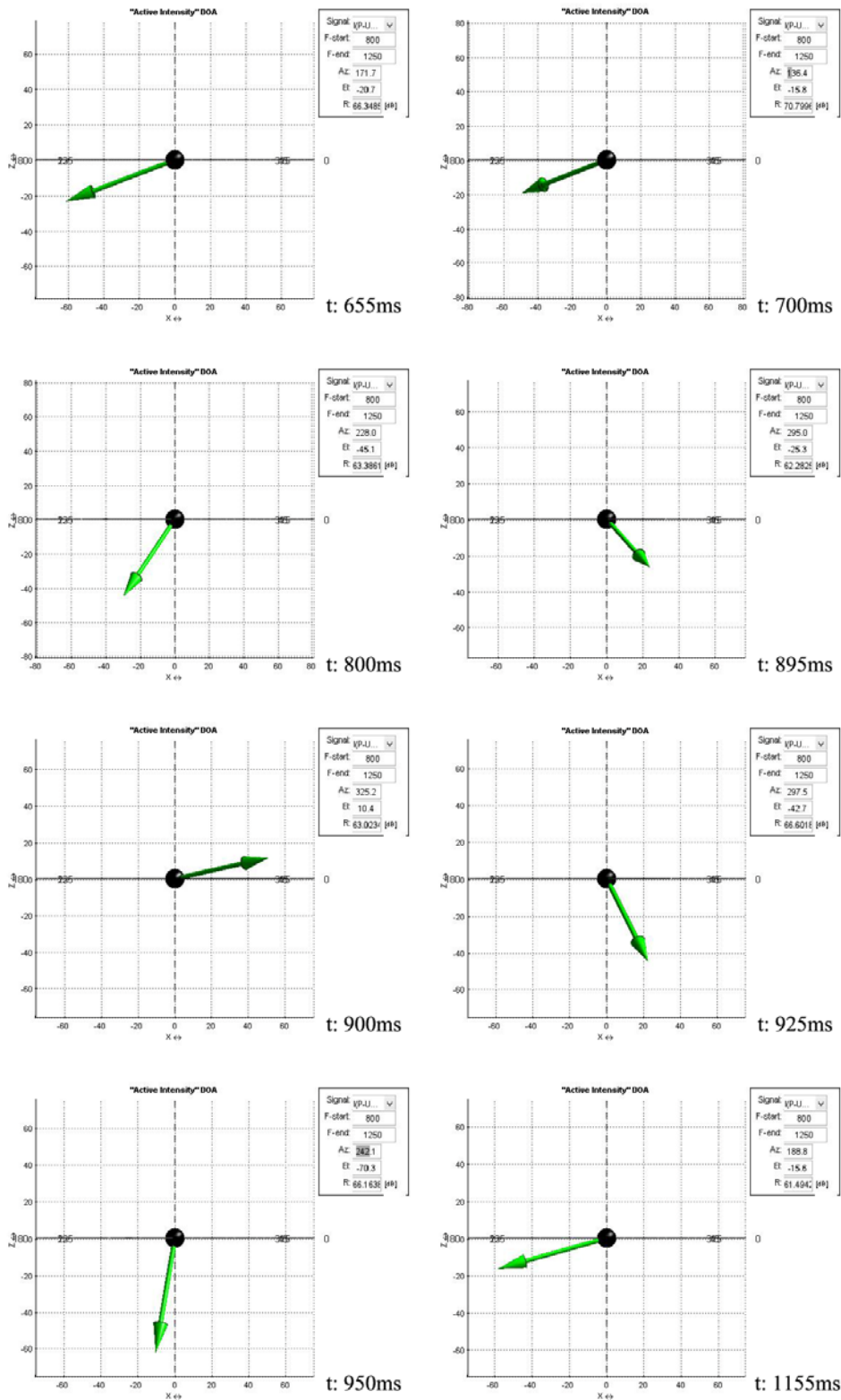


Figure 6.13. Intensity vectors, S_1R_1 , 1 kHz, t: 655 to 1155ms, XZ axis, Süleymaniye Mosque

A closer look into the data is provided for S_1R_1 filtered for 1 kHz over both pressure and intensity impulse responses. The aim of this trial is to provide the possible relation in between turning points and energy flow decay returns, in other words, to seek validation of the non-exponential energy decay formation detected over pressure impulses. Pressure impulse response is analyzed through Multi-Slopes code. The decay parameters for S_1R_1 filtered for 1 kHz are presented in Table 6.1. Bayesian decay model with relevant decay slopes and the turning point time are indicated on the Schroeder decay graph given in Figure 6.14.

For the same data (S_1R_1 , 1 kHz), next, intensity impulse responses are generated by a Matlab code developed within the context of this thesis research. Initially, pressure and 3D velocity files are imported within the code for relevant multiplication to get arrays of sound intensity impulses. Later, the data is filtered by an IIR filter, in which lower and upper limits of the central frequency can be defined. The filtered intensity impulses, separately for (intensity-x, intensity-y and intensity-z) are then smoothed by a moving filter for neighboring data points, in order to provide representative averages over specified time spans. Finally, the 2D vectors are plotted for different axes, in this case specifically XZ that shows flow vector turning patterns within the Mosque through *mihrab* section. By the help of vector plot code it is also possible to animate direction changes in desired time instances.

The intensity flow vector outputs for a close up time span from 1137 to 1170 ms for every 3 ms are presented in Figure 6.15. It should be noted that both in Figure 6.14 and Figure 6.15, time 0 is the start of recording. Thus, there is a time gap until the balloon pop is completed. The direct sound line is important in that respect, which is around 300 ms, as can be observed both in pressure and intensity impulses. Observing both sound pressure energy decay (Figure 6.14) and intensity vector flow results (Figure 6.15), it could be stated that the turning point, where the linear decay terms of two exponential energy decays intersect, is around 1140 to 1150 ms (or around 800 ms after direct sound). That means there is an energy flow direction

change within this time interval, when the steeper early energy decay is overlapped with the shallower later decay due to the energy exchange mechanisms within the space. Coinciding time interval for turning point and flow vector return is significant in validating Bayesian estimated decay parameters, and thus multi-slope formation, with real-size active intensity vector data analysis.

Table 6.1. Decay parameters for impulse response collected at S₁R₁, filtered for 1000 Hz, at probe field tests, Süleymaniye Mosque

Decay parameters	S ₁ R ₁ 1000 Hz
A_0 (dB)	-85.50
A_1 (dB)	-6.95
T_1 (s)	4.64
A_2 (dB)	-10.47
T_2 (s)	6.98
BIC (Neper)	11186 (2 slopes)

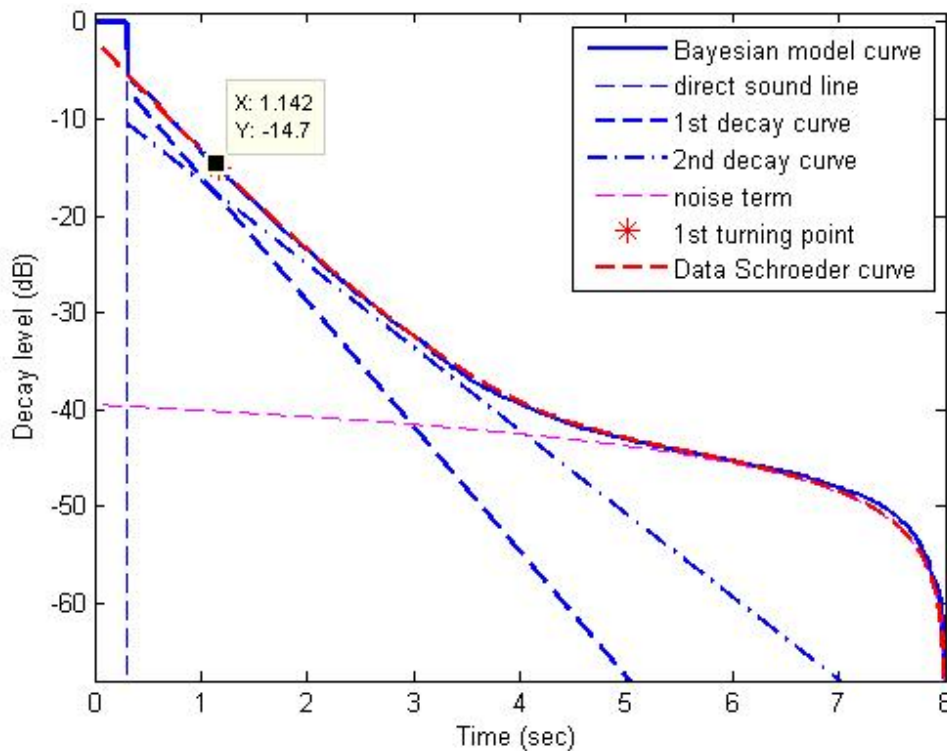


Figure 6.14. Comparison between Schroeder curve and the model curve, S₁R₁, a double-slope model derived from the room impulse response, band pass-filtered at 1000 Hz, at probe field tests in Süleymaniye Mosque

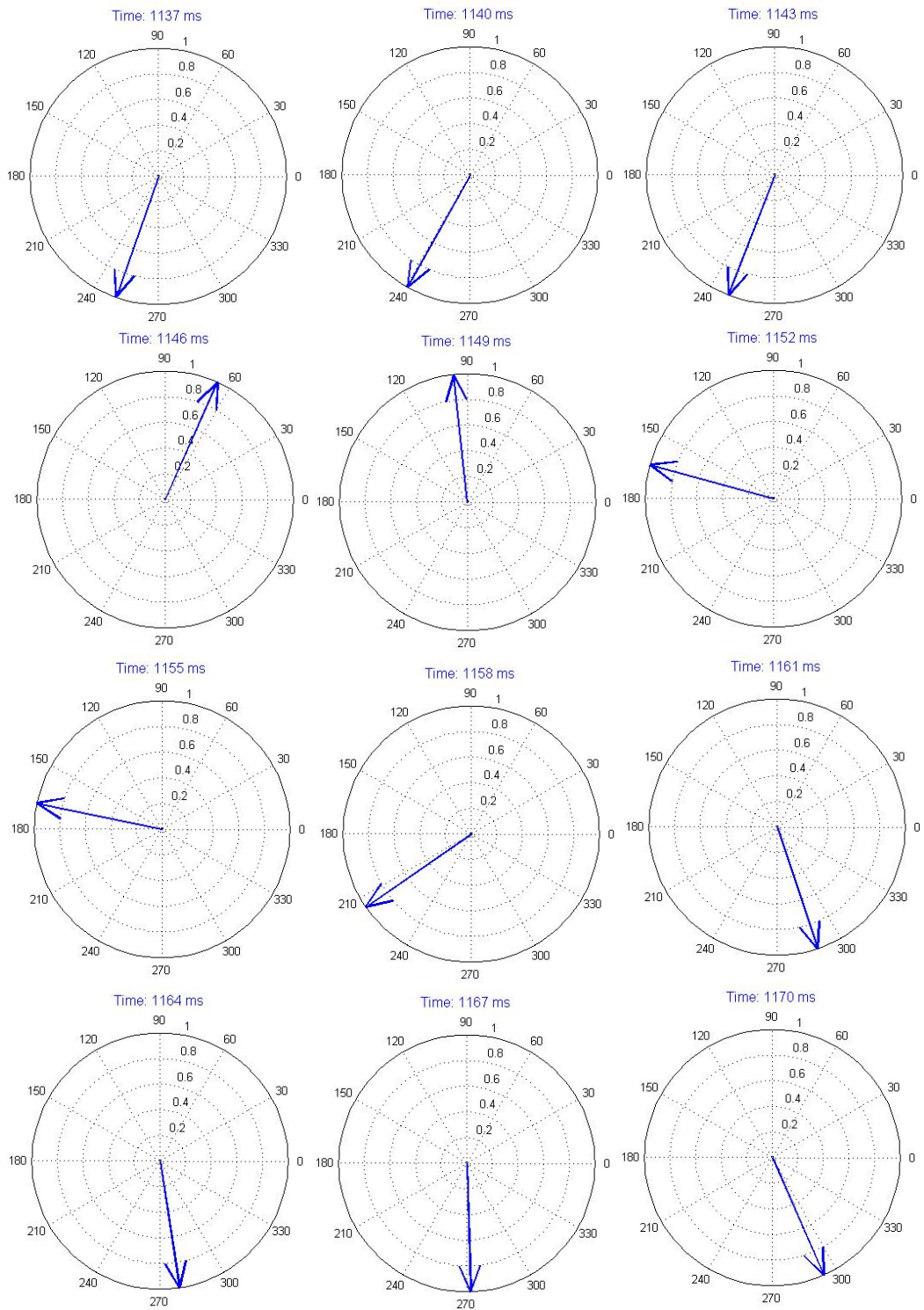


Figure 6.15. Intensity vectors, S_1R_1 , 1 kHz, t: 1137 to 1170 ms, XZ axis, Süleymaniye Mosque

An important reason for the energy divergence within the space is the absorptive and reflective sound area break-up in between carpet and stone and/or plastered brick upper shell and wall surfaces. Specifically for lower octave bands the difference in between carpet or plaster (today's) are not significantly deviate from each other. For that reason the sound flow just differs in the manner of raising the energy concentration in the dominating central *mihrab* wall section by 1 to 2 meters upward the receiver zone in compare to a reflective floor.

Together with the materials' sound absorption characteristics, the geometrical features and/or architectural divisions in form of central dome, secondary dome and secondary side domes with their characterizing dimensions and heights from the floor together with main axial plan dimensions, are the dominating properties in effect of acoustical coupling formation. The multi-slope decay formation is estimated to be primarily the result of the energy division in between the upper central zone of the mosque -in between the four elephant feet in plan, and approximately where the pendentives of the main dome are started at the section on the boundaries-, and the side aisles underneath the secondary dome structures (Sü Gül, et al., 2014b).

The acoustical effects of floor -and/or overall surface materials' sound absorption areas- can better be analyzed through a case which has a totally reflective floor, in compare to Süleymaniye Mosque with carpet floor finish in its current state. For that reason, floor finish material over developed DEM of Süleymaniye Mosque is replaced from carpet to marble. Detailed DEM time dependent solution results are presented under Section 5.3 and detailed DPE results are given under Appendix C. Figure 6.16 to Figure 6.17, summarize the spatial energy distribution and flow vector analysis results for floor with marble. As shown in Figure 6.16, spatial sound energy distributions for 2 s time solution at 1 kHz is selected to be a representative case. Closer before and after this time period the energy accumulation zones do not show a significant shift.

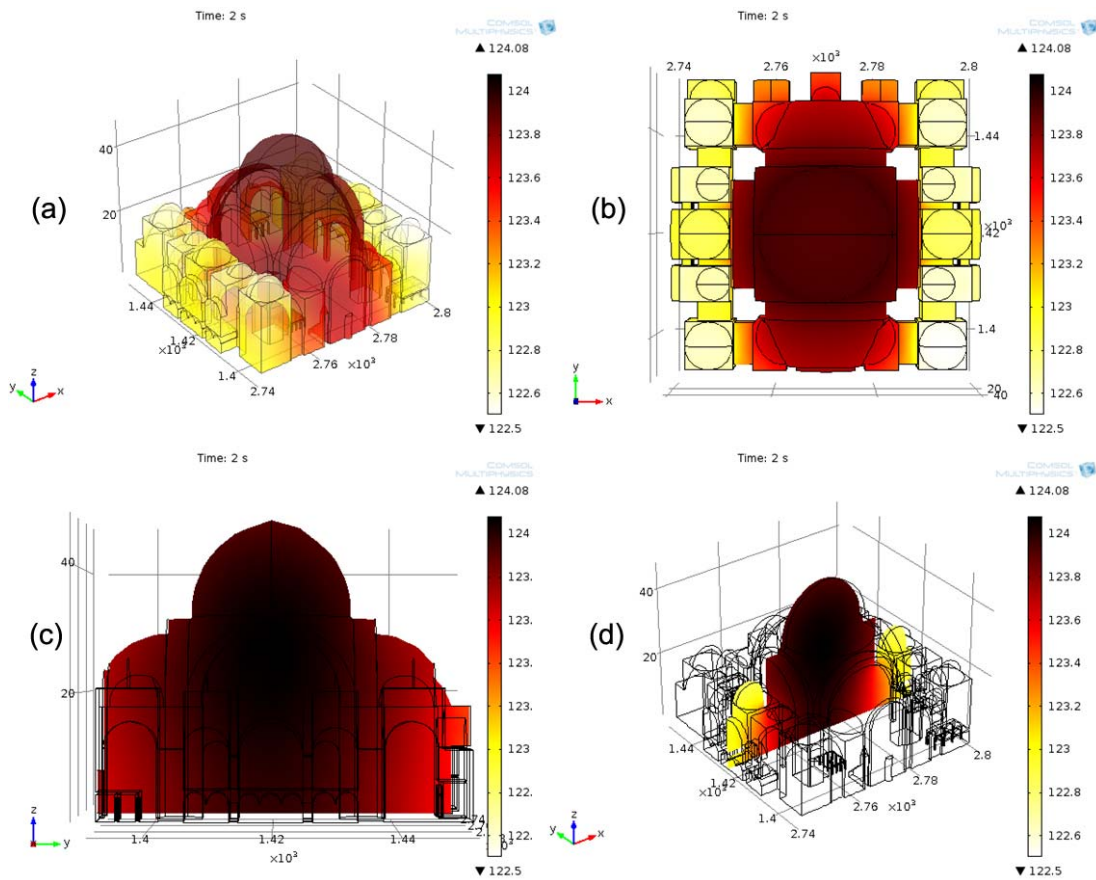


Figure 6.16. Spatial sound energy level (dB) distribution, marble floor for 1 kHz; volume and slice plots of Süleymaniye Mosque DEM solution, for time: 2 s. a) axonometric view, b) plan view, c) section through the *mihrab* wall, central axis, d) section parallel to the *mihrab* wall, central axis.

As can be observed from spatial sound energy distributions in Figure 6.16 and flow vectors in Figure 6.17, the central zone underneath the main dome do not indicate a significant energy fragmentation on the mihrab axis. Energy distribution is much even, and the deviations from floor zones to upper parts of the main dome are not significant (less than 1dB). On the other hand, for floor with carpet, there is a significant separation on the section for over and below the pendentive zone. For floor with marble, the inverse section parallel to the mihrab wall axis, the side aisles underneath mezzanine floors show relatively lower sound intensity levels, similar to that of floor with carpet, representing a typical coupled volume case.

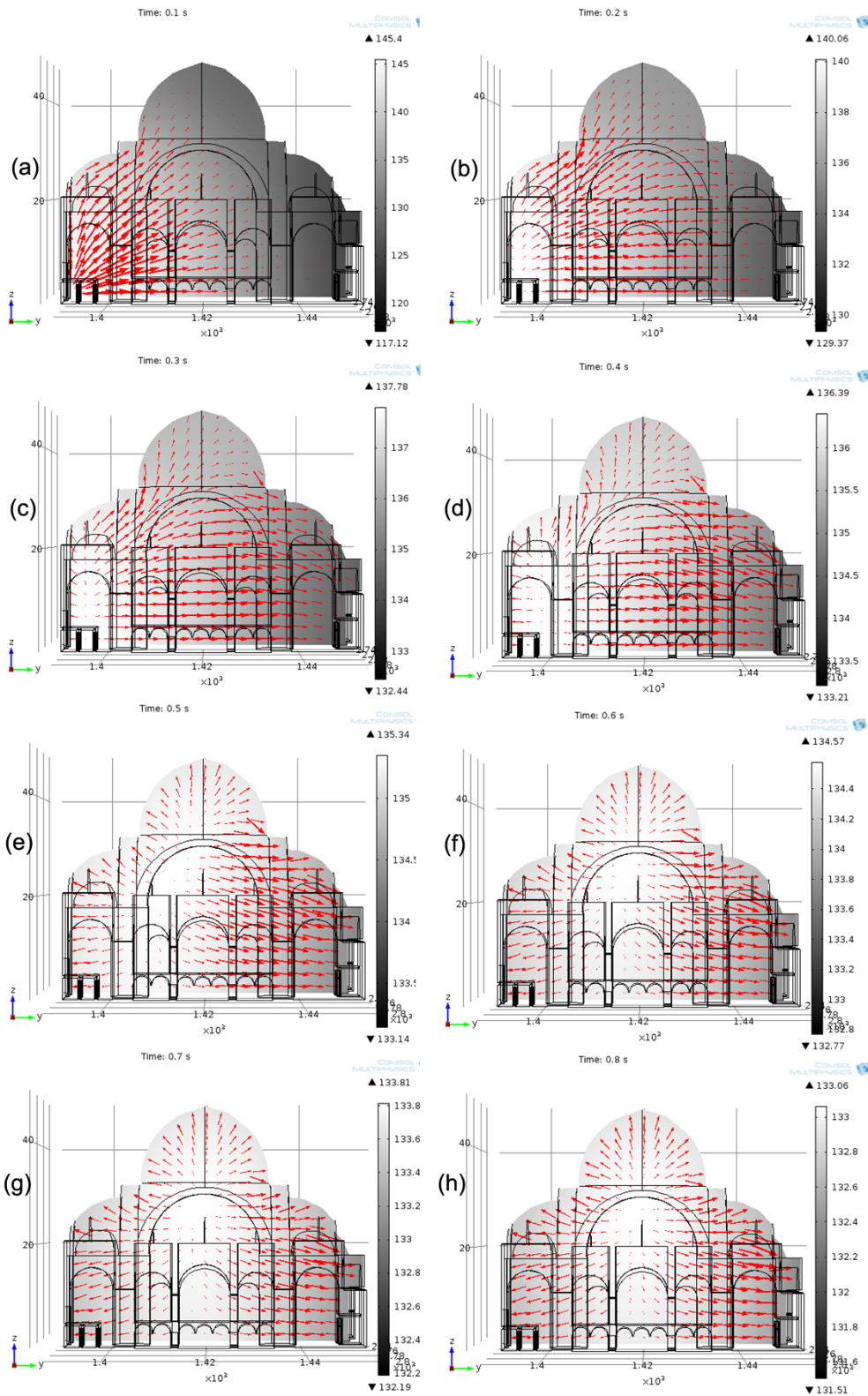


Figure 6.17. Two-dimensional mapping of flow vectors, marble floor for 250 Hz; a) time: 0.1s, b) time: 0.2s, c) time: 0.3s, d) time: 0.4s, e) time: 0.5s, f) time: 0.6s, g) time: 0.7s, h) time: 0.8s, Süleymaniye Mosque

For both cases, floor with carpet or marble, flow return is around $0.7 \text{ s} - 0.9 \text{ s}$. Basic deviation is that the focal point of energy concentration is at the center of main dome for floor with carpet, while in marble floor trial the focal point is at the center of the Mosque over total height. The lowering of the focal point towards prayer zone causes a more homogenous distribution of sound from that center outwards the rest of the Mosque volume. As a result, the energy zones overlap and multi-slope formation is impeded. This initial hypothesis is not only supported by the spatial energy distribution and flow vector analysis, but as well with decay parameter estimations.

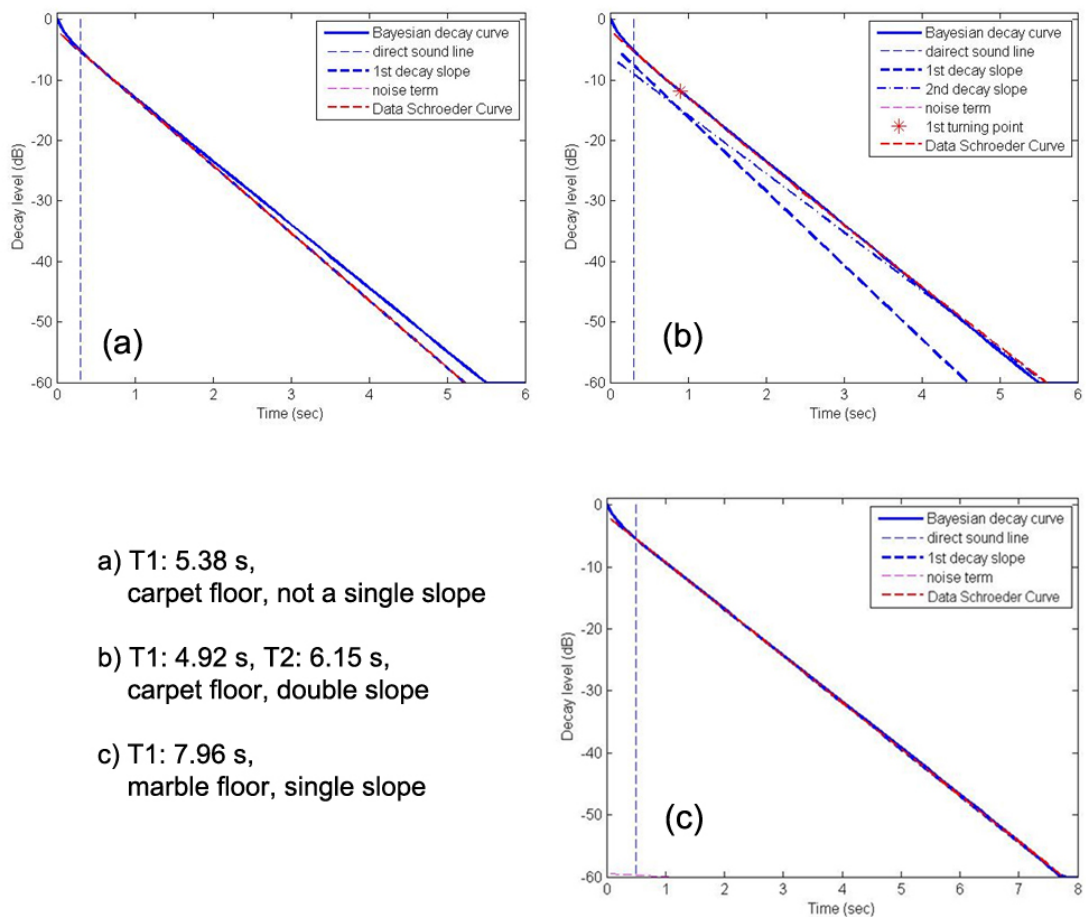


Figure 6.18. Süleymaniye Mosque, DEM multi-slope analysis results, S_1R_4 , 1 kHz; a) carpet floor - 1 slope, refuted, b) carpet floor - 2 slopes, a) marble floor - 1 slope

In Figure 6.24, double slope formation of DEM solution with carpet floor of the Mosque over a sample receiver position (S_1R_4) at 1 kHz is compared with the single slope formation of DEM solution with marble floor for the same source-receiver configuration and 1/1 octave band. As can be observed from Figure 6.24, Süleymaniye Mosque with carpet floor indicates distinctive double slope decay for the given case, but a marble floor finish for the same case results in single slope energy decay, highlighting the significance of absorptive floor material in un-even distribution of sound field and so-called multi-slope energy decay formation.

6.5. MULTI-SLOPE FORMATION WITHIN SÜLEYMANIYE MOSQUE AND HAGIA SOPHIA IN RELATION TO BASIC ARCHITECTURAL PARAMETERS

The aim of this section is initially to assess the dissimilar sound field of Hagia Sophia in compare to Süleymaniye Mosque, due to volumetric, geometric and material input. In order to further discuss about multi-slope formation within the super-structures, initially reverberation time distributions over 1/1 octave bands are compared for Hagia Sophia, measured in different times, to Süleymaniye Mosque's most recent field tests (Figure 6.19).

In Figure 6.19, DTU and UNIFE indicates measurements taken in 2000 under the supervision of CAHRISMA project (2003). Hagia Sophia field tests held in 2000 (2003), highlights that T30 values in overall are higher than field test results of ODTÜ-2014 measurements, that are held within the context of this thesis research. The drop of T30 values out in most recent measurements below 250 Hz in Hagia Sophia is expected to be the result of barrier wall separating one side aisle from main volume over the whole longitudinal length, which was present within the space during field tests due to ongoing restorations (Figure 6.20). Out of single layer gypsum board connected to back studs/profiles in certain intervals, it is probable that the system behaved as an effective low frequency membrane absorber. On the other

hand, the mid to – high frequency drop in T30 values for ODTÜ-2014 measurements in compare to pre 2000 restorations is the most probable result of present scaffolding for on-going restorations that are re-built after 2012 (Figure 6.21). Thus, the presence of additional architectural elements/constructions within the space during ODTÜ-2014 measurements has resulted in a drop of 1 to 2 seconds in overall frequency spectrum for reverberation times. On the other hand, the trend of the sound decay over frequency spectrum is similar for overall Hagia Sophia field tests, and T30 values still are relatively much higher than those of Süleymaniye Mosque for 250 Hz and above.

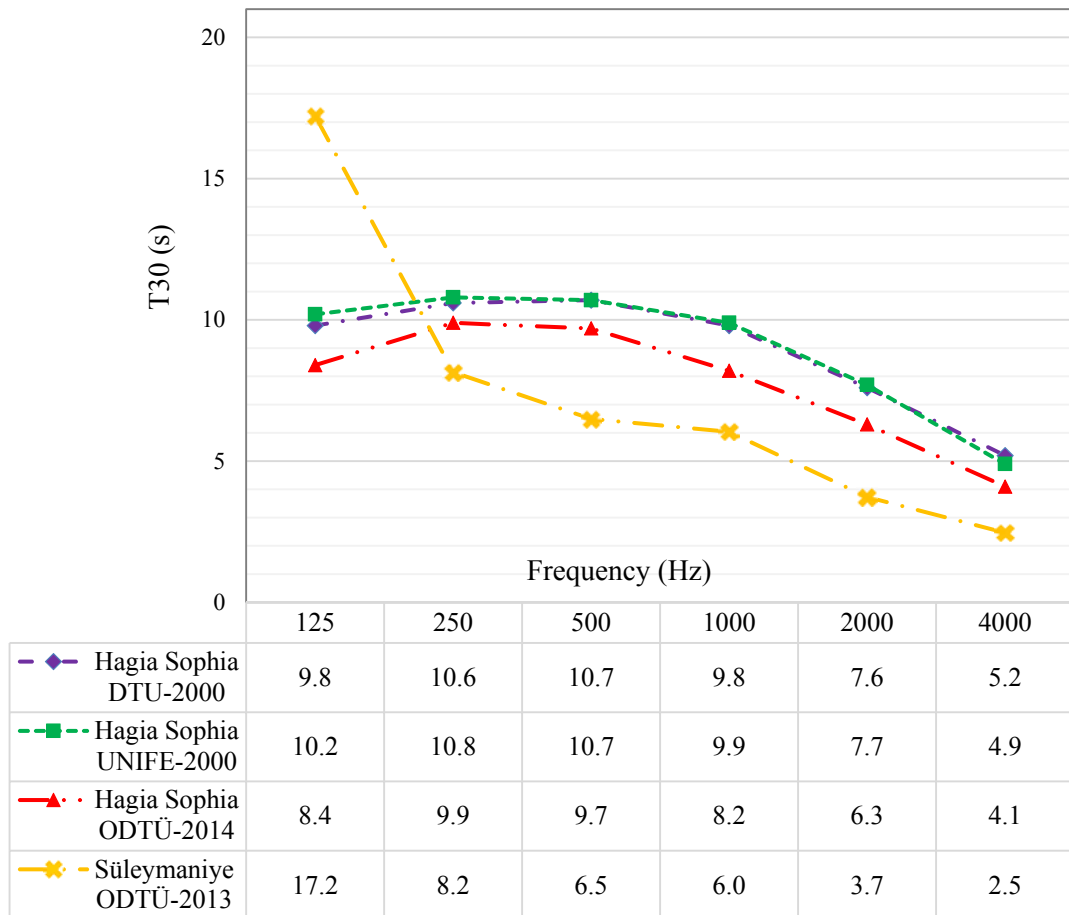


Figure 6.19. Comparison of different T30 field test results of Hagia Sophia and comparison with T30 field test results of Süleymaniye Mosque, 1/1 octave bands



Figure 6.20. Barrier wall separating left aisle from the main space, for providing security zone in ongoing 2014 restorations, Hagia Sophia (*Source: photographed by the author*)



Figure 6.21. Photo of main dome and scaffoldings, Hagia Sophia in 2014 (*Source: photographed by the author*)

T30 comparison graphs as given in Figure 6.22 provide a general insight for the acoustical fields within two mega structures. DIRAC post-processed data for the first 30 dB drop in energy decay, regardless of multiple slopes, indicate that frequencies over 250 Hz have significantly higher decay rate in classical terms of reverberation for Hagia Sophia in compare to Süleymaniye Mosque. This result is expected considering the doubling of acoustical volumes, which is roughly around 100,000 m³ for Süleymaniye Mosque, whereas roughly around 200,000 m³ for Hagia Sophia. The plan schemes of two structures are compared in Figure 7.1, indicating the considerable differences in size even in plan layout.

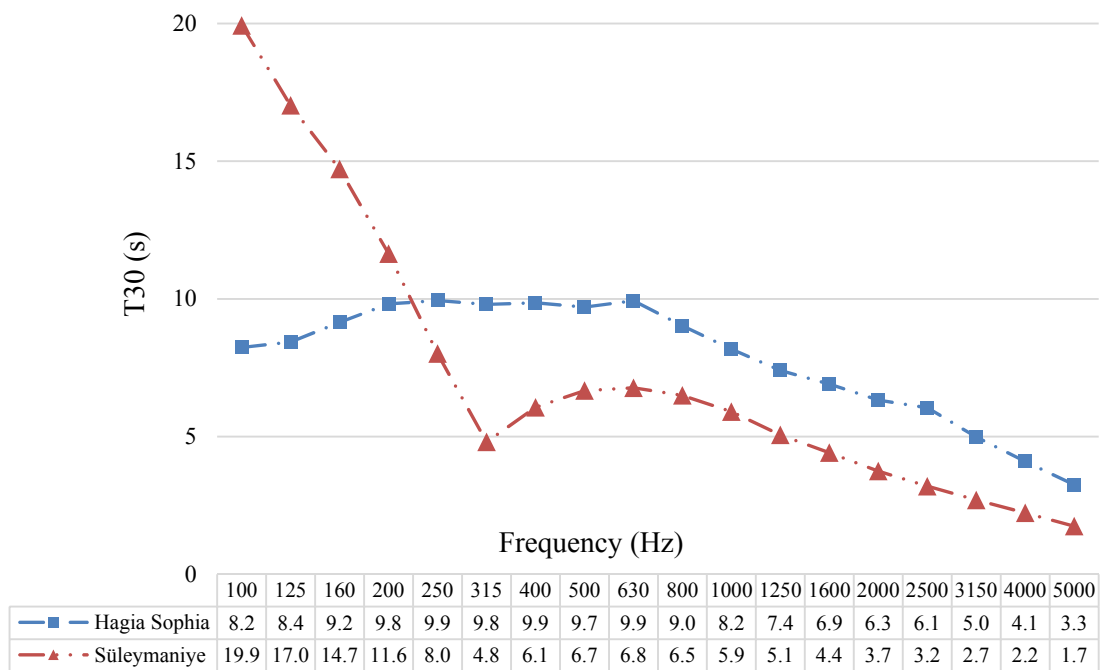


Figure 6.22. Comparison of T30 for Süleymaniye Mosque and Hagia Sophia , 1/3 octave bands

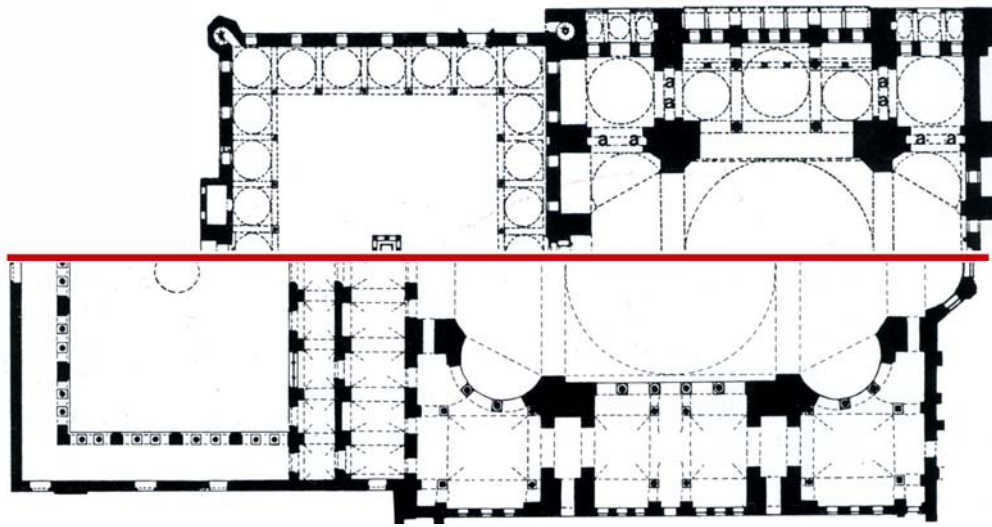


Figure 6.23. Partial plans of Süleymaniye (above) and Hagia Sophia (below) (Source: produced by the author)

Another significant aspect in relation to reverberation, aside from the interior volumes, is the interior finish materials. Marble floor cover in Hagia Sophia in compare to carpet floor finish in Süleymaniye Mosque is also very much effective in increasing decay rates specifically over mid-to high frequencies. To discuss about multi slope formation within two mega structures as a common variable decay slopes per octave bands are compared. Relative multiple slope decay formation analysis results over 1/1 octave bands are compared in bar graphs for average, maximum and minimum number of decay slopes in Figure 6.24 and Figure 6.25.

It can clearly be observed that Süleymaniye Mosque in measured source and receiver locations provides greater number of decay slopes (non-exponential energy decay formation) in overall frequency spectrum. This outcome highlights that, the volume of Hagia Sophia being much greater than that is of Süleymaniye Mosque -so that the global reverberation over specific octaves- has not provided the circumstance for higher decay rates. The effect of material absorption in terms of creating absorptive versus reflective zones (carpet versus marble), is much dominating than the very high reverberation within spaces for providing multiple decay rates. Air absorption is

much greater over 2 kHz, so specifically for Hagia Sophia there is an increasing trend of multi-slope formation in those upper band frequency range.

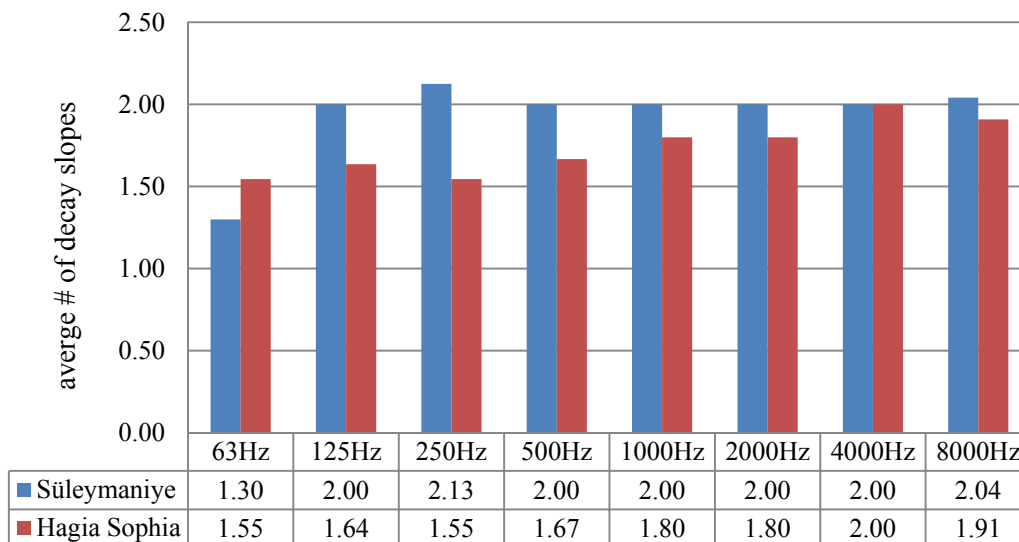


Figure 6.24. Average # of decay slopes per 1/1 octave bands, comparison of Süleymaniye Mosque to Hagia Sophia

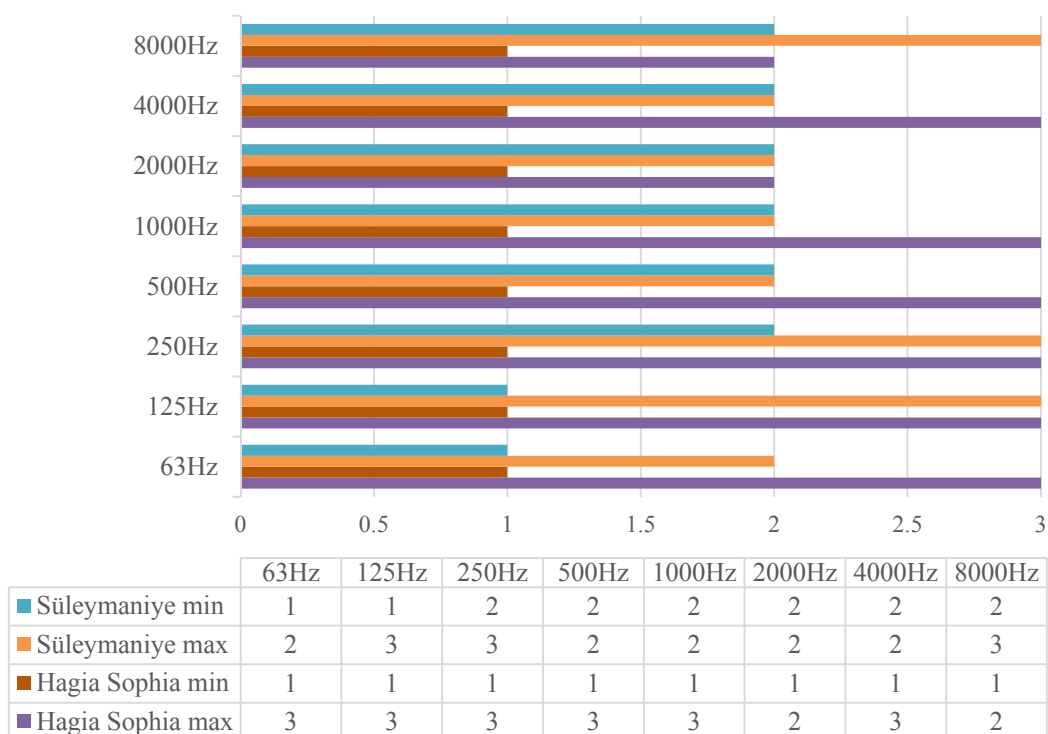


Figure 6.25. Minimum and maximum # of decay slopes per 1/1 octave bands, comparison of Süleymaniye Mosque to Hagia Sophia

On the other hand, as highlighted in Figure 5.18 for certain source and receiver configurations the maximum number of decay rates per octave bands in Hagia Sophia are much greater than Süleymaniye Mosque, specifically for S₂R₅ and S₂R₆, as of in a typical coupled space. This instance is due to the right side aisle (under gallery) measurement locations, where the sound source and receiver are both at the virtual room with lower natural reverberation. The existence of acoustical coupling in between sub-spaces within cathedrals have been previously proved by couple of researchers (Anderson & Anderson, 2000; Magrini & Magnani, 2005; Martellotta, 2009). Similarly, in Hagia Sophia case for mentioned measurement locations, the coupled space or secondary volume that provides energy feedback is the main space underneath the central dome axis of Hagia Sophia, whereas the energy deficient first volume is the virtually separated zone of side aisles underneath gallery space with lower natural reverberation time -where the source and receiver are both located-.

An important point is that, side aisles of Süleymaniye Mosque, behind large major arches carrying the central dome, are not restricted as much as arcades separating side aisles of Hagia Sophia. The aperture size, as an important architectural variable for acoustical coupling, indicates that in Süleymaniye Mosque the whole space behaves much even in terms of volumetric distribution, so can be named under single volume spaces. However, the aperture sizes of Hagia Sophia, arches of side arcades, are not large enough that these auxiliary spaces could not be interpreted as within the same volume of the central space (Figure 6.26).



Figure 6.26. Arches of Süleymaniye Mosque (above) and Hagia Sophia (below) (Source: anonymous)

To conclude, providing a much even sound distribution considering reflective interior finish materials, overall assessment of Hagia Sophia indicates lower number of decay rates. By Hagia Sophia field analysis, field data are acquired over a real-size monumental space. The outcomes support the argument on the contribution of absorptive versus reflective floor case to non-exponential energy decay formation that is previously proved and/or highlighted by simulated Süleymaniye DEM solutions.

On the other hand, for certain source and receiver configurations, the space coupling provides the circumstances much closer to coupled space concept, so that for these locations the number of decay rates are at maximum at overall frequency range, more specifically observed as triple slopes out of five over eight octave bands. This final outcome indicates the necessity of further investigations on non-exponential sound energy decays underneath the aisles of Hagia Sophia, but this time to be called under

the title of coupled spaces with real apertures instead of single spaces with virtual apertures that is searched under this thesis topic.

6.6. EVALUATION OF DATA COLLECTION AND DATA ANALYSIS METHODS

In this research, data is collected from both field tests and simulations. Field tests, held within the monumental structures with a complete set of acoustical measurement equipment, are more reliable in compare to simulations as they provide the real data. The field measurements organized at late hours with minimum background noise levels are crucial for obtaining best signal to noise ratios. Delivery of the equipment to the site and the setup of the field measurements in terms of the positions of sound source and receivers are some of the important issues to be managed within field test procedure. There is necessity to shape the set of field test procedure before field measurements by means of preliminary simulation analyses and, then, build the field test procedure in order to achieve the most efficient in-situ acoustical data.

Field tests are held by two different sets of acoustical measurement equipment in this research initially for analyzing decay parameters and next for validating decay returns. Standard room acoustic parameter measurement set-up includes an omni-power sound source, a held-held analyzer with incorporated pressure microphone, amplifiers and software for signal generation and post processing. Intensity measurement set-up includes a USP probe with incorporated pressure and particle velocity sensors, an omni-power sound source, amplifiers and software for signal generation and post processing. Comparing the two measurements, the major difference is the use of pressure microphone versus the joint use of pressure and velocity sensors/transducers (intensity probes). However, the second set up produces data in 4 channels as opposed to single channel measurement scheme in the former.

Pressure microphones only measure the potential energy field, which is proportional to the square of pressure. Intensity probes, on the other hand, are instrumental to measure energy density, which is the sum of both potential and kinetic energy densities, thus proportional to the sum of the squares of pressure and particle velocity. Energy density is more spatially uniform and more reliable quantity to use for reverberation time and other parametric calculations. Thus, using energy density leads to fewer measurements to accurately describe a room. Besides, specifically at low frequencies, the signal to noise ratio is also increased by the use of intensity probes in comparison to classical pressure microphones, as proved by previous research (Nutter et al., 2007).

Impulse responses obtained by a pressure microphone can provide the estimations on energy decay parameters as of RT, T30, C80, STI *etc.* used in classical room acoustics assessments. However, pressure microphones can only provide one dimensional information in form of pressure over time, without any information on direction in 3D. On the other hand, three particle velocity sensors (located in 3 axis; x, y and z) coupled to one pressure sensor, as in 3D-USP probe, can provide the 3D mapping of the space. With 3D-USP probes, all other energy decay parameters over pressure impulses obtained by a single pressure microphone can also be gathered, but as well sound intensity impulses for each direction can be measured. Sound intensity is a vector associated with the product of sound pressure and particle velocity averaged over time windows, which quantifies the amount of sound power that propagates through a unit area. By plotting sound intensity vectors over time, energy flow patterns can be depicted/visualized and energy exchange mechanism in relation to non-exponential energy decay formation can be examined as done in this study. Such a comprehensive examination was not possible with the sole use of a pressure microphone in field measurements.

There are some other advantages of using intensity probes. For instance, specific acoustic impedance is related with the ratio of pressure to the particle velocity, and is

a useful quantity to determine the reflection or absorption coefficients of materials. In other words, intensity probes, for now in a limited frequency range, introduce an alternative method to impedance tube and reverberation chamber methods for estimating material's sound absorption and/or scattering coefficients. More important is that these tests are non-destructive and can be held in situ without the necessity of collecting or reforming of the sample materials in specific sizes. One basic disadvantage is that the initial investment for the system is still much costly in compare to a standard room acoustics measurement set-up and or impedance-tube set up. Furthermore, the technology of particle velocity sensors/transducers and measurement techniques are very recent and still developing in room acoustics and in-situ acoustical performance analyses of materials. This research is one of the few studies in room acoustics, by its application on a monumental structure.

The type of sound source signal is especially significant in providing high signal to noise ratios. In this study, for both pressure microphone and intensity probe measurements various source signals are tested, including “continuous digital signals” as of e-sweep, MLS, MLS-pink and “impulsive human-made noise” as of balloon pop and wood clap. Those signals have differences in terms of frequency content, pattern, directionality and signal strength over time. In overall, the results highlight that e-sweep as a digital signal possesses the highest signal to noise ratios, but may contain distortion for very long capture/impulse lengths. Therefore, the data should be carefully selected over multiple-recordings for the same location or cleared out for the distorted time span as long as it provides sufficient time window for energy decay analysis. In intensity measurements, on the other hand, impulsive balloon signal has been much usable specifically for over 1 kHz, considering signal-to-noise ratios as well as their clear shut off time. Signal generation by wood clap, in this study in overall, has provided the weakest signal strength/power over the frequency spectrum, thus the lowest signal to noise ratios. For that reason, the data obtained by wood clap are not included in later data analysis.

Computer aided simulation is the second method exercised in data collection, following to field tests. Ray-tracing based acoustical simulations are instrumental in assessing the spaces before field tests or in the very beginning of research, when there is no knowledge over probable outcomes. They are also directive in highlighting critical locations to be assessed in field tests. For after field tests, computer simulations provide the ground for practical experimental analysis, either by changing/testing materials or source and receiver locations. Simulations are free of background noise that persist in the real environment, which drops the noise floor in a sound energy decay curve and increases the analyzable decay range. Thus, it is more probable to observe higher number of decay rates in a simulated data, which is the most ideal case but still not likely to occur in a real environment. For that reason, the caution should be paid over the very late decays and higher number of decay rates in the assessment of multi-slope energy decay formation out of simulated data.

DEM as applied in this research is another computational analytic technique for both data acquisition and analysis of simulated data. This technique is applied for understanding/examining the energy exchange mechanisms that can cause multi-slope energy decay formation within the space. DEM is a very recent statistical analysis model for its applications in room acoustics. It is first time applied in such an over-scale real structure, for the acoustical field analysis of Süleymaniye Mosque.

The method is based on the theory of diffusion of particles instead of wave phenomena. In finite element modeling for overall frequency range the meshing size depends on the mean free path of the room rather than the wavelength of interest. This results in much minimized mesh dimensions and so much feasible computation times in comparison to computations depending upon the wave theory.

This study basically focuses on the spatial energy distribution and flow vector plots that can be gathered out of DEM solution, for examining energy fragmentations and energy exchanges within a single space. Besides that, for any receiver location within

the coordinate system (volume), point responses can be obtained in form of intensity impulses. Out of intensity impulses energy flow decays can be obtained, which are significant for detection of the turning point (intersection of different linear decay terms within a non-exponential decay) location (in time and level) in relation to that same data gathered out of pressure impulse responses. These point responses out of DEM solution are also important for comparison or for to be validated by the intensity impulses gathered through particle velocity sensors (USP probes) in the field tests.

Exercised over an existing monumental structure within the context of this study, the DEM solution findings are significant in revealing more specific causes of multi-slope decay formation within single volume structures with specific geometric attributes. It should be emphasized that DEM application by finite element modeling is an emerging practical and scientific method of room acoustics predictions, particularly for in-depth sound field analysis. Thus, it can find many grounds in room acoustics applications, as in this case, and should be utilized as an acoustical analysis tool over existing structures or as an acoustical design tool for virtual or future spaces.

In addition to DEM analysis, in phase of post-processing of the collected data -or as of data analysis tools- some commercial software are utilized, including DIRAC and Analyzer, for classical room acoustics parameter estimations. These type of software are practical for immediate estimation of objective acoustical metrics. However, for further scientific investigation of the data, in this case the non-exponential energy decays, more sophisticated or specialized analysis methods/codes are needed. The dependability of Bayesian framework in room acoustics' coupling studies (coupled spaces) in comparison to visual inspection and ratio based coupling quantifiers are previously discussed under Section 2.4.4. in detail. MultiSlopes code that relies on the Bayesian decay parameter estimation and decay model selection, as an approximated model to the Schroeder integrated real data, can be used a reliable tool

for investigating and detecting decay parameters (number of slopes, decay rates, decay levels, turning point) within a sound energy decay.

As necessitated for in-depth data analysis and for processing the signals obtained in form of impulse responses (pressure or intensity), post-processing in this research does not only rely on commercial software, but also Matlab codes developed specifically within the context of this research. Signal processing is vital for an in-depth scientific investigation in acoustics, in order to have a better control of the analysis over the data and for computation of parameters or phenomenon that are searched after. It is significant that the researcher to develop his/her own tools of analysis or even data collection methods for carrying the research and/or science one step forward, regardless of whether they have applied before or not. Such an approach may broaden/introduce new tools on data collection and analysis. The research methods used and developed in this thesis research, the achievements in reliable data collection and their joint analyses/interpretation are expected to be guiding for further analyses and developments in this field.

CHAPTER 7

CONCLUSION

Within the context of this study sound fields of two multi-domed superstructure cases, namely Süleymaniye Mosque and Hagia Sophia, are analyzed. Assessment of acoustical coupling until now has basically been studied to define the peculiar sound field within acoustically coupled enclosures in which multiple-slope energy decays can often be observed. The key concern of this study has been to reveal the potential of multiple-slope energy decay formation in over-size *single space* structures with particular geometry and distribution of materials. The interpretation of the acquired data is carried in order to broaden the definition of “the coupled volume system” with an emphasis on invisible sources and apertures of acoustical coupling in a “single volume system”.

Following to the detection of non-exponential energy decay (multiple slopes) formation in case structures -by real size field measurements and acoustical simulations-, the probable reasons are further investigated by different techniques including decay parameter estimations and diffusion equation modeling. Data collection over the prototype case, Süleymaniye Mosque, provided scientific grounds to discuss not only acoustical coupling but also sound field of the Mosque for before and after specific restorations as well as for its original state.

In order to examine the acoustical comfort levels of Süleymaniye Mosque for its current state and to discuss the changes occurred in relation to the main repairs undergone in its life time, in-situ acoustical tests are held in 2013 -right after the final restoration work performed during 2007-2011. Those recent data are then compared

with the previously-published in-situ measurement data, characterizing the acoustical condition of the Mosque after 1969's and 1980's restorations. Acoustical simulations are performed to represent and discuss activity patterns for the occupied state. Simulations are also utilized to discuss about different effects of material changes within the Mosque for its original state. Findings can be briefed as follows:

- the acoustical field of the Mosque as a result of architectural form-geometry and interior material factors exhibits the presence of very high reverberation times in all field tests, especially at low frequencies.
- field tests taken after most recent restoration work indicate some enhancement in terms of reverberation control for mid to high frequencies. However, low frequency T30 values varying in between 12 s to 17 s still indicate boomy/muddy sound field, which is a major problem especially in terms of speech intelligibility within the Mosque.
- the simulations for full occupancy of the Mosque for its current state, indicate almost one half of the T30 values for low frequency range and relatively lower values for mid to high frequency range in compare to field test results for unoccupied condition. This means when the Mosque is fully occupied, as in a typical Friday's sermon, reverberation time as a basic indicator is much closer to the optimum range.
- the Mosque is found to suffer from high background noise levels due to the mechanical systems introduced to the structure during 2007-2011 restorations. In order to decrease the fan noise of electrical panels located right across to the mihrab wall at the 1st balcony level, measures such as box-in-box construction, silencers, or acoustical cabinet design are strongly recommended.
- such of a high reverberation and background noise is even worse for today's practice, with the application of electro-acoustic enhancement/reinforcement, in compare to its initial use for natural sound.

The discussion on the original state of acoustics within Süleymaniye Mosque relies on acoustical simulations over tuned acoustical model by gathered field-test data and material and geometry input for its initial state. Findings can be briefed as follows:

- major architectural form and volume features of the Mosque has not been altered much from the very beginning. However, over major restoration works, interior finish materials specifically plaster and paints have been renewed. Material changes is the basic reason for differences in acoustical conditions within the Mosque in different periods mostly for its original state.
- use of sound absorptive lime based plasters in original state to achieve high sound absorption is especially beneficial to frequencies in relation to the articulation of speech.
- burnt-clay pots taught to cure the low frequency sound energy built-up within the Mosque, as well as to provide acoustical asymmetry in overcoming acoustical defects as of sound foci and/or echo formation.
- the results pointed out the necessity of further investigations on the acoustical properties of historical lime-based plasters belonging to the Ottoman Period and their raw materials characteristics contributing to the acoustical features of the historical mosque structures.

Other precautions that Sinan applied for the sake of acoustics in our belief, or that are concurrently resulted to be positive in terms of room acoustics conditions of Süleymaniye Mosque, can be briefed as follows:

- position of the Mosque in a courtyard protects itself from environmental noise, which is sufficient for the time when traffic or other environmental noise was not present.
- particular geometrical configuration of multi dome superstructure and interrupted square plan-layout with elements such as mahfil's and piers helps to overcome fluttering echoes and room modes.

- sound scattering elements such as muqarnas, 'kündekari' and glazed surfaces provides much even distribution of sound at mid to high frequencies through the prayer zone as can be observed from field test results for different receiver positions.

It is very remarkable that 'Sinan the Architect' has taken many precautions in design of Süleymaniye Mosque, which have positive results for speech intelligibility, while those precautions aid live reverberance for augmenting the spiritual effects expected from such a volume of a religious space. In 16th century, when the technology was deficient of computer-aided simulation tools, or acoustical field measurement equipment and even when the acoustical parameters as of reverberation time had not defined by then, with a naked ear calibrating the room for a proper acoustic response desires much respect.

The technology that are beyond its time, as of lime based plasters and linen additives applied within the composition of plasters, as well as *Sebu* technique should further be investigated in order to scientifically prove their contribution to the acoustical features of Süleymaniye Mosque and to recover it as in the original acoustical comfort conditions. The sensitivity over acoustics for specific function, so for the human comfort, is very obvious for Sinan's time. This approach should be a motivation for today's scientific research with much developed acoustical technology.

Above mentioned issues have been naturally raised, during the research steps, as to be some additional but significant research findings and discussion points. Back to the focus of this study, both simulated and field tested data are analyzed initially for multiple slope decay formation within single spaces of super-volumes of selected cases. The single spaces for both cases are sheltered by one central dome supported by semi-domes and transitional elements, depicting the major geometrical figure. The methodology of the research involves joint use of in-situ acoustical

measurements, acoustical modeling/simulation methods and computational analyses. Bayesian analysis approach is applied in quantifying multiple-slope decay parameters.

For Süleymaniye Mosque, both acoustical simulations and field tests are applied. Pre-field simulation study aims to direct/aid following field tests for probable multi-slope decay formation. The mosque model in post-field simulations is approximated to field test conditions for further experimental analysis. Findings of Decay Parameter Estimations (DPE) of Süleymaniye Mosque for field and simulated data can be briefed as follows:

- initial results for selected source-receiver configurations indicate double and triple slopes for field tests and even more slope natures for simulations at various frequency bands.
- the increasing multi-slope formation trend in high frequencies in simulations in compare to field tests is due to the absence of noise.
- there is no significant deviation in average number of slopes per source locations, and the trend for both field and simulation results are similar.
- number of decay slopes are slightly higher for receivers underneath side corner domes and slightly higher for source in front of *mihrab* and underneath central dome.
- variations of source-receiver configurations for both simulations and field tests are statistically insignificant, indicating an even distribution of sound throughout the mosque.
- in field tests triple slopes have been mostly observed at 250 Hz, which is a very critical band when 1/3 octave bands are observed. The sharp decrease of decay time (T30) from 200 Hz to 250 Hz may be indicating the presence of volume absorbers, in this case numerous *Sebu* voids, should be further investigated.

The DPE investigations in Süleymaniye Mosque out of measured and simulated impulse response data have proved the hypothesis of even a single space with particular geometrical features and material input, which are basically reflective central main dome upper zone versus absorptive cubic lower floor zone, can provide the circumstances for multiple-slope decay formation. The answers of the mechanism of why multi-slope decay may occur in such an architectural scheme are further investigated by Diffusion Equation Model (DEM) application in a finite element solution and in-site intensity probe measurements.

Multiple decay, or mostly double decay, phenomena has been searched for coupled spaces until recently. One major conclusion of this study is that even a single space with nondiffuse sound field can provide the circumstances for multiple-slope decay formation. In order to illuminate/reveal the probable reasons of non-exponential sound energy decays within such an architectural venue, namely Süleymaniye Mosque, sound energy distributions and energy flows are investigated. DEM is applied for modeling interior sound field of the monument and intensity probe measurements are held for validation of DEM results. Findings can be briefed as follows:

- results indicate good agreement for overall energy decay time estimations among experimental field and DEM results.
- spatial sound energy distribution and energy flow vector analysis indicate the upper central dome-structure to be the potential energy accumulation/concentration zone, contributing to the later energy decays.
- the multi-slope decay formation is estimated to be primarily the result of the energy division in between the upper central zone of the mosque -in between the four elephant feet in plan, and approximately where the pendentives of the main dome are started at the section on the boundaries-, and the side aisles underneath the secondary dome structures (see Figure 7.1).

- concentration of sound absorption at specific locations, in other words the uneven distribution of absorption coefficients, creates the nondiffuse field at corresponding ranges of the frequency spectrum.
- the energy divergence within the space is the absorptive and reflective sound area break-up in between carpet and stone and/or plastered brick upper shell and wall surfaces.
- for lower octave bands the difference in between sound absorption performance of carpet or plaster does not deviate from each other as much as for mid to high frequencies. For that reason, the sound flow just differs in the manner of raising the energy concentration in the dominating central mihrab wall section by 1 to 2 meters upward the receiver zone in compare to a reflective floor.

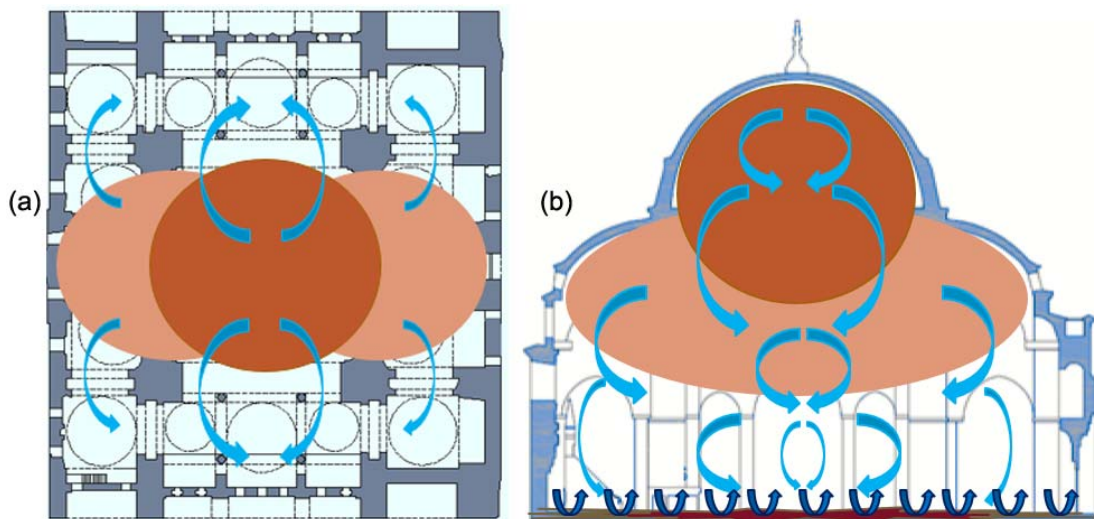


Figure 7.1. Conceptual plan (a) and section (b) views for energy flows of Süleymaniye Mosque
(Source: produced by the author)

In order to better highlight and scientifically discuss about the effects on absorptive versus reflective surface, floor finish material over developed DEM of Süleymaniye Mosque is changed from carpet to marble in simulations. Findings out of the revised model solved for 1 kHz are briefed as follows:

- for Süleymaniye Mosque -floor to be marbled-, the central zone underneath the main dome do not indicate a significant energy fragmentation on section passing centrally by the mihrab axis (Figure 7.2-b).
- energy distribution is much even within the central zone and the deviations from floor zones to upper parts of the main dome are not significant (Figure 7.2-b), in compare to the real case to the floor with carpet (Figure 7.2-a).
- at the central section cut parallel to the mihrab wall axis, the side aisles underneath mezzanine floors show relatively lower sound intensity levels, similar to that of floor with carpet and they represent a typical coupled volume case.
- flow vector plots also highlight the energy fragmentation in between domed upper structure and cubic lower floor zone, for floor with carpet (Figure 7.3-a), while for the floor with marble (Figure 7.3-b) the distribution of sound form the focal point is creating a much even and un-fragmented energy zone.
- basic deviation is that the focal point of energy concentration is at the center of main dome for floor with carpet (Figure 7.3-a), while in marble floor trial the focal point is at the center of the Mosque over total height (Figure 7.3-b).
- lowering of the focal point towards prayer zone, causes a more homogenous distribution of sound from that center outwards the rest of the Mosque volume. As a result, the energy zones overlap and multi-slope formation is impeded.
- decay parameter estimations for a sample point response indicated a double slope formation of DEM solution with carpet floor of the Mosque, while the same location resulted in a single slope formation of DEM solution with marble floor.

It should also be noted that, all these discussions are over the unoccupied space, for better correlation with practical results of field tests. For the real case of floor with carpet, when the Mosque is fully occupied as of in a Friday's sermon, the separation zones of energy fragmentation will be even greater because the absorption of the

floor will be increased. This will conclude that the multi-slope formation will be at most and perceived even greater for occupied mosque.

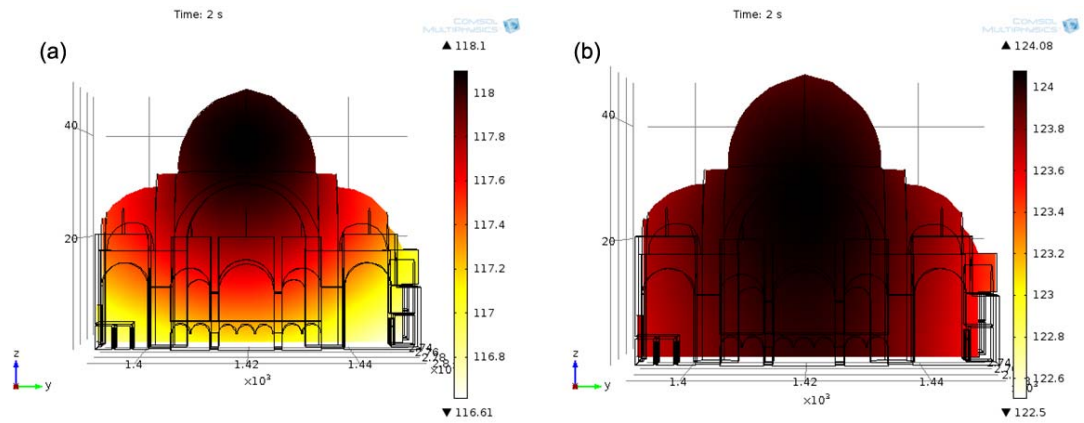


Figure 7.2. Spatial sound energy distribution comparison of Süleymaniye Mosque floor finishes; carpet floor (a) versus marble floor (b), time dependent DEM solution, mihrab wall section, 1 kHz, t: 2s`

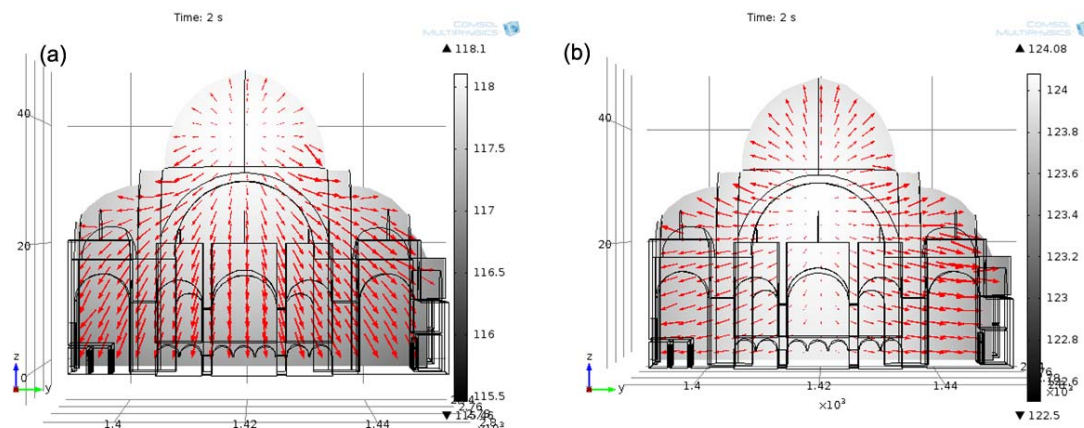


Figure 7.3. Flow vector distribution comparison of Süleymaniye Mosque floor finishes; carpet floor (a) versus marble floor (b), time dependent DEM solution, mihrab wall section, 1 kHz, t: 2s

Exercised over an existing monumental structure, the DEM solution findings are significant in revealing more specific causes of multi-slope decay formation within single volume structures with specific geometric and material attributes. It should be emphasized that the DEM application by finite element modeling is a practical and scientific method of room acoustics predictions, particularly for in-depth sound field analysis. As an outcome of this study, this unique application of DEM over a real-

size structure, will open and/or motivate a new generation tool for room acoustics estimations whether as a design tool for virtual spaces (concept designs), or for renovation of existing ones.

On the other hand, 3D impulse response measurements by the use of sound intensity (particle velocity) probes declare an even more reliable and scientific tool for discussing such scientifically in-depth research questions. The intensity probe measurements out of this study support the simulated DEM data in general specifically for the data averaged over a larger time window frame, but have dissimilarities for data averaged over shorter time windows due to individual reflections from close-by reflective surfaces in the real environment. Depending upon the purpose of use, both small and large window frames can be applied. In this case larger time windows are more representative for visualizing energy flow patterns within the reverberant tail.

The supportive case for discussions over multi-slope decay occurrence in a multi-domed upper shell structure formation is Hagia Sophia. The findings out of Hagia Sophia multi-slope decay analysis results are briefed as follows:

- there is an increasing trend of multiple slope formation towards high frequencies.
- all the surfaces within the room are in reflective range and dominating effect of air absorption over 2 kHz may have caused this energy divergence within the space by augmenting the nondiffuse sound field formation at high frequency spectrum.
- as of in a typical coupled volume space; the source is within the energy deficient room (side aisles) and the energy surplus room which is the central volume of Hagia Sophia sheltered by the main dome is coupled to the aisle space as of a reverberation chamber.

- most probably due to the above mentioned fact, measurements for source and receiver locations underneath the side galleries have provided higher number of decay slopes.

In acoustical terms basic differences from standpoint of energy decays in between Süleymaniye Mosque and Hagia Sophia, are that the former has a carpeted floor and a smaller volume and later has a marbled floor with a double sized interior volume in compare to the former. The acoustical field and multiple-slope decay formation comparison of both super-structures are briefed as follows:

- octave bands over 250 Hz have significantly higher decay rate, in classical terms of reverberation estimates, for Hagia Sophia in comparison to Süleymaniye Mosque; this result is expected considering the doubling of acoustical volume from Hagia Sophia to Süleymaniye Mosque.
- Süleymaniye Mosque in measured source and receiver locations provides greater number of decay slopes in overall frequency spectrum in compare to Hagia Sophia; this outcome highlights that, the volume of Hagia Sophia being much greater than that is of Süleymaniye Mosque has not provided the circumstance for higher decay rates.
- the effect of material absorption in terms of creating absorptive versus reflective zones (carpet versus marble), is much dominating than the very high reverberation within spaces for providing multiple decay rates.
- on the other hand, for certain source and receiver configurations the maximum number of decay rates per octave bands in Hagia Sophia are much greater than Süleymaniye Mosque.
- this instance is due to the right side aisle (under gallery) measurement locations. As of in a typical coupled space -as observed in cathedrals-, the sound source and receiver are both in the room with lower natural reverberation and the room with higher reverberation, that is the main space underneath the central dome axis of Hagia Sophia, provides energy feedback

and/or energy flow from this energy surplus main volume to energy deficient underneath gallery/aisle volumes.

- side aisles of Süleymaniye Mosque, behind large major arches carrying the central dome, are not restricted as much as arcades separating side aisles of Hagia Sophia; the aperture size, as an important architectural variable for acoustical coupling, indicates that in Süleymaniye Mosque the whole space behaves much even in terms of volumetric distribution, so can be named under single volume spaces. However, the aperture sizes of Hagia Sophia, arches of side arcades, are not large enough that these auxiliary spaces could not be interpreted as within the same volume of the central space.

To conclude, providing a much even sound distribution considering reflective interior finish materials, overall assessment of Hagia Sophia indicates lower number of decay rates. On the other hand, for certain source and receiver configurations, the space coupling provides the circumstances much closer to coupled space concept, so that for these locations the number of decay rates are at maximum in overall frequency range. It should be emphasized that Hagia Sophia for under balcony locations behave as a classical coupled volume system, and for other locations can be compared within the context of single spaces as of in Süleymaniye Mosque.

As a final summary of this study, going through over various acoustical data collection and data analysis techniques, results proved that energy fragmentation in support of acoustical coupling is due to both materials' sound absorption characteristics and their distributions as well as volumetric inter-space relations and the dome effect -augmenting the energy in reflective focal zone-. Central dome, secondary dome and secondary side domes with their characterizing dimensions and heights from the floor together with main axial plan dimensions are the dominating properties in effect of acoustical coupling formation.

It should be noted once more that the absorptive floor finish is not the only reason for nondiffuse acoustical field and it is supported by the geometrical features;

- the basic geometrical attribute that affects the energy fragmentation (so the nondiffuse acoustical environment) is the main central dome, with its excessive size and height from the ground.
- the occurrence of multiple decays indicate that the phenomenon is very susceptible even to very low reverberation time differences and material (absorption) changes.

Whether this multiple slope energy decay formation in monumental religious spaces is a useful/contributing phenomenon or not to the subjective acoustical impressions, is another important research question. The answers necessitate further investigations as in form of subjective (psycho-acoustic) testing and hopefully will be a topic of a future scientific investigation. The insights out of this study in terms of multiple decay formation and its subjective evaluation in relation to the mosque or sacred function are briefed in the following;

- for a classical coupled volume system as being the highlight of this study, there is a very interesting sound decay; composed of early and late energy parts (Figure 7.4). Late part of the decay serves for higher reverberance, whereas the early part serves for a higher clarity. So the coupled rooms have the potential of meeting these two conflicting requirements specifically beneficial for concert hall acoustics, as this non-exponential sound decay becomes an important design tool in recent years.

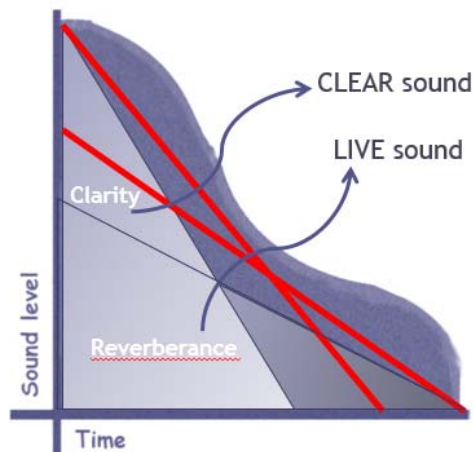


Figure 7.4. Conceptual sketch for early (clarity) and late (reverberance) sound contribution of non-exponential energy decay (Source: produced by the author)

- in a mosque speech intelligibility is one major parameter for understanding the praying orders or sermons of imam, whereas the call for prayer namely ‘*ezan*’ still necessitates the augmentation of the male voice for the envelopment and spaciousness of the spiritual space.
- in a mosque, too high of a reverberation time distracts intelligibility while too low of it generates a dead space which is not appropriate for spiritual ceremonies.
- in that respect, non-exponential energy decay with early decay that contributes to the clarity versus later decays that contribute to the reverberance completes the desired acoustical sensation of a grandeur religious volume.

Intentionally or not, the resulting occurrence of multiple-slopes within such religious/sacred super-structures has ended up with fitting the desired acoustical environments, which as well has contributed for them to be called out as the world’s most significant architectural master-pieces.

BIBLIOGRAPHY

Abdelazeez, K., Hammad, R.N. and Mustafa, A.A. "Acoustics of King Abdullah Mosque." *J. Acoust. Soc. Am.* 90.3 (1991): 1441-1445.

Abdou, A.A. "Measurement of Acoustical Characteristics of Mosques in Saudi Arabia." *J. Acoust. Soc. Am.* 113.3 (2003a): 1505-1517.

Abdou, A.A. "Comparison of the Acoustical Performance of Mosque Geometry using Computer Model Studies." *Eighth International IBPSA Conference*, Eindhoven, Netherlands, (2003b): 39-46.

Abel, J.S, Bryan, N.J., Huang, P.P., Kolar, M.A. and Pentcheva, B.V. "Estimating Room Impulse Responses from Recorded Balloon Pops." *129th Convention of Audio Engineering Society*, November 4-7 2010, San Francisco, CA, USA, 2010.

Abel, J.S. Woszczyk, W., Ko, D., Levine, S., Hong, J., Skare, T., Wilson, M.J., Coffin, S. and Lopez-Lezcano, F. "Recreation of the Acoustics of Hagia Sophia in Stanford's Bing Concert Hall for the Concert Performance and Recording of Cappella Romana." *International Symposium on Room Acoustics*, 9-11 June 2013, Toronto, Canada, 2013.

Acar, S. "Süleymaniye'nin Düşündürdükleri", *Tasarım* 102 (2000): 108-117.

Ahnert, W., Feistal, S. and Behrens, T. "Speech Intelligibility Prediction in very Large Sacral Venues." *ICA 2013*, 2 - 7 June, Montreal, Canada, 2013.

Akgündüz, A and Öztürk, S., Baş, Y. *Kiliseden Müzeye Ayasofya Camii*. İstanbul: Osmanlı Araştırmaları Vakfı, 2006.

Anderson, J.S. and Anderson, M.B. "Acoustic Coupling Effects in St Paul's Cathedral, London." *J. Sound and Vib.* 236.2 (2000): 209-225.

ASHRAE, Standards of American Society of Heating, Refrigerating and Air Conditioning Engineers, 2013.

Aydın, A. *Acoustical Characteristics of Historical Turkish Baths*. Unpublished Master's Thesis. Middle East Technical University, Department of Architecture, Ankara, 2008.

Barkan, L.O. *Süleymaniye Camii ve İmareti İnşaatı*. 1st vol. c2. Ankara: Türk Tarih Kurumu Matbaası, 1972.

Barron, M. *Auditorium Acoustics and Architectural Design*. London: E&FN Spon, 1993.

Beranek, L.L. *Noise and Vibration Control*. NY: McGraw-Hill, 1971.

Billon, A., Valeau, V., Sakout, A. and Picaut, J. "On the Use of a Diffusion Model for Acoustically Coupled Rooms." *J. Acoust. Soc. Am.* 120.4 (2006): 2043-2054.

Billon, A., Picaut, J. and Sakout, A. "Prediction of the Reverberation Time in High Absorbent Room Using a Modified-Diffusion Model." *J. Appl. Acoust.* 69 (2000): 68-74.

Bos, H.L., Van Den Oever, M.J.A. and Peters, O.C.J.J. (2002) "Tensile and Compressive Properties of Flax Fibers for Natural Fiber Reinforced Composites." *J. Mat. Sci.* 7 (2002): 1683-1692.

Bradley, D.T. and Wang, L.M., 2005. "The Effects of Simple Coupled Volume Geometry on the Objective and Subjective Results from Nonexponential Decay." *J. Acoust. Soc. Am.* 118.3 (2005): 1480-1490.

Bradley, D.T. and Wang, L.M., 2007. "Comparison of Measured and Computer-Modeled Objective Parameters for an Existing Coupled Volume Concert Hall." *Build. Acoust.* 14.2 (2007): 79-90.

Bradley, D.T. and Wang, L.M. "Quantifying the Double Slope Effect in Coupled Volume Room Systems." *Build. Acoust.* 16.2 (2009): 105-123.

Bradley, D.T. and Wang, L.M. "Optimum Absorption and Aperture Parameters for Realistic Coupled Volume Spaces Determined from Computational Analysis and Subjective Testing Results." *J. Acoust. Soc. Am.* 127.1 (2010): 223-232.

Bree, H.E., P. Leussink, P., Korthorst, M., Jansen, H., Lammerink, T. and Elwenspoek, M. "The Microflown: a novel device measuring acoustical flows, Sensors and Actuators." *A-Physical*, 54 (1996): 552-557.

Bryan, N.J. and Abel, J.S. "Methods for Extending Room Impulse Responses beyond Their Noise Floor." *129th Convention of Audio Engineering Society*, November 4-7 2010, San Francisco, CA, USA, 2010.

CAHRISMA, Conservation of the Acoustical Heritage by the Revival and Identification of Sinan's Mosques' Acoustics. Project No: ICA3-CT-1999-00007 Work package 2, Deliverables. Istanbul: Yıldız Technical University, 2001.

CAHRISMA, *Acoustical Properties of Domed Spaces and Optimum Acoustical Conditions for Domed Mosques*. Combined Deliverable (D29-D34-D35), Project Number: ICA3-CT-1999-00007. İstanbul: Yıldız Technical University, 2003.

Cantay, T. *Süleymaniye Camii*. İstanbul: EREN Yayıncılık, 1989.

Cantay, G. "Süleymaniye Camii 2007-2011 Onarımlarında Bezeme Programıyla ilgili Çalışmalar." *Restorasyon* 3 (2011): 80-111.

Carvalho, A.P. and Monteiro, C.G. "Comparison of the Acoustics of Mosques and Catholic Churches." *ICSV16*, Kraków, Poland, 2009.

Carvalho, P.O. and Freitas, C.T. "Acoustical Characterization of the Central Mosque of Lisbon." *Forum Acusticum*, Aalborg, Denmark, 2011.

Chiang, W., Lin, W., Chen, Y. and Hu, H. "Variable Acoustics Design of a Small Proscenium Concert Hall." *J. Asian Arch. and Build. Eng.* 305 (2009): 299-305.

Christensen, C.L., Koutsouris, G., and Rindel, J.H. "The ISO 3382 Parameters: Can We Simulate Them? Can We Measure Them?" *International Symposium on Room Acoustics*, June 9-11 June 2013, Toronto, Canada, 2013.

Chu, Y. and Mak, C.M., 2009. "Early Energy Decays in Two Churches in Hong Kong." *Appl. Acoust.* 70 (2009): 579-587.

Cremer, L. and Müller, H.A. "Coupled Rooms." *Principles and Applications of Room Acoustics*. 1st vol. London: Elsevier, 1978. 261-292.

Çelik, S. *Süleymaniye Külliyesi: Malzeme, Teknik ve Süreç*. Ankara: Atatürk Kültür Merkezi, 2009.

Dalmay, P., Smith, A., Chotard, T., Sahay-Turner, P., Gloaguen, V. and Krausz, P. "Properties of Cellulosic Fiber Reinforced Plaster: Influence of Hemp or Flax Fibers on the Properties of Set Gypsum", *J. Mat. Sci.* 45, (2010): 793-803.

Egan, M.D. *Architectural Acoustics*. Ed. B.J. Clark. New York: McGraw-Hill, 1988.

El-khateeb, A.A. and Ismail, M.R. "Sounds from the Past: the Acoustics of Sultan Hassan Mosque and Madrasa." *Build. Acoust.* 14.2 (2007): 109-132.

Ermann, M. "Coupled Volumes: Aperture Size and the Double-Sloped Decay of Concert Halls." *Build. Acoust.* 12 (2005): 1-14.

Ermann, M. and Johnson, M. "Exposure and Materiality of the Secondary Room and its Impact on the Impulse Response of Coupled-Volume Concert Halls." *J. Sound Vib.* 284 (2005): 915-931.

Ersen, A., Nilgün, O., Akbulut, S.S. and Yıldırım, B.Ş. "Süleymaniye Camii 2007-2010 Yılları Restorasyonu ve Restorasyon Kararları." *Restorasyon* 3 (2011): 6-27.

Eröz, F. "Sinan ve Mimari Akustik." *TAKDER 10th National Acoustics Congress*, 16-17 December 2013, Yıldız Technical University, İstanbul, (2013): 11-20.

Escolano, J., Navarro, J.M. and López, J.J. "On the Limitation of a Diffusion Equation Model for Acoustic Predictions of Rooms with Homogeneous Dimensions." Letter to the Editor. *J. Acoust. Soc. Am.* 128.4 (2010): 1586-1589.

Esen, S., Tunç, N., Telatar, S., Tavukçuoğlu, A., Caner-Saltık E.N. and Demirci, Ş. "Manisa Çukur Hamam'ın Onarımına Yönelik Malzeme Çalışmaları." *2nd National Construction Materials Congress and Exhibition*, 6-8 October 2004, İstanbul, (2004): 494-505.

Everest, F.A. *The Master Handbook of Acoustics*. New York: McGraw-Hill, 1994.

Eyice, S. *Ayasofya*. Vol. 1-3. İstanbul: Yapı Kredi, 1984.

Eyring, C.F. "Reverberation Time Measurements in Coupled Rooms." *J. Acoust. Soc. Am.* 3.2 (1931): 181-206.

Eyüpgiller, K. "Restitüsyon ve Renovasyon." *Bir Şaheser Süleymaniye Külliyesi*, Ed. S. Mülayim. Ankara: T.C. Kültür ve Turizm Bakanlığı, 2007. 193-232.

Fausti, P., Pompoli R. and Prodi, N. "Comparing the Acoustics of Mosques and Byzantine Churches." *CIPA XIXth International Symposium*, Antalya, Turkey, 2003.

Hamadah, H.A. and Hamouda, H.M. "Assessment of Speech Intelligibility in Large Auditoria Case Study: Kuwait State Mosque." *Appl. Acoust.* 54.4 (1998): 273-289.

Harris, C.M. and Feshbach, H. "On the Acoustics of Coupled Rooms." *J. Acoust. Soc. Am.* 22.5 (1950): 572-578.

ISO 3382-1, 2009. *Acoustics - Measurement of Reverberation Time of Rooms with Reference to other Acoustical Parameters*. ISO, 2009.

İrteş, S. "Kalemişi, Cam ve Revzen." *Bir Şaheser Süleymaniye Külliyesi*. Ed. S. Mülayim. Ankara: T.C. Kültür ve Turizm Bakanlığı, 2007. 293-328.

Jing, Y. *On the Use of Transport and Diffusion Equations for Room-Acoustics Predictions*. Unpublished Thesis PhD. Graduate Faculty of Rensselaer Polytechnic Institute, Troy, NY, 2009.

Jing, Y. and Xiang, N. "A Modified Diffusion Equation for Room-Acoustic Prediction." Letter to the Editor. *J. Acoust. Soc. Am.* 121.6 (2007): 3284-3287.

Jing, Y. and Xiang, N. "Visualizations of Sound Energy across Coupled Rooms using a Diffusion Equation Model." Express Letter. *J. Acoust. Soc. Am.* 124.6 (2008a): 360-365.

Jing, Y. and Xiang, N. "On the Use of a Diffusion Equation Model for Sound Energy Flow Prediction in Acoustically Coupled Spaces." *Proceedings of the COMSOL Conference*, Boston, 2008b.

Jing, Y. and Xiang, N. "On Boundary Conditions for the Diffusion Equation in Room Acoustic Prediction: Theory, Simulations, and Experiments." *J. Acoust. Soc. Am.* 123.1 (2008c): 145-153.

Kahler, H. and Mango, C. *Hagia Sophia*. New York: Frederick A. Praeger, 1967.

Karabiber, Z. "Avrupa Birliđi 5. Çerçeve Programı Kapsamında Sinan Camileri Üzerine bir Araştırma: CAHRISMA Projesi." *Tasarım* 102 (2000): 74-83.

Kayılı, M. "Sinan ve Boşluklu Rezonatörler." *Gazi Üniversitesi Müh. Mim. Fak. Dergisi* 3.1-2 (1988a): 1-17.

Kayılı, M. "Mimar Sinan'ın Camilerindeki Akustik Verilerin Deđerlendirilmesi." *Mimarbaşı Koca Sinan: Yaşadığı Çağ ve Eserleri*. İstanbul: T.C. Başbakanlık Vakıflar Genel Müdürlüğü, 1988b. 545-555.

Kayılı, M. "Evolution of Acoustics and Effect of Worship Buildings on It." *Proceedings of the 3rd European Congress on Forum Acusticum*, 16-20 September 2002, Seville, Spain, 2002.

Kleiner, M., Klepper, D.L. and Torres, R.R. *Worship Space Acoustics*. Fort Lauderdale: J. Ross Publishing, 2010.

Klenbauer, W.E., White, A. and Matthews, H. *Hagia Sophia*. London: Scala Publishers, 2004.

Kolay, I.A. and Çelik, S. (2006). "Ottoman Stone Acquisition in the Mid-Sixteenth Century: The Süleymaniye Complex in Istanbul." *Muqarnas*, 23, 251-272.

- Kuban, D.A. "Symbol of Ottoman Architecture: The Süleymaniye." *Ottoman Architecture*, Suffolk: Antique Collectors' Club, 2010. 277-294.
- Kuttruff, H. *Room Acoustics*. New York: Elsevier, 1991.
- Kuttruff, H. "Coupled Rooms." *Room Acoustics*. London: E&FN Spon, 2000. 142-145.
- Kütükoğlu, M.S. *XX. Asra Erişen İstanbul Medreseleri*. Ankara: Türk Tarih Kurumu, 2000.
- Long, M. *Architectural Acoustics*. London: Elsevier, 2006.
- Lyle, C.D. "Recommendations for Estimating Reverberation Times in Coupled Rooms." *Acoust. Lett.* 5.2 (1981): 35-38.
- Maekawa, Z. and Lord, P., 1994. *Environmental and architectural acoustics*. London: E&FN Spon.
- Magrini, A. and Magnani, L. "Models of the Influence of Coupled Spaces in Christian Churches." *Build. Acoust.* 12.2 (2005): 115-139.
- Mainstone, R.J. *Hagia Sophia: Architecture, Structure and Liturgy of Justinian's Great Church*. London: Thames and Hudson, 1988.
- Makrinenko, L.I. *Acoustics of Auditoriums in Public Buildings*. Trans. R. S. Ratner. Ed. J. S. Bradley. New York: ASA, 1994.
- Mark, R. and Çakmak, A.Ş. *Hagia Sophia: from the Age of Justinian to the Present*. Cambridge: Cambridge University Press, 1992.
- Martellotta, F. "Identifying Acoustical Coupling by Measurements and Prediction-Models for St. Peter's Basilica in Rome." *J. Acoust. Soc. Am.* 126.3 (2009): 1175-1186.
- Mehta, M, Johnson, J. and Rocafort, J. "Coupled Spaces." *Architectural Acoustics: Principles and Design*. New Jersey: Prentice-Hall, 1999. 220-222.
- Meissner, M. "Computational Studies of Steady-State Sound Field and Reverberant Sound Decay in a System of Two Coupled Rooms." *Cent. Eur. J. Phys.* 5.3 (2007): 293-312.
- Meissner, M. "Acoustic Energy Density Distribution and Sound Intensity Vector Field inside Coupled Spaces." *J. Acoust. Soc. Am.* 132.1 (2012): 228-238.

Mungan, I. "Strüktür Çözümü." *Bir Şaheser Süleymaniye Külliyesi*. Ed. S. Mülayim. Ankara: T.C. Kültür ve Turizm Bakanlığı, 2007.

Naylor, G.M. "ODEON: Another Hybrid Room Acoustical Model." *Appl. Acoust.* 38 (1993): 131-143.

Necipoglu-Kafadar, G. (1985). "The Süleymaniye Complex in İstanbul: an interpretation." *Muqarnas*, 3, 92-117.

Neftçi, A. "Kubbe ve Örtüde Dolaşım." *Bir Şaheser Süleymaniye Külliyesi*. Ed. S. Mülayim. Ankara: T.C. Kültür ve Turizm Bakanlığı, 2007. 103-124.

Nijs, L., Jansens, G., Vermeir, G. and Voorden, M., 2002. "Absorbing surfaces in ray-tracing programs for coupled spaces." *Appl. Acoust.*, 63, 611-626.

Nutter, D.B., Leishman, T.W., Sommerfeldt, S.D. and D.B. Jonathan. "Measurement of Sound Power and Absorption in Reverberation Chambers using Energy Density." *J. Acoust. Soc. Am.* 121.5 (2007): 2700-2710.

Orfali, W.A. "Sound Parameters in Mosques." *153rd Meeting of ASA*, Salt Lake City, UT, 2007.

Oyhon, E. and Etingü, B. "Hagia Sophia, Church of Divine Wisdom". *Churches in İstanbul*. İstanbul: YKY, 1999. 39-41.

Picaut, J., Simon, L. and Polack, J.D. "A Mathematical Model of Diffuse Sound Field Based on a Diffusion Equation." *Acta Acustica* 83 (1997): 614-621.

Prodi, N. and Marsilo, M. "On the Effect of Domed Ceiling in Worship Spaces: a Scale Model Study of a Mosque." *Build. Acoust.* 10.2 (2003): 117-134.

Radikal, http://www.radikal.com.tr/turkiye/256_bos_kupun_sirri-1028387, last visited on 17th July 2013.

Rindel, J.H. "The Use of Computer Modeling in Room Acoustics." *J. Vib. Eng.* 3 (2000): 219-224.

Saatçi, S. "Temelden Aleme İnşaat Süreci." *Bir Şaheser Süleymaniye Külliyesi*. Ed. S. Mülayim. Ankara: T.C. Kültür ve Turizm Bakanlığı, 2007. 57-74.

Schmidt, A.M.D. and Kirkegaard, P.L. "On Architectural Acoustics Design Using Computer Simulation." *Eleventh International Congress on Sound and Vibration*, St. Petersburg, Russia, 2004.

Schroeder, M. R. "New Method of Measuring Reverberation Time." *J. Acoust. Soc. Am.* 37 (1965): 409-412.

Su'arez, R., Sendra, J.J., Navarro, J. and Le'on, A.L. "The Acoustics of the Cathedral-Mosque of C'ordoba, Proposals for Architectural Intervention." *Acta Acustica* 90 (2004): 362-375.

Summers, J.E., Torres, R.R. and Shimizu, Y. "Statistical-Acoustics Models of Energy Decay in Systems of Coupled Rooms and Their Relation to Geometrical Acoustics." *J. Acoust. Soc. Am.* 116.2 (2004): 958-969.

Summers, J.E., Torres, R.R., Shimizu, Y. and Dalenback, B.L. "Adapting a Randomized Beam-axis Tracing Algorithm to Modeling of Coupled Rooms via Late-part Ray Tracing." *J. Acoust. Soc. Am.*, 118.3 (2005): 1491-1502.

Sü, Z. *Systematic Investigations on Energy Decays in Acoustically Coupled Spaces Using the Scale-Model Technique*. Unpublished Master's Thesis. Graduate Faculty of Rensselaer Polytechnic Institute, Troy, NY, 2006.

Sü, Z. and Yılmaz, S. "The Acoustical Characteristics of the Kocatepe Mosque in Ankara, Turkey." *Arch. Sci. Rev.* 51.1 (2008): 21-30.

Sü Gül, Z. and Çalışkan, M. "Acoustical Considerations in the Design of Heydar Aliyev Center Auditorium." *Proceedings of the International Symposium on Room Acoustics, ISRA 2010*, 29-31 August 2010, Melbourne, Australia, 2010.

Sü Gül, Z., Xiang N. and Çalışkan, M. "Investigations on Multi-Slope Sound Energy Decays in Domed Structures." *Proceedings of Inter-Noise 2012*, 19-22 August 2012, New York, USA, 2012.

Sü Gül, Z. and Çalışkan, M. "Impact of Design Decisions on Acoustical Comfort Parameters: Case Study of Doğramacızade Ali Paşa Mosque." Technical Note. *App. Acoust.* 74 (2013a). 834-844.

Sü Gül, Z. and Çalışkan, M. "Acoustical Design of Turkish Religious Affairs Mosque." *The 21st International Congress on Acoustics (ICA)*, 2-7 June 2013, Montreal, Canada, 2013b.

Sü Gül, Z., Xiang N. and Çalışkan, M. "Multiple-Slope Sound Energy Decay Investigations in Single Space Enclosures with Specific Geometrical and Material Attributes." *166th Meeting of the Acoustical Society of America*, San Francisco, California, 2013c.

Sü Gül, Z., Çalışkan, M. and Tavukçuoğlu, A. "2007-2011 Onarımları Sonrası Süleymaniye Camii'nin Akustik Özellikleri: Ölçüm ve Değerlendirmeler." *TAKDER*

10th National Acoustics Congress, 16-17 December 2013, Yıldız Technical University, İstanbul, (2013d): 21-28.

Sü Gül, Z., Tavukçuoğlu, A., Çalışkan, M. “A Discussion on the Acoustics of Süleymaniye Mosque for its Original State.” *9th International Symposium on Conservation of Monuments in the Mediterranean Basin (MONUBASIN)*, 3-5 June 2014, Middle East Technical University, Ankara, 2014a.

Sü Gül, Z., Xiang, N. and Çalışkan, M. “Sound Field Analysis of Monumental Structures by the Application of Diffusion Equation Model.” *COMSOL Conference 2014*, 17 - 19 September, Cambridge, UK, 2014b.

Sü Gül, Z., Xiang, N. and Çalışkan, M. “Investigations on Acoustical Coupling within Single-Space Monumental Structures using a Diffusion Equation Model.” *168th Meeting of the Acoustical Society of America*, 27-31 October 2014, Indianapolis, Indiana, 2014c.

Sü Gül, Z., Çalışkan, M. and Tavukçuoğlu, A. “Geçmişten Günümüze Süleymaniye Camii Akustiği. *Megaron*. 9.3 (2014d): 201-216.

Tavukçuoğlu, A., Aydın, A. and Çalışkan, M. “Tarihi Türk Hamamlarının Akustik Nitelikleri: Özgün Hali ve Bugünkü Durumu.”, *TAKDER 9th National Acoustics Congress*, 26-27 May 2011, Ankara, 2011.

Tijs, E., Botts, J. Bree, H.E. and Arato, E. “Acoustic Particle Velocity enabled Methods to Assess Room Acoustics.” *Euronoise*, 26-28 October 2009, Edinburgh, UK, 2009.

Topaktaş, L. *Acoustical Properties of Classical Ottoman Mosques, Simulation and Measurements*. Unpublished Thesis PhD. Graduate School of Natural and Applied Sciences, Middle East Technical University, Ankara, Turkey, 2003.

Topaktaş, L., Çalışkan, M. and Bakırer, Ö. “Evaluation of Acoustical Characteristics of Cenabi Ahmet Pasha Mosque: Simulation and Measurements” *Proceedings of 17th ICA*, Roma, Italy, 2001.

T.R. Prime Ministry Directorate General of Foundations Archive. *Süleymaniye Camii Belgeleri*. Ankara, 2011.

Utami, S.S. *An Acoustical Analysis of Domes Coupled to Rooms with Special Application to the Darussolah Mosque, in East Java, Indonesia*. Unpublished Master's Thesis. Department of Physics and Astronomy, Brigham Young University, Provo, UT, 2005.

Valeau, V., Picaut, J. and Hodgson, M. "On the Use of a Diffusion Equation for Room-Acoustic Prediction." *J. Acoust. Soc. Am.* 119.3 (2006): 1504-1513.

Weitze, C.A., Christensen, C.L., and Rindel, J.H. "Comparison between In-situ Recordings and Auralizations for Mosques and Byzantine Churches." *Joint Baltic-Nordic Acoustical Meeting*, Copenhagen, Denmark, 2002a.

Weitze, C.A., Rindel, J.H., Christensen, C.L., and Gade, A.C. "The Acoustical History of Hagia Sophia Revived through Computer Simulation." *Forum Acusticum*, Seville, Spain, 2002b.

Wester, E.N. and Mace, B.R. "A Statistical Analysis of Acoustical Energy Flow in Two Coupled Rectangular Rooms." *Acta Acustica* 84 (1998): 114-121.

Xiang, N. and Goggans, P.M. "Evaluation of Decay Times in Coupled Spaces: Bayesian Parameter Estimation." *J. Acoust. Soc. Am.* 110.3 (2001): 1415-1424.

Xiang, N. and Goggans, P.M. "Evaluation of Decay Times in Coupled Spaces: Bayesian Decay Model Selection." *J. Acoust. Soc. Am.* 113 (2003): 2685-2697.

Xiang, N., Goggans, P.M., Jasa, T. and Kleiner, M. "Evaluation of Decay Times in Coupled Spaces: Reliability Analysis of Bayesian Decay Time Estimation." *J. Acoust. Soc. Am.* 117 (2005): 3707-3715.

Xiang, N., Jing, Y. and Bockman, A.C. "Investigation of Acoustically Coupled Enclosures Using a Diffusion-Equation Model." *J. Acoust. Soc. Am.* 126.3 (2009): 1189-1198.

Xiang, N., Robinson, P., and Botts, J. "Comments on 'Optimum Absorption and Aperture Parameters for Realistic Coupled Volume Spaces Determined from Computational Analysis and Subjective Testing Results.'" Letter to the *Editor. J. Acoust. Soc. Am.* 127 (2010): 2539-2542.

Xiang, N., Goggans, P.M., Jasa, T. and Robinson, P. "Bayesian Characterization of Multiple-Slope Sound Energy Decays in Coupled-Volume Systems." *J. Acoust. Soc. Am.* 129.2 (2011): 741-752.

Xiang, N., Escolano, J., Navarro, J.M. and Jing, Y. "Investigation on the Effect of Aperture Sizes and Receiver Positions in Coupled Rooms." *J. Acoust. Soc. Am.* 133.6 (2013): 3975-3985.

Yılmaz, Y. *Kanuni Vakfıyesi Süleymaniye Külliyesi*. Ankara: Vakıflar Genel Müdürlüğü, 2008.

APPENDIX A

SIMULATION RESULTS

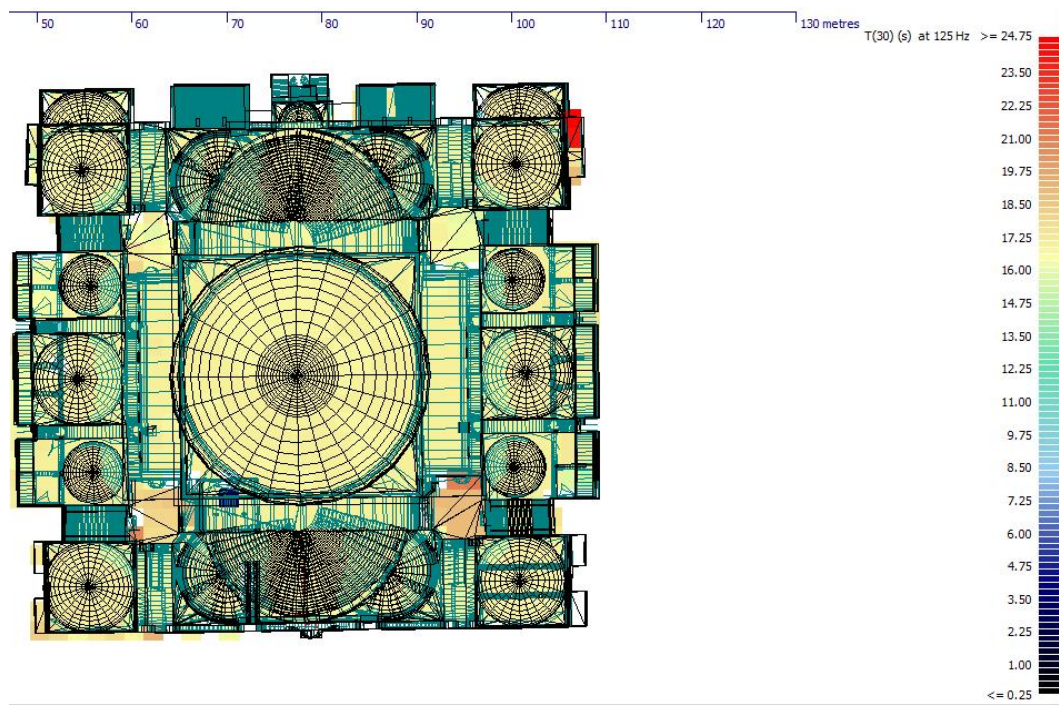


Figure A.1. T30 distribution map, 125 Hz, Süleymaniye Mosque

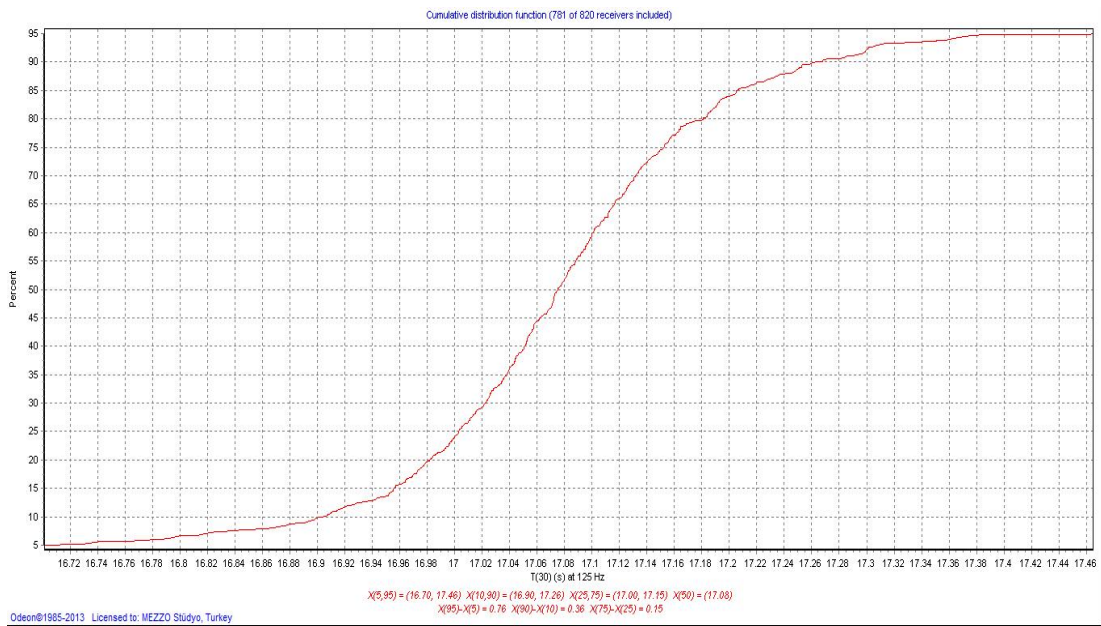


Figure A.2. T30 cumulative distribution graph, 125 Hz, Süleymaniye Mosque

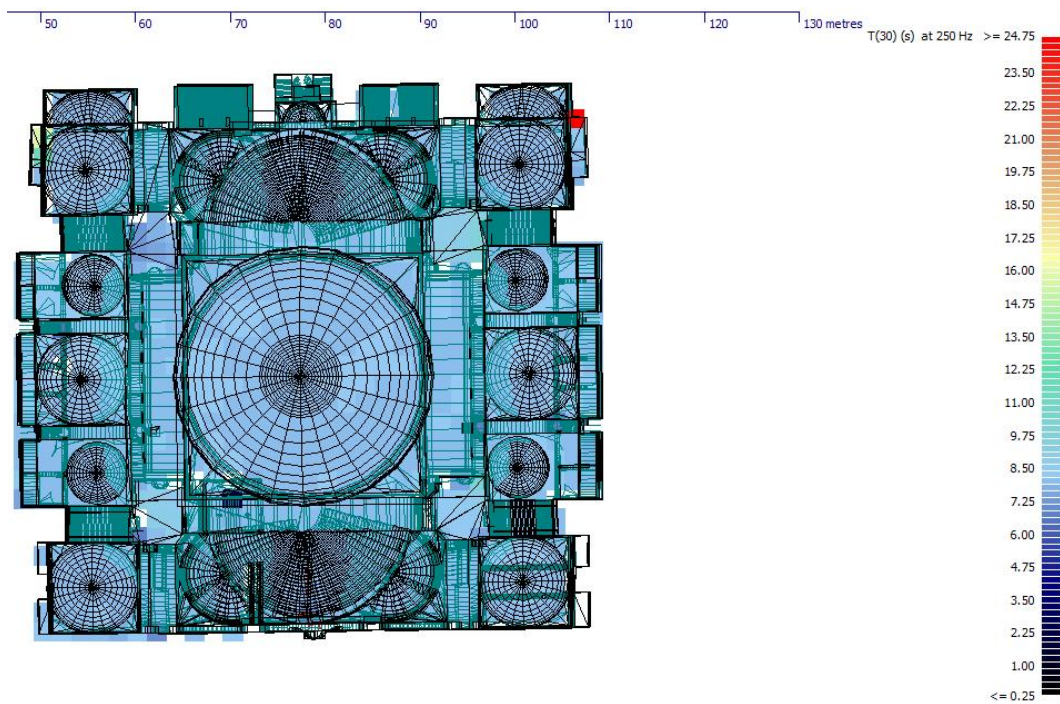


Figure A.3. T30 distribution map, 250 Hz, Süleymaniye Mosque

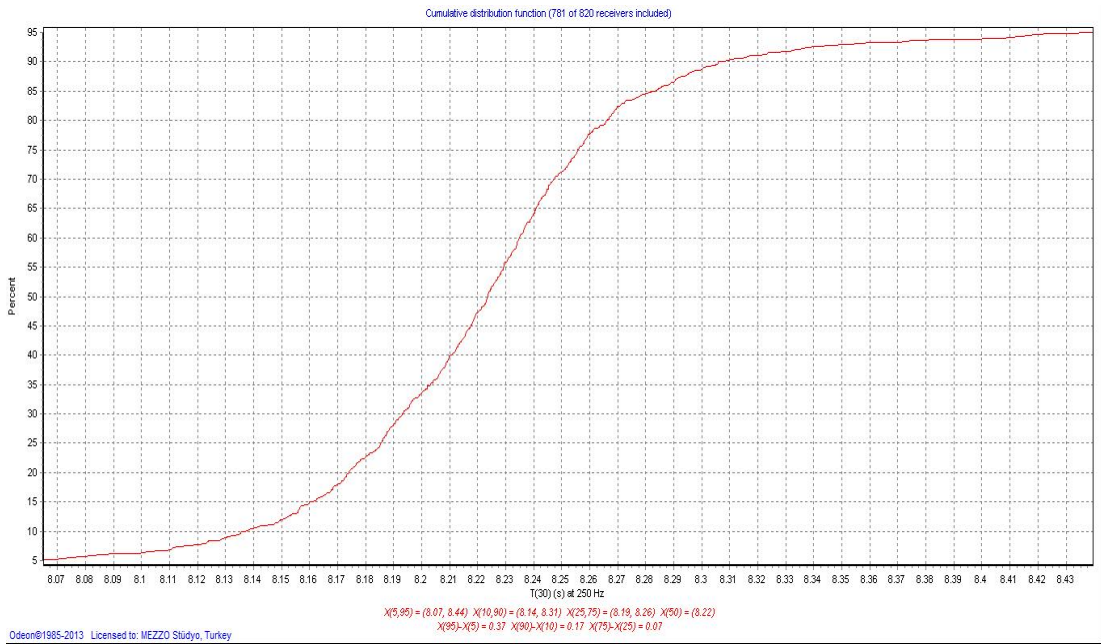


Figure A.4. T30 cumulative distribution graph, 250 Hz, Süleymaniye Mosque

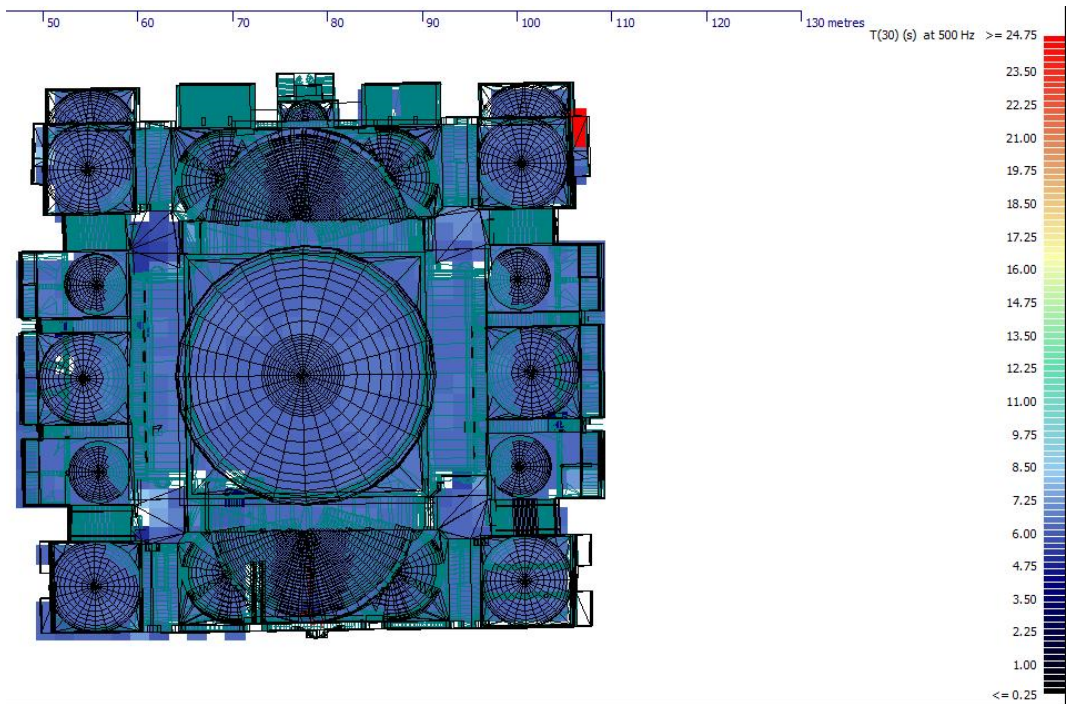


Figure A.5. T30 distribution map, 500 Hz, Süleymaniye Mosque

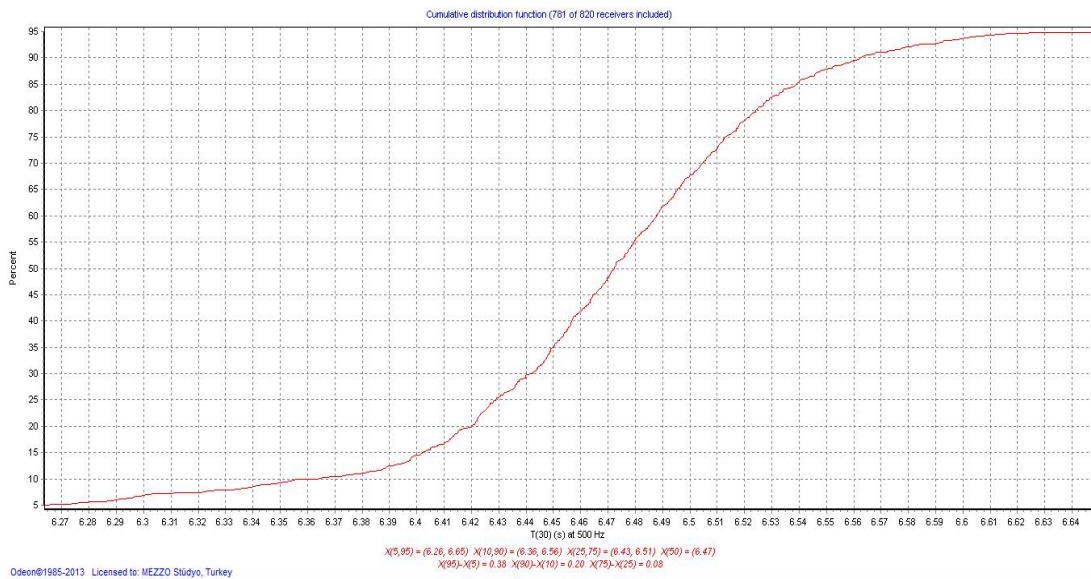


Figure A.6. T30 cumulative distribution graph, 500 Hz, Süleymaniye Mosque

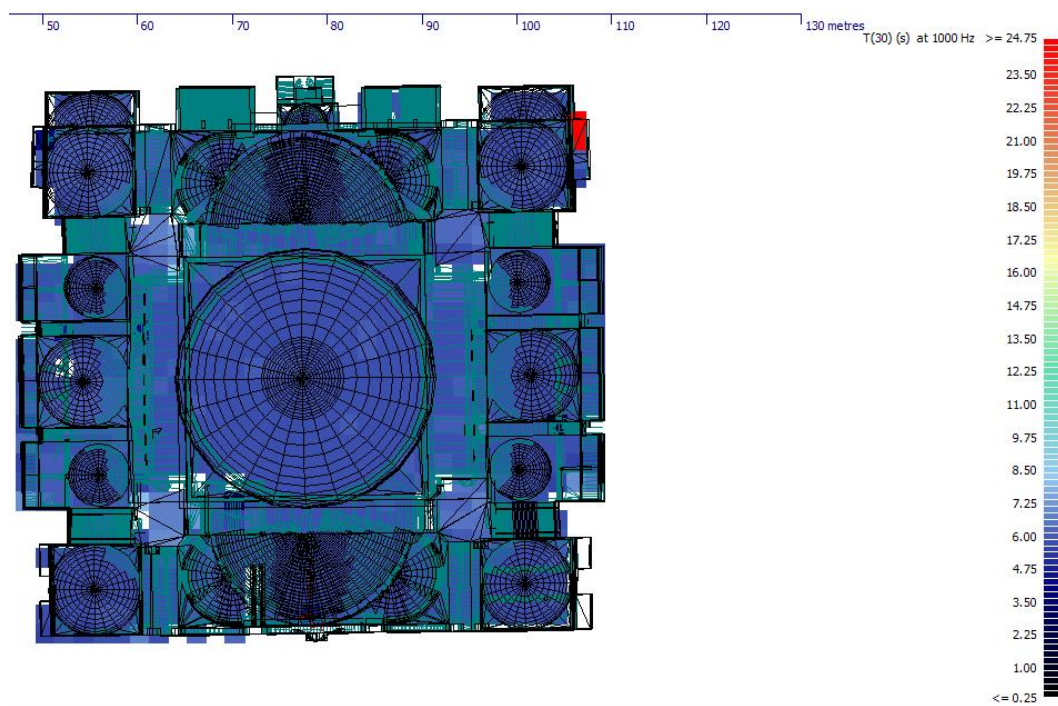


Figure A.7. T30 distribution map, 1000 Hz, Süleymaniye Mosque

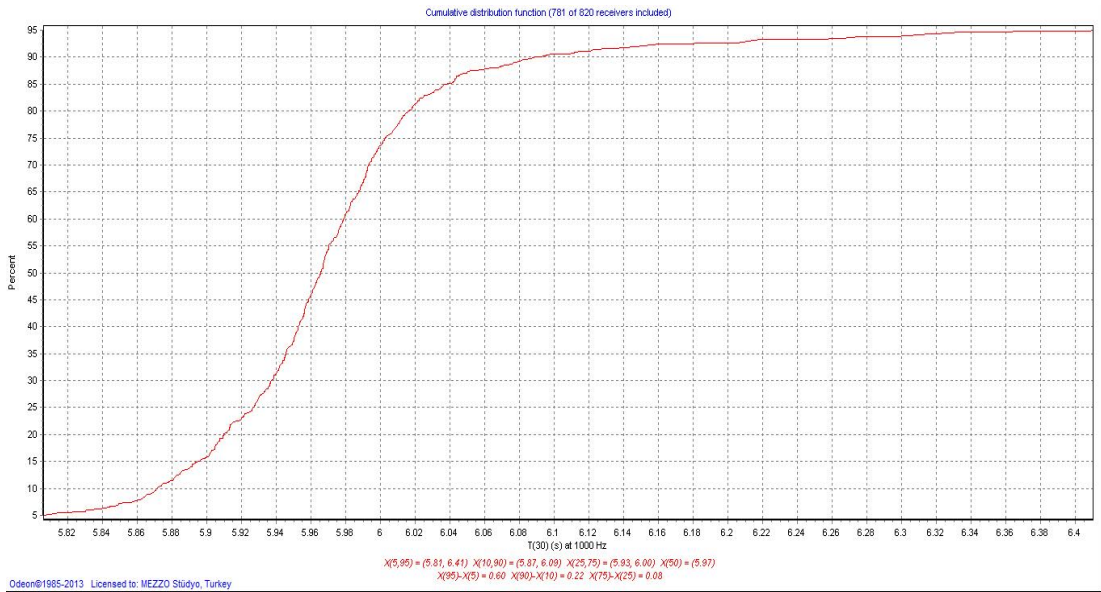


Figure A.8. T30 cumulative distribution graph, 1000 Hz, Süleymaniye Mosque

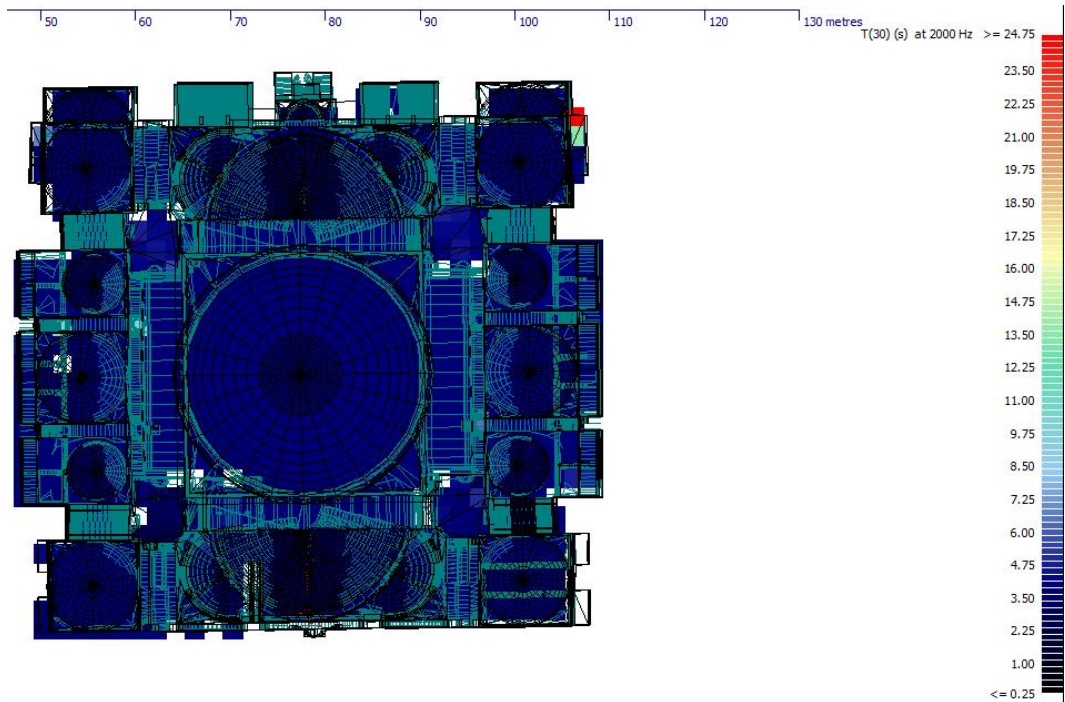


Figure A.9. T30 distribution map, 2000 Hz, Süleymaniye Mosque

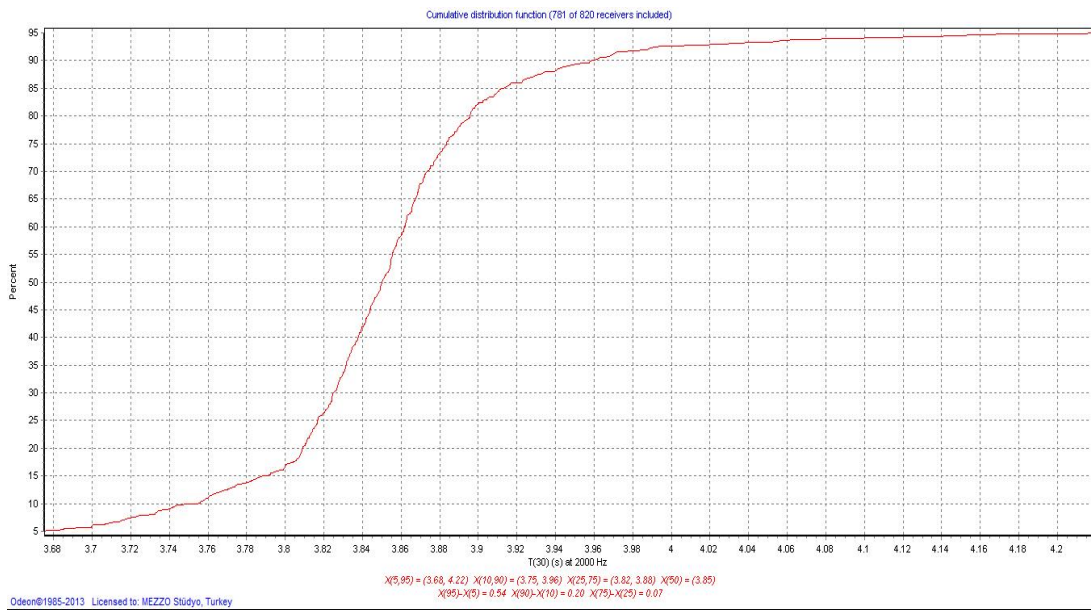


Figure A.10. T30 cumulative distribution graph, 2000 Hz, Süleymaniye Mosque

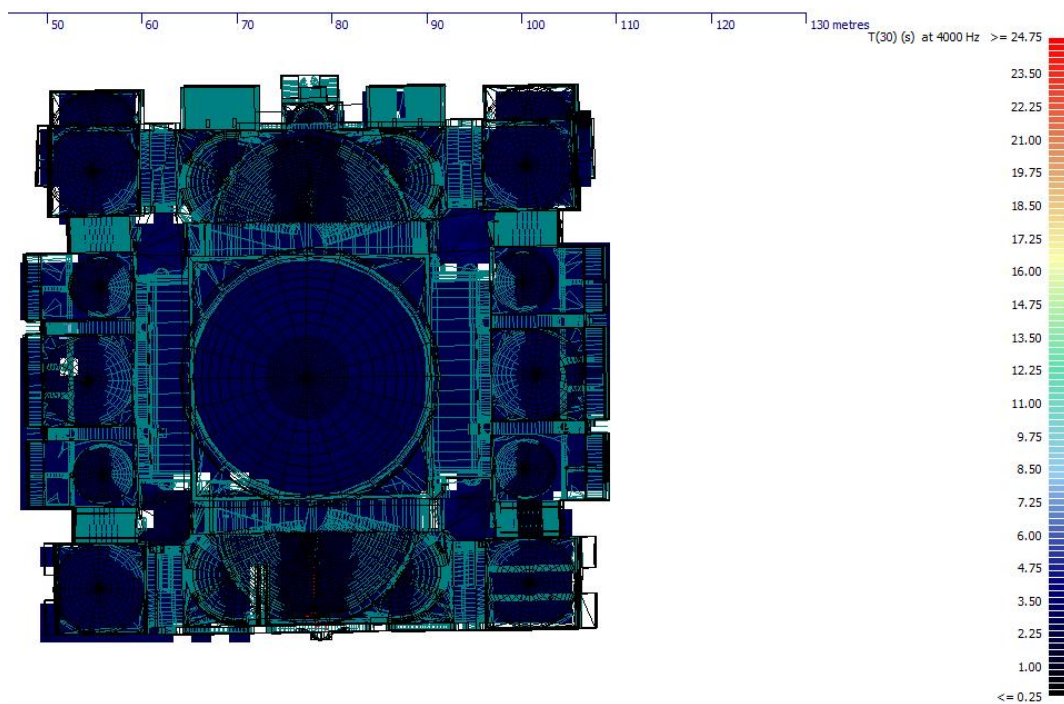


Figure A.11. T30 distribution map, 4000 Hz, Süleymaniye Mosque

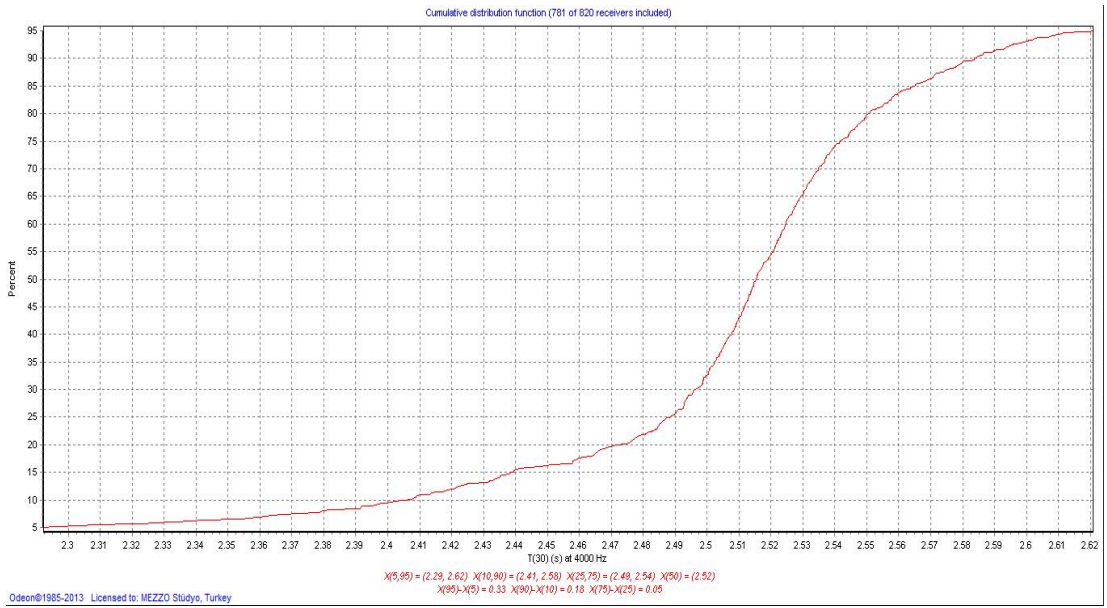


Figure A.12. T30 cumulative distribution graph, 4000 Hz, Süleymaniye Mosque

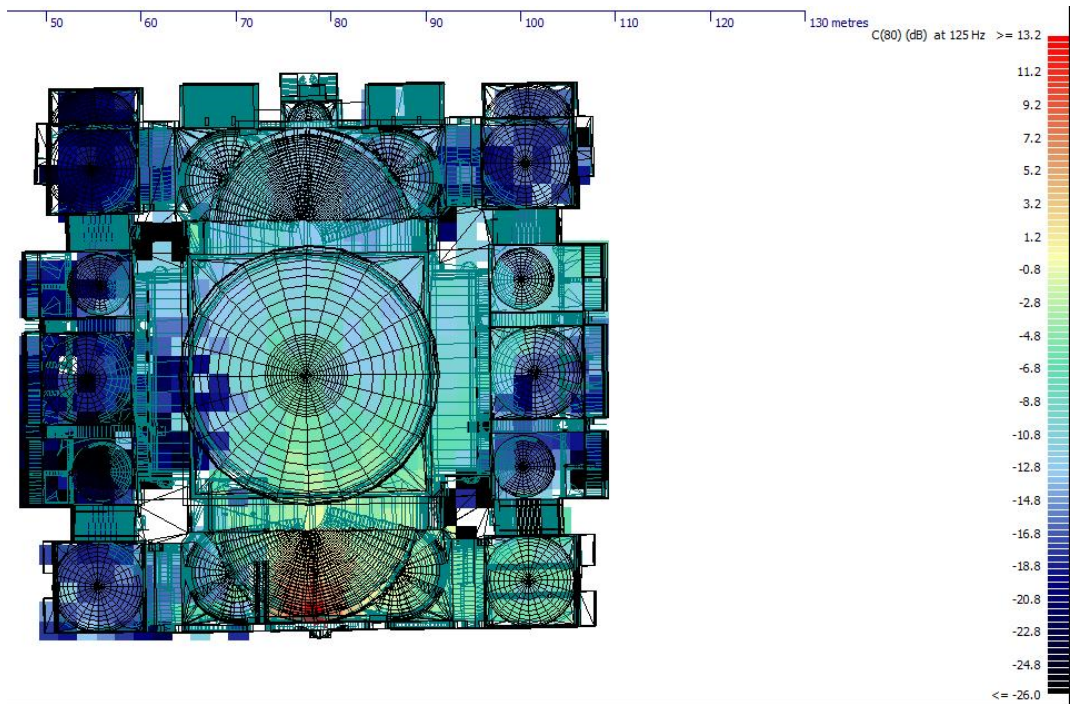


Figure A.13. C80 distribution map, 125 Hz, Süleymaniye Mosque

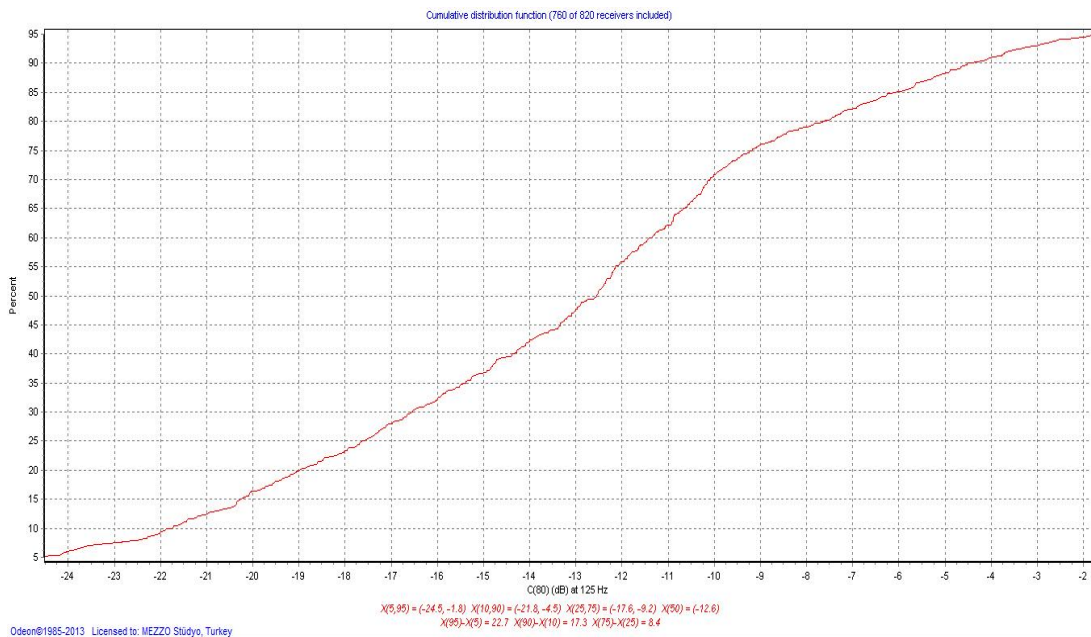


Figure A.14. C80 cumulative distribution graph, 125 Hz, Süleymaniye Mosque

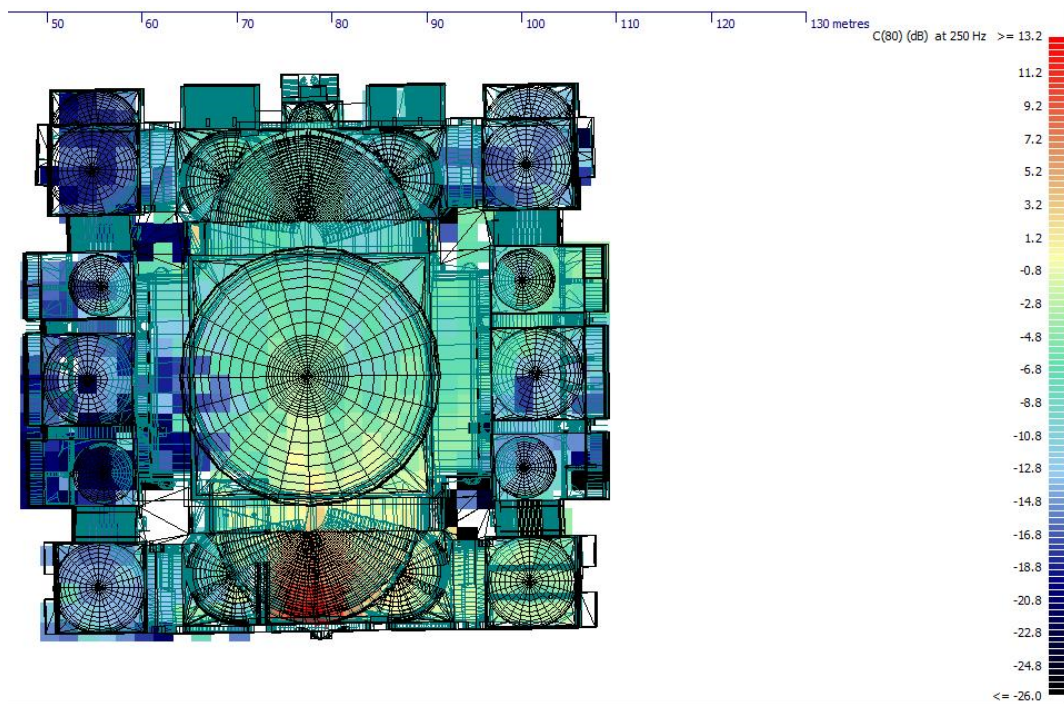


Figure A.15. C80 distribution map, 250 Hz, Süleymaniye Mosque

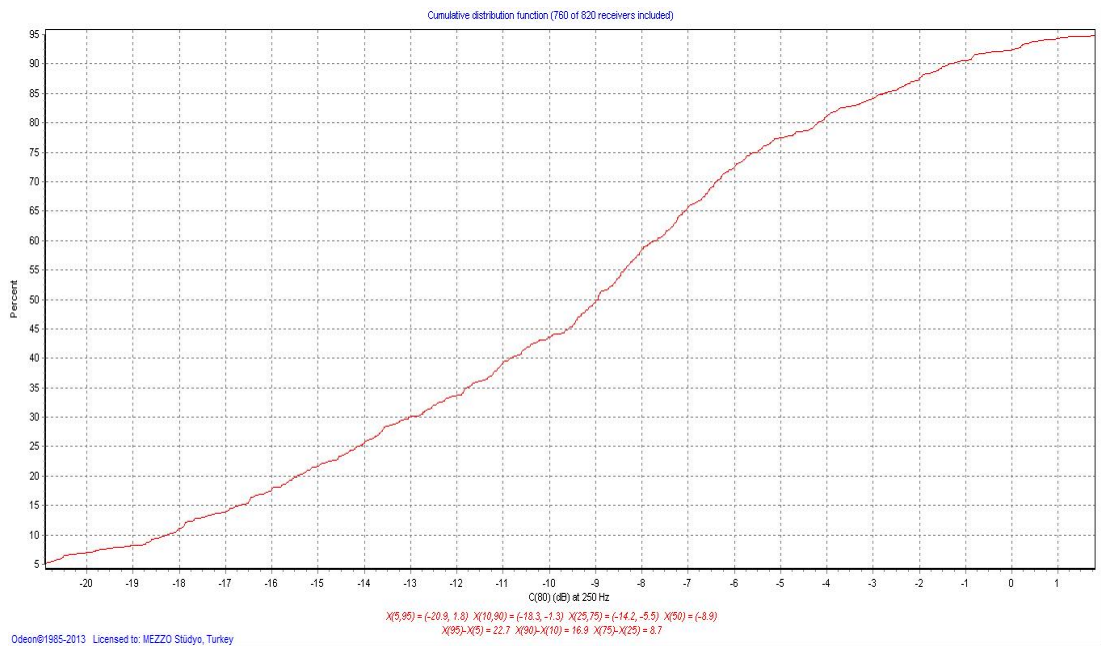


Figure A.16. C80 cumulative distribution graph, 250 Hz, Süleymaniye Mosque

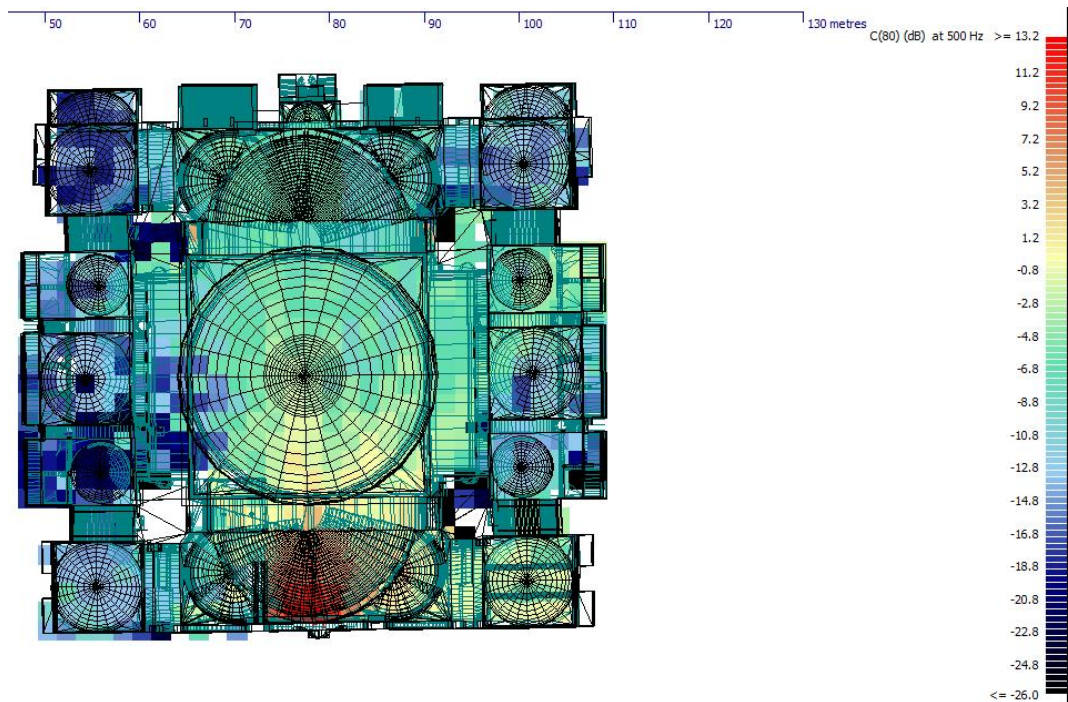


Figure A.17. C80 distribution map, 500 Hz, Süleymaniye Mosque

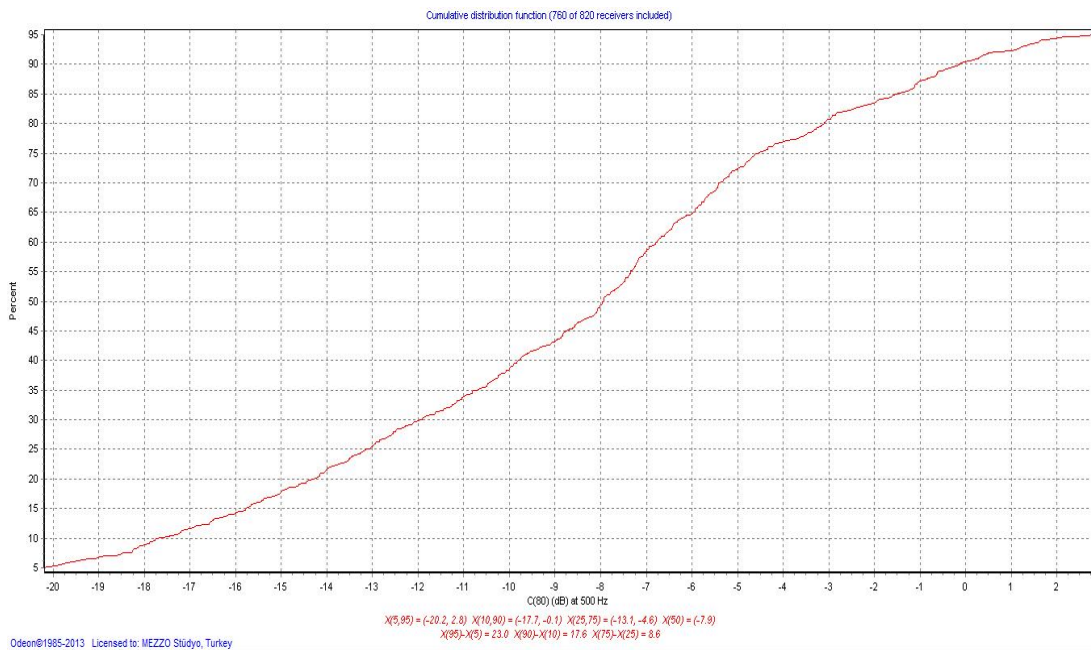


Figure A.18. C80 cumulative distribution graph, 500 Hz, Süleymaniye Mosque

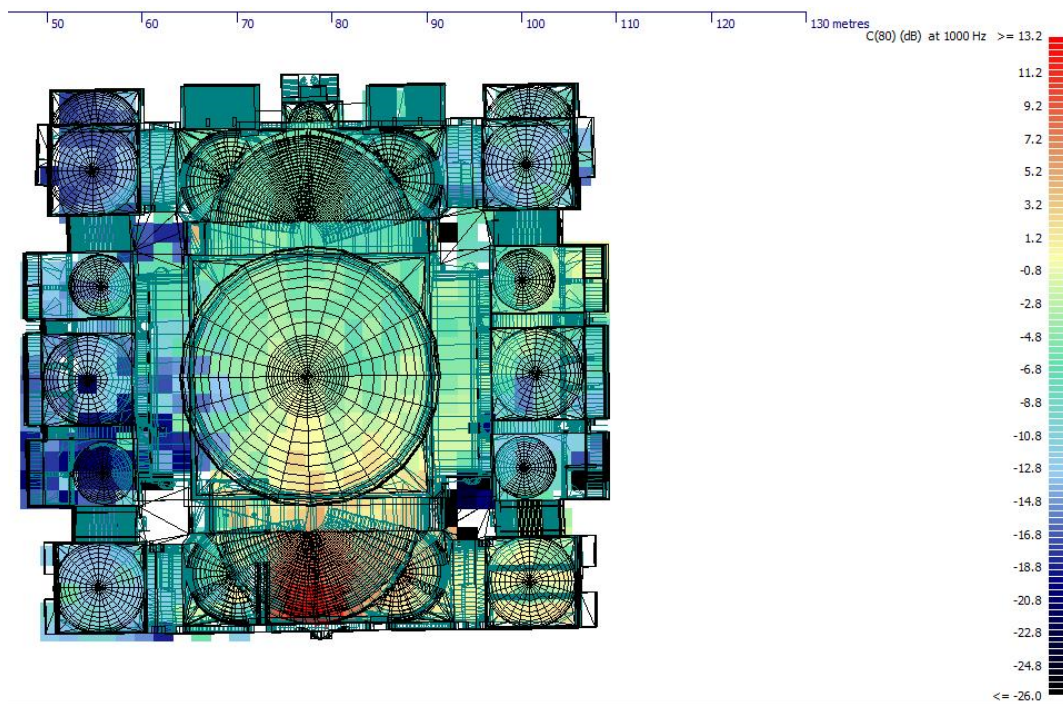


Figure A.19. C80 distribution map, 1000 Hz, Süleymaniye Mosque

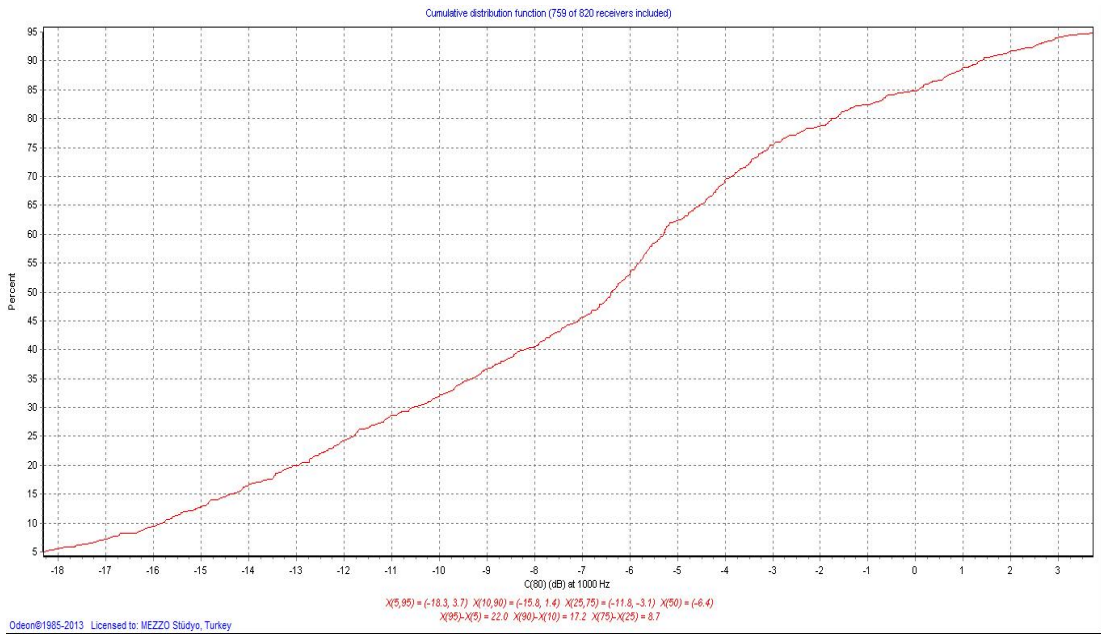


Figure A.20. C80 cumulative distribution graph, 1000 Hz, Süleymaniye Mosque

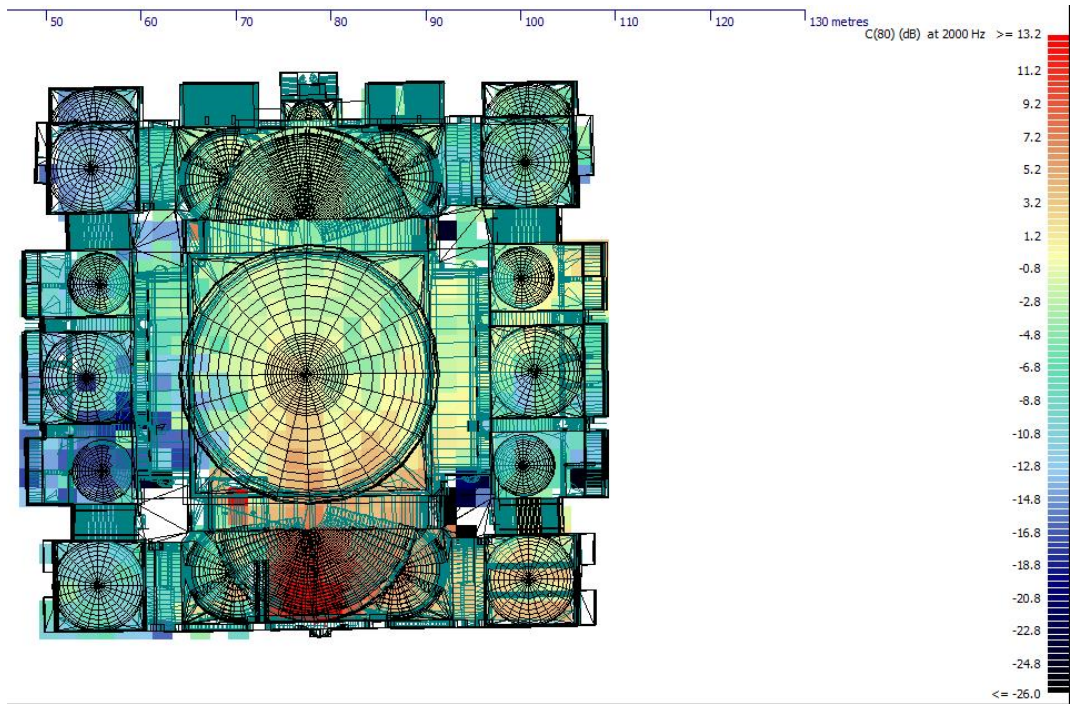


Figure A.21. C80 distribution map, 2000 Hz, Süleymaniye Mosque

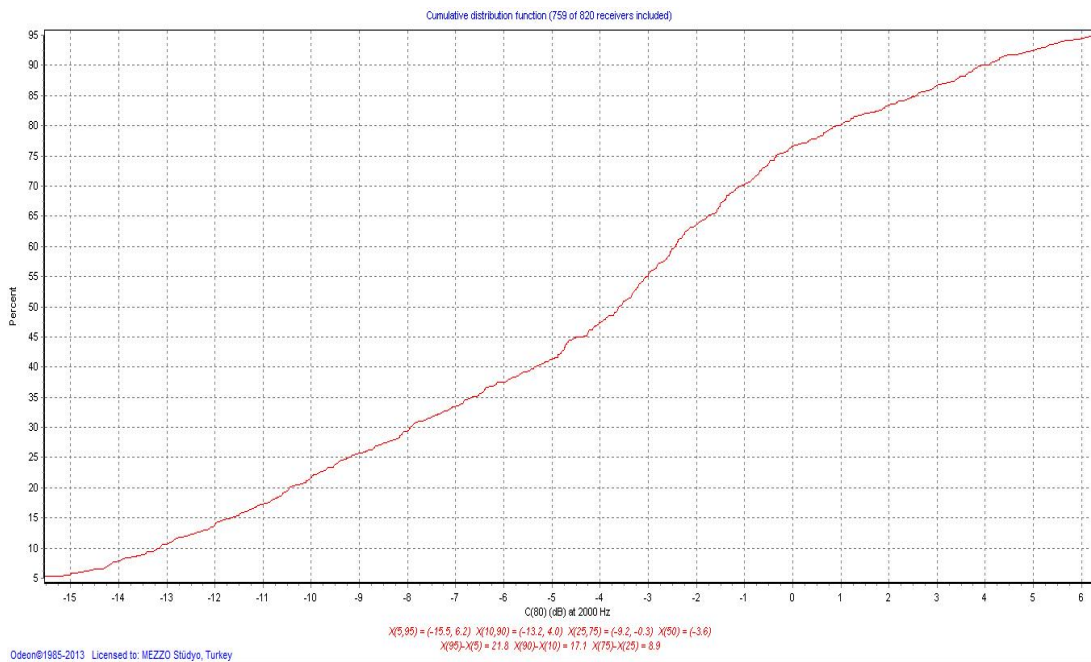


Figure A.22. C80 cumulative distribution graph, 2000 Hz, Süleymaniye Mosque

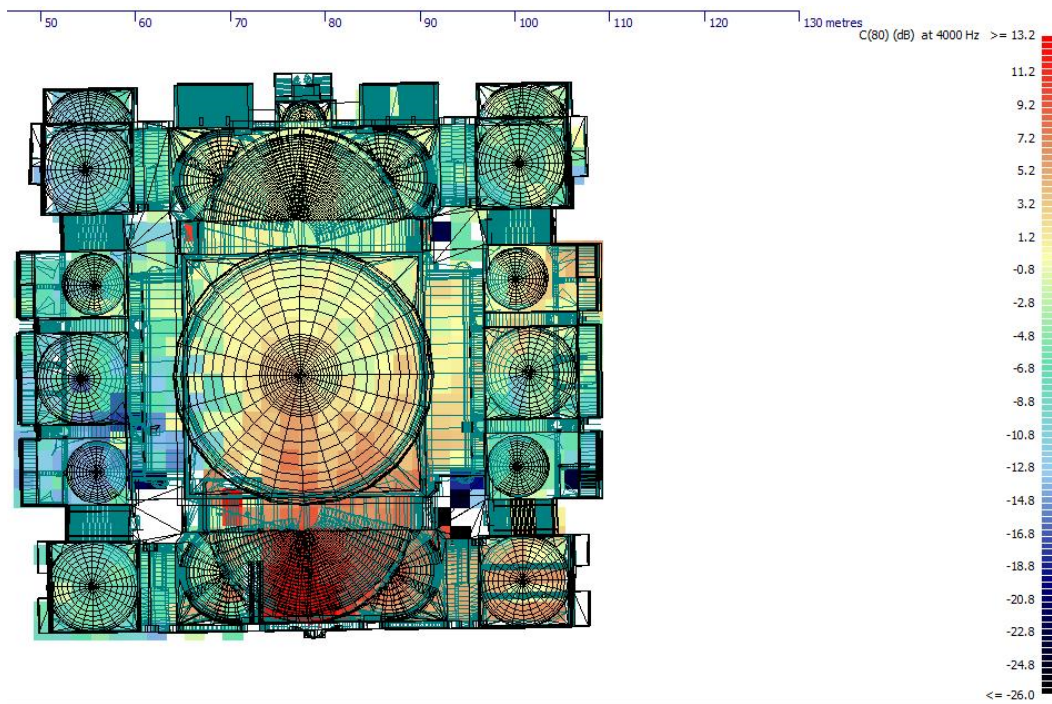


Figure A.23. C80 distribution map, 4000 Hz, Süleymaniye Mosque

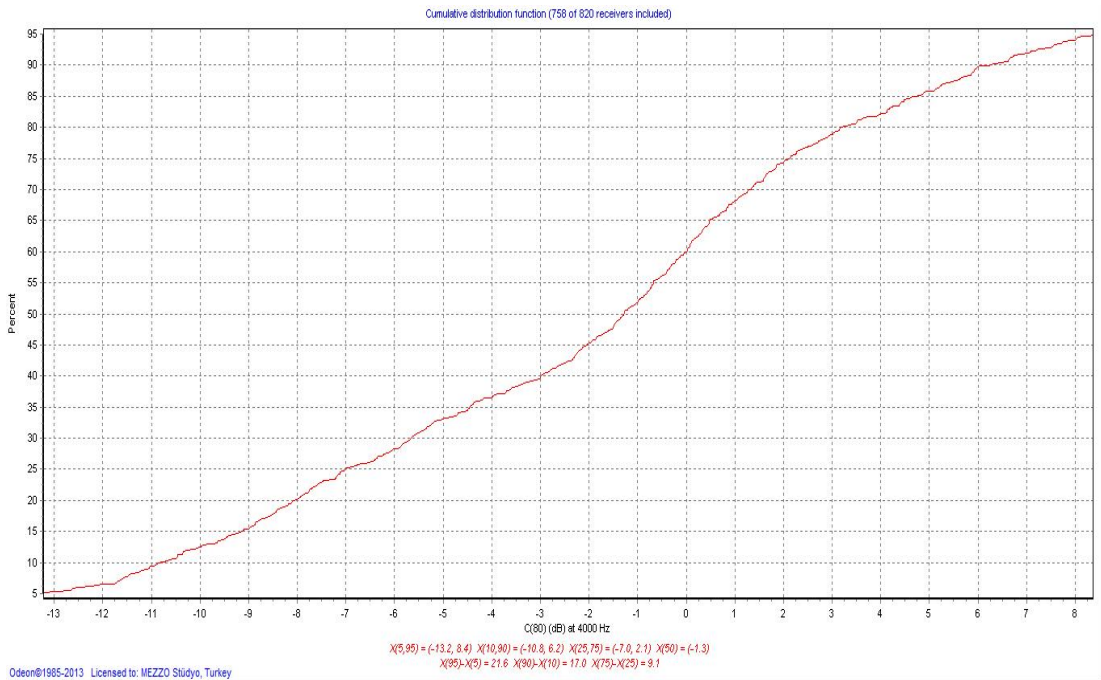


Figure A.24. C80 cumulative distribution graph, 4000 Hz, Süleymaniye Mosque

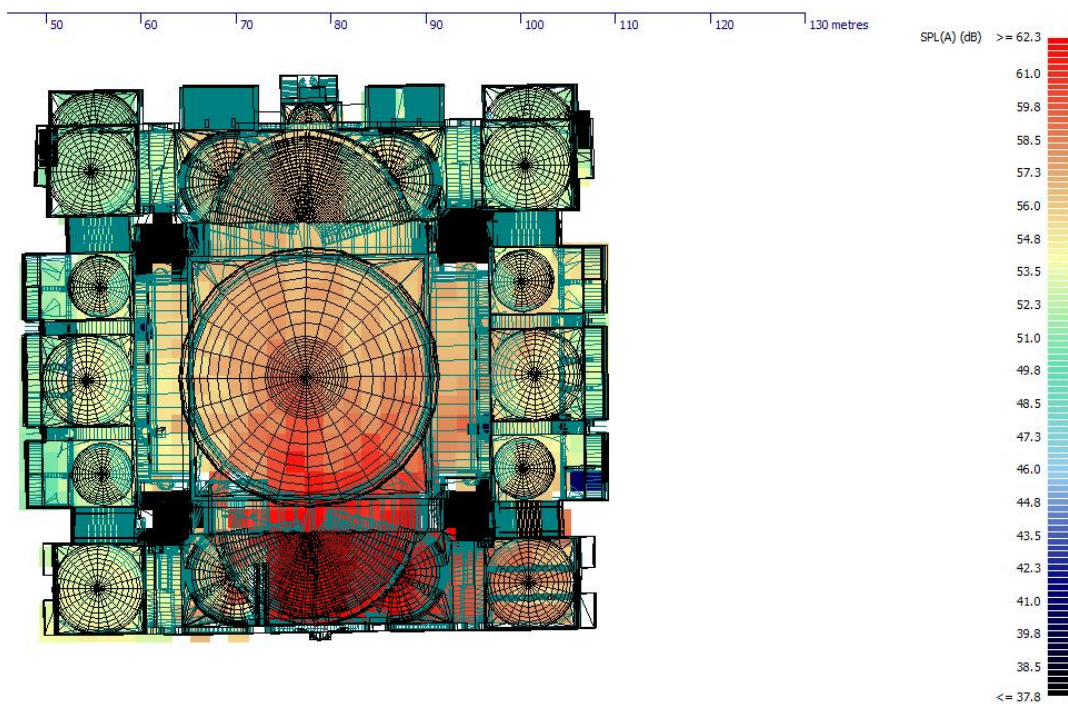


Figure A.25. SPL(A) distribution map, Süleymaniye Mosque

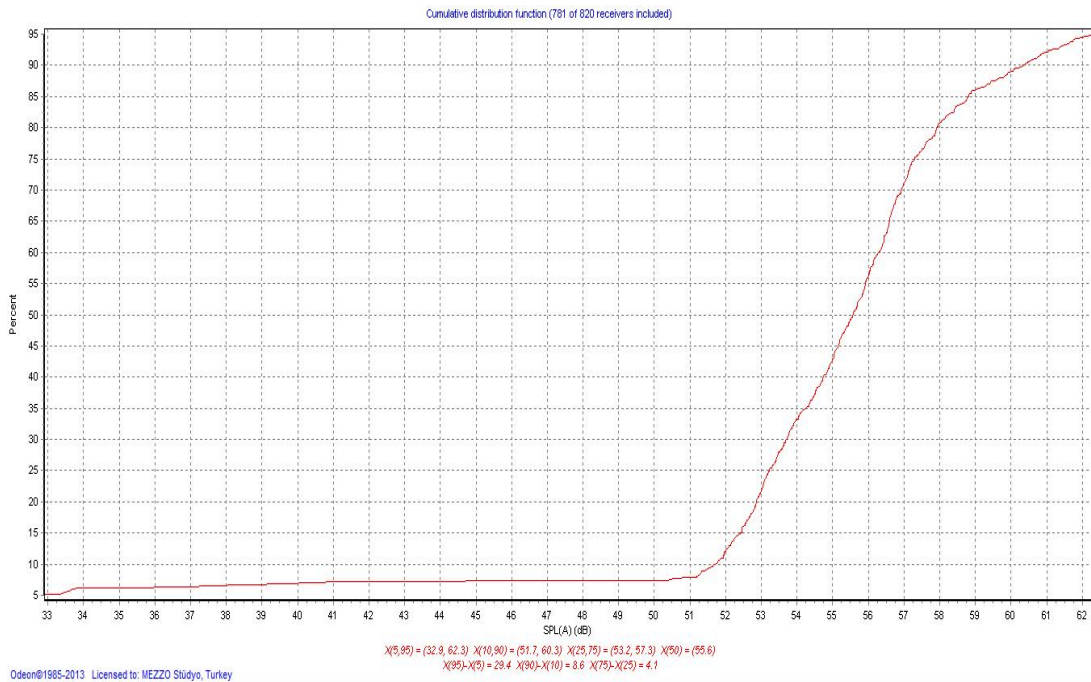


Figure A.26. SPL(A) cumulative distribution graph, Süleymaniye Mosque

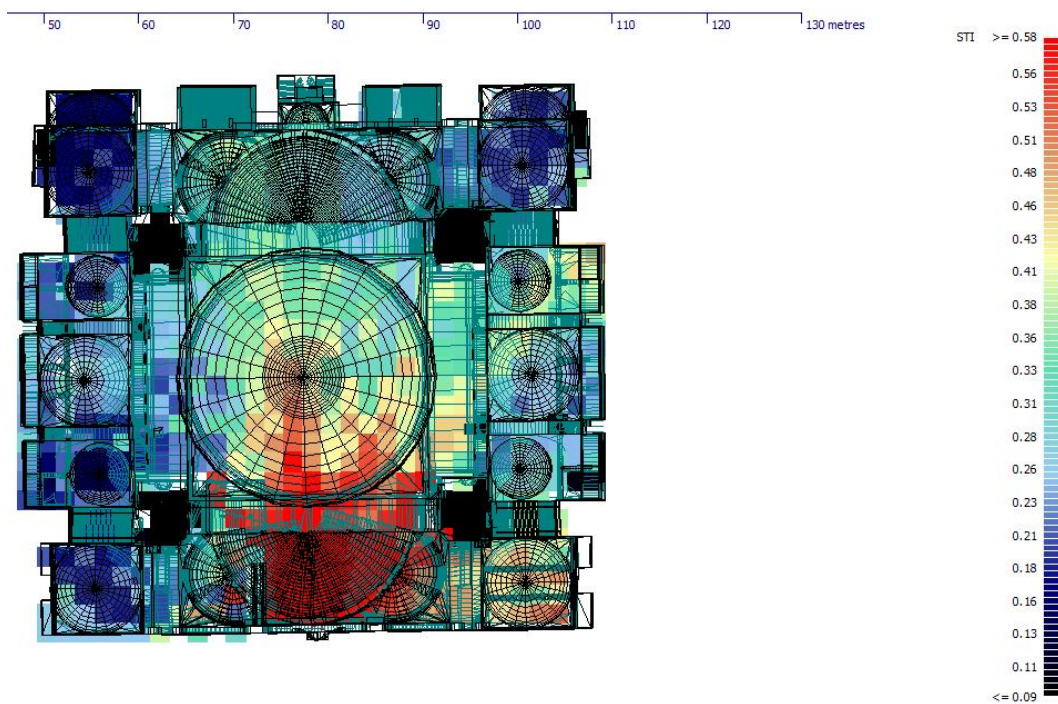


Figure A.27. STI distribution map, Süleymaniye Mosque

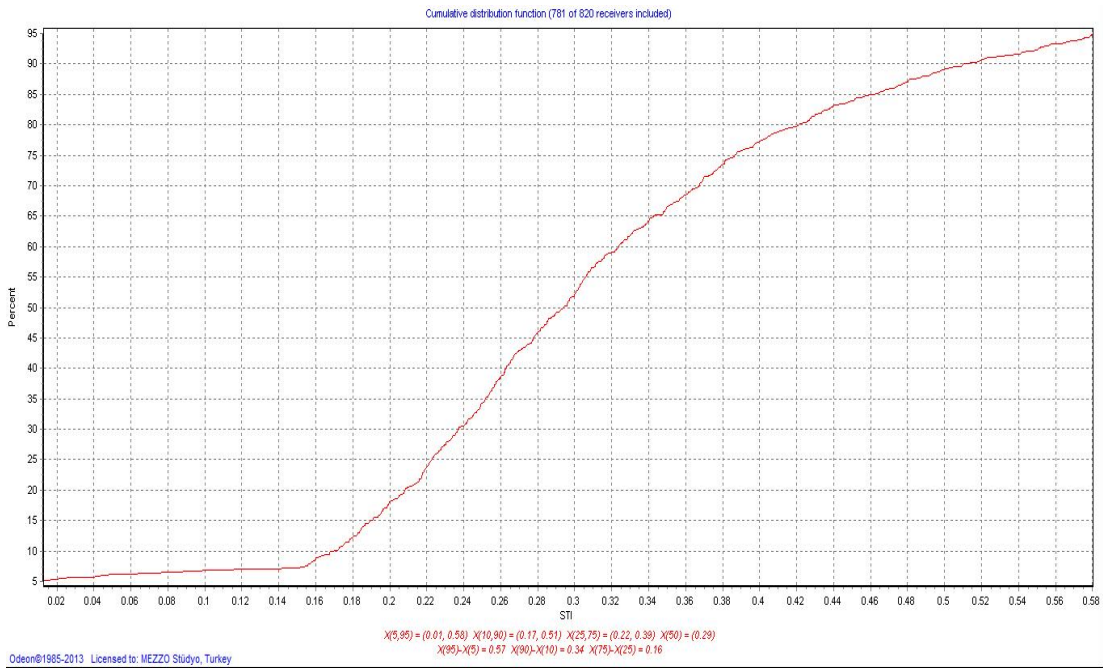


Figure A.28. STI cumulative distribution graph, Süleymaniye Mosque

APENDIX B

DPE RESULTS

Table B.1. Süleymaniye Mosque multi-slope analysis results, overall pre-field simulation data; number of decay/slope, decay rates (s) over frequency for different source-receiver configurations

Receiver Source #		Frequency (Hz)						
		125	250	500	1000	2000	4000	8000
R1 S1	# of slope (S)	1	1	1	2	2	3	4
	decay rates (s)	T1:9.8	T1:9.2	T1:8.3	T1:5.3 T2:7.8	T1:3.9 T2:7.4	T1:2.4 T2:4.7 T3:9.0	T1:1.2 T2:2.3 T3:4.4 T4:9.8
R2 S1	# of slope (S)	1	1	1	2	2	3	4
	decay rates (s)	T1:9.8	T1:9.5	T1:8.4	T1:5.0 T2:8.0	T1:4.19 T2:8	T1:2.6 T2:4.7 T3:9	T1:1.6 T2:2.8 T3:5.9 T4:12.7
R3 S1	# of slope (S)	1	1	1	2	2	3	4
	decay rates (s)	T1:9.8	T1:9.3	T1:8.4	T1:5.5 T2:8.0	T1:4.2 T2:7.59	T1:2.5 T2:4.5 T3:8.8	T1:1.28 T2:2.73 T3:7.49 T4:14.0
R5 S1	# of slope (S)	1	1	1	2	2	3	4
	decay rates (s)	T1:9.8	T1:9.3	T1:8.4	T1:5 T2:8	T1:3.99 T2:7.27	T1:2.5 T2:4.56 T3:8.41	T1:1.6 T2:2.9 T3:5.9 T4:12.5

Table B.1 (continued)

R6 S1	# of slope (S)	1	1	1	2	2	3	4
	decay rates (s)	T1:9.7	T1:9.2	T1:8.2	T1:5.2 T2:8.0	T1:4.2 T2:7.59	T1:2.5 T2:4.4 T3:9.8	T1:1.5 T2:3.0 T3:5.7 T4:12.0
R7 S1	# of slope (S)	1	1	2	2	2	3	4
	decay rates (s)	T1:9.9	T1:9.3	T1:7 T2:9	T1:5.3 T2:7.9	T1:4.14 T2:7.46	T1:2.6 T2:4.8 T3:9.0	T1:1.5 T2:3.1 T3:6.0 T4:12.0
R8 S1	# of slope (S)	1	1	1	2	2	3	4
	decay rates (s)	T1:10	T1:9.4	T1:8.5	T1:5.0 T2:8.0	T1:4.14 T2:7.46	T1:2.5 T2:4.56 T3:8.41	T1:1.5 T2:3.1 T3:5.8 T4:13.0
R10 S1	# of slope (S)	1	1	1	2	2	3	4
	decay rates (s)	T1:10	T1:9.36	T1:8.5	T1:5.6 T2:7.9	T1:4.21 T2:7.51	T1:2.51 T2:4.5 T3:8.53	T1:1.6 T2:3.4 T3:7.0 T4:12.0
R11 S1	# of slope (S)	1	1	1	2	2	3	4
	decay rates (s)	T1:9.8	T1:9.3	T1:8.2	T1:5.5 T2:8.1	T1:4.3 T2:7.51	T1:2.78 T2:4.7 T3:8.81	T1:1.5 T2:2.8 T3:5.9 T4:12.3
R12 S1	# of slope (S)	1	1	1	2	2	3	4
	decay rates (s)	T1:9.8	T1:9.3	T1:8.4	T1:6.4 T2:10.3	T1:4.2 T2:7.59	T1:2.54 T2:4.5 T3:8.69	T1:1.47 T2:2.3 T3:4.5 T4:10.5
R13 S1	# of slope (S)	1	1	1	2	2	3	4
	decay rates (s)	T1:9.9	T1:9.3	T1:8.4	T1:6.4 T2:10	T1:4.3 T2:7.51	T1:2.77 T2:4.8 T3:8.98	T1:1.47 T2:2.29 T3:4.5 T4:10.5

Table B.1 (continued)

R15 S1	# of slope (S)	1	1	1	2	2	3	4
	decay rates (s)	T1:10	T1:9.2	T1:8.5	T1:5.1 T2:8.2	T1:4.14 T2:7.61	T1:2.54 T2:4.4 T3:8.7	T1:1.6 T2:3.2 T3:6.6 T4:13.2
R16 S1	# of slope (S)	1	1	1	2	2	3	4
	decay rates (s)	T1:9.8	T1:9.5	T1:8.4	T1:5.4 T2:8.1	T1:4.21 T2:7.78	T1:2.44 T2:4.6 T3:8.65	T1:1.79 T2:3.6 T3:7.98 T4:13.1
R17 S1	# of slope (S)	1	1	1	2	2	3	4
	decay rates (s)	T1:9.8	T1:9.3	T1:8.6	T1:5.6 T2:8.1	T1:4.3 T2:7.7	T1:2.5 T2:4.8 T3:9.1	T1:1.2 T2:2.5 T3:4.3 T4:10.1
R18 S1	# of slope (S)	1	1	1	2	2	3	4
	decay rates (s)	T1:9.7	T1:9.1	T1:8.3	T1:6.3 T2:9.5	T1:4.3 T2:7.4	T1:2.5 T2:4.5 T3:9	T1:1.5 T2:3.1 T3:5.8 T4:13.0
R19 S1	# of slope (S)	1	1	1	2	2	3	4
	decay rates (s)	T1:9.8	T1:9.2	T1:8.4	T1:5.3 T2:7.8	T1:4.32 T2:7.55	T1:2.44 T2:4.2 T3:8.65	T1:1.2 T2:2.3 T3:4.4 T4:11.0
R20 S1	# of slope (S)	1	1	1	2	2	3	4
	decay rates (s)	T1:9.6	T1:9.2	T1:8.2	T1:5.5 T2:7.9	T1:4.3 T2:7.83	T1:2.63 T2:4.6 T3:9	T1:1.59 T2:2.58 T3:5.42 T4:13.2
R21 S1	# of slope (S)	1	1	1	2	2	3	4
	decay rates (s)	T1:9.8	T1:9.3	T1:8.7	T1:5.0 T2:8.2	T1:4.43 T2:7.92	T1:2.5 T2:4.5 T3:8.81	T1:1.2 T2:2.4 T3:4.5 T4:9.8

Table B.1 (continued)

R22 S1	# of slope (S)	1	1	1	2	2	3	4
	decay rates (s)	T1:10	T1:9	T1:8.5	T1:5.1 T2:8	T1:4.43 T2:7.95	T1:2.54 T2:4.6 T3:8.69	T1:1.2 T2:2.3 T3:4.4 T4:10.7
R23 S1	# of slope (S)	1	1	1	2	2	3	4
	decay rates (s)	T1:9.7	T1:9.1	T1:8.2	T1:4.01 T2:7.73	T1:3.91 T2:7.68	T1:2.2 T2:3.8 T3:8.4	T1:1.3 T2:2.6 T3:4.5 T4:11
R24 S1	# of slope (S)	1	1	1	2	2	3	4
	decay rates (s)	T1:10	T1:9.1	T1:8.3	T1:4.87 T2:7.91	T1:4.1 T2:7.8	T1:2.2 T2:3.9 T3:8.4	T1:1.97 T2:2.31 T3:4.48 T4:10
R25 S1	# of slope (S)	1	1	1	2	2	3	4
	decay rates (s)	T1:10	T1:9.26	T1:8.1	T1:5.15 T2:8.63	T1:4.1 T2:7.7	T1:2.39 T2:3.8 T3:8.5	T1:1.19 T2:2.1 T3:4.3 T4:10
R26 S1	# of slope (S)	1	1	1	2	2	3	4
	decay rates (s)	T1:10	T1:9.4	T1:8.4	T1:5.38 T2:8.58	T1:4 T2:7.26	T1:2.5 T2:4.5 T3:8.41	T1:1.64 T2:3.37 T3:7.3 T4:12
R27 S1	# of slope (S)	1	1	1	2	2	3	4
	decay rates (s)	T1:9.5	T1:9.46	T1:8.3	T1:5.38 T2:8.58	T1:3.88 T2:7.09	T1:2.54 T2:4.4 T3:8.69	T1:1.65 T2:2.85 T3:6 T4:12
R28 S1	# of slope (S)	1	1	1	2	2	3	4
	decay rates (s)	T1:9.7	T1:9.3	T1:8.3	T1:5.4 T2:8.58	T1:4.43 T2:7.92	T1:2.5 T2:4.55 T3:8.41	T1:1.19 T2:2.31 T3:4.5 T4:10

Table B.1 (continued)

R29 S1	# of slope (S)	1	1	1	2	2	3	4
	decay rates (s)	T1:9.7	T1:9	T1:8.0	T1:5.58 T2:8.68	T1:4.07 T2:7.54	T1:2.21 T2:4.06 T3:8.26	T1:1.3 T2:2.3 T3:3.9 T4:9.6
R30 S1	# of slope (S)	1	1	1	2	2	3	4
	decay rates (s)	T1:9.6	T1:9.1	T1:8.1	T1:5.73 T2:8.49	T1:4.15 T2:7.4	T1:2.1 T2:4.0 T3:10	T1:1.3 T2:2.2 T3:3.6 T4:9.6
R31 S1	# of slope (S)	1	1	1	2	2	3	4
	decay rates (s)	T1:10	T1:9.5	T1:8.3	T1:4.92 T2:8.58	T1:4.1 T2:7.6	T1:2.17 T2:4.17 T3:9.49	T1:1.3 T2:2.6 T3:6.1 T4:9
R32 S1	# of slope (S)	1	1	1	2	2	3	3
	decay rates (s)	T1:9.5	T1:8.7	T1:7.8	T1:4.81 T2:8.60	T1:3.22 T2:7.18	T1:1.75 T2:3.26 T3:5.4	T1:1.1 T2:1.6 T3:3.8
R33 S1	# of slope (S)	1	1	1	2	2	3	3
	decay rates (s)	T1:10	T1:9.3	T1:8.2	T1:5.49 T2:8.65	T1:4.16 T2:7.3	T1:2.2 T2:4.5 T3:10.1	T1:1.5 T2:2.9 T3:8
R34 S1	# of slope (S)	1	1	1	2	2	3	4
	decay rates (s)	T1:10	T1:9.2	T1:8.1	T1:4.6 T2:8.15	T1:3.93 T2:7	T1:2 T2:4.0 T3:8.6	T1:1.2 T2:2.3 T3:4.5 T4:11
R1 S2	# of slope (S)	1	1	1	2	2	3	4
	decay rates (s)	T1:9.6	T1:9.1	T1:8.3	T1:4.6 T2:7.8	T1:3.86 T2:7.5	T1:2.6 T2:4.7 T3:9	T1:1.17 T2:2.37 T3:4.57 T4:10

Table B.1 (continued)

R7 S2	# of slope (S)	1	1	1	2	2	3	4
	decay rates (s)	T1:10	T1:9.6	T1:8.5	T1:5.0 T2:7.9	T1:4 T2:7.1	T1:2.8 T2:5.18 T3:9.5	T1:1.55 T2:2.91 T3:6.15 T4:11.8
R10 S2	# of slope (S)	1	1	1	2	2	3	4
	decay rates (s)	T1:9.8	T1:9.3	T1:8.2	T1:5.5 T2:8	T1:4 T2:7.6	T1:2.85 T2:5.10 T3:9.3	T1:1.65 T2:3.1 T3:7 T4:11.8
R13 S2	# of slope (S)	1	1	1	2	2	3	4
	decay rates (s)	T1:10	T1:9.5	T1:8.5	T1:5 T2:7.8	T1:4.01 T2:7.08	T1:2.85 T2:5.38 T3:9.5	T1:1.57 T2:3.19 T3:7.2 T4:11.6
R16 S2	# of slope (S)	1	1	1	2	2	3	4
	decay rates (s)	T1:10	T1:9.3	T1:8.5	T1:4.9 T2:7.9	T1:3.99 T2:7.51	T1:3 T2:5.7 T3:10	T1:1.6 T2:3.38 T3:7.5 T4:12
R17 S2	# of slope (S)	1	1	1	2	2	3	3
	decay rates (s)	T1:9.6	T1:9.3	T1:8.5	T1:4.9 T2:7.9	T1:4.19 T2:7.1	T1:3 T2:5.7 T3:10	T1:1.7 T2:3.5 T3:9.7
R28 S2	# of slope (S)	1	1	1	2	2	3	3
	decay rates (s)	T1:9.7	T1:9.4	T1:8.4	T1:4.6 T2:8.2	T1:3.67 T2:6.99	T1:1.94 T2:3.93 T3:9	T1:1.1 T2:2.4 T3:6
R29 S2	# of slope (S)	1	1	1	2	2	3	3
	decay rates (s)	T1:9.8	T1:9.3	T1:8.3	T1:5.5 T2:9.4	T1:4 T2:7.1	T1:2.7 T2:4.5 T3:9	T1:1.3 T2:2.6 T3:8
R32 S2	# of slope (S)	1	1	1	2	2	3	4
	decay rates (s)	T1:9.9	T1:9	T1:8	T1:5.5 T2:9.1	T1:3.8 T2:6.99	T1:2.3 T2:4.1 T3:8.2	T1:1.1 T2:2 T3:3.2 T4:9.4

Table B.1 (continued)

R1 S3	# of slope (S)	1	1	1	2	2	3	3
	decay rates (s)	T1:9.6	T1:9	T1:8.1	T1:5.4 T2:8.6	T1:3.76 T2:6.88	T1:2.5 T2:4.4 T3:8.5	T1:1.4 T2:2.8 T3:8
R7 S3	# of slope (S)	1	1	1	2	2	3	4
	decay rates (s)	T1:9.9	T1:9.2	T1:8.3	T1:5.42 T2:8.8	T1:4.05 T2:7.4	T1:2.8 T2:4.9 T3:7.6	T1:1.55 T2:2.91 T3:6.15 T4:11.8
R10 S3	# of slope (S)	1	1	1	2	2	3	3
	decay rates (s)	T1:9.8	T1:9.3	T1:8.1	T1:5.5 T2:9	T1:4.01 T2:6.84	T1:2.8 T2:4.7 T3:8.9	T1:1.8 T2:3.5 T3:8.9
R13 S3	# of slope (S)	1	1	1	2	2	3	3
	decay rates (s)	T1:9.9	T1:9.3	T1:8.1	T1:5.46 T2:8.8	T1:4.01 T2:6.85	T1:2.8 T2:5 T3:9	T1:1.9 T2:3.5 T3:8.4
R16 S3	# of slope (S)	1	1	1	2	2	3	4
	decay rates (s)	T1:9.9	T1:9.3	T1:8.4	T1:5.7 T2:9	T1:4.46 T2:7.46	T1:3 T2:5.4 T3:9	T1:1.61 T2:3.37 T3:7.46 T4:10.8
R17 S3	# of slope (S)	1	1	1	2	2	3	3
	decay rates (s)	T1:9.8	T1:9.3	T1:8.4	T1:5.37 T2:8.6	T1:3.79 T2:6.76	T1:3.08 T2:5.5 T3:8.7	T1:1.7 T2:3.4 T3:9.2
R28 S3	# of slope (S)	1	1	1	2	2	3	3
	decay rates (s)	T1:9.7	T1:9.2	T1:8.1	T1:5.49 T2:8.8	T1:3.95 T2:6.77	T1:2.7 T2:4.7 T3:8.3	T1:1.8 T2:3.3 T3:8.3
R29 S3	# of slope (S)	1	1	1	2	2	3	3
	decay rates (s)	T1:10	T1:9.2	T1:8.2	T1:5.69 T2:8.79	T1:3.85 T2:6.8	T1:2.4 T2:4.5 T3:8.9	T1:1.5 T2:3.3 T3:8.3
R32 S3	# of slope (S)	1	1	1	2	2	3	3
	decay rates (s)	T1:9.6	T1:8.9	T1:8.1	T1:5.4 T2:8.5	T1:3.7 T2:6.6	T1:2.5 T2:4.4 T3:8.5	T1:1.4 T2:2.8 T3:8.2

Table B.1 (continued)

R1 S4	# of slope (S)	1	1	1	2	2	3	4
	decay rates (s)	T1:9.8	T1:9.47	T1:8.2	T1:5.26 T2:8.67	T1:4.15 T2:7.09	T1:2.97 T2:4.75 T3:9.03	T1:1.65 T2:2.9 T3:5.6 T4:9.7
R7 S4	# of slope (S)	1	1	1	2	2	3	4
	decay rates (s)	T1:9.9	T1:9.56	T1:8.4	T1:5.27 T2:8.73	T1:4.15 T2:7.4	T1:2.7 T2:5.3 T3:9.26	T1:1.6 T2:3 T3:5.4 T4:10
R10 S4	# of slope (S)	1	1	1	2	2	3	4
	decay rates (s)	T1:9.8	T1:9.3	T1:8.3	T1:5.45 T2:8.67	T1:4.15 T2:7.2	T1:2.88 T2:4.68 T3:9.18	T1:1.5 T2:2.5 T3:5.3 T4:10.1
R13 S4	# of slope (S)	1	1	1	2	2	3	4
	decay rates (s)	T1:9.6	T1:9.2	T1:8.2	T1:4.6 T2:8.15	T1:3.79 T2:7.06	T1:1.9 T2:4.7 T3:9.9	T1:0.99 T2:2.25 T3:6.2 T4:12.4
R16 S4	# of slope (S)	1	1	1	2	2	3	4
	decay rates (s)	T1:9.9	T1:9.3	T1:8.3	T1:5 T2:8.49	T1:3.9 T2:7.2	T1:2.5 T2:4.75 T3:8.9	T1:1.3 T2:2.2 T3:4.5 T4:9.7
R17 S4	# of slope (S)	1	1	1	2	2	3	4
	decay rates (s)	T1:9.8	T1:9.4	T1:8.6	T1:5.45 T2:8.5	T1:4.15 T2:7.4	T1:2.4 T2:4.62 T3:9.3	T1:2 T2:2.9 T3:5.7 T4:11
R28 S4	# of slope (S)	1	1	1	2	2	3	3
	decay rates (s)	T1:9.6	T1:9.3	T1:8.6	T1:5 T2:8.5	T1:3.89 T2:7.33	T1:2.41 T2:4.75 T3:8.9	T1:1.6 T2:2.7 T3:9.7

Table B.1 (continued)

R32 S4	# of slope (S)	1	1	1	2	2	3	3
	decay rates (s)	T1:9.8	T1:9.3	T1:8.3	T1:4.68 T2:8.13	T1:3.78 T2:6.82	T1:2.6 T2:4.9 T3:9	T1:0.94 T2:2.4 T3:6
R1 S5	# of slope (S)	1	1	1	2	2	3	4
	decay rates (s)	T1:9.9	T1:9.4	T1:8.2	T1:5.32 T2:8.4	T1:4 T2:7.09	T1:2.9 T2:4.8 T3:9.13	T1:1.62 T2:2.69 T3:6.04 T4:11.9
R7 S5	# of slope (S)	1	1	1	2	2	3	4
	decay rates (s)	T1:9.8	T1:9.2	T1:8.4	T1:5.44 T2:8.59	T1:4 T2:7.09	T1:2.93 T2:4.71 T3:9.56	T1:1.4 T2:2.85 T3:6.3 T4:11.9
R10 S5	# of slope (S)	1	1	1	2	2	3	4
	decay rates (s)	T1:9.8	T1:9.3	T1:8.4	T1:5.19 T2:8.5	T1:3.94 T2:7.24	T1:3.1 T2:5.9 T3:8.9	T1:1.6 T2:3 T3:7.1 T4:11.8
R16 S5	# of slope (S)	1	1	1	2	2	3	4
	decay rates (s)	T1:9.8	T1:9.2	T1:8.2	T1:4.45 T2:8.15	T1:3.79 T2:7.06	T1:2.1 T2:4.6 T3:9.02	T1:1 T2:1.9 T3:5 T4:5.13
R17 S5	# of slope (S)	1	1	1	2	2	3	3
	decay rates (s)	T1:9.8	T1:9.4	T1:8.5	T1:5.45 T2:7.27	T1:4.1 T2:7.27	T1:2.3 T2:4.4 T3:8.7	T1:1.32 T2:3.19 T3:9.86
R28 S5	# of slope (S)	1	1	1	2	2	3	4
	decay rates (s)	T1:10	T1:9.37	T1:8.4	T1:5.25 T2:8.45	T1:4 T2:7.09	T1:2.5 T2:4.4 T3:8.8	T1:1.6 T2:3.82 T3:8.8 T4:12.8
R29 S5	# of slope (S)	1	1	1	2	2	3	4
	decay rates (s)	T1:9.7	T1:9.1	T1:7.9	T1:4.67 T2:8.05	T1:3.82 T2:7	T1:1.6 T2:3.9 T3:9.07	T1:1.12 T2:2.6 T3:5.68 T4:11

Table B.1 (continued)

R32 S5	# of slope (S)	1	1	1	2	2	3	4
	decay rates (s)	T1:9.8	T1:9.2	T1:8.0	T1:5.16 T2:8.32	T1:4 T2:6.9	T1:2.9 T2:5 T3:9.13	T1:1.6 T2:2.94 T3:5.95 T4:12.0
R7 S6	# of slope (S)	1	1	1	2	2	3	4
	decay rates (s)	T1:9.7	T1:9.3	T1:8.4	T1:5.23 T2:8.4	T1:3.85 T2:6.89	T1:2.56 T2:4.65 T3:9.02	T1:1.40 T2:2.65 T3:5.74 T4:12.3
R10 S6	# of slope (S)	1	1	1	2	2	3	4
	decay rates (s)	T1:9.9	T1:9.3	T1:8.3	T1:5.13 T2:8.3	T1:3.85 T2:6.8	T1:2.56 T2:4.5 T3:9.02	T1:1.36 T2:2.69 T3:5.85 T4:11.8
R13 S6	# of slope (S)	1	1	1	2	2	3	4
	decay rates (s)	T1:9.8	T1:9.2	T1:8.3	T1:5.39 T2:8.22	T1:3.85 T2:6.89	T1:2.56 T2:4.65 T3:9.02	T1:1.36 T2:2.5 T3:5.4 T4:12.1
R16 S6	# of slope (S)	1	1	1	2	2	3	4
	decay rates (s)	T1:9.9	T1:9.3	T1:8.4	T1:5.23 T2:8.4	T1:4 T2:6.89	T1:2.56 T2:4.65 T3:9.02	T1:1.49 T2:2.62 T3:4.61 T4:12.1
R17 S6	# of slope (S)	1	1	1	2	2	3	4
	decay rates (s)	T1:9.9	T1:9.3	T1:8.4	T1:5.5 T2:8.39	T1:4 T2:6.89	T1:2.60 T2:4.59 T3:8.84	T1:1.47 T2:2.50 T3:4.69 T4:10.6
R28 S6	# of slope (S)	1	1	1	2	2	3	4
	decay rates (s)	T1:9.8	T1:9.3	T1:8.4	T1:5.15 T2:8.6	T1:3.93 T2:6.8	T1:2.60 T2:4.59 T3:8.83	T1:1.48 T2:2.52 T3:4.65 T4:10.3

Table B.1 (continued)

R29 S6	# of slope (S)	1	1	1	2	2	3	4
	decay rates (s)	T1:9.7	T1:9.47	T1:8.3	T1:5.5 T2:8.6	T1:3.94 T2:7.05	T1:2.49 T2:4.38 T3:9	T1:1.47 T2:2.3 T3:4.5 T4:10.6
R32 S6	# of slope (S)	1	1	1	2	2	3	4
	decay rates (s)	T1:9.8	T1:9.2	T1:8.2	T1:4.86 T2:8.28	T1:3.7 T2:6.7	T1:2.56 T2:4.5 T3:9.02	T1:1.41 T2:2.6 T3:5.5 T4:12.3

Table B.2. Süleymaniye Mosque multi-slope analysis results, overall field measurement data; number of decay/slope, decay rates (s) over frequency for different source-receiver configurations

Source Receiver #		Frequency (Hz)							
		63	125	250	500	1000	2000	4000	8000
S1 R1	# of slope (S)	2	2	2	2	2	2	2	2
	decay rates (s)	T1:11 T2:22	T1:12 T2:20	T1:7.7 T2:14	T1:5.8 T2:9.0	T1:5.3 T2:7.8	T1:3.6 T2:7.0	T1:2.3 T2:3.8	T1:1.3 T2:2.3
S1 R2	# of slope (S)	2	2	2	2	2	2	2	2
	decay rates (s)	T1:14 T2:22	T1:13 T2:19	T1:10 T2:16	T1:6 T2:9.8	T1:5.6 T2:8.0	T1:4.0 T2:6.4	T1:2.6 T2:4.1	T1:1.5 T2:2.2
S1 R3	# of slope (S)	1	2	2	2	2	2	2	2
	decay rates (s)	T1:18	T1:15 T2:19	T1:10 T2:15	T1:6.2 T2:10	T1:5.6 T2:8	T1:3.7 T2:5.7	T1:2.6 T2:4.2	T1:1.4 T2:2.1
S1 R4	# of slope (S)	1	2	2	2	2	2	2	3
	decay rates (s)	T1:19	T1:14 T2:19	T1:11 T2:15	T1:5.8 T2:10	T1:5.2 T2:8.0	T1:3.9 T2:6.2	T1:2.5 T2:4	T1:0.49 T2:1.11 T3:1.83
S1 R5	# of slope (S)	1	2	2	2	2	2	2	2
	decay rates (s)	T1:18	T1:15 T2:21	T1:11 T2:15	T1:6.1 T2:10	T1:5.7 T2:7.7	T1:4.2 T2:6.3	T1:2.7 T2:4.1	T1:1.47 T2:2.16
S1 R6	# of slope (S)	1	2	3	2	2	2	2	2
	decay rates (s)	T1:18	T1:14 T2:21	T1:8.4 T2:14 T3:17	T1:6.2 T2:10	T1:5.6 T2:8	T1:4.1 T2:6.2	T1:2.8 T2:4.2	T1:1.5 T2:2.14

Table B.2 (continued)

S2 R1	# of slope (S)	1	2	2	2	2	2	2	2
	decay rates (s)	T1:19	T1:15 T2:18	T1:10 T2:15	T1:6.2 T2:10	T1:5.5 T2:8	T1:4 T2:6.5	T1:2.5 T2:4.1	T1:1.55 T2:2.23
S2 R2	# of slope (S)	1	1	2	2	2	2	2	2
	decay rates (s)	T1:18	T1:17	T1:11 T2:15	T1:6.2 T2:10	T1:5.7 T2:7.9	T1:4.1 T2:6.7	T1:2.6 T2:4.1	T1:1.56 T2:2.21
S2 R4	# of slope (S)	2	3	2	2	2	2	2	2
	decay rates (s)	T2:15 T2:22	T1:13 T2:16	T1:11 T2:15 T3:23	T1:6.2 T2:9.7	T1:5.4 T2:7.8	T1:4.0 T2:6.6	T1:2.4 T2:4.0	T1:1.50 T2:2.23
S2 R6	# of slope (S)	1	2	2	2	2	2	2	2
	decay rates (s)	T1:18	T1:15 T2:20	T1:11 T2:15	T1:6.4 T2:9.9	T1:5.4 T2:7.3	T1:4.1 T2:6.6	T1:2.5 T2:4.0	T1:1.53 T2:2.21
S2 R8	# of slope (S)	1	2	2	2	2	2	2	2
	decay rates (s)	T1:18	T1:13 T2:20	T1:9.3 T2:14	T1:6 T2:9.8	T1:4.7 T2:8.0	T1:2.6 T2:4.8	T1:1.6 T2:3.0	T1:1.26 T2:2.08
S3 R2	# of slope (S)	1	2	2	2	2	2	2	2
	decay rates (s)	T1:19	T1:14 T2:21	T1:8.6 T2:15	T1:6.0 T2:9.6	T1:5.4 T2:7.9	T1:3.8 T2:5.7	T1:2.5 T2:3.8	T1:1.51 T2:2.24
S3 R5	# of slope (S)	1	2	2	2	2	2	2	2
	decay rates (s)	T1:18	T1:15 T2:20	T1:9.8 T2:15	T1:6.2 T2:10	T1:5.3 T2:7.7	T1:4.1 T2:6.2	T1:2.6 T2:4.0	T1:1.55 T2:2.09
S3 R7	# of slope (S)	1	2	3	2	2	2	2	2
	decay rates (s)	T1:18	T1:15 T2:20	T1:8.9 T2:13 T3:17	T1:6.1 T2:9.4	T1:5.4 T2:8	T1:3.9 T2:6.1	T1:2.4 T2:4.0	T1:1.33 T2:2.00
S6 R3	# of slope (S)	2	2	2	2	2	2	2	2
	decay rates (s)	T1:14 T2:21	T1:13 T2:18	T1:10 T2:15	T1:6.1 T2:9.9	T1:5.3 T2:7.8	T1:4.1 T2:5.9	T1:2.5 T2:4.1	T1:1.55 T2:2.22
S6 R5	# of slope (S)	1	2	2	2	2	2	2	2
	decay rates (s)	T1:18	T1:15 T2:19	T1:8.8 T2:15	T1:5.5 T2:7.6	T1:5.3 T2:7.3	T1:4.0 T2:6.1	T1:2.6 T2:3.7	T1:1.53 T2:1.98

Table B.2 (continued)

S6 R6	# of slope (S)	2	2	2	2	2	2	2	2
	decay rates (s)	T1:16 T2:21	T1:13. T2:19	T1:10. T2:15	T1:6.1 T2:9.8	T1:5.7 T2:7.5	T1:4.1 T2:6.1	T1:2.4 T2:3.8	T1:1.4 T2:2.10

Table B.3. Süleymaniye Mosque multi-slope analysis results, overall post-field simulation data; number of decay/slope, decay rates (s) over frequency for different source-receiver configurations

Source Receiver #		Frequency (Hz)						
		125	250	500	1000	2000	4000	8000
S1 R1	# of slope (S)	2	1//2	2//3	2	2	2//3	3
	decay rates (s)	T1:10.3 T2:16.6	T1:8.42 T2:12.62	T1:5.35 T2:10	T1:4.64 T2:8.54	T1:3.76 T2:7.52	T1:2.32 T2:5.04	T1:1.18 T2:2.39 T3:5.90
S1 R2	# of slope (S)	2	2	2	2	2	2	3
	decay rates (s)	T1:9.9 T2:19.0	T1:9.62 T2:16.42	T1:7.20 T2:14.1	T1:4.78 T2:8.58	T1:3.79 T2:7.01	T1:2.60 T2:5.14	T1:1.19 T2:2.40 T3:5.58
S1 R3	# of slope (S)	2	2	2	2	2//3	2//3	2
	decay rates (s)	T1:12.6 T2:25.3	T1:9.75 T2:16.5	T1:7.17 T2:13.2	T1:5.23 T2:9.87	T1:3.58 T2:5.7 T3: 10	T1:2.91 T2:6.69	T1:1.75 T2:4.17 T3:11.76
S1 R4	# of slope (S)	2	1//2	2	2	2//3	3	3
	decay rates (s)	T1:12.3 T2:22.4	T1:8.34 T2:13.72	T1:7 T2:13.8	T1:4.98 T2:8.77	T1:2.68 T2:5.21 T3:10.1	T1:1.84 T2:3.62 T3:8.31	T1:1.21 T2:3 T3:9.75
S1 R5	# of slope (S)	3	2	2	2	2	3	3
	decay rates (s)	T1:10.7 T2:17.7 T3:28	T1:10 T2:15	T1:7.35 T2:13.0	T1:5.4 T2:11.0	T1:4.51 T2:10.3	T1:2.95 T2:4.96 T3:10.8	T1:1.8 T2:3.8 T3:10.8
S1 R6	# of slope (S)	2	2	2	2	2//3	3	3
	decay rates (s)	T1:12.1 T2:25.5	T1:9.8 T2:15	T1:7.1 T2:13.2	T1:5.4 T2:11.5	T1:4.45 T2:10.6	T1:2.95 T2:4.96 T3:11.1	T1:1.8 T2:3.3 T3:10.7

Table B.3 (continued)

S2 R1	# of slope (S)	2	1//2	2	2	2	3	3
	decay rates (s)	T1:10.1 T2:19.2	T1:9.46 T2:15.82	T1:7.19 T2:14.2	T1:5.2 T2:10.8	T1:4 T2:8	T1:2.46 T2:4.53 T3:10.5	T1:1.29 T2:2.99 T3:10.22
S2 R2	# of slope (S)	2	1//2	2	2	2//3	3	3
	decay rates (s)	T1:12 T2:26.4	T1:9.84 T2:15.09	T1:7.07 T2:12.8	T1:5.4 T2:11.2	T1:4.51 T2:10.6	T1:2.57 T2:4.55 T3:11.1	T1:1.8 T2:3.8 T3:12
S2 R4	# of slope (S)	2//3	2	2	2	2	3	3
	decay rates (s)	T1:12.2 T2:25.1	T1:9.56 T2:15.9	T1:7.5 T2:14	T1:5.4 T2:11.2	T1:4.8 T2:12.7	T1:2.43 T2:4.57 T3:11.0	T1:1.6 T2:3.5 T3:12.7
S2 R6	# of slope (S)	2//3	1//2	2	2	2	2//3	3
	decay rates (s)	T1:10 T2:16 T3:28	T1:9.9 T2:16	T1:7.5 T2:14	T1:7.1 T2:13.2	T1:4.6 T2:11	T1:3.6 T2:9.9	T1:1.69 T2:4.64 T3:13.2
S2 R8	# of slope (S)	1//2	1//2	2	2	2	2	3
	decay rates (s)	T1:9.8 T2:19	T1:8.7 T2:15.3	T1:5.97 T2:12.5	T1:4.5 T2:8.4	T1:2.69 T2:6.09	T1:1.8 T2:4.69	T1:1.14 T2:2.34 T3:6
S3 R2	# of slope (S)	1	1	2	2	2	2	3
	decay rates (s)	T1:14	T1:11.6	T1:6.02 T2:10.8	T1:5.4 T2:10.4	T1:4 T2:7.8	T1:3.05 T2:7.2	T1:1.35 T2:2.9 T3:8.8
S3 R5	# of slope (S)	2//3	2	2	2	2	2	3
	decay rates (s)	T1:10.5 T2:16.2 T3:28.9	T1:9.16 T2:15.2	T1:7.24 T2:13.1	T1:5.4 T2:10.3	T1:3.99 T2:7.6	T1:3.05 T2:7.41	T1:1.5 T2:3.01 T3:8.98
S3 R7	# of slope (S)	2//3	2	2	2	2	2	3
	decay rates (s)	T1:12.7 T2:25	T1:10.16 T2:16	T1:7 T2:13.1	T1:5.4 T2:10.2	T1:4.04 T2:7.4	T1:3.05 T2:7.1	T1:1.47 T2:2.82 T3:8.58

Table B.3 (continued)

S4 R3	# of slope (S)	2	2	2	2	2	2	3
	decay rates (s)	T1:10.4 T2:20.5	T1:8.5 T2:13.75	T1:7 T2:13	T1:5.44 T2:10.1	T1:3.99 T2:8.2	T1:2.9 T2:6.9	T1:1.4 T2:2.95 T3:9.2
S4 R5	# of slope (S)	2	1//2	2//3	2	2	2	3
	decay rates (s)	T1:12.2 T2:20.1	T1:8.2 T2:14.2	T1:6.9 T2:13.2	T1:5.3 T2:10.1	T1:4.04 T2:8.3	T1:3.05 T2:7	T1:1.5 T2:2.99 T3:9.6
S4 R6	# of slope (S)	2//3	2	2	2	2//3	2//3	3//4
	decay rates (s)	T1:10.2 T2:16.9 T3:28.1	T1:10.16 T2:16.4	T1:7.7 T2:13.3	T1:5.6 T2:11	T1:3.99 T2:6.5 T3:12.0	T1:3.05 T2:7.3	T1:1.52 T2:2.81 T3:8.8

* // indicates impulses that are weak cases of the higher number of slope

Table B.4. Hagia Sophia multi-slope analysis results, overall field data; number of decay/slope, decay rates (s) over frequency for different source-receiver configurations versus DIRAC post-processed T30 data

Source Receiver #		Frequency (Hz)							
		63	125	250	500	1000	2000	4000	8000
S1 R1	T30 (s)	7.77	8.52	9.89	9.53	7.81	6.19	4.32	2.69
	# of slope (S)	1/2	1	1	1	1/2	2	2	2
	decay rates (s)	T1:7 T2:12	T1:8.6	T1:10	T1:9.3	T1:6.61 T2:8.89	T1:5.4 T2:7.6	T1:2.9 T2:5.3	T1:2.4 T2:3.3
S1 R2	T30 (s)	8.25	8.96	9.80	12.25*	8.85	10.36*	5.95*	2.80
	# of slope (S)	1	1/2	1/2	NA	1	NA	NA	2
	decay rates (s)	T1:8.5	T1:8.4	T1:9.4	NA	T1:7.74	NA	NA	T1:2.6 T2:3.4
S1 R3	T30 (s)	8.03	8.81	9.89	10.01	8.34	6.45	4.61	2.85
	# of slope (S)	1	1	1	2	1	1	1	2
	decay rates (s)	T1:8.3	T1:8.8	T1:9.8	T1:8.68 T2:10.9	T1:8.2	T1:6.3	T1:4.8	T1:2.5 T2:3.5
S1 R4	T30 (s)	8.36	8.43	9.88	9.70	8.19	6.23	4.45	2.69
	# of slope (S)	2	1/2	1/2	2	2/3	2/3	2/3	2/3
	decay rates (s)	T1:7.0 T2:10	T1:7.7 T2:10	T1:8.8 T2:11	T1:8.7 T2:10.9	T1:6.69 T2:9.47	T1:5.2 T2:7.2	T1:3.0 T2:5.5	T1:1.7 T2:3.5

Table B.4 (continued)

S1 R5	T30 (s)	8.24	8.91	9.83	9.78	8.22	6.43	4.67	2.85
	# of slope (S)	1/2	1	1	1/2	2	2	2	2
	decay rates (s)	T1:8.8	T1:9.2	T1:9.8	T1:8.90	T1:6.69	T1:5.4	T1:4.0	T1:2.5
				T2:11.3	T2:9.47	T2:7.6	T2:5.7	T2:3.7	
S2 R1	T30 (s)	9.75	8.88	9.89	9.45	8.18	6.46	4.63	2.85
	# of slope (S)	1	2	1/2	1	2	2	2	2
	decay rates (s)	T1:8.6	T1:7.7	T1:8.5	T1:9.4	T1:6.90	T1:5.7	T1:3.5	T1:2.0
		T2:10	T2:10		T2:9.34	T2:8.0	T2:5.6	T2:3.6	
S2 R2	T30 (s)	8.24	8.92	9.94	10.13	8.52	6.43	4.66	2.90
	# of slope (S)	1	1/2	1/2	1	1/2	2	2	1/2
	decay rates (s)	T1:8.6	T1:9.0	T1:9.7	T1:9.44	T1:8.1	T1:6.0	T1:3.8	T1:2.7
						T2:7.5	T2:5.6	T2:3.9	
S2 R3	T30 (s)	8.20	8.97	10.07	9.64	8.15	6.52	4.76	2.93
	# of slope (S)	1	2	1	1	1/2	1	2	1
	decay rates (s)	T1:8.5	T1:8.2	T1:9.7	T1:9.37	T1:7.93	T1:6.4	T1:3.8	T1:3.1
		T2:10					T2:5.6		
S2 R5	T30 (s)	6.93	8.19	8.99	9.07	7.71	5.89	3.91	2.29
	# of slope (S)	2/3	2/3	2/3	2/3	2	2	2	2
	decay rates (s)	T1:3.9	T1:4.0	T1:4.1	T1:5.47	T1:5.14	T1:3.9	T1:2.2	T1:1.9
		T2:7.9	T2:8.7	T2:9.3	T2:11.1	T2:9.81	T2:7.6	T2:5.1	T2:3.3
		T3:10	T3:10	T3:11					
S2 R6	T30 (s)	8.11	8.55	9.74	9.19	8.04	6.26	4.34	2.64
	# of slope (S)	2/3	2/3	2/3	2/3	2/3	2	2/3	2
	decay rates (s)	T1:5.6	T1:4.5	T1:6.0	T1:6.38	T1:5.30	T1:4.5	T1:2.1	T1:2.3
		T2:10	T2:9.1	T2:10	T2:10.5	T2:8.70	T2:7.7	T2:4.1	T2:3.5
			T3:11	T3:12	T3:13.0	T3:13.1		T3:5.8	
S3 R1	T30 (s)	7.7	8.8	9.9	9.6	8.0	6.2	4.4	2.4
	# of slope (S)	2	1	1	1/2	2	2	2/3	2
	decay rates (s)	T1:7.4	T1:8.8	T1:9.8	T1:9.59	T1:6.61	T1:5.3	T1:3.0	T1:2.1
		T2:12			T2:9.10	T2:7.4	T2:5.3	T2:3.7	

* results in red indicates deviations from overall T30, indicating echo or flutter echo formation for that specific location and octave band, thus the data is excluded in the averaging of results

APPENDIX C

DEM RESULTS

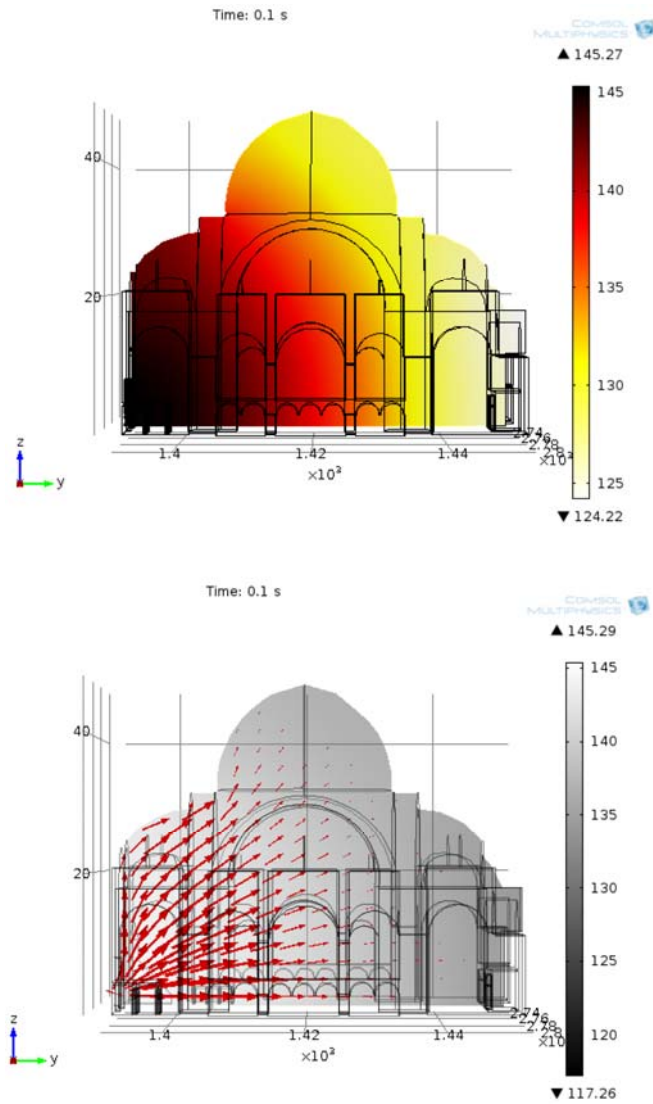


Figure C.29. Süleymaniye Mosque DEM result for 250 Hz, t: 0.1s, carpeted floor, mihrab wall section spatial sound energy level (dB) distribution (above), 2D-flow vector plot (below)

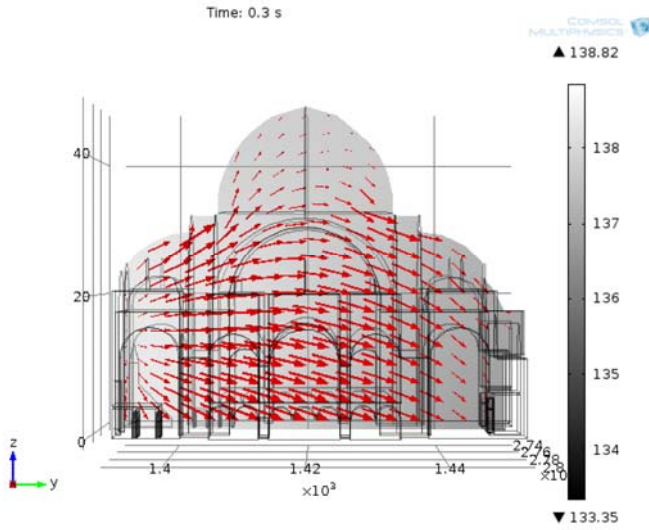
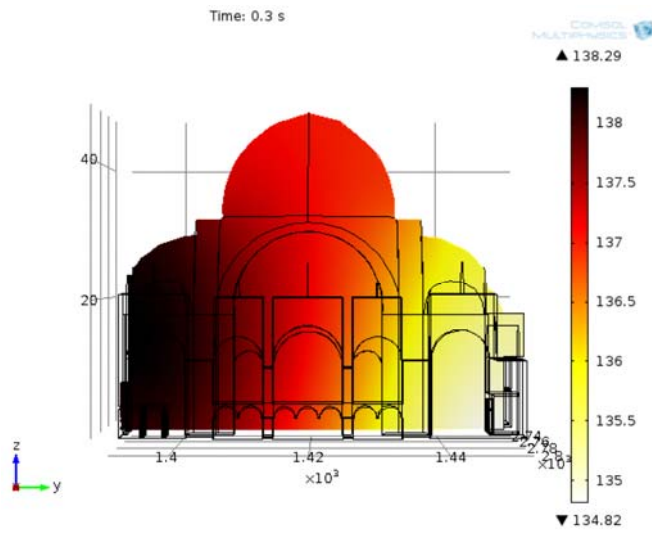


Figure C.30. Süleymaniye Mosque DEM result for 250 Hz, t: 0.3s, carpeted floor, mihrab wall section spatial sound energy level (dB) distribution (above), 2D-flow vector plot (below)

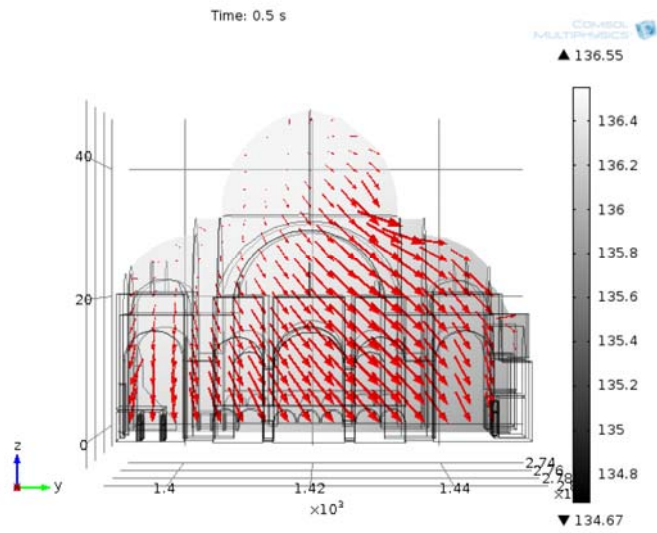
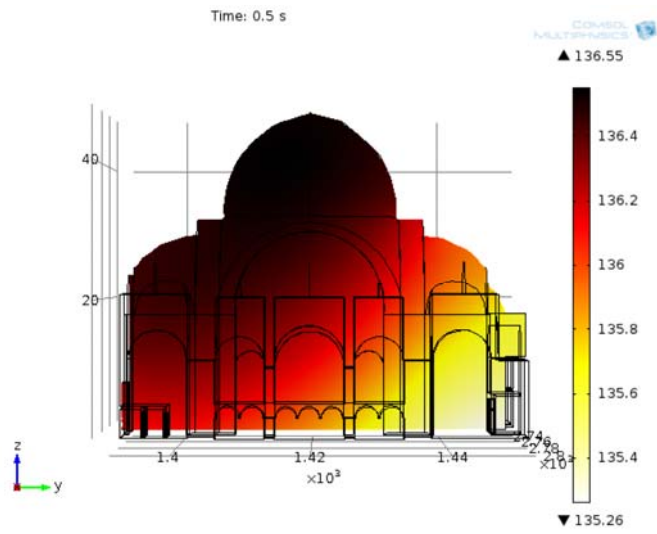


Figure C.31. Süleymaniye Mosque DEM result for 250 Hz, t: 0.5s, carpeted floor, mihrab wall section spatial sound energy level (dB) distribution (above), 2D-flow vector plot (below)

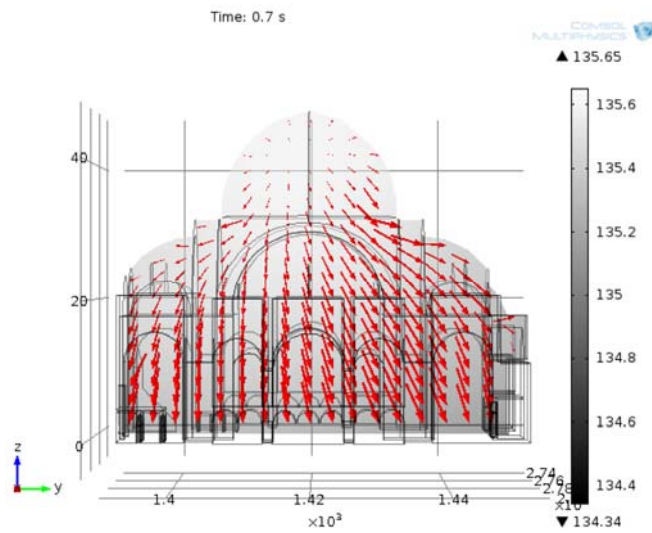
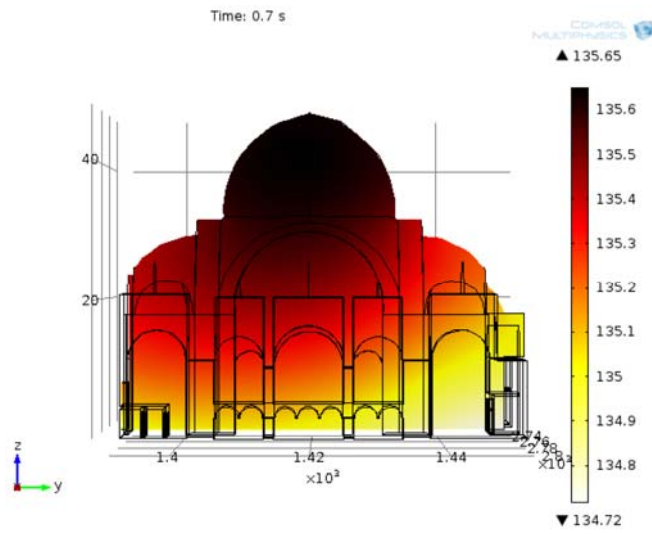


Figure C.32. Süleymaniye Mosque DEM result for 250 Hz, t: 0.7s, carpeted floor, mihrab wall section spatial sound energy level (dB) distribution (above), 2D-flow vector plot (below)

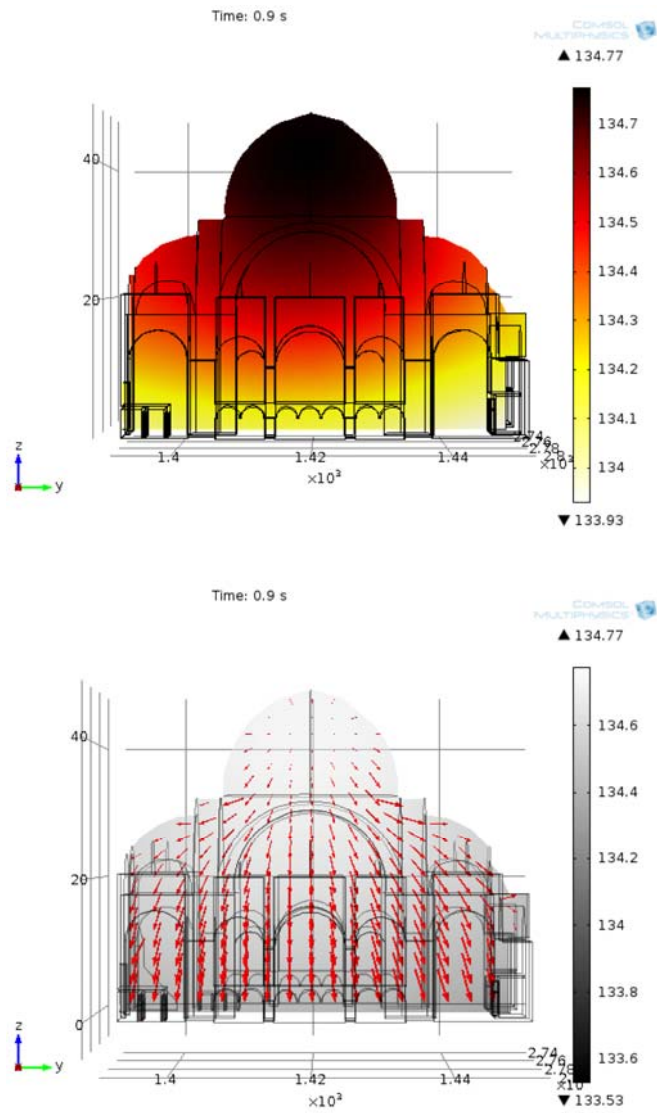


Figure C.33. Süleymaniye Mosque DEM result for 250 Hz, t: 0.9s, carpeted floor, mihrab wall section spatial sound energy level (dB) distribution (above), 2D-flow vector plot (below)

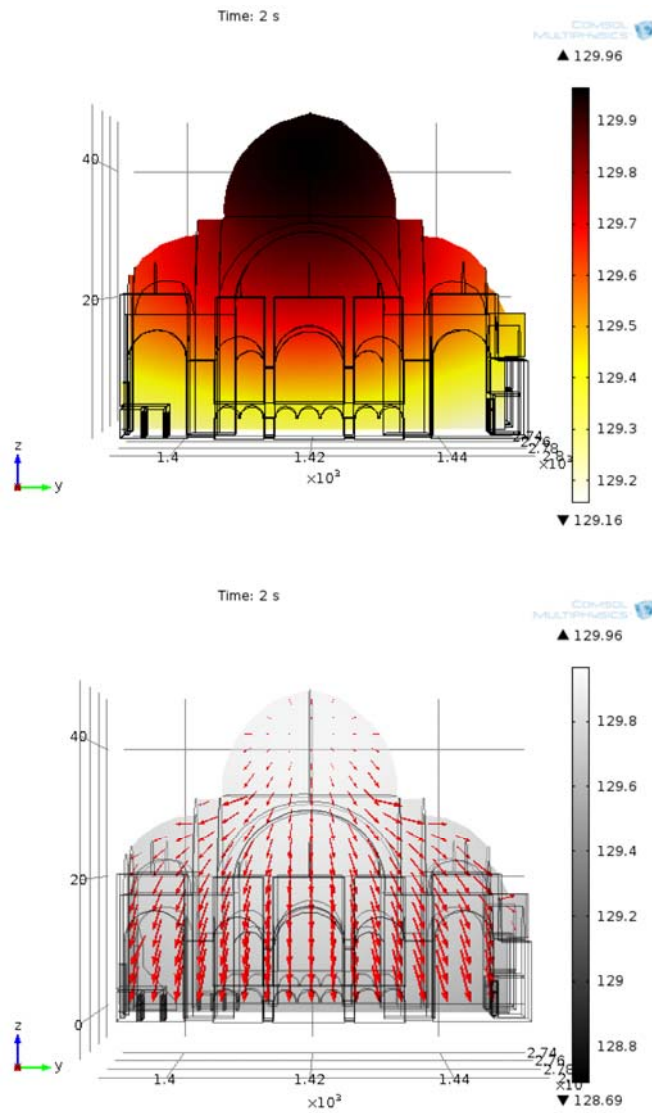


Figure C.34. Süleymaniye Mosque DEM result for 250 Hz, t: 2s, carpeted floor, mihrab wall section spatial sound energy level (dB) distribution (above), 2D-flow vector plot (below)

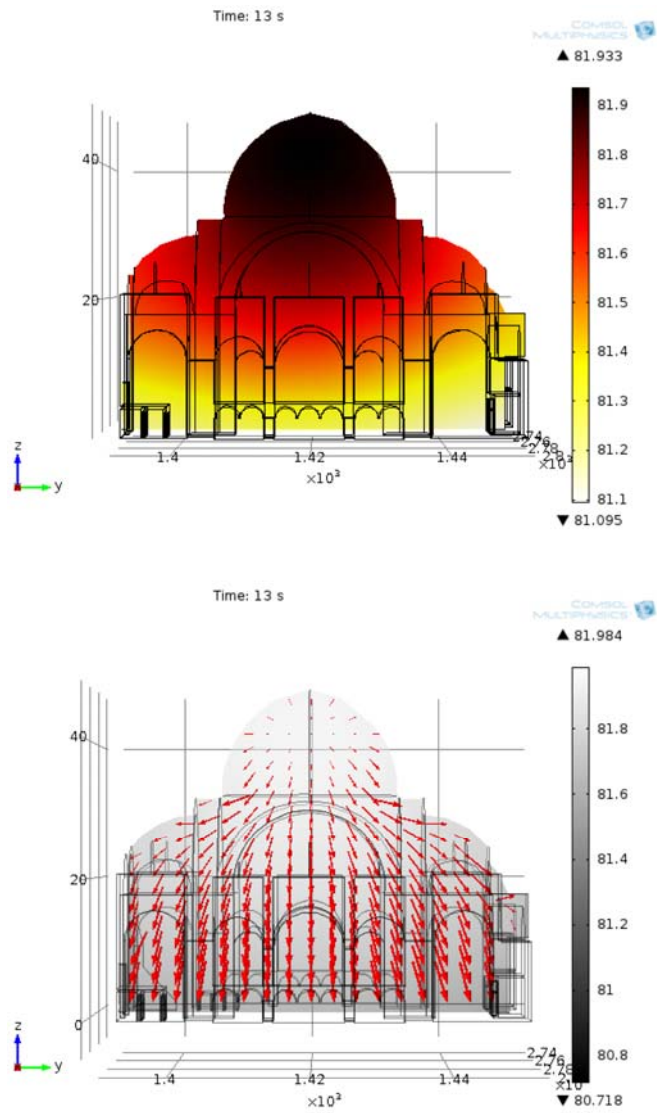


Figure C.35. Süleymaniye Mosque DEM result for 250 Hz, t: 13s, carpeted floor, mihrab wall section spatial sound energy level (dB) distribution (above), 2D-flow vector plot (below)

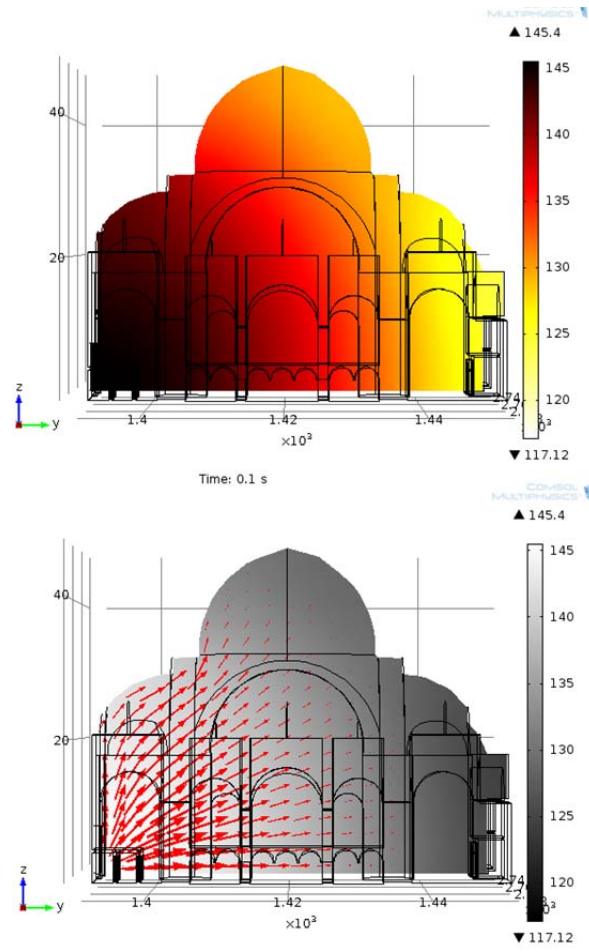


Figure C.36. Süleymaniye Mosque DEM results for 1 kHz, t: 0.1s, marbled floor, mihrab wall section spatial sound energy level (dB) distribution (above), 2D-flow vector plot (below)

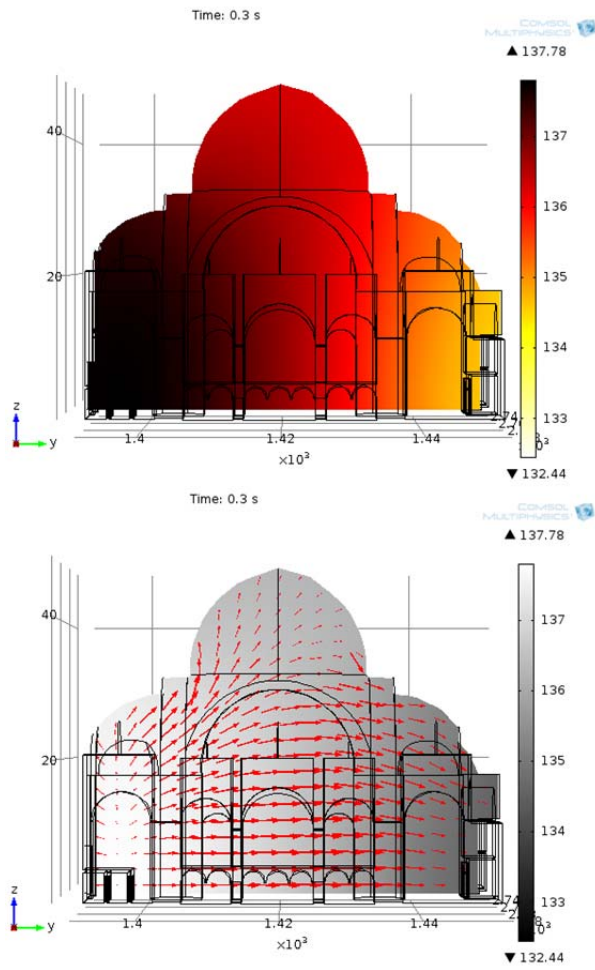


Figure C.37. Süleymaniye Mosque DEM results for 1 kHz, t: 0.3s, marbled floor, mihrab wall section spatial sound energy level (dB) distribution (above), 2D-flow vector plot (below)

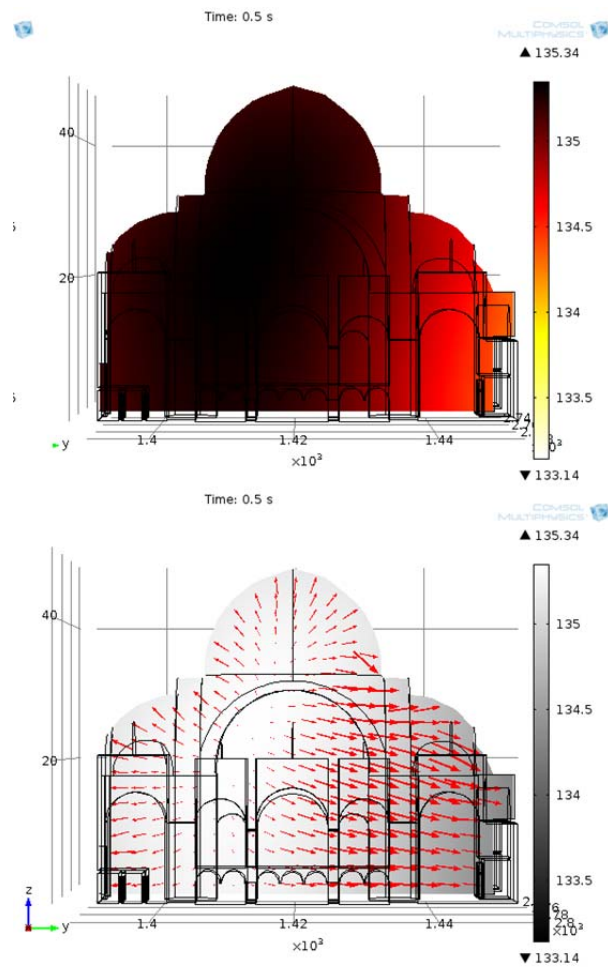


Figure C.38. Süleymaniye Mosque DEM results for 1 kHz, t: 0.5s, marbled floor, mihrab wall section spatial sound energy level (dB) distribution (above), 2D-flow vector plot (below)

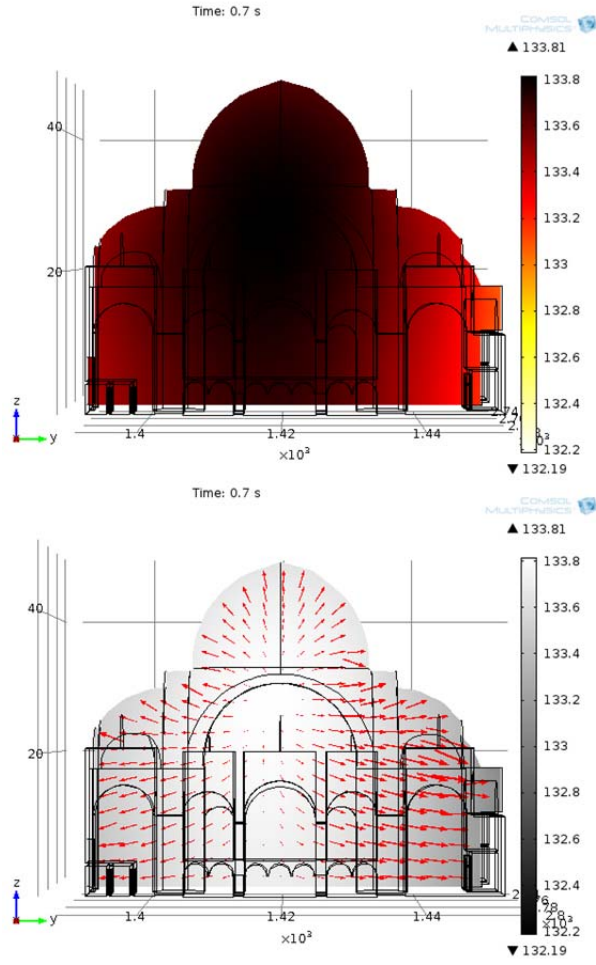


Figure C.39. Süleymaniye Mosque DEM results for 1 kHz, t: 0.7s, marbled floor, mihrab wall section spatial sound energy level (dB) distribution (above), 2D-flow vector plot (below)

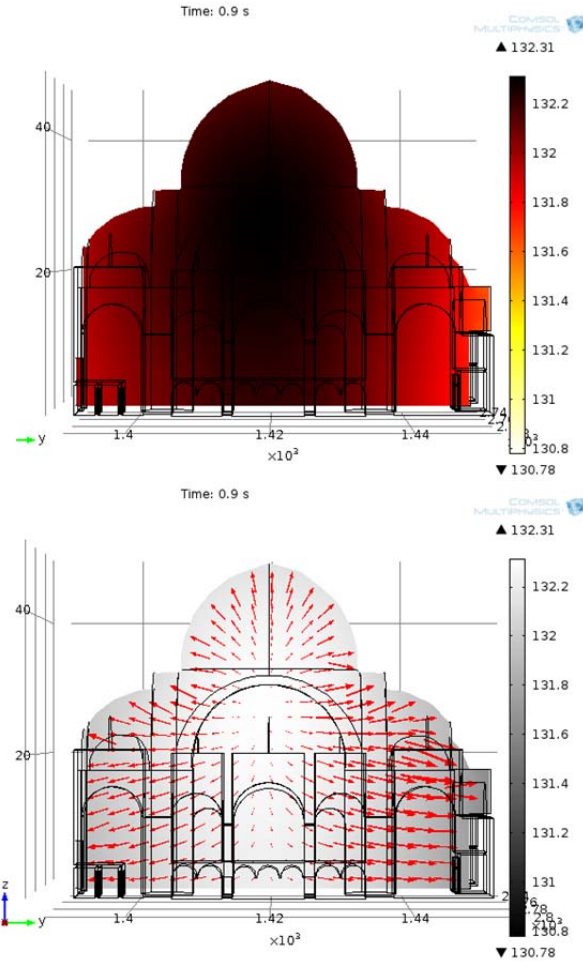


Figure C.40. Süleymaniye Mosque DEM results for 1 kHz, t: 0.9s, marbled floor, mihrab wall section spatial sound energy level (dB) distribution (above), 2D-flow vector plot (below)

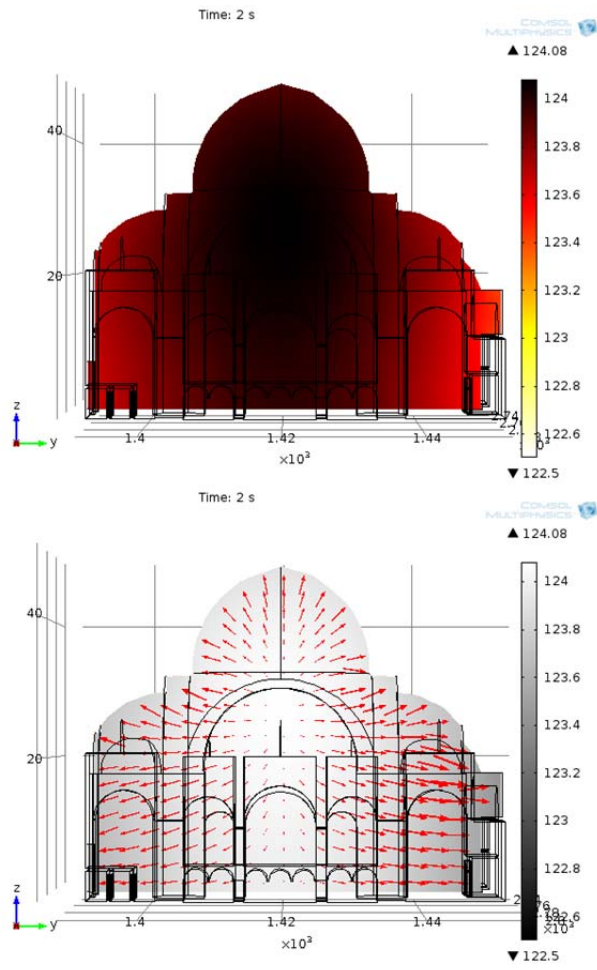


Figure C.41. Süleymaniye Mosque DEM results for 1 kHz, t: 2s, marbled floor, mihrab wall section spatial sound energy level (dB) distribution (above), 2D-flow vector plot (below)

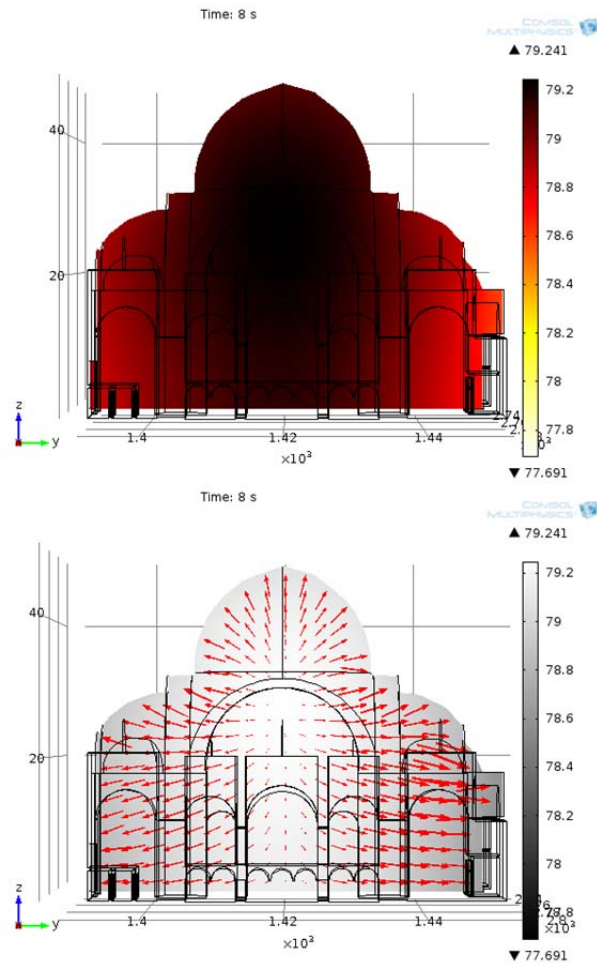


Figure C.42. Süleymaniye Mosque DEM results for 1 kHz, t: 8s, marbled floor, mihrab wall section spatial sound energy level (dB) distribution (above), 2D-flow vector plot (below)

APPENDIX D

INTENSITY PROBE RESULTS

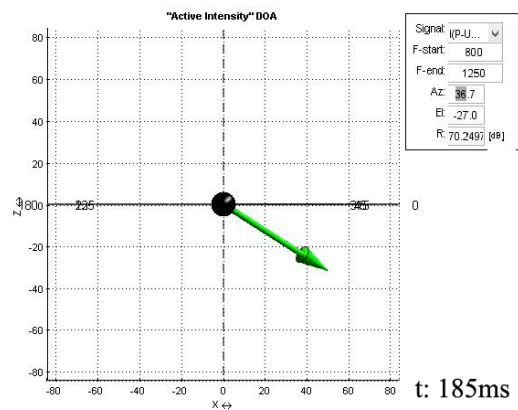
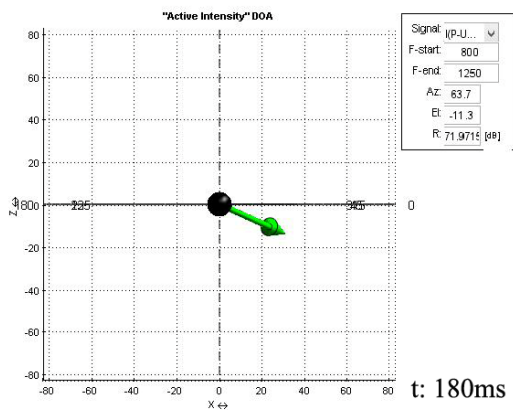
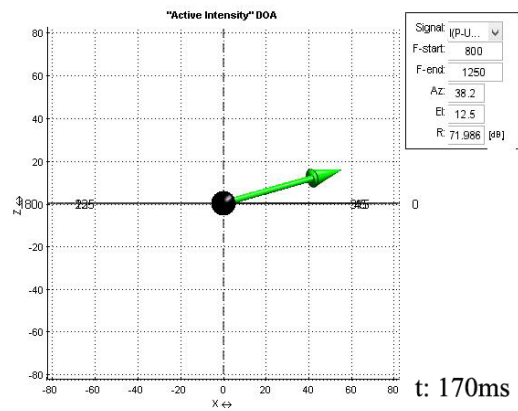
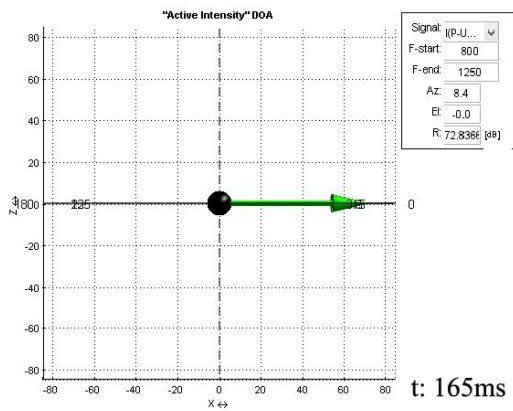
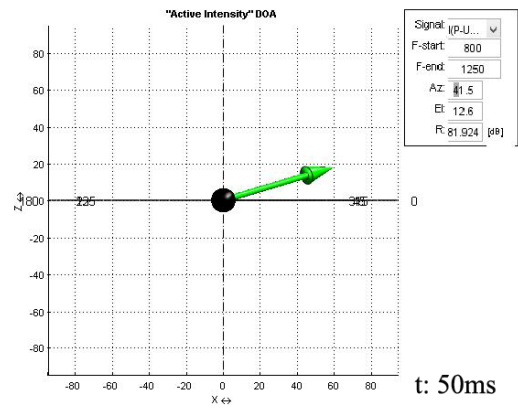
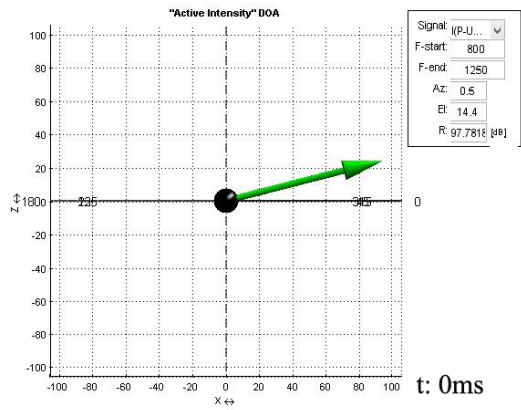


Figure D.43. Intensity vectors, R1S1, 1kHz, t: 0 to 185ms, XZ coordinates, Süleymaniye

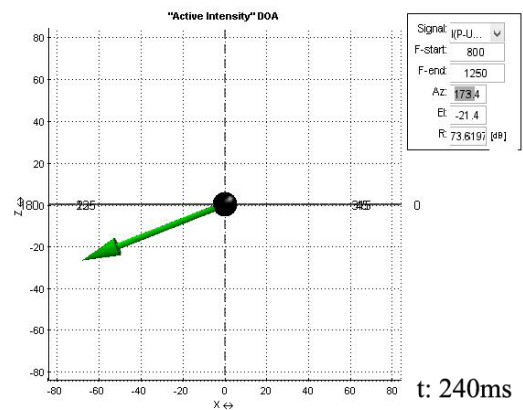
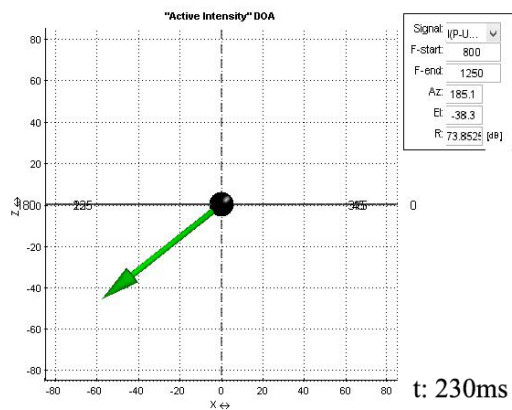
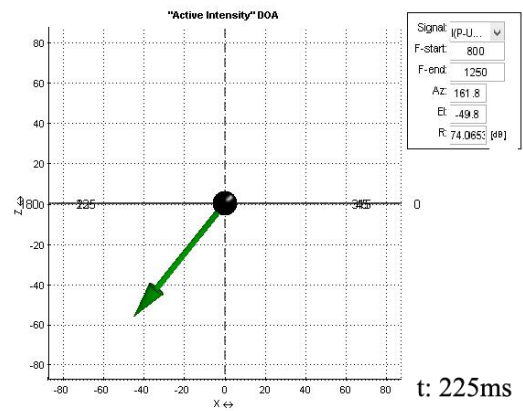
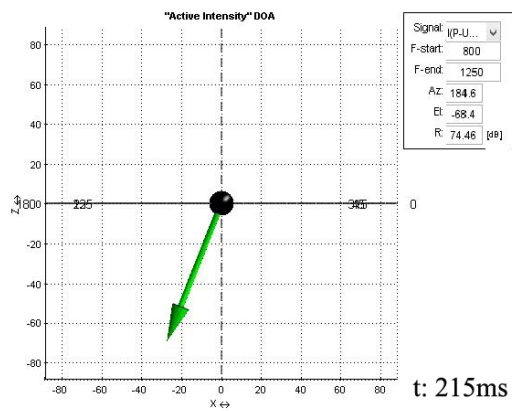
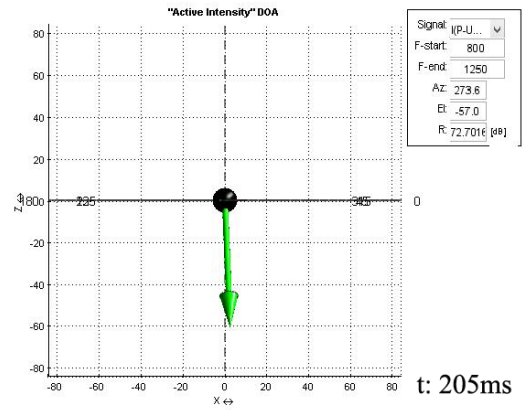
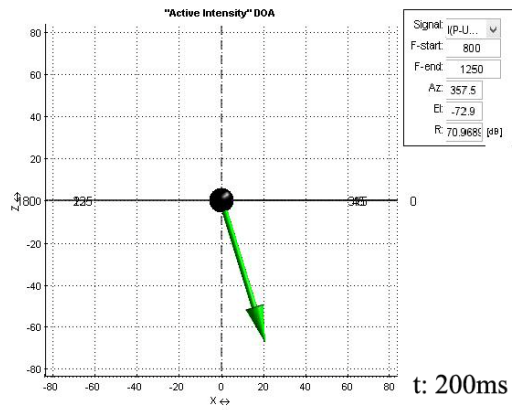


Figure D.44. Intensity vectors, R1S1, 1kHz, t: 200 to 240ms, XZ coordinates, Süleymaniye

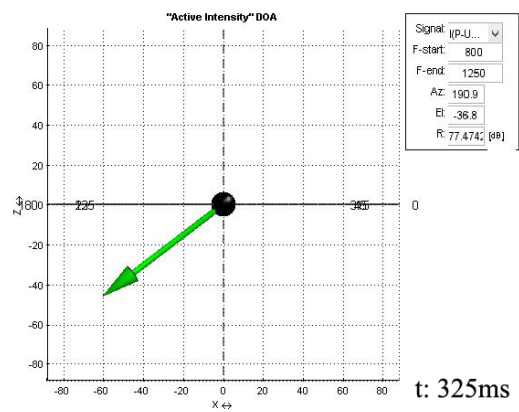
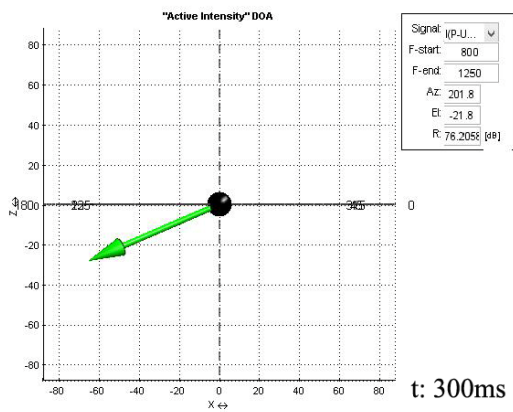
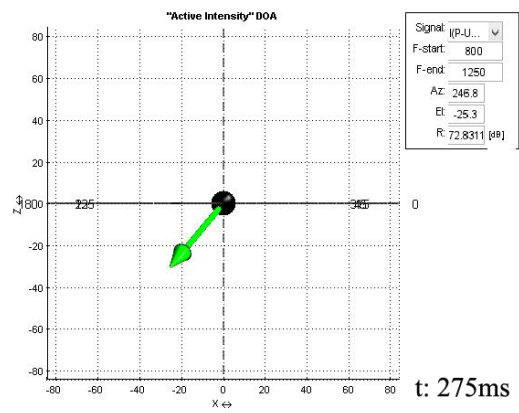
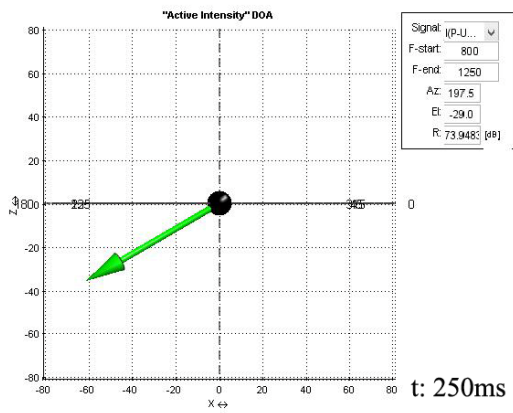
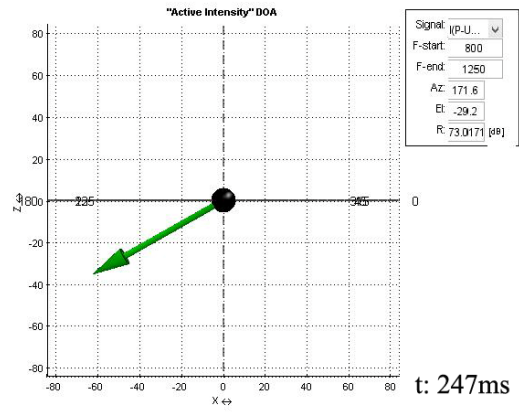
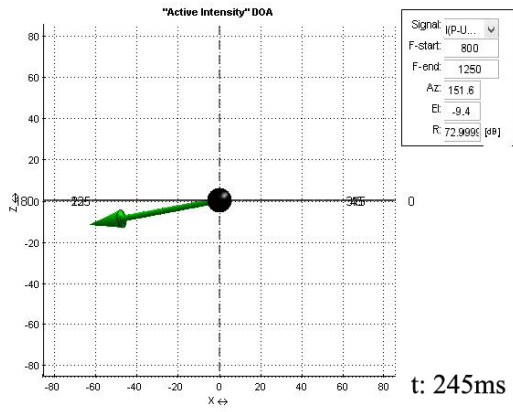


Figure D.45. Intensity vectors, R1S1, 1kHz, t: 245 to 325ms, XZ coordinates, Süleymaniye

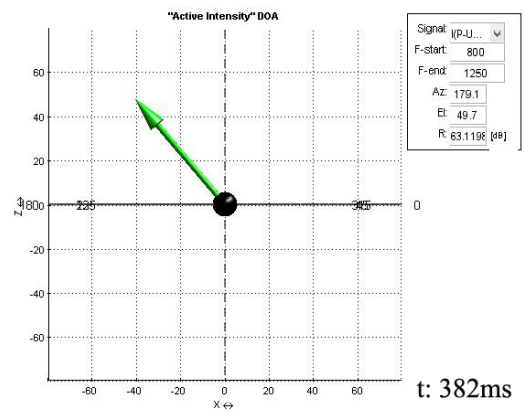
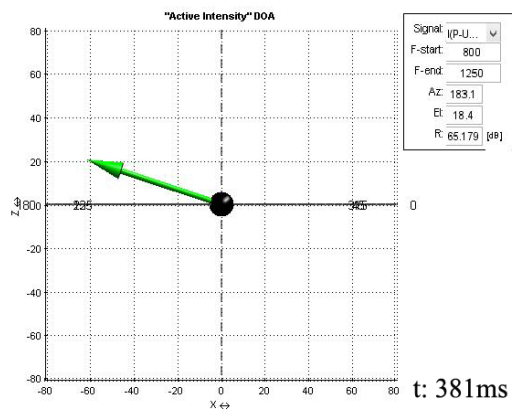
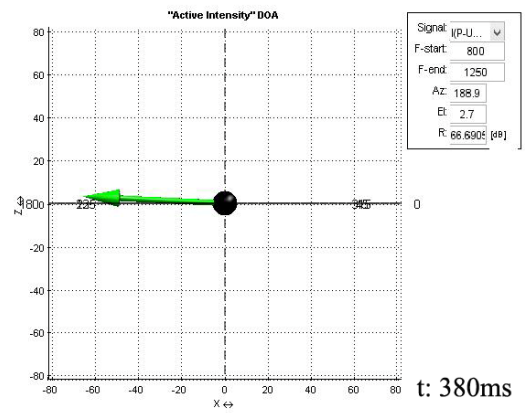
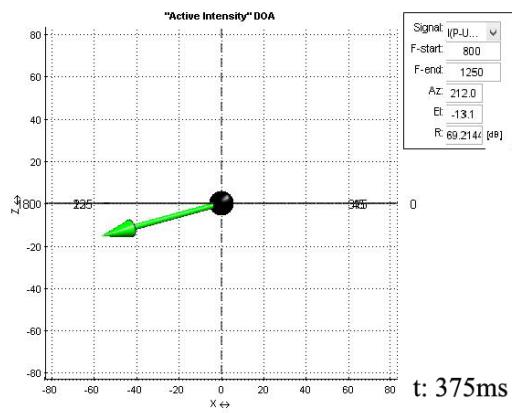
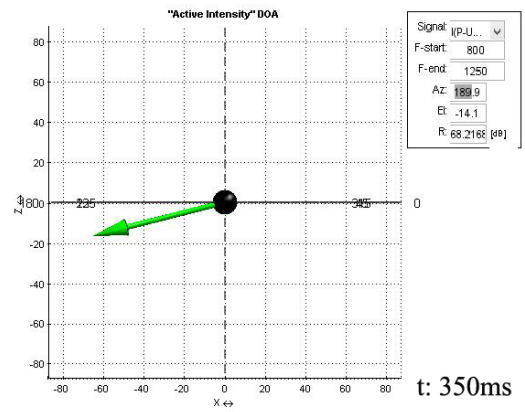
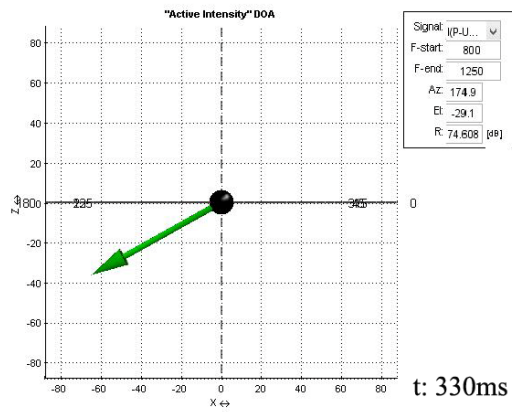


Figure D.46. Intensity vectors, R1S1, 1kHz, t: 230 to 382ms, XZ coordinates, Süleymaniye

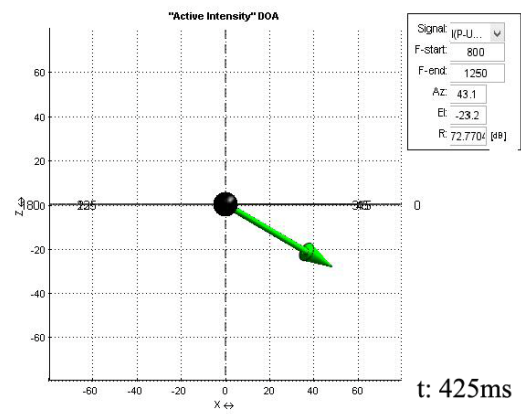
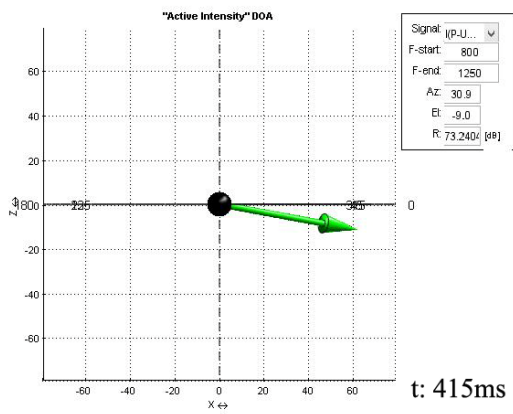
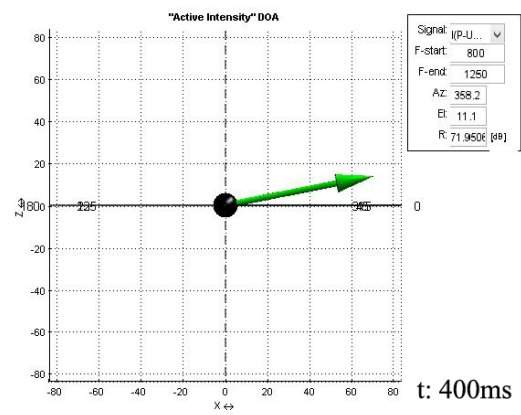
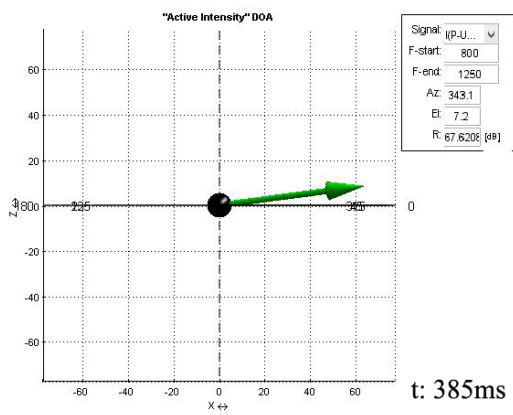
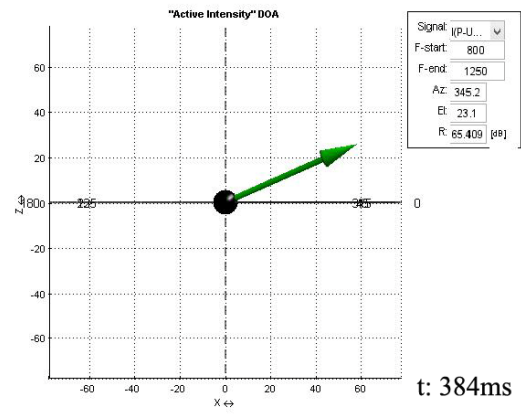
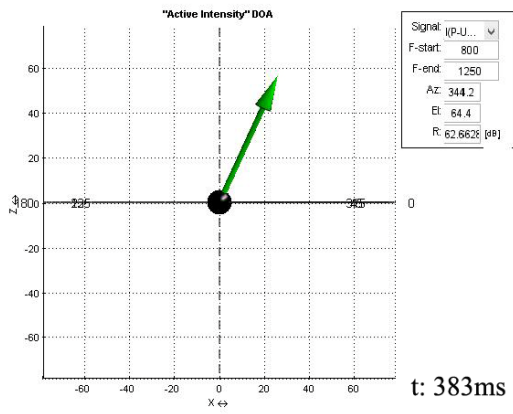


Figure D.47. Intensity vectors, R1S1, 1kHz, t: 283 to 425ms, XZ coordinates, Süleymaniye

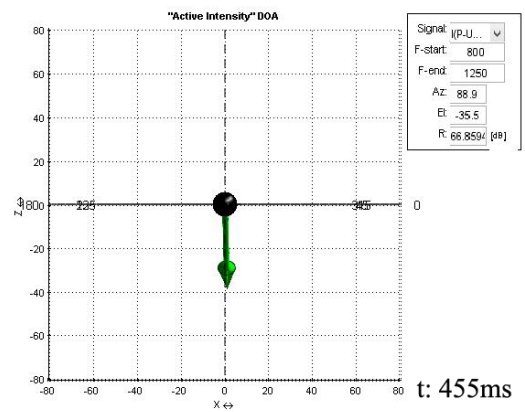
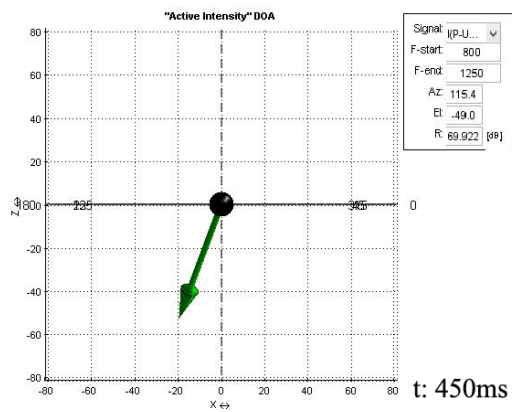
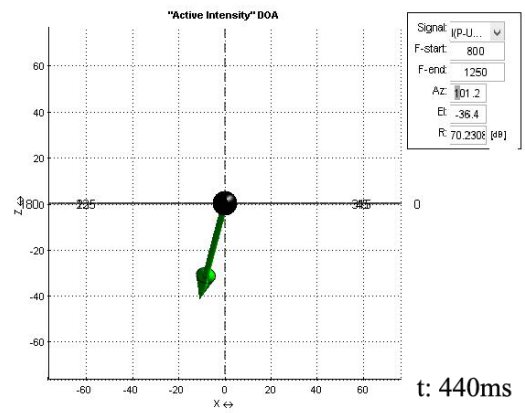
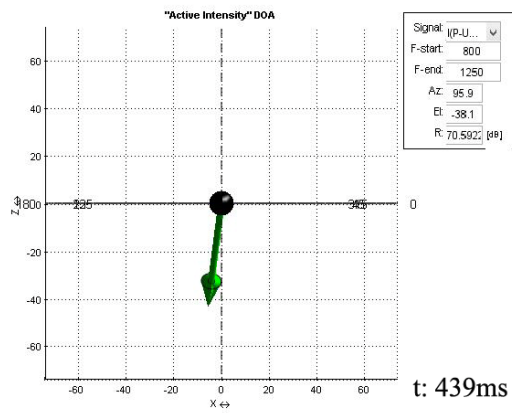
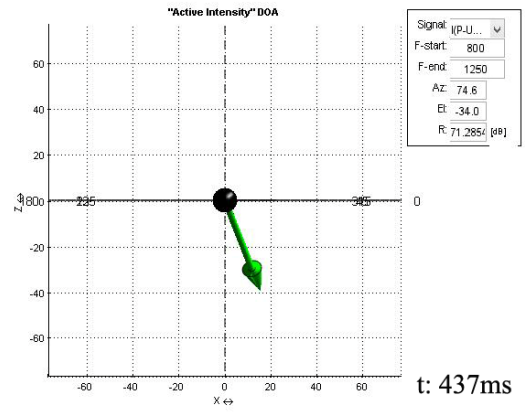
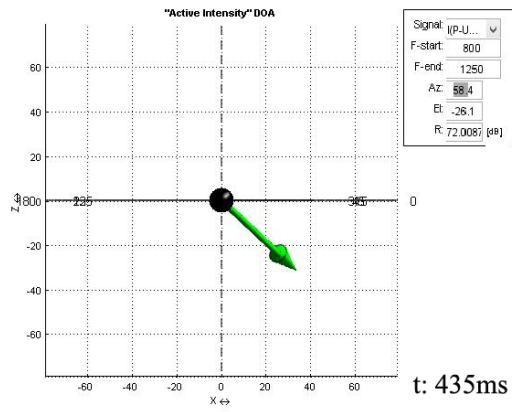


Figure D.48. Intensity vectors, R1S1, 1kHz, t: 435 to 455ms, XZ coordinates, Süleymaniye

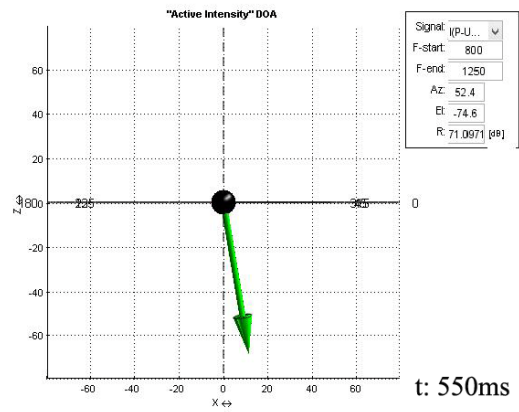
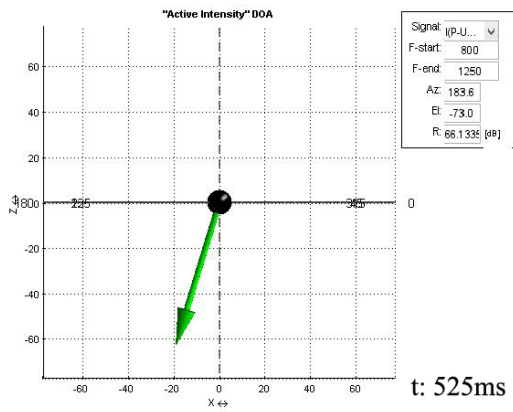
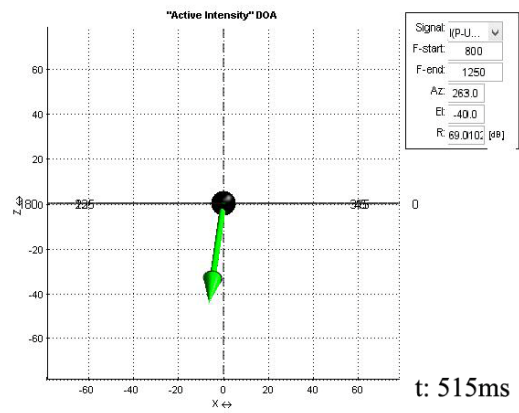
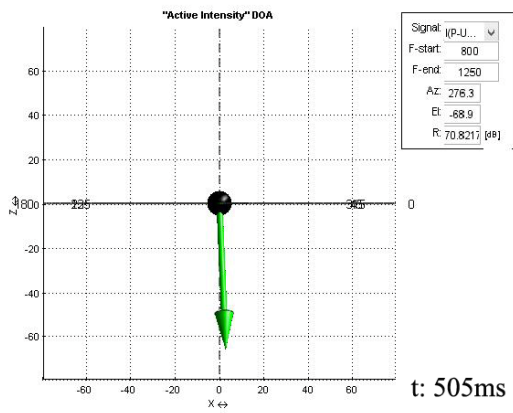
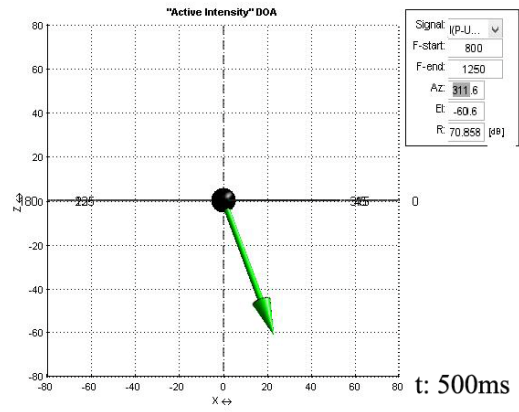
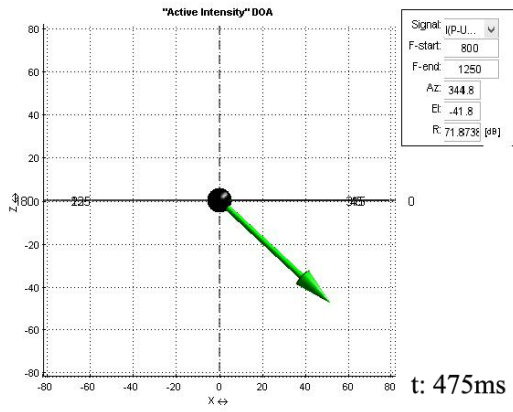


Figure D.49. Intensity vectors, R1S1, 1kHz, t: 475 to 555ms, XZ coordinates, Süleymaniye

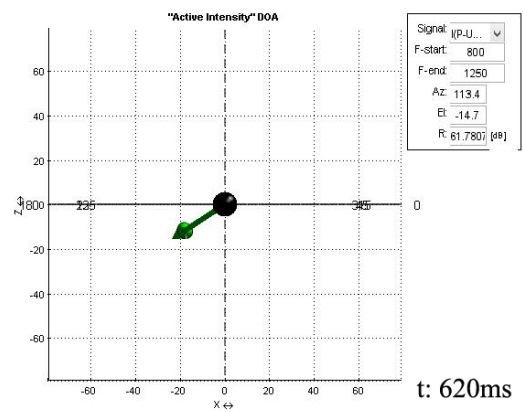
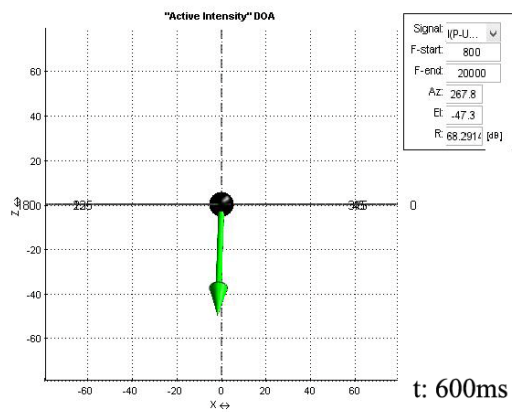
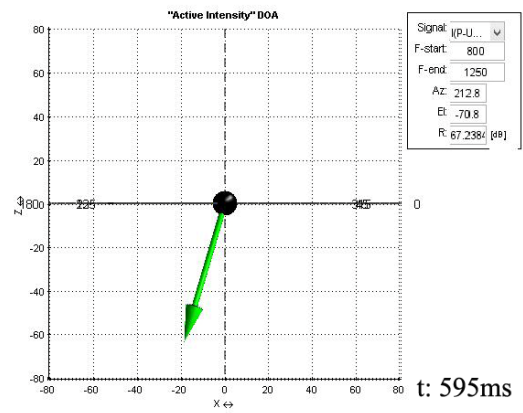
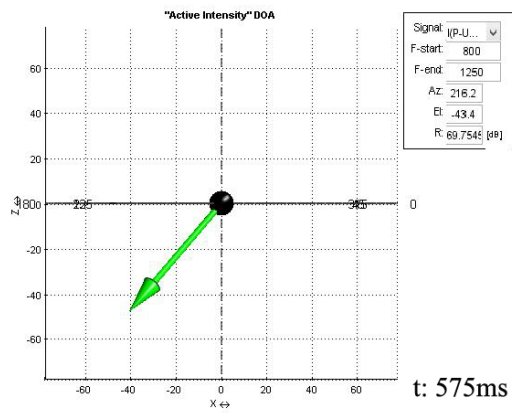
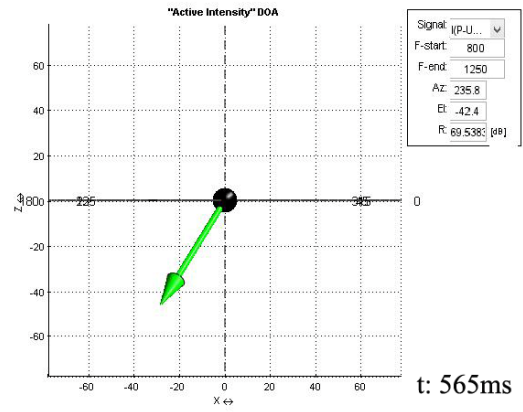
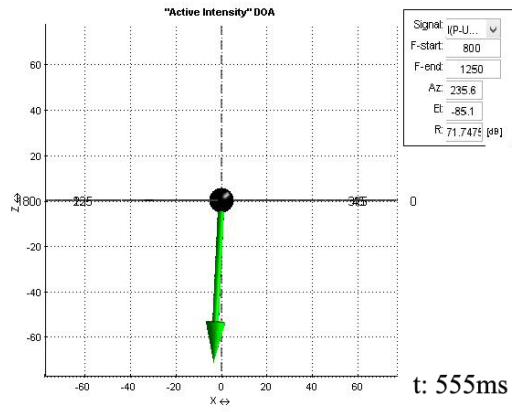


Figure D.50. Intensity vectors, R1S1, 1kHz, t: 555 to 620ms, XZ coordinates, Süleymaniye

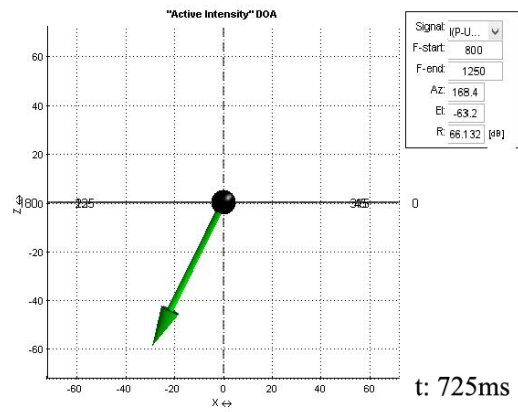
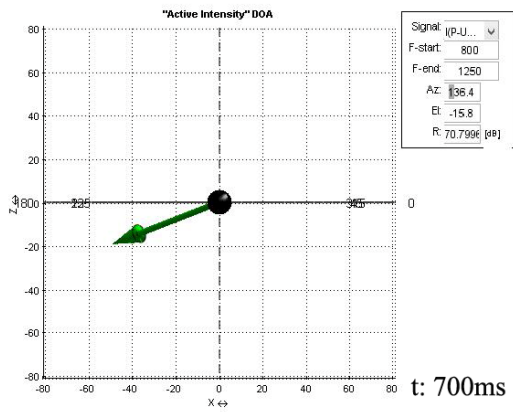
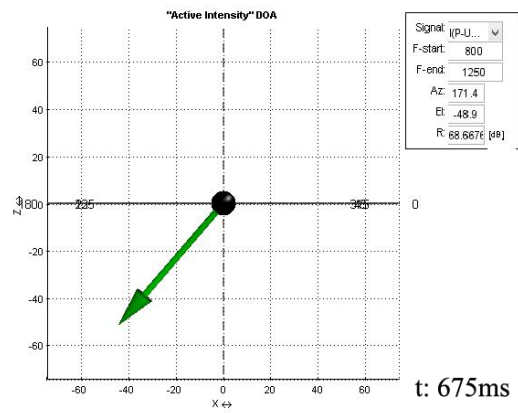
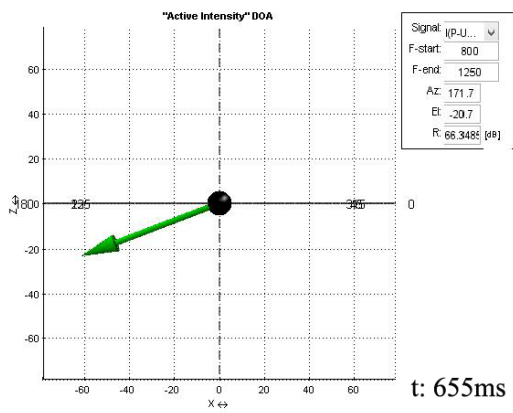
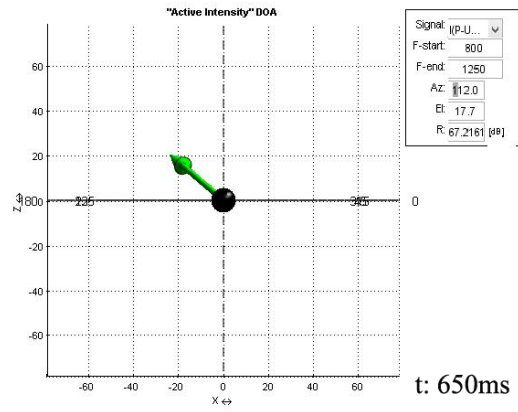
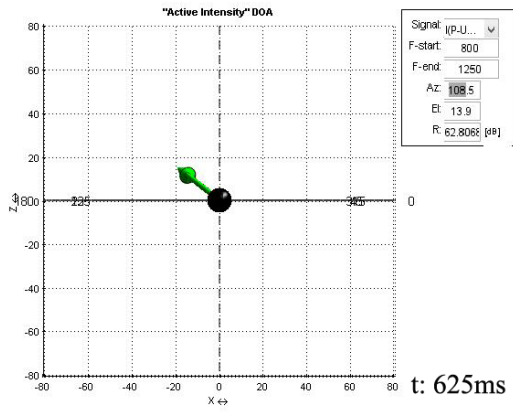


Figure D.51. Intensity vectors, R1S1, 1kHz, t: 625 to 725ms, XZ coordinates, Süleymaniye

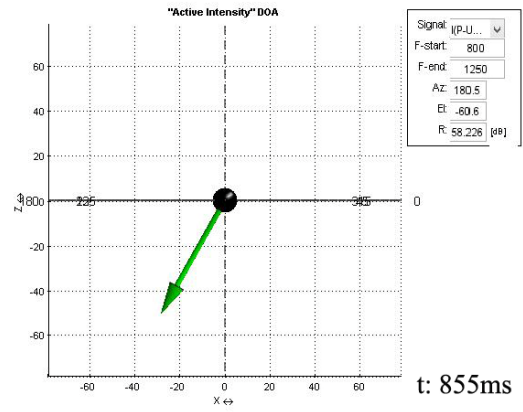
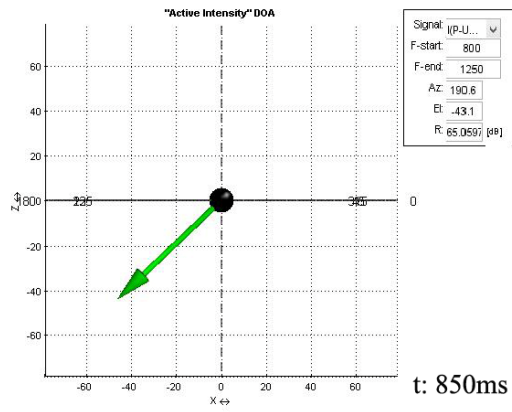
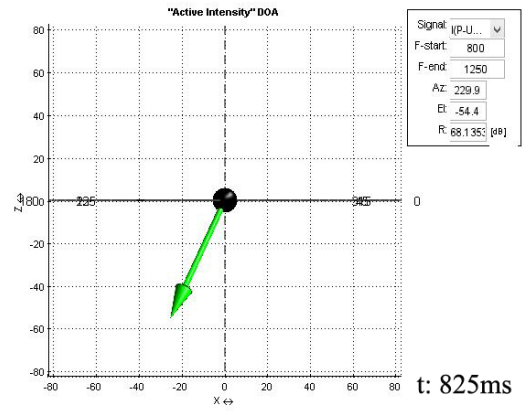
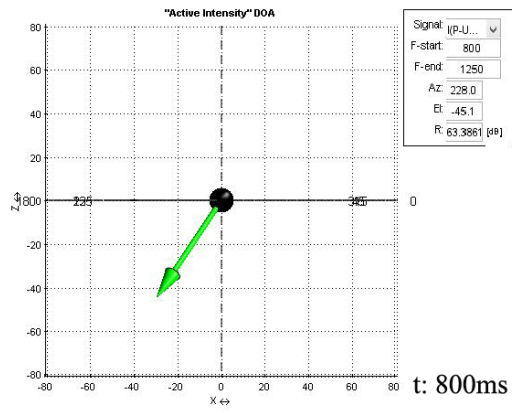
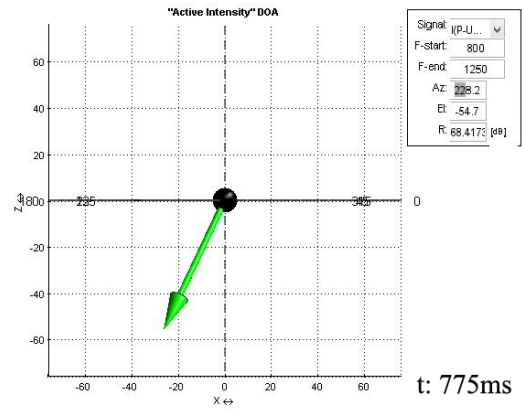
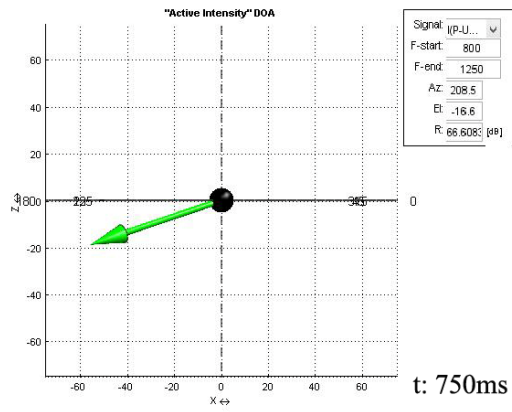


Figure D.52. Intensity vectors, R1S1, 1kHz, t: 750 to 855ms, XZ coordinates, Süleymaniye

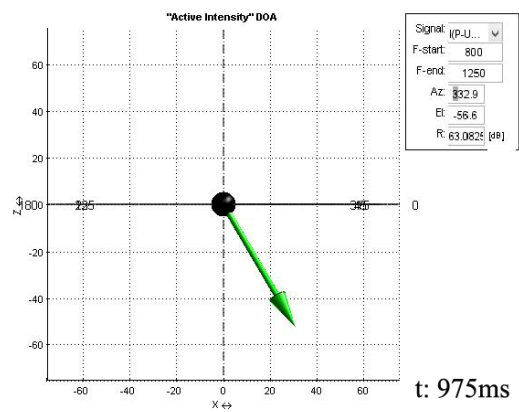
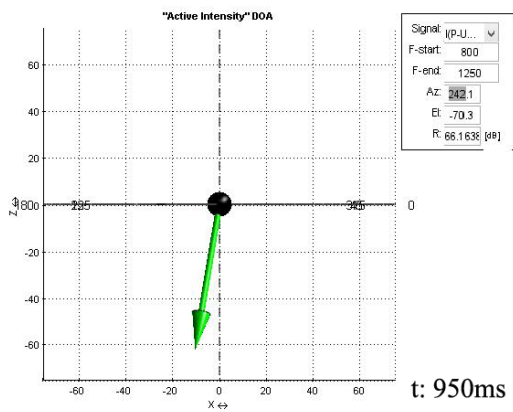
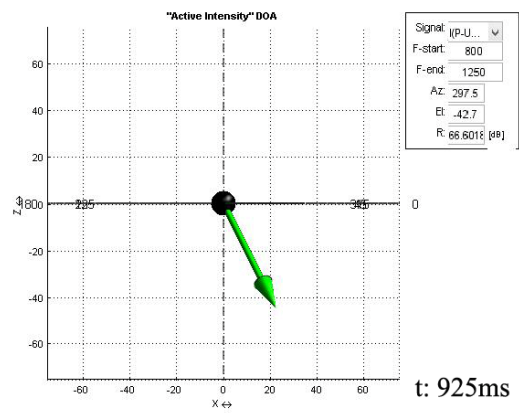
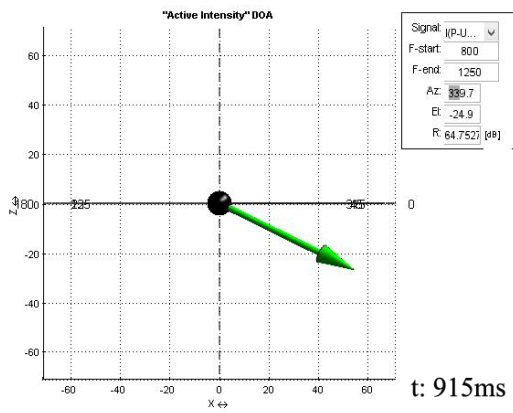
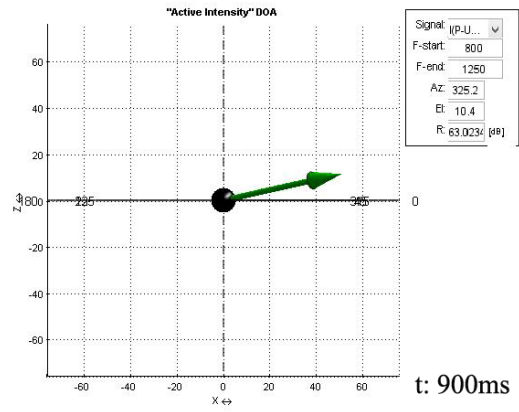
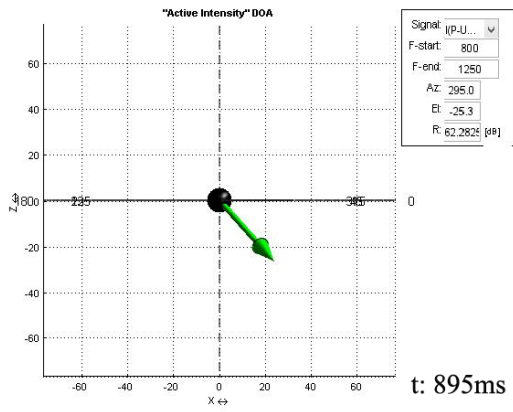


Figure D.53. Intensity vectors, R1S1, 1kHz, t: 895 to 975ms, XZ coordinates, Süleymaniye

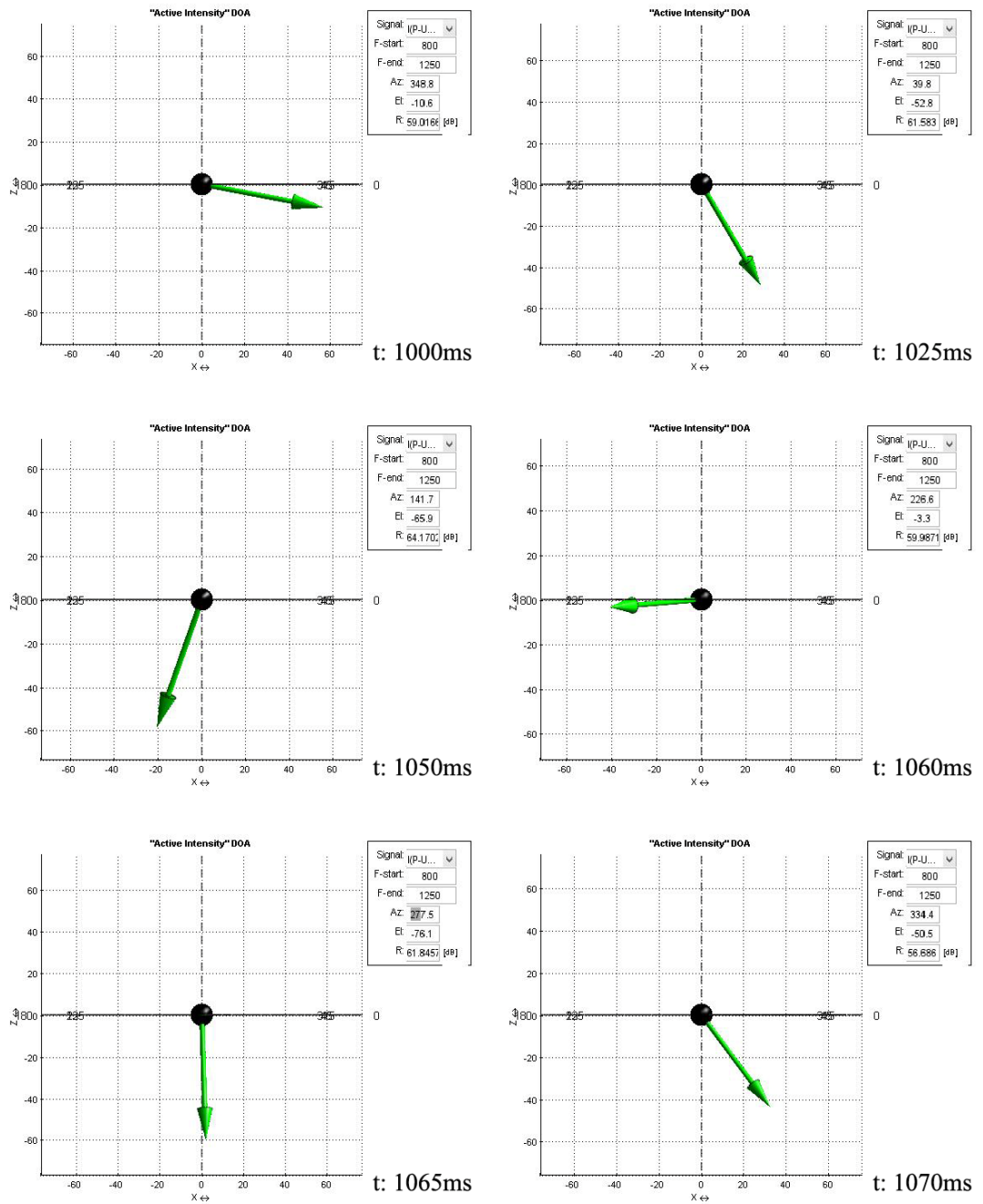


Figure D.54. Intensity vectors, R1S1, 1kHz, t: 1000 to 1070ms, XZ coordinates, Süleymaniye

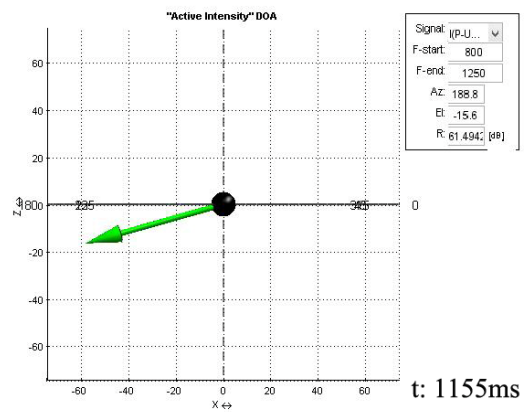
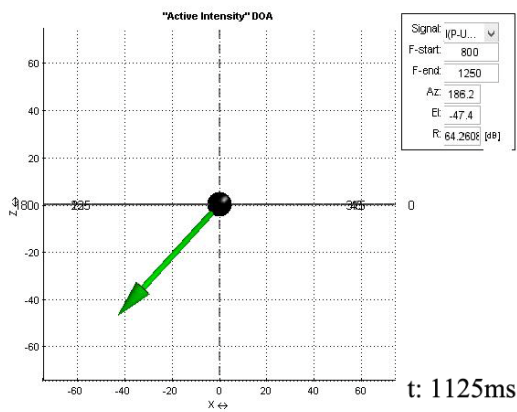
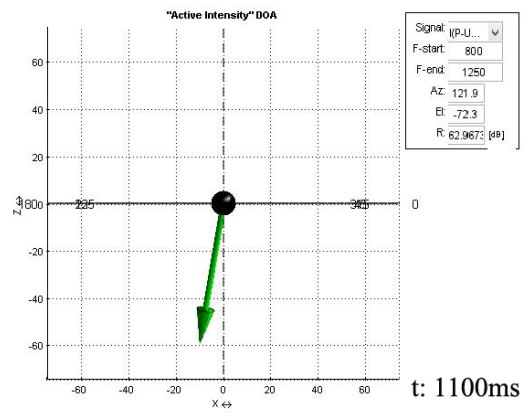
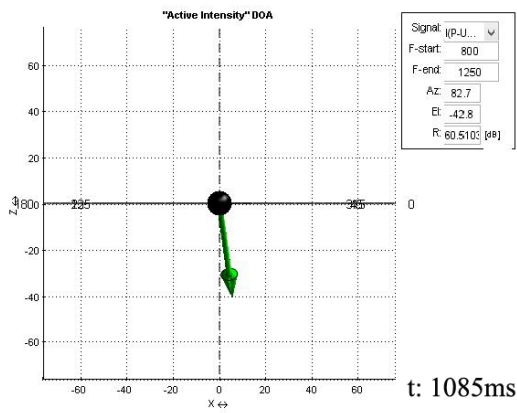
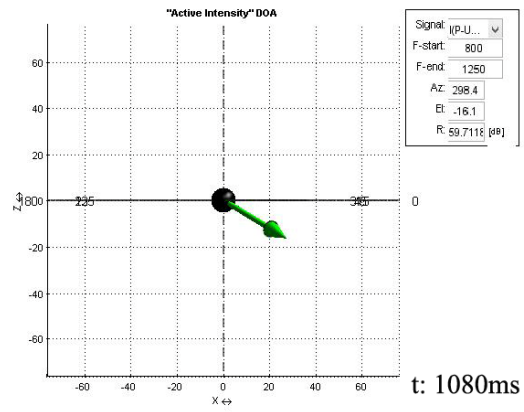
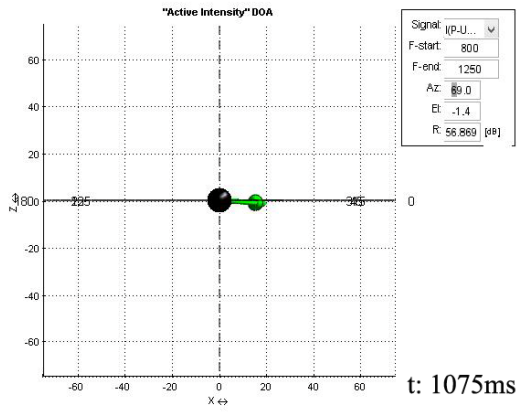


Figure D.55. Intensity vectors, R1S1, 1kHz, t: 1075 to 1155ms, XZ coordinates, Süleymaniye

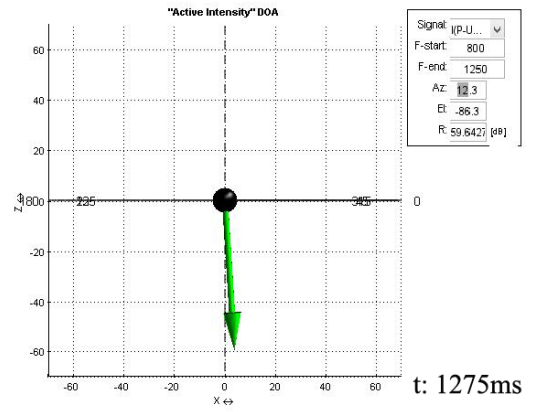
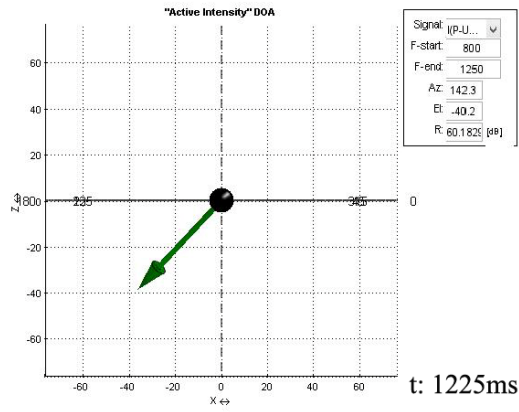
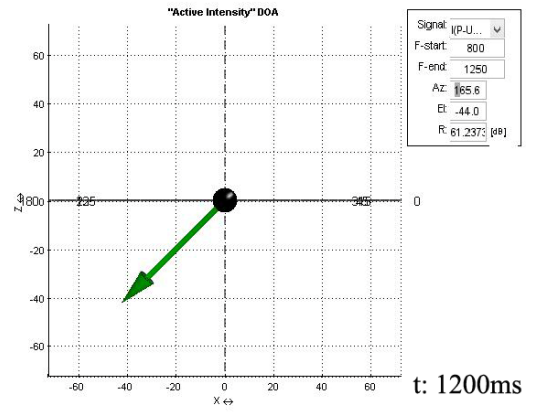
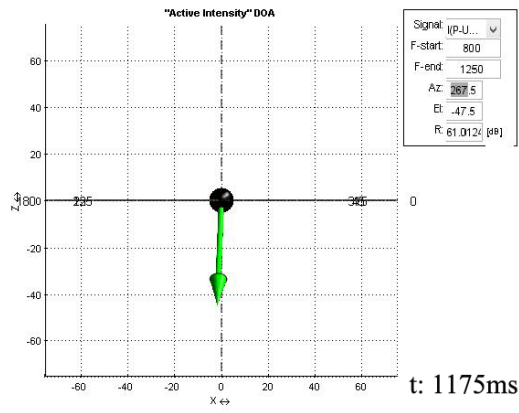
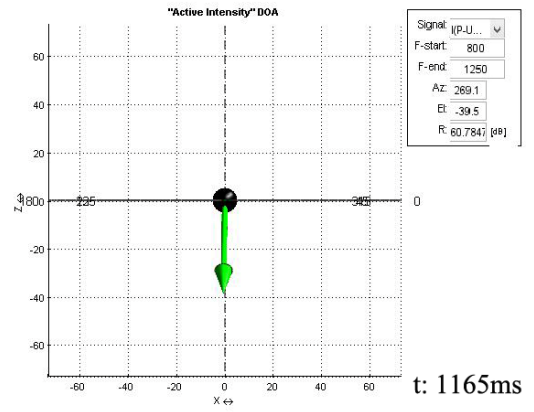
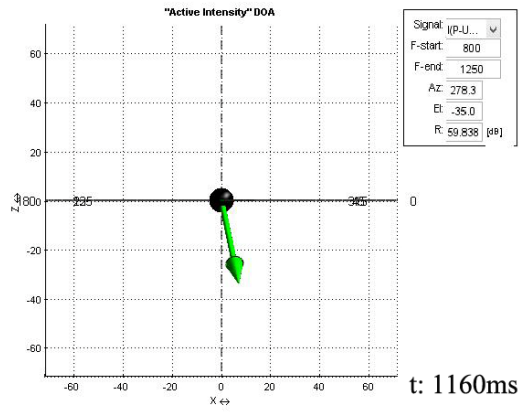


Figure D.56. Intensity vectors, R1S1, 1kHz, t: 1160 to 1275ms, XZ coordinates, Süleymaniye

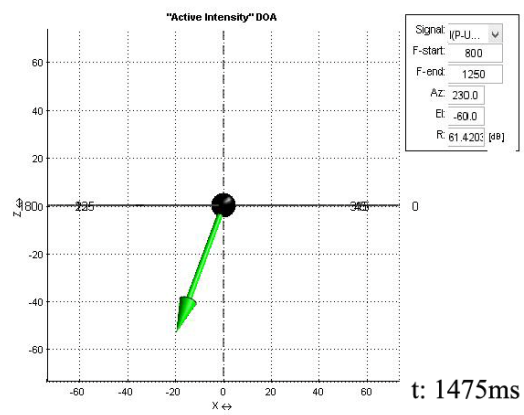
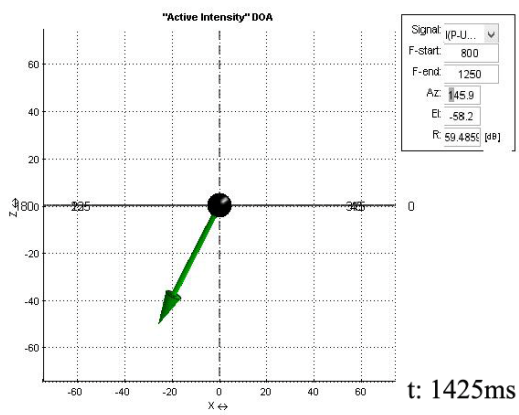
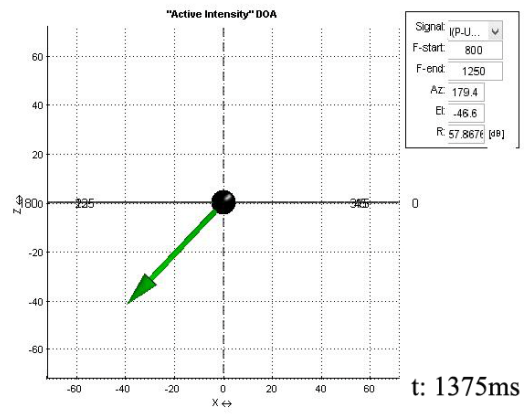
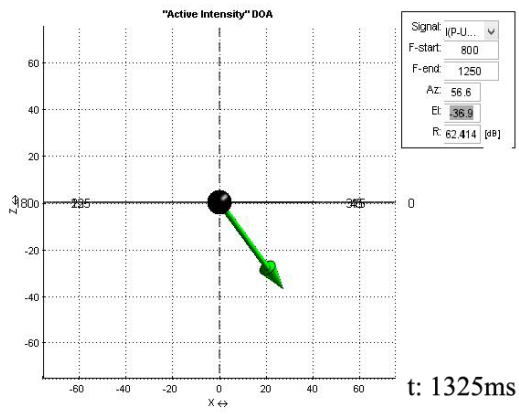


Figure D.57. Intensity vectors, R1S1, 1kHz, t: 1375 to 1475ms, XZ coordinates, Süleymaniye

CURRICULUM VITAE

PERSONAL INFORMATION

Surname, Name: Sü Gül, Zühre

Nationality: Turkish (TC)

Date and Place of Birth: 7 March 1980, Antalya

Marital Status: Married

Phone: +90 312 210 18 25

Fax: +90 312 210 18 26

email: zuhre@mezzostudyo.com

EDUCATION

Degree	Institution	Year of Graduation
MS	Rensselaer Polytechnic Institute (RPI), Graduate Program in Architectural Acoustics, Troy, NY, USA	2006
MFA	Bilkent University, Department of Interior Architecture and Environmental Design, Ankara, Turkey	2004
BArch	Middle East Technical University (METU), Department of Architecture, Ankara, Turkey	2002
High School	Yüce Science High School, Ankara, Turkey	1997

HONORS/AWARDS

Professional:

- ‘Globally Born Incubator Finalist Nominee Award’ by Turkish Ministry of Industry, November, 2012.

Academic:

- 2006 Medallist of Robert B. Newman Award for Merit in Architectural Acoustics. ‘For Excellence in the Study of Acoustics and in its Application to Architecture’, NY, USA, 2006.
- Second price in the Best Student Paper Award competition in the area of Architectural Acoustics for the June 2006 Acoustical Society of America meeting in Providence, RI, USA.
- Commendation from 2006 ASA Student Design Competition, ‘A City Municipal Building, including a Council Chambers and Courtroom.’
- Graduation with the 3rd Honour from Yüce Science High School, 1995-1997.

Sports:

- 6 gold, 4 silver and 2 bronze medals including the 1st and 2nd awards in Turkish National Championships as a licensed swimmer, 1991-1993.

WORK EXPERIENCE

Year	Place	Enrollment
2009 - Present	Mezzo Stüdyo Ltd., Ankara, Turkey	General Manager
2013 - Present	Bilkent University, Department of Interior Architecture and Environmental Design, Ankara, Turkey	Part-time Instructor
2006 -2008	Russ Berger Design Group (RBDG), Dallas, TX, USA	Architect – Acoustician
2005 - 2006	Rensselaer Polytechnic Institute (RPI), Graduate Program in Architectural Acoustics, Troy, NY,USA	Research Assistant
2003 -2005	Bilkent University, Department of Interior Architecture and Environmental Design, Ankara, Turkey	Teaching Assistant
2002-2003	Kural Architecture, Ankara, Turkey	Architect
2001	Kural Architecture, Ankara, Turkey	Intern Architect
2000	Tepe Construction, Antalya, Turkey	Intern Architect

MEMBERSHIPS

- National Council of Acoustical Consultants, of USA (company membership)
- Full Member, ASA Acoustical Society of America
- TMMOB Turkish Architectural Chamber Membership

PUBLICATIONS

- 1*. Sü Gül, Z., Çalışkan, M. and Tavukçuoğlu, A. “Geçmişten Günümüze Süleymaniye Camii Akustiği.” *Megaron*, 9.3 (2014): 201-216.
- 2*. Sü Gül, Z., Xiang, N. and Çalışkan, M. “Investigations on Acoustical Coupling within Single-Space Monumental Structures using a Diffusion Equation Model.” *168th Meeting of the Acoustical Society of America*, 27-31 October 2014, Indianapolis, Indiana, 2014.
3. Sü Gül, Z. (2014). “Konforun Üç Bilinmeyenli Denklemi 2014, 3. Bölüm, X: Akustik”. *Konsept Projeler*, 42 (2014): 98-108.
- 4*. Sü Gül, Z., Xiang, N. and Çalışkan, M. “Sound Field Analysis of Monumental Structures by the Application of Diffusion Equation Model.” *COMSOL Conference 2014*, 17 - 19 September, Cambridge, UK, 2014.
- 5*. Sü Gül, Z., Tavukçuoğlu, A., Çalışkan, M. “A Discussion on the Acoustics of Süleymaniye Mosque for its Original State.” *9th International Symposium on Conservation of Monuments in the Mediterranean Basin (MONUBASIN)*, 3-5 June 2014, Middle East Technical University, Ankara, 2014.
6. Sü Gül, Z. and Çalışkan, M. “Acoustical Considerations in Design and Construction of Turkish Contractors Association Headquarters”, *167th Meeting of the Acoustical Society of America*, 5-9 May 2014, Providence, Rhode Island, USA.
7. Sü Gül, Z. and Çalışkan, M. “Heydar Aliyev Merkezi Oditoryumu Akustik Tasarım Süreci; the Acoustic Design Process for the Auditorium at the Heydar Aliyev Center” *Yapı*, March (2014): 144-150.
- 8*. Sü Gül, Z., Çalışkan, M. and Tavukçuoğlu, A. “2007-2011 Onarımları Sonrası Süleymaniye Camii’nin Akustik Özellikleri: Ölçüm ve Değerlendirmeler.” *TAKDER 10th National Acoustics Congress*, 16-17 December 2013, Yıldız Technical University, İstanbul, (2013): 21-28.
- 9*. Sü Gül, Z., Xiang N. and Çalışkan, M. “Multiple-Slope Sound Energy Decay Investigations in Single Space Enclosures with Specific Geometrical and Material Attributes.” *166th Meeting of the Acoustical Society of America*, San Francisco, California, 2013.
- 10*. Sü Gül, Z. and Çalışkan, M. “Acoustical Design of Turkish Religious Affairs Mosque.” *The 21st International Congress on Acoustics (ICA)*, 2-7 June 2013, Montreal, Canada, 2013.

- 11*. Sü Gül, Z. and Çalışkan, M. "Impact of Design Decisions on Acoustical Comfort Parameters: Case Study of Doğramacızade Ali Paşa Mosque." *Technical Note. App. Acoust.* 74 (2013). 834-844.
- 12*. Sü Gül, Z., Xiang N. and Çalışkan, M. "Investigations on Multi-Slope Sound Energy Decays in Domed Structures." *Proceedings of Inter-Noise 2012*, 19-22 August 2012, New York, USA, 2012.
13. Sü Gül, Z. and Çalışkan, M. "Acoustical Design of Underground Stations within Warsaw Metro System Phase II" *9th National Acoustics Congress, TAKDER, ODTÜ*, 26-27 May 2011, Ankara, Turkey.
- 14*. Odabaş, E., Sü Gül, Z. and Çalışkan, M. "Acoustical Design of Doğramacızade Ali Paşa Mosque and Assessment of Acoustical Characteristics by Real Size Measurements" *9th National Acoustics Congress, TAKDER, ODTÜ*, 26-27 May 2011, Ankara, Turkey.
15. Sü Gül, Z. and Çalışkan, M. "Acoustical Considerations in the Design of Heydar Aliyev Center Auditorium." *Proceedings of the International Symposium on Room Acoustics, ISRA 2010*, 29-31 August 2010, Melbourne, Australia, 2010.
16. Sü Gül, Z. and Çalışkan, M. "Acoustical Design of Inner Galleries in Heydar Aliyev Center" *Proceedings of 20th International Congress on Acoustics, ICA 2010*, 23-27 August 2010, Sydney, Australia.
17. Sü, Z. and Yılmaz, S. "The Acoustical Characteristics of the Kocatepe Mosque in Ankara, Turkey." *Arch. Sci. Rev.* 51.1 (2008): 21-30.
18. Sü, Z. and Çalışkan, M. "Acoustical Design and Noise Control in Metro Stations: Three Cases in Ankara Metro System." *Building Acoustics*, 14.3 (2007): 231-249.
19. Sü, Z. and Xiang, N. "Further Investigations on Acoustically Coupled Spaces using Scale-Model Technique" *Acoustical Society of America and Acoustical Society of Japan: Fourth Joint Meeting*, 28 November,-2 December 2006, Honolulu, Hawaii, USA.
20. Sü, Z. *Systematic Investigations on Energy Decays in Acoustically Coupled Spaces Using the Scale-Model Technique*. Unpublished Master's Thesis. Graduate Faculty of Rensselaer Polytechnic Institute, Troy, NY, 2006.
21. Xiang, N., Jasa, T. and Sü, Z. "Schroeder Decay Function Decomposition for Sound-Energy Decay Analysis of Acoustic Coupled-Volume Systems." *Wespac IX: The 9th Western Pacific Acoustics Conference*, 26-28 June 2006, Seoul, Korea.

22. Sü, Z., Xiang, N. and Summers, J. E. “Experimental investigations of acoustically coupled spaces” *Acoustical Society of America: 151st Meeting*, 5-9 June 2006, Providence, Rhode Island, USA.
23. Sü, Z. and Yilmazer, S. “The Acoustical Performance Analysis of Bilkent Amphitheater: Proposal for Acoustical Renovation.” *Architectural Science Review*, 49.2 (2006): 167-178.
24. Arslan, S., Sü, Z. and Çalışkan, M. “Contribution of the Computer Simulation to the Process of Design in the Courses of Architectural Acoustics: A Study of 500 Seated Concert Hall.” *Proceedings of Turkish Acoustical Society (TAKDER): 7th National Congress*, 17 -19 November 2004, Cappadocia. Nevşehir: TAKDER, 2004.
25. Sü, Z. *Acoustical Performance Analysis of Bilkent University Amphitheater - ODEON*. Unpublished Master’s Thesis. Bilkent University, Department of Interior Architecture and Environmental Design, Ankara, Turkey, 2004.

* *Journal and proceeding papers published or presented in relation and as an outcome to this thesis research.*